Using NMR to Study Protein-Ligand Interactions

A thesis submitted to the Board of the Faculty of Physical Sciences of the University of Oxford in partial fulfilment of the requirements for the degree of Doctor of Philosophy

Martine I. Abboud

St John's College, Oxford

Michaelmas Term, 2016

Abstract

Using NMR to Study Protein-Ligand Interactions

Martine I. Abboud ***DPhil Thesis***
St John's College, University of Oxford ***Michaelmas Term, 2016***

The work described in this thesis focused on the use of nuclear magnetic resonance spectroscopy (NMR) to study two classes of metallo enzymes – the Fe(II)- and 2-oxoglutarate (2OG)-dependent dioxygenases and the metallo β-lactamases (MBLs). These enzymes are involved in clinically important biological processes, *i.e.* the hypoxic response and antimicrobial resistance, respectively. Both protein systems are interesting from an NMR perspective because they have dynamic regions involved in catalysis and ligand interactions. The work included mechanistic studies, protein-ligand interaction studies, and method development for inhibitor discovery.

NMR was applied to study the human prolyl hydroxylase domain-containing protein 2 (PHD2), which is crucially involved in the chronic hypoxic response. The results reveal that binding of the *C*- and the *N*-terminus of the oxygen dependent degradation domains CODD and NODD, respectively, induce different interactions with PHD2. The substitution of a single amino acid, as occurs with PHD2 variants linked to erythrocytosis and breast cancer, can alter the selectivity of PHD2 towards its ODD substrates. Studies with the *Trichoplax adhaerens* PHD provide insights into the evolutionary substrate preference of the PHDs. Using ^{13}C-labelled peptidyl-substrates; NMR was applied to investigate proposed 'alternative' PHD2 substrates/interaction partners. The product release mechanism of PHD2 was investigated using NMR; the results reveal that the presence of 2OG strongly discriminates between the binding of CODD and hydroxylated CODD to PHD2. NMR was also applied to monitor PHD2 kinetics and inhibition. Competition and displacement assays were designed and applied to investigate PHD inhibitor binding modes. Comparative studies on the activities and selectivities of PHD inhibitors in clinical trials should aid in the work on the therapeutic manipulation of the natural hypoxic response.

Protein-observe ^{19}F-NMR was used to study the São Paolo MBL (SPM-1). The results provide new structural insights into SPM-1 catalysis and the requirements for inhibitor development. They also reveal that the hydrolysed β-amino acid products of MBL catalysis can bind to SPM-1. They illustrate the utility of ^{19}F-NMR for detecting metal chelation, which is not always readily tractable in studies on metallo enzyme inhibition, new binding modes, and stereoisomer binding/epimerisation in solution. The interaction of a cyclobutanone analogue, a broad-spectrum MBL inhibitor, with SPM-1 was investigated. A combination of ^{1}H, ^{19}F, ^{13}C-NMR and crystallographic analyses reveal that cyclobutanone binding may mimic formation of the oxyanion tetrahedral intermediate in β-lactam hydrolysis. The susceptibility of avibactam, the first clinically useful non-β-lactam β-lactamase inhibitor, to MBL-catalysed hydrolysis was studied. The results reveal that avibactam is not an MBL inhibitor and a poor substrate of most members of all three clinically relevant subclasses of MBLs. In some cases, avibactam undergoes slow hydrolysis in a process different from that observed with serine β-lactamases.

Overall, the results illustrate the utility of NMR for studying dynamic aspects of enzyme catalysis and inhibitor binding.

Contents

Acknowledgments

I should like to thank Prof Christopher Schofield for believing in me, even before I have joined Oxford. His guidance and supervision have enormously helped me to develop as a scientist. I would like to thank him for giving me the opportunity to join Oxford and for encouraging me to work on various fascinating and rewarding projects. During my DPhil time, I have discovered a genuine enthusiasm for scientific research and a massive perseverance, which have undoubtedly been enhanced by his support and positive attitude. I learned from him how to supervise students and help them to achieve their potential. I am eternally grateful. Thanks also go to Prof Timothy Claridge for his fantastic guidance and for our endless discussions throughout my degree. He has been great at always finding time for his students and at passing on his amazing knowledge in simple ways. I felt that I belong to the NMR family. Thank you.

I owe a huge amount to Dr Ivanhoe Leung, for all his guidance and his confidence in my abilities. He introduced me to the NMR world and gave me hands-on instrument knowledge. My initial lack of technical ability was no obstacle to his patience and skill in showing me the ropes. Equal gratitude must be extended to Dr Rasheduzzaman Chowdhury, the crystal wizard, for introducing me to the PHD world. He has helped me in so many ways, each of which is sincerely appreciated. Thanks to Dr Jürgen Brem for introducing me to the fascinating MBL world. I would like to thank Dr Richard Hopkinson; our brainstorming sessions have uplifted my spirit and helped me to grow. His help and encouragement have extended beyond my project and I am truly grateful. Huge thanks go to the entire CJS group, for being excellent colleagues and friends. Special thanks go to Adam and Wendy for all their day-to-day help and advice. Massive thanks go to Kerstin Lippl, James Holt-Martyn, Dr Cyrille Awesome Thinnes, Dr Tzu-Lan Yeh, Dr Lucia Serran, and others, for prosperous collaborations. Individual contributions are listed in each chapter. Too many other people have contributed to my enjoyment to name. Tremendous thanks go to Suzana Markolovic, my twinnie, for cheering me up and for her non-stop support. Joanna, Becky, Bobojon, KD, Marina, Sarah, Louise, Mike, Marios, David, Duncan, Jake, Ollie, Thomas, Val, Jenny, Akane, and all CJS members have been great spirits and empowering souls to be around. Thanks to Richard, Tristan (Dr Smart III), Gareth (the grumpy guy), and Suzana for extensively proofreading this thesis and for their thorough comments. I owe you loads. Huge thanks to Dr Joshua Makepeace, my college advisor, for all his support and to my funding body, the Biochemical Society, for the Krebs Memorial Award; I could not have done it otherwise.

Astronomical thanks to my parents, the people who brought me to this world and helped me to overcome all of its obstacles with a smile on their face. No words can describe how grateful I am. You brought me up to more than I could be. My successes belong in a large part to you. I absolutely love you.

Finally, I would like to dedicate this thesis to my Godfather who passed away the day I had my interview to join Oxford. You have been my guardian angel.

Abbreviations

$[L]_0$	total ligand concentration
$[P]_0$	total protein concentration
Δ_{max}	maximal difference in chemical shift observed
Δ_{obs}	difference in chemical shift observed
2D	two-dimensional
2OG	2-oxoglutarate
2TY	2-tryptone/yeast extract
A	absorbance
***apo*-enzyme**	enzyme without bound ions
APS	ammonium persulphate
B_0	applied magnetic field
BcII	*Bacillus cereus* MBL
BL	β-lactamase
BLA	β-lactam antibiotic
BTFA	3-bromo-1,1,1-trifluoroacetone
CA	carbonic anhydrase
CBP	CREB binding protein
CCD	charge-coupled device
CD	circular dichroism
CODD	*C*-terminal oxygen dependent degradation domain
COSY	correlation spectroscopy
CphA	*Aeromonas hydrophila* AE036 carbapenemase
CPMG	Carr-Purcell-Meiboom-Gill
CTX-M	cefotaxime-resistant SBL from Munich
DBO	diazabicyclooctane
DHB	2,5-dihydroxybenzoic acid
DMSO	dimethyl sulphoxide
DNA	deoxyribonucleic acid
dNTP	deoxyribonucleotides
DSBH	double-stranded β-helix

DTT	dithiothreitol
EDTA	ethylenediaminetetraacetic acid
EPO	erythropoietin
ESI	electrospray ionisation
FEZ	*Fluoribacter (Legionella) gormanii* ATCC 33297(T) lactamase
FIH	factor inhibiting hypoxia-inducible factor
GIM	German imipenemase
Glc*N*Ac	*N*-acetyl glucoseamine
Glut	glucose transporter
HEPES	4-(2-hydroxyethyl)-1-piperazineethanesulfonic acid
HIF	hypoxia-inducible factor
HMBC	heteronuclear multiple bond correlation
HP	high purity
HPLC	high-performance liquid chromatography
HRE	hypoxia response element
HRV	human rhinovirus
HSQC	heteronuclear single quantum correlation
hyCODD	hydroxylated CODD
hyHIF	hydroxylated HIF
hyNODD	hydroxylated NODD
IC_{50}	half maximal inhibitory concentration
IDH	isocitrate dehydrogenase
IMP	imipenemase
IPTG	isopropyl β-D-1-thiogalactopyranoside
kbp	kilo-base pairs
k_{cat}	catalytic constant
K_D	dissociation constant
K_{Dapp}	apparent K_D
K_i	inhibition constant
K_M	Michaelis-Menten constant
KPC	*Klebsiella pneumoniae* carbapenemase
LC-MS	liquid chromatography-mass spectrometry

m/z	mass-to-charge ratio
MALDI	matrix assisted laser desorption/ionisation
MBL	metallo β-lactamase
MS	mass spectrometry
MS-MS	tandem mass spectrometry
Mur*N*Ac	*N*-acetylmuramic acid
NDM	New Delhi MBL
NMR	nuclear magnetic resonance spectroscopy
NODD	*N*-terminal oxygen dependent degradation domain
NOE	nuclear Overhauser effect
NOESY	nuclear Overhauser effect spectroscopy
NOG	*N*-oxalyl glycine
OD	optical density
ODD	oxygen-dependent degradation domain
OXA	oxacillin-resistant carbapenemase
P99	*Enterobacter cloacae* strain P99 β-lactamase
PBP	penicillin-binding protein
PCR	polymerase chain reaction
PDB	protein data bank
PHD	prolyl hydroxylase domain containing enzyme
PMSF	phenylmethanesulfonylfluoride
ppm	parts per million
PROJECT	periodic refocusing of *J* evolution by coherence transfer
pVHL	von Hippel-Lindau protein
qToF	quadruple time of flight
Rf	radio frequency
RNA	ribonucleic acid
rpm	rounds per minute
SBL	serine β-lactamase
SDS-PAGE	sodium dodecylsulfate polyacrylamide gel electrophoresis
SOC	super optimal broth catabolite repressing
SPM	São Paulo MBL

T_1	longitudinal relaxation time constant
T_2	transverse relaxation time constant
TCA	tricarboxylic acid
TEM	*Temoniera* lactamase
TEMED	tetramethylethylenediamine
TFA	trifluoroacetic acid
ToF	time of flight
Tris	tris(hydroxymethyl)aminomethane
Tris-D_{11}	deuterated Tris
trNOE	transferred nuclear Overhauser effect
UPLC	ultraperformance liquid chromatography
UV	ultra-violet
VCB	pVHL-Elongin C-Elongin B complex
VGEF	vascular endothelial growth factor
VIM	Verona integron-encoded MBL
Vis	visible
v_{max}	maximum velocity
WHO	world health organisation
wLOGSY	water-ligand observed gradient spectroscopy
wt	wildtype
δ_0	initial chemical shift
δ_{max}	maximal shift observed
δ_{obs}	chemical shift observed
λ	wavelength

List of Contributions from Others

Individual contributions are listed in each chapter. This list is meant to give a summary of the work done by others which contributed to the results described in this thesis.

- **Crystallography**: Dr Rasheduzzaman Chowdhury (Chapter 2, PHD2 and its clinical variants) and Dr Philip Hinchliffe (Dr James Spencer's group, Bristol) (Chapter 5, Y58C SPM-1 and Chapter 6, SPM-1.cyclobutanone complex).
- **Peptide Synthesis**: Kerstin Lippl (Chapter 2, taODD, eEF2 and Rbp1 peptides).
- **Protein Production**: Kerstin Lippl (Chapter 2, taPHD), Dr Rasheduzzaman Chowdhurry (Chapter 2, PHD2 clinical variants), and Dr Jürgen Brem (Chapter 6, Y152C SPM-1 and Chapter 7, CphA and VIM-4).
- **Assays**: Kerstin Lippl (Chapter 2, competitive hydroxylation assays), Dr Lucia Serran (Chapter 2, VCB fluorescence polarisation assay), Dr Tom McAllister (Chapter 3, fluorescence polarisation assay help), and Prof Jean-Marie Frère, Liège (Chapter 7, inhibition assays).
- **Chemical Synthesis**: Dr Cyrille Thinnes and James Holt-Martyn (Chapter 4, IOX4 and GSK1278863), Dr Marina Demetriades (Chapter 4, FG2216), Dr Klaus-Daniel Umland (Chapter 5, ML302 and ML302F), Dr Anna Rydzik (Chapter 5, isoquinoline), Dr Jarrod Johnson and Dr Anthony Krismanich (Dr Gary Dmitrienko's group, Waterloo) (Chapter 6, cyclobutanone analogue).
- **Biophysical Techniques**: Dr Jasmin Mecinovic (Chapter 3, MS analyses), Dr Ivanhoe Leung (Chapter 3, protein NMR), Dr Anne Makena (Chapter 5, CD analyses), and Dr Christian Damblon, Liège (Chapter 7, VIM-4-mediated product characterisation and Raman analyses).

Chapter 1. Introduction

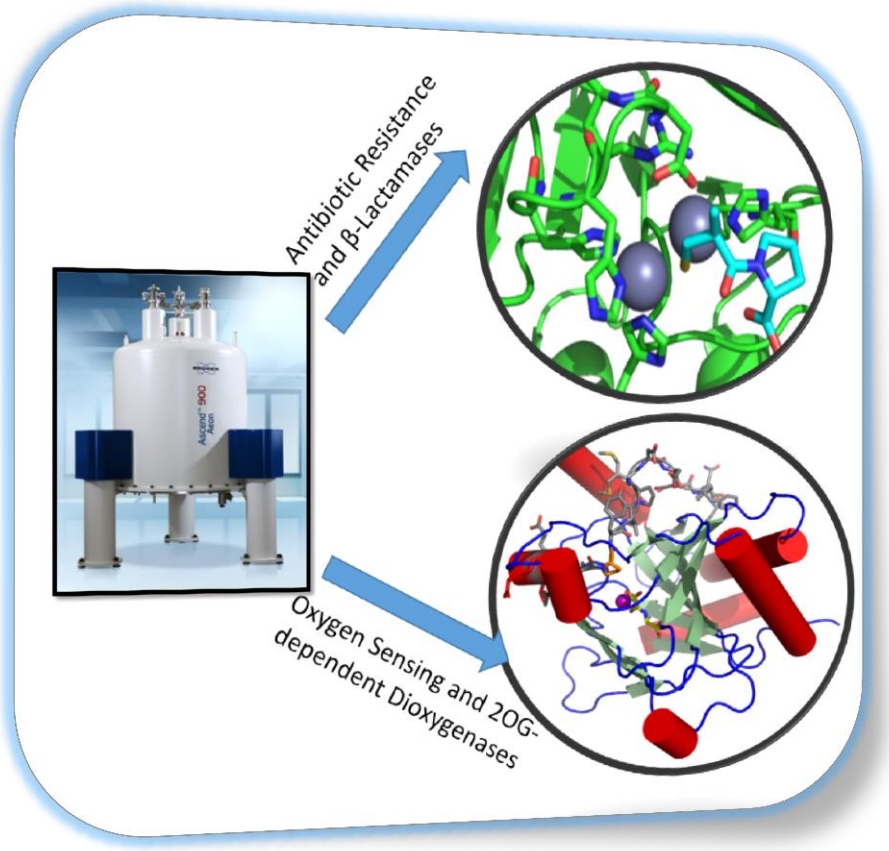

Chapter 1. Contents

1.1. Biological Systems Studied

The work described in this thesis principally focused on applying nuclear magnetic resonance spectroscopy (NMR) and other biophysical methods to probe the functions, mechanisms, structures, and inhibitory potential of two classes of metallo enzymes: the Fe(II)- and 2-oxoglutarate (2OG)-dependent dioxygenases, and the metallo β-lactamases. An introduction to each enzyme class is provided is given below.

1.1.1. Prolyl Hydroxylase Domains and Other 2-Oxoglutarate Dependent Dioxygenases

1.1.1.1. The Hypoxic Response

Dioxygen is essential to aerobic life. Limitations in the supply of adequate O_2 result in the state of hypoxia.[1] In humans and other higher animals, the chronic response to limiting oxygen availability involves the context-dependent upregulation of multiple genes including those encoding for erythropoietin (EPO), a protein hormone inducing red blood cell production, vascular endothelial growth factor (VEGF), and glucose transporter (GLUT1).[2] These responses work collectively to increase oxygen supply by stimulating angiogenesis, vasodilation, and erythropoiesis, whilst others increase anaerobic respiration by upregulating glycolysis.[3] The upregulation of expression in response to hypoxia is mediated by the α,β-heterodimeric hypoxia-inducible factors (HIFs).[4] Although the HIF-mediated response is not involved in acute hypoxic response and non-HIF processes are also involved in the cellular response to hypoxia, HIF is considered a 'master regulator' of the chronic hypoxic response in animals.[5] Under hypoxic conditions, HIF-α subunits accumulate in the nucleus and dimerise with HIF-β[6] enabling them to bind HIF-response elements (HREs) in DNA promoter regions (5'-G/ACGTG-3') that activate the transcription of selected genes.[7] HIF-α, but not HIF-β subunit of HIF, is regulated by O_2.[8] Under normoxia (*i.e.* non-limiting oxygen

levels), HIF-α is targeted for degradation *via* the ubiquitin-proteasome system by binding to the von Hippel-Lindau tumour suppressor protein (pVHL), which constitutes the substrate recognition component of an E3 ubiquitin complex **(Figure 1.1)**.[9] Therefore, in normoxic cells, HIF-α levels are normally low or not detected.[10] pVHL binding to HIF-α is strongly promoted by hydroxylation of proline residues in the HIF-α oxygen-dependent degradation domain (ODD) (Pro-402 and Pro-564 in HIF-1α, Pro-405 and Pro-531 in HIF-2α, and Pro-492 in HIF-3α) allowing for its ubiquitination and degradation by the proteasome.[11] HIF-α hydroxylation is mediated by a family of non-haem Fe(II)- and 2-oxoglutarate (2OG)-dependent prolyl-4-*trans*-hydroxylase domain proteins (PHD1-3).[12] (See our recent review).[13]

1.1.1.2. Cellular and Physiological Aspects

There are three forms of human HIF-α (HIF-1/2/3α) which have different, though sometimes overlapping, roles in upregulating different sets of HIF-target genes **(Figure 1.2)**. Although HIF-1α and HIF-2α are closely related, they play substantially non-redundant roles; the inactivation of either results in different phenotypes.[14] HIF-2α is more important in the regulation of renal EPO, whereas HIF-1α regulates expression of carbonic anhydrase and glycolysis-related genes, such as pyruvate dehydrogenase kinase.[15] The factors leading to different regulation of various HIF-target genes are not well understood. HIF-3α is the most distally related of the three human HIF-α isoforms and, in some splicing arrangements, encodes for a polypeptide that antagonises HRE-dependent gene expression.[16]

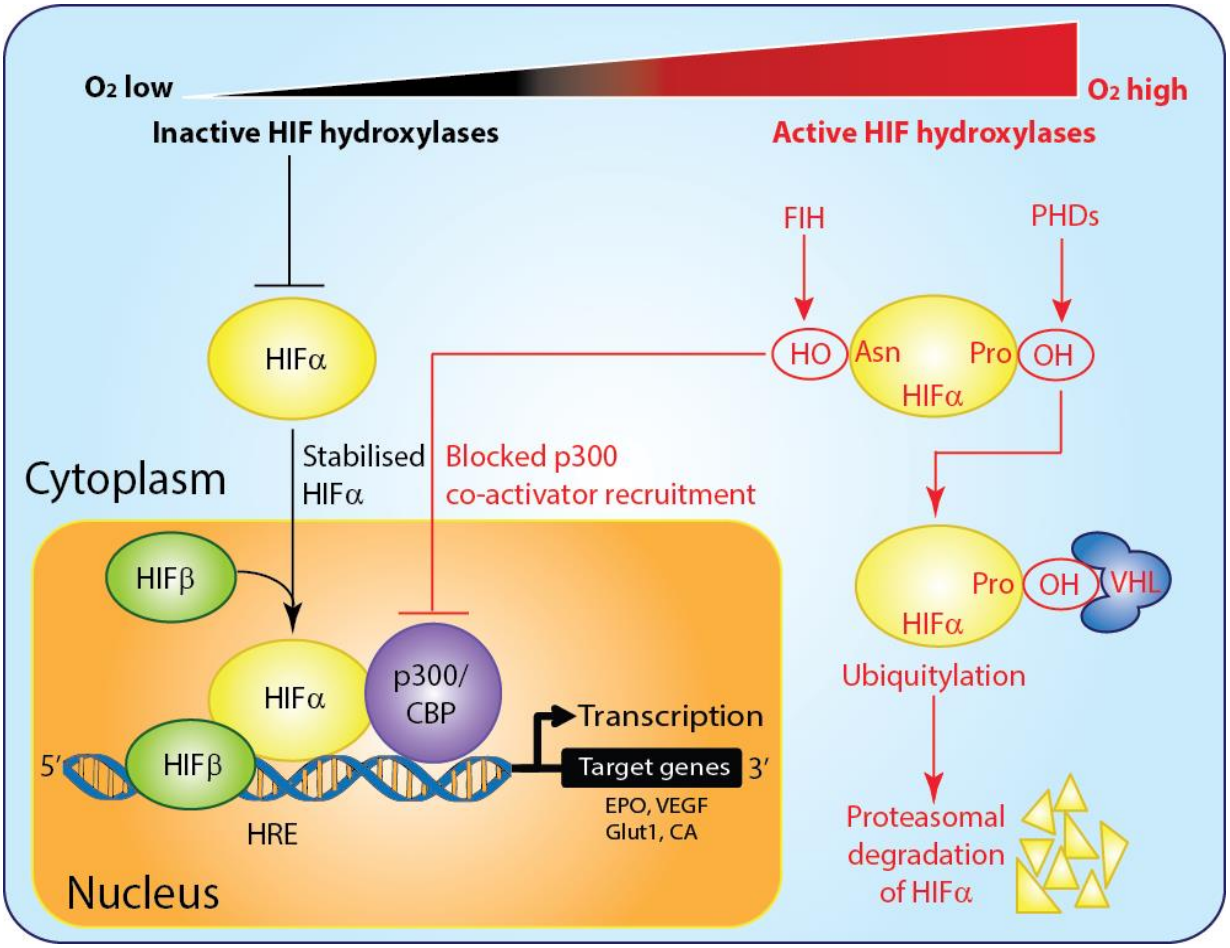

Figure 1.1. Outline cellular response to hypoxia and normoxia. *A simplified scheme depicting the cellular response to hypoxia and normoxia in animals. PHD: prolyl hydroxylase domain, HIF: hypoxia inducible factor, FIH: factor inhibiting HIF, VHL: von Hippel-Lindau protein, CBP: CREB binding protein, HRE: hypoxia response element, EPO: erythropoietin, VEGF: vascular endothelial growth factor, Glut1: glucose transporter, CA: carbonic anhydrase.*

There are three human PHD isoforms which are involved in oxygen-dependent HIF hydroxylation. A fourth putative human PHD, PHD4, has also been reported, but PHD4 possesses a transmembrane domain which is *N*-glycosylated and is bound to the endoplasmic reticulum membrane (with its catalytic domain inside the lumen), suggesting it is unlikely to be involved in the HIF-mediated response even though its overexpression in cultured neuroblastoma cells reduced HIF-α levels.[17] In terms of localisation, at least in some cells,

PHD1 is exclusively observed in the nucleus and PHD2 is more predominantly found in the cytoplasm, though nuclear activity for it has been reported.[18] PHD3 is reported to be homogeneously distributed in both cellular compartments.[19] Based on mRNA expression patterns, PHD2 seems to be ubiquitously expressed, whereas PHD3 is more dominant in the heart and PHD1 in the testes.[20] Gene-knockout studies suggest PHD2 is the most important PHD isoform in most human tissues.[20-21] The *C*-terminally positioned catalytic domains of PHD1-3 are highly conserved; however, the *N*-terminal regions differ substantially; PHD2 has an *N*-terminal MYND-type zinc finger domain, PHD3 lacks a significant *N*-terminus, and PHD1 has a uncharacterised, apparently disordered domain.[22] PHD1-2 catalyse hydroxylation of both the *C*-terminal ODD (CODD) and the *N*-terminal ODD (NODD) of HIF-α, whereas PHD3 preferentially hydroxylates CODD, although it can catalyse hydroxylation of NODD on prolonged incubation. There is some preliminary evidence that PHD3 is biased to the regulation of HIF-2α, whilst PHD2 preferentially interacts with HIF-1α.[12] PHD2 is substantially the most abundant HIF prolyl hydroxylase in normoxia and its suppression has dominant effects in raising levels of HIF-1α in normoxic cells.[18] PHD3 levels are strongly induced in hypoxia (in a HIF-dependent manner), suggesting the presence of a negative feedback mechanism in the HIF system.[12] This differential behaviour might be beneficial from a therapeutic perspective as PHD2 inhibition might be predicted to broadly activate HIF response under resting conditions, whilst PHD3 inhibition might selectively augment the response to hypoxia in certain tissues (*e.g.* the heart).[20] The following sections focus on summarising the biochemical, mechanistic, and structural properties of PHD2, the most studied of the PHDs.

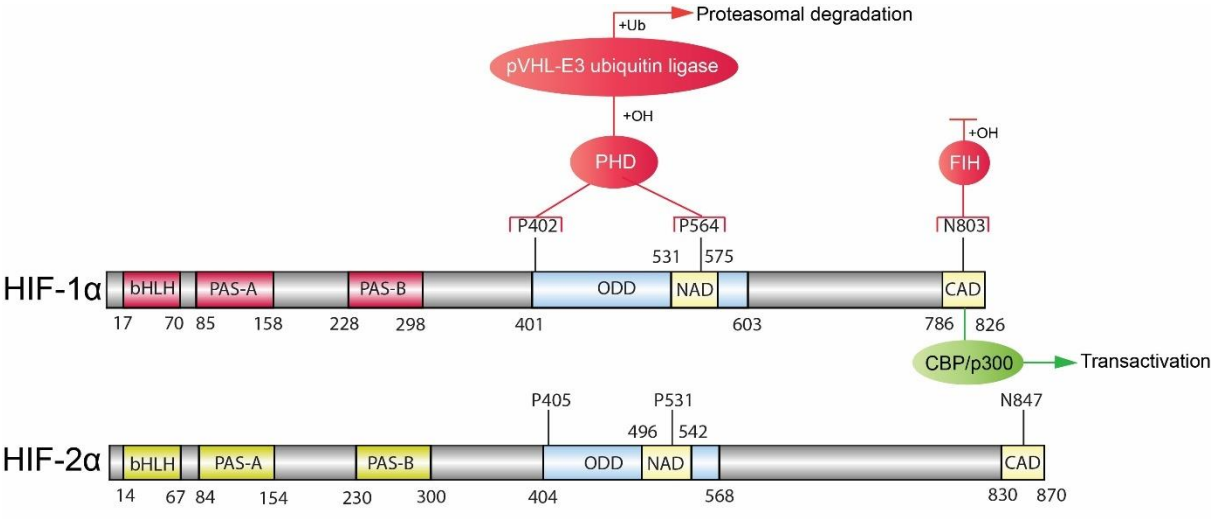

Figure 1.2. Outline scheme of HIF-1 and HIF-2. *The figure highlights the similarities between HIF-1 and HIF-2.*

1.1.1.3. Functional and Catalytic Aspects

An extensive body of evidence arising from studies with isolated proteins, cellular, and animal work, involving biochemistry, genetics, and pharmaceutical methods, supports the proposal that PHD-catalysed HIF-α hydroxylation is limited by oxygen availability. The PHDs are well adapted to act as oxygen sensors; PHD2, the most important of the human PHDs, reacts unusually slowly with dioxygen[23] which is partly attributed to the relatively tight binding of the iron-ligated water to Asp-315$_{PHD2}$, one of the main metal-binding residues.[24] The PHDs belong to a family of structurally related non-haem Fe(II)- and 2OG-dependent-dioxygenases which contain a 'distorted' double-stranded β-helix (DSBH or jelly roll) structure that supports iron and 2OG-binding residues. The DSBH fold is made of eight β-strands which occur in an antiparallel manner and fold in a helical manner to form two β-sheets (a major β-sheet made of β-strands I, VIII, III, and VI, and a minor β-sheet made of β-sheets II, VII, IV, and V).[25] In the case of PHD2, a catalytic triad of His-313$_{PHD2}$, Asp-315$_{PHD2}$, and His-374$_{PHD2}$ residues coordinates the Fe(II) ion in the active site (PDB ID:

2G1M). The 2OG-binding site is adjacent to that of Fe(II), and is buried within the major and minor β-sheets of the DSBH. 2OG coordinates the active site metal *via* one of its carboxylate oxygens and its amide α-carbonyl oxygen and is stabilised by ionic interactions between its carboxylate and Arg-383$_{PHD2}$ **(Figure 1.3)**.[26]

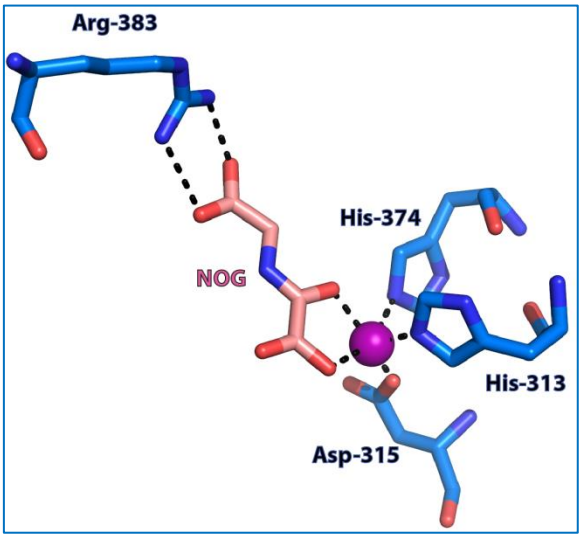

Figure 1.3. Active site view of PHD2 highlighting metal-binding residues and *N*-oxalyl glycine (NOG), a 2OG analogue, coordination (PDB ID: 8HQR).[24]

During catalysis, the PHDs catalyse the post-translational modification of HIF-1α by hydroxylating Pro-564 residue of CODD and/or Pro-402 residue of NODD. The proposed consensus mechanism for 2OG oxygenases involves the incorporation of one oxygen atom from molecular oxygen to the HIF substrate and of the other to carbon dioxide; this hydroxylation event is coupled to the oxidation of 2OG into succinate.[27] The proposed mechanism is an ordered sequential process in which 2OG, then substrate, and then oxygen binding occurs. After substrate hydroxylation, the product leaves the active site before release of succinate. 2OG coordinates to the metal centre in a bidentate manner. The substrate binds in close proximity to the active site without coordinating the metal ion directly. Binding of the substrate is proposed to displace a third water ligand from the active site Fe(II), leaving a vacant coordination site for oxygen to bind. An oxidative decarboxylation reaction then

generates CO_2, succinate, and a highly oxidising Fe(IV)-oxo intermediate, which reacts with the substrate, likely (at least, in some cases) *via* a radical mechanism to insert an oxygen into the nearest substrate C-H bond. It is proposed that CO_2 release from the active site occurs after reaction of the iron-bound-2OG and dioxygen, but prior to substrate hydroxylation, in part because of the electrostatic interaction between the non-coordinating C-1 carboxylate of 2OG and the polar Arg-252_{PHD2} residue.[24] During the course of the cycle, the reactive Fe(IV) species is reduced back to the Fe(III), and subsequently the Fe(II) oxidation state **(Figure 1.4)**.

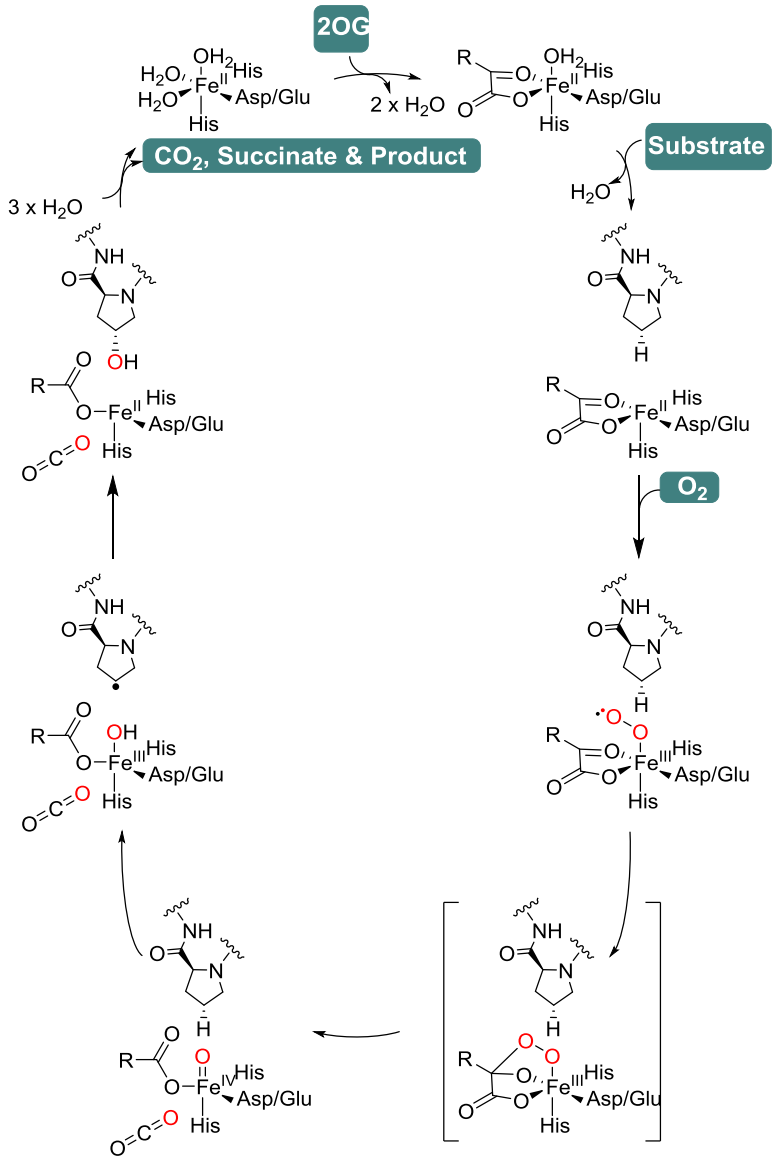

Figure 1.4. Outline consensus mechanism for catalysis by 2OG-dependent dioxygenases.

1.1.1.4. Structural Aspects of the PHDs

Structural studies using crystallography and NMR have revealed that the importance of a mobile loop in PHD2 (residues 237-254) during CODD hydroxylation. Upon CODD binding, the loop folds over the active site to entrap the substrate, stabilising the PHD2.Fe(II).2OG.CODD complex (for structures, see PDB ID: 3HQR[24] and PDB ID: 2G1M[26]) **(Figure 1.5)**. The hydroxylation sites of both HIF-1α NODD and CODD occur within a conserved Leu-X-X-Ala-Leu-Pro motif.[28] Leu-$562_{HIF\text{-}1\alpha}$ and Ala-$563_{HIF\text{-}1\alpha}$ of the LXXLAP motif form hydrophobic interactions with PHD2.[24] Point- and deletion-mutagenesis studies suggest that Leu-$574_{HIF\text{-}1\alpha}$, 10 residues downstream of Pro-564 in HIF-1α, is required for recruiting PHD2 to HIF-1α CODD (but not NODD) prolyl hydroxylation and, consequently, pVHL binding.[29]

The conformation of the prolyl rings plays crucial roles in both the binding of non-hydroxylated HIF-α of the PHDs and the binding of hydroxylated HIF-α to pVHL. The target HIF-1α proline adopts the C^4-*endo* conformation when bound to PHD2; the C^4-*endo* conformation is required for reaction of the [Fe^{IV}=O] intermediate with the C^4-*trans* prolyl hydrogen atom.[30] However, in *trans*-4-hydroxyproline rings, a stereoelectronic effect arising from the N–C^5–C^4–O gauche effect biases the pyrrolidine ring towards the C^4-*exo* conformation in order to maximise delocalisation of electron density through the σ-bond framework.[24, 30] This C^4-*trans*-conformation of the hydroxylated prolyl residues of HIF-1α is important for pVHL binding, which has a 1,000-fold higher affinity to hydroxylated CODD HIF-1α than to non-hydroxylated CODD, supporting the proposal that post-translational hydroxylation accounts for pVHL selectivity.[31] The hydroxylated Pro-402 and Pro-564 HIF-1α bind independently to the same pocket in pVHL, thereby signalling for proteolysis by hydroxylation of either NODD or CODD.[28]

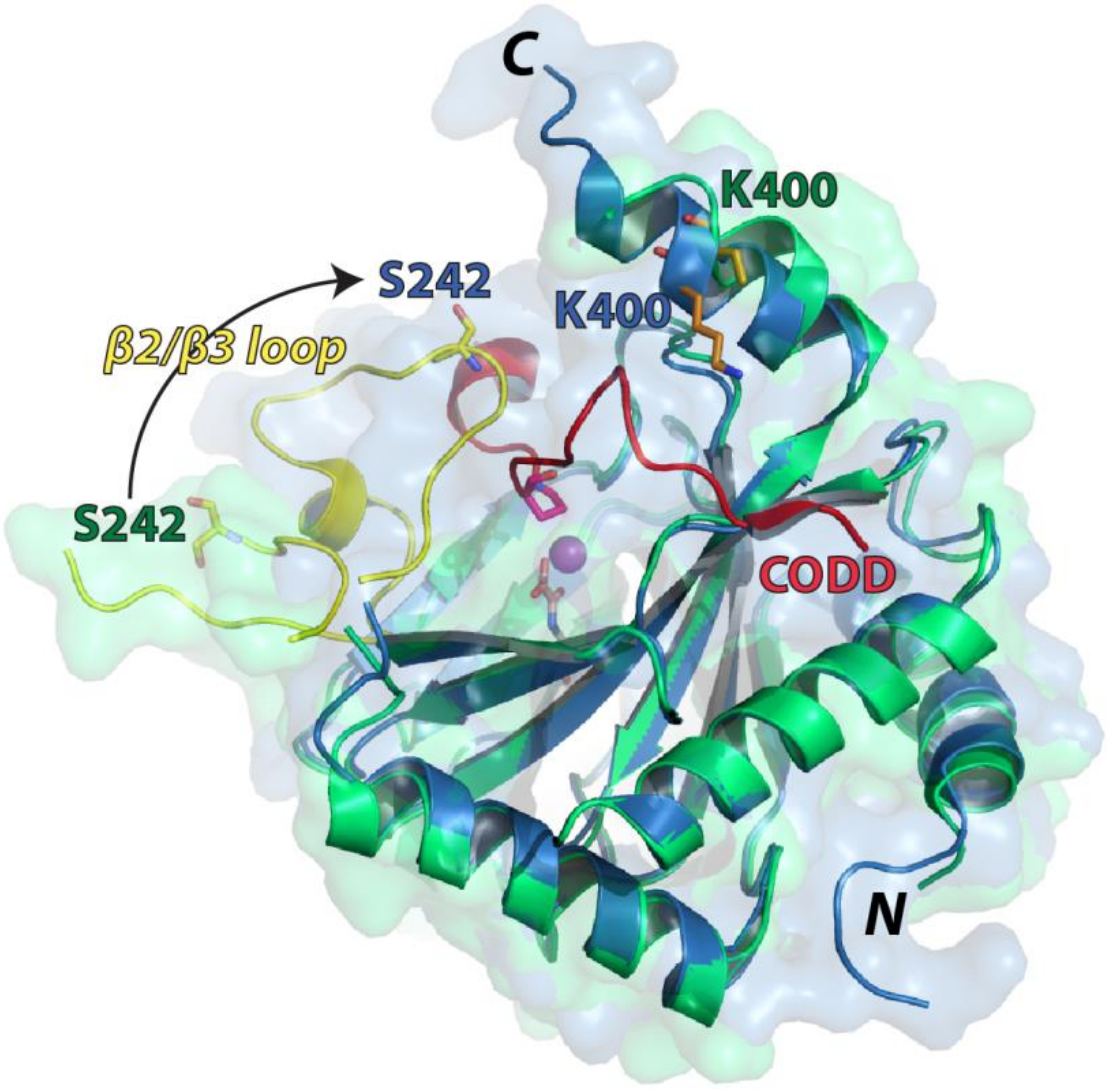

Figure 1.5. View from a crystal structure of PHD2 (green, PDB ID: 2G1M) overlaid with PHD2.CODD complex (blue, PDB ID: 3HQR). *The PHD2 residues 237-254, which adopt a finger-like β2β3 conformation in the PHD2 crystal form (PDB ID: 2G1M),*[32] *fold to adopt a loop conformation in the PHD2.CODD structure entirely enclosing the Pro-564$_{HIF\text{-}1\alpha}$ region and the PHD2 active site in a substantial induced fit mechanism, with the Cα position of Ser-242$_{PHD2}$ differing by 18 Å between the two structures. Additionally, Cα position of Lys-400$_{PHD2}$ in the C-terminal of α4 helix differs by 2.5 Å between both structures.*[13]

1.1.2. Penicillin-Binding Proteins (PBPs) and β-Lactamases

1.1.2.1. Antibiotic Resistance

Antibiotic resistance is a growing major global health threat.[33] The World Health Organisation (WHO) report on antimicrobial resistance suggests that a post-antibiotic era in which common infections and minor injuries can kill is a very real possibility in the 21st century.[34] Hospital-acquired infections account for a growing rate of mortality and represent an increasing financial burden. It is estimated that within the UK, 8.2% of hospitalised patients contract a hospital-acquired infection costing the UK National Health Service > £1 billion per year.[35] β-Lactams (*e.g.* penicillins, cephalosporins, and carbapenems) remain the most important class of antibiotics, representing 60%[36] of all antibiotics used **(Figure 1.6)**. Today, however, the use of these life-saving β-lactam antibiotics (BLAs) is threatened by antimicrobial resistance.[37]

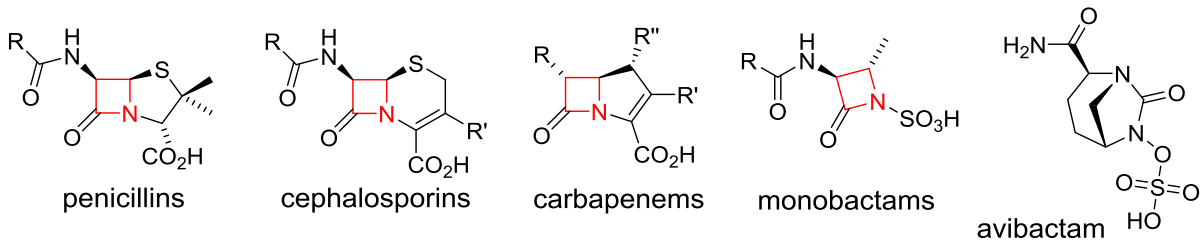

Figure 1.6. Major classes of clinically used β-lactams and avibactam. *The β-lactam core is highlighted in red.*

1.1.2.2. Peptidoglycan Cross-Linking and Penicillin-Binding Proteins

BLAs act as antibacterials by inhibiting peptidoglycan cross-linking in bacterial cell walls. Peptidoglycan is a highly cross-linked polymer composed of glycan strands with peptide cross-links. Peptidoglycan is unique to bacteria and its presence is essential for maintaining the structural integrity of the cell; it constitutes an excellent target for selective toxicity. The glycan strands of peptidoglycans consist of alternating units of two amino sugars, *N*-acetyl glucosamine (Glc*N*Ac) and *N*-acetyl muramic acid (Mur*N*Ac), which are

linked by β-(1,4)-glycosidic bonds. A peptide stem is attached to each Mur*N*Ac unit and forms a cross-link with the peptide stem of an adjacent glycan unit. The peptide side chains are linked together by extensive cross-linking reactions catalysed by penicillin-binding proteins (PBPs). PBPs react with the D-Ala-D-Ala terminus of a pentapeptide *via* a nucleophilic active site serine residue, forming a Ser-D-Ala acyl-enzyme intermediate, with release of terminal D-Ala. The carbonyl carbon of the sub-terminal D-Ala is then attacked by the side chain of an amine donor to cleave the ester linkage of the acyl-enzyme and form a cross-linking peptide amide bond **(Figure 1.7)**.[38]

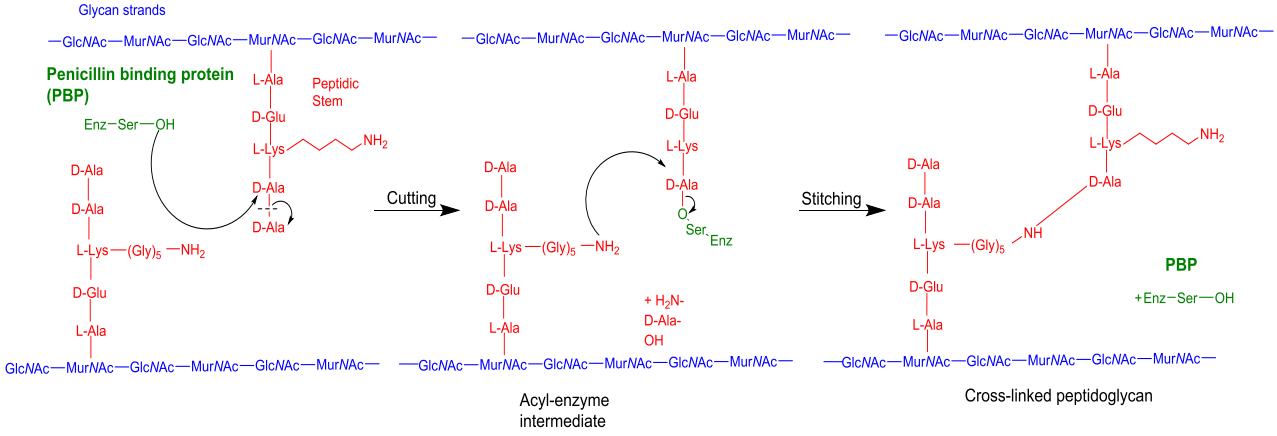

Figure 1.7. Outline peptidoglycan cross-linking in a Gram-positive bacterial cell wall.

1.1.2.3. β-Lactam Mode of Action

BLAs are characterised by the presence of a four-membered β-lactam which is proposed to resemble a strained conformation of the terminal D-Ala-D-Ala unit in the substrate. BLAs bind in the active site of the transpeptidase enzymes where they form an acyl-enzyme complex with the active site serine.[38a] This acyl-enzyme complex is sterically blocked for attack by the pentapeptide nucleophilic residue and hence, the covalently bound β-lactam is a long lived inhibitor of PBPs blocking peptidoglycan cross-linking. BLAs side chains have been optimised to achieve better activities.[39] (See our recent review).[40]

1.1.2.4. Lactamases and their Mode of Action

Whilst BLAs remain extremely important antibacterials, many bacteria have evolved efficient resistance mechanisms. These include PBP mutations that lower efficient binding of BLAs, and the production and modification of porins and efflux pumps to export BLAs.[41] The most important mechanism of resistance in Gram-negative bacteria is probably the production of β-lactamases (BLs), which catalyse β-lactam hydrolysis.[42] According to the Ambler classification, β-lactamases can be subdivided into four classes: class A (penicillinases), class B (carbapenemases), class C (cephalosporinases), and class D (oxacillinases) based on structural and mechanistic characteristics.[43]

Class A, C, and D are serine-β-lactamases (SBLs) which use an active-site nucleophilic serine residue to catalyse the hydrolysis of the β-lactam ring **(Figure 1.8A)**. Similar to the PBPs, SBLs have an active site nucleophilic serine residue **(Figure 1.8B)**. However, the interaction of a β-lactam antibiotic substrate with an SBL leads to the formation of an unstable acyl-enzyme complex susceptible to fast hydrolysis.[44]

Class B are metallo β-lactamases (MBLs), which use zinc ions in their active site to hydrolyse the β-lactam ring **(Figure 1.8D)**.[45] There are three subclasses of the class B MBLs, B1-B3, which are distinguished by variations to their conserved αββα MBL core fold and in their metal ion usage. The B1 and B3 MBLs use two Zn(II) ions and the B2 enzymes use only one Zn(II) ion in catalysis. The B2 enzymes are inhibited by binding a second Zn(II) ion. The B1 MBLs are presently the largest group and, probably, the most clinically relevant. [43, 46] See **Table 1.1** for the differences and similarities between different subclasses of Class B MBLs.

The two zinc binding sites of the B1 MBLs are termed Zn1 and Zn2. Using the standard class B β-lactamase (BBL) numbering,[47] the Zn1 is coordinated in a tetrahedral

geometry by three histidine ligands (His116, His118 and His196) and a bridging water/hydroxide ion (Wat1) and is also known as the 3H site. The Zn2, DCH, site involves a trigonal bipyramidal coordination with the Asp120, Cys221, and His263 metal binding ligands, Wat1, and an additional apical water molecule (Wat2).[38b] The β-lactam is proposed to bind at the active site metal centre, with its carbonyl oxygen interacting with Zn1. Zn2 coordinates the carboxyl group of the five- or six-membered ring fused to the β-lactam.[48]

Hydrolysis of the β-lactam is believed to occur *via* nucleophilic attack of a hydroxide ion onto the carbonyl carbon of the β-lactam, followed by C-N bond cleavage. The Zn ions are proposed to coordinate the nucleophilic hydroxide, lowering the pK_a of the bound water molecule.[46] Nucleophilic attack by the hydroxide ion bound to Zn1 and Zn2 leads to the formation of a tetrahedral intermediate. Zn1 has been proposed to act as a Lewis acid that coordinates the β-lactam carbonyl oxygen and polarises the carbonyl bond to facilitate nucleophilic attack by the metal-bound hydroxide ion **(Figure 1.8C)**.[49] Zn2 has been proposed to be more important in substrate binding, C-N bond cleavage, and intermediate stabilisation.[46] Breakdown and cleavage of the lactam derived C-N bond has been proposed to occur either following lactam nitrogen protonation or without initial nitrogen protonation, the latter leading to the accumulation of an anionic nitrogen intermediate whose protonation can be rate-limiting.[50] The protonation of the anionic nitrogen is proposed to precede the release of the hydrolysed product and the regeneration of the active enzyme. The source of the proton is suggested to be either a water molecule bound to Zn2 in the *apo*-enzyme, bulk water entering the active site, or a proton from the carboxylic acid moiety formed upon β-lactam hydrolysis.[51] Monobactams are not hydrolysed by MBLs, possibly because they bind with their sulfonate group between Zn sites, with consequent displacement of the catalytic hydroxide.[52]

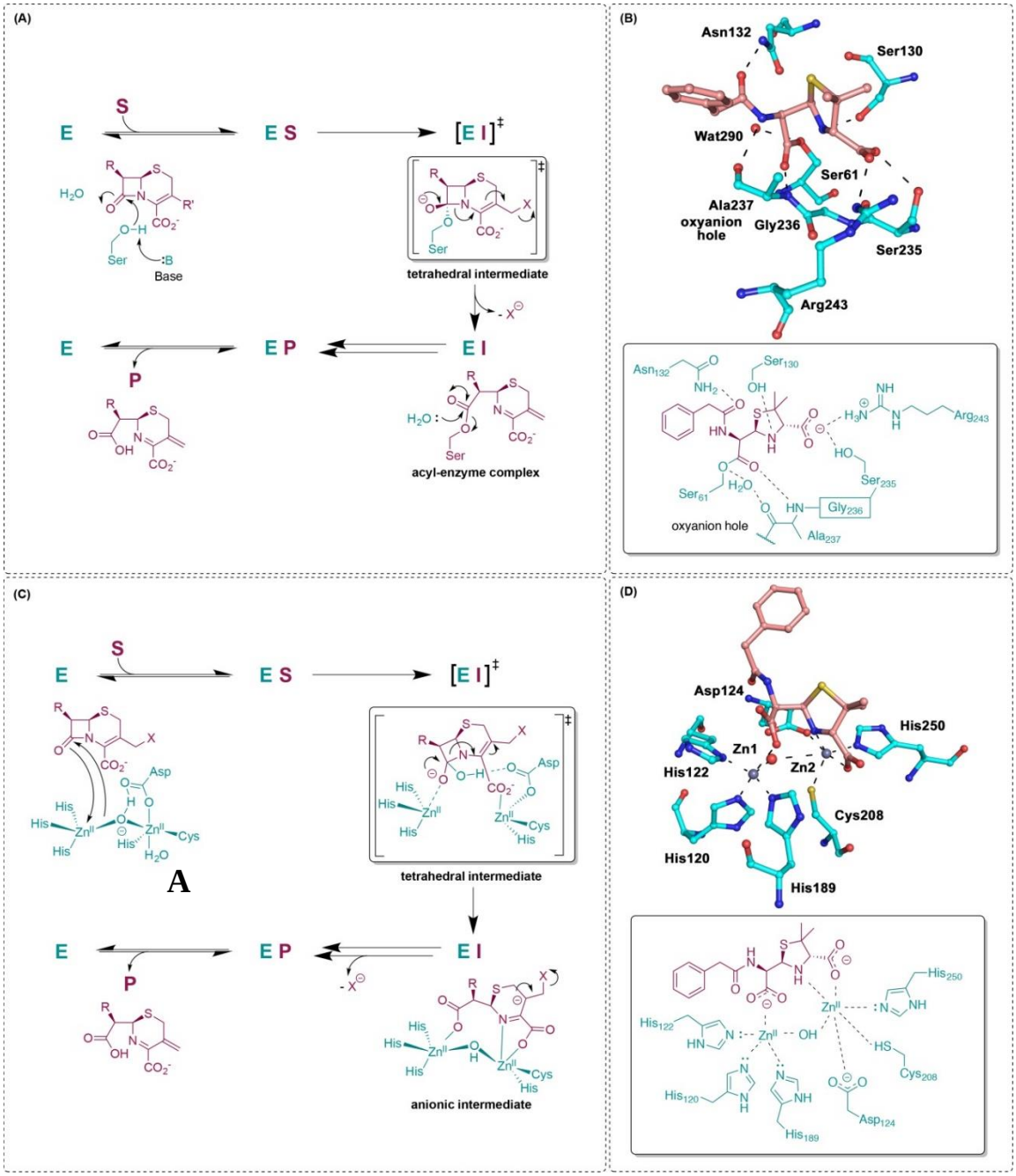

Figure 1.8. Outline mechanisms of action of (A) the serine and (C) the metallo-β-lactamases. ***(A)*** *Class A, C, and D are serine-β-lactamases (SBLs) which employ a nucleophilic active-site serine to catalyse hydrolysis of the amide bond of the β-lactam ring.* ***(C)*** *Class B are metallo β-lactamases (MBLs) which use Zn ions in their active site.*[53] *Note that in each case the mechanism proceeds via a tetrahedral intermediate.* ***(B)*** *Active site view from a crystal structure of TEM-1 (cyan), a Class A SBL, as acylated by penicillin G (pink) (PDB ID: 1FQG).*[54] ***(D)*** *Active site view from a crystal structure of NDM-1 (cyan) complexed with hydrolysed penicillin G (pink) (PDB ID: 4EYF).*[55] *Figure used with permission from Future Science Publishing Group.*[40]

Table 1.1. Table highlighting the similarities and differences between different subclasses of Class B metallo β-lactamases.[56]

	B1	B2	B3
Metal content and enzyme activity	Maximum activity as di-zinc species	Mostly active as mono-zinc species	Maximum activity as di-zinc species*
Zn1 site	Tetrahedral coordination: His116, His196, His196, and a water molecule (3H site)	His116 is replaced by Asn116 (with respect to B1 and B3 MBLs)	Conserved 3H site**
Zn2 site	Trigonal pyramidal coordination: Asp120, Cys221, His263, and two water molecules (DCH site)	Mostly conserved DCH site	Zn2 is bound to Asp120, His121, and His263 (DHH site). Cys221 is replaced by Ser221 (with respect to B1 and B2 MBLs)
Functional similarity	Similar mechanism to B3 MBLs	Different mechanism to B1/B3 MBLs	Similar mechanism to B1 MBLs
Substrate profile	Broad-spectrum activity (except monobactams)	Mainly carbapenemases	Broad-spectrum activity (except monobactams)
Oligomerisation state	Mostly monomers	Mostly monomers	Mostly monomers***

All residue numbers are given according to the standard BBL numbering.[47]

**GOB MBL, a B3 MBL, is mostly active as a mono-zinc species.[57]*

***His116 of the 3H site is replaced by Gln116 in GOB-type MBLs.[57]*

****L1, a B3 MBL from Stenotrophomonas maltophilia, is mostly a homotetramer.[58]*

1.1.2.5. Challenges in the Antimicrobial Resistance Field

Inhibitors of Class A β-lactamases, *e.g.* clavulanic acid,[59] have been successful in extending the lifetime of the penicillins. The novel non-β-lactam-containing avibactam has been recently reported as a broad spectrum serine β-lactamase inhibitor.[60] However, MBLs are not inhibited by any of the currently available SBL inhibitors.[61] MBLs have broad-spectrum activity and can catalyse the hydrolysis of almost all β-lactams except monobactams.[62] A major challenge in developing clinically useful MBL inhibitors is achieving the requisite breadth of selectivity for the different types of clinically relevant

MBLs, which are mostly, but not exclusively, B1 subclass MBLs [*e.g.* New Delhi MBLs (NDMs),[63] Imipenemases (IMPs), and Verona-encoded Integron MBLs (VIMs)[64]], which differ in mobile regions surrounding their active sites.[56] Therefore, novel clinically-relevant MBL inhibitors should have a broad-spectrum of activity, should not interfere with human enzymes possessing the same MBL αβ/βα fold (of which there are many),[65] and should ideally be resistant to common mechanisms of bacterial resistance. Accordingly, unravelling the biophysical and biochemical properties of MBLs (and their mode(s) of action) is of major interest.

1.2. Biological Applications of NMR Spectroscopy

NMR is one of the most powerful biophysical techniques to study proteins and their interactions/reactions in solution. NMR relies on the magnetic properties of atomic nuclei to inform on their chemical environments; using appropriate methods, information on the connectivity of nuclei, as well as their spatial proximity to distally-bonded atoms can be attained.[66] Unlike other powerful biophysical methods, *e.g.* X-ray crystallography and electron microscopy, NMR enables analysis of proteins in aqueous solutions. NMR can thus provide important information on protein structure, dynamics, interactions with binding partners, and catalytic activities under physiologically-relevant conditions. In general, protein function(s) depends on interactions with ligands, such as substrates, metal ions, and other regulatory binding partners.[67] Understanding the biological functions of proteins therefore usually requires a deep knowledge of these protein-ligand recognition events at the atomic level. Moreover, information on protein structure and dynamics and knowledge of ligand binding modes/affinities are essential for efficient structure-guided drug design.[68]

The main objective of the work reported in this thesis was to apply NMR spectroscopy techniques to study different aspects of 2OG-dependent dioxygenases and β-

lactamase-mediated antibacterial resistance. Both systems are interesting from an NMR perspective because of their dynamic structural elements involved in catalysis and ligand interactions. The work includes mechanistic studies, protein-ligand interaction studies, and method development for inhibitor discovery. A variety of NMR-based biophysical methods are available and enable characterising protein-ligand interactions.[69] These methods adopt either a ligand-observe NMR approach, or a protein-observe NMR approach, as discussed hereafter.

1.2.1. Ligand-Observe NMR Methods

Ligand-observe NMR methods aim to identify and characterise the binding activity of ligands to their receptor proteins by observing the changes of the ligand molecule upon its interaction with the protein. Unlike other methods (see below) ligand-observe methods are not necessarily limited by protein size and do not require isotopic protein labelling; however, as signals for the protein are not observed, direct analysis of the ligand binding site is not afforded. Despite this limitation, indirect information on the binding site may be attained by competition experiments employing 'reporter' ligands, which are known to bind at particular sites. Several NMR parameters, which can be easily obtained readily with high sensitivity, serve as a gauge for the binding activity of a ligand to a receptor; these include changes in chemical-shifts, nuclear Overhauser effects (NOEs), diffusion constants, and relaxation times.[70] These approaches are often complementary and have different advantages.

1.2.1.1. Protein-Ligand Binding Equilibria

The binding affinity of a ligand to its protein receptor may be defined by its dissociation constant (K_D). K_D equates to the free (unbound) ligand concentration [L] in solution when half of the total protein receptor sites are saturated by the ligand. In its simplest form, the binding of small-molecule ligands to proteins follows a bimolecular association

interaction with second-order kinetics [**equation (1.1)**] whereby the association of a ligand (L) to a receptor protein (P) is in equilibrium with the complex (PL) with k_{on} and k_{off} (these being the association and dissociation rate constant, respectively). The bimolecular rate constant (k_{on}) reflects the probability of the free protein and ligand forming the PL complex. The unimolecular rate constant (k_{off}) is inversely proportional to the lifetime of the bound PL complex before its dissociation.[71]

$$P + L \underset{k_{off}}{\overset{k_{on}}{\rightleftharpoons}} PL \qquad \textbf{(1.1)}$$

K_D is then given by **equation (1.2)**:

$$K_D = \frac{[P][L]}{[PL]} = \frac{k_{off}}{k_{on}} \qquad \textbf{(1.2)}$$

Estimates for k_{off} can be obtained by assuming diffusion-controlled association (on-rate) of 10^7 $s^{-1}.M^{-1}$ even though k_{on} can vary (from less than 10^4 to 10^{11}).[72] Estimates of k_{off} are important for the interpretation of NMR binding experiments in which different conditions for the exchange between the free and bound state of the ligand apply. In the case of a fast exchange on the chemical-shift time scale, k_{off} is much larger than $\Delta\omega$ ($k_{off} >> \Delta\omega$) where $\Delta\omega$ is the chemical shift difference in $rad.s^{-1}$ of signals in the bound and free state, such that $\Delta\omega = 2\pi\Delta\nu$ (where $\Delta\nu$ is the chemical shift difference of the signals in Hz). In the case of an intermediate exchange on the NMR time scale, $k_{off} \approx \Delta\omega$. For a slow exchange on the chemical-shift time scale, k_{off} is much smaller than $\Delta\omega$ ($k_{off} << \Delta\omega$). At faster k_{off} values, signals appear at a position equivalent to the weighted-average of the chemicals shifts of the bound and free ligand, whilst at slower k_{off} values, two separate signals for a ligand-bound and a ligand-free state will appear.[73] **Equation (1.2)** can be transformed into a quadratic

equation (1.3) where [PL] is the concentration of protein ligand complex, and $[P]_0$ and $[L]_0$ are the total concentrations of protein and ligand, respectively.

$$[PL] = \frac{(K_D + [P]_0 + [L]_0) - \sqrt{(K_D + [P]_0 + [L]_0)^2 - 4[P]_0[L]_0}}{2} \quad \textbf{(1.3)}$$

At a given $[P]_0$, $[L]_0$, and K_D, the actual [PL] can be calculated.[71]

1.2.1.2. ^{1}H NMR experiments

1.2.1.2.1. Direct Observation

^{1}H NMR is usually most useful for ligand binding studies when the difference in size between the ligand and its receptor protein is large. In this situation, the free and bound ligand populations exhibit distinct NMR parameters that can be differentiated. A free (small-molecule) ligand, with a short rotational correlation time, tumbles fast in solution; however, when it becomes part of a larger protein-ligand complex, it tumbles slower with a larger rotational correlation time and enhanced transverse relaxation rate R_2 (and hence, shorter transverse relaxation time T_2). These differences lead to changes in chemical shifts, peak intensities, linewidths, and diffusion coefficients for the observed ligand[74] **(Figure 1.9)**. One drawback of direct ligand observation by ^{1}H NMR is that it is mostly suitable for K_D measurements of relatively weak binders (K_D ranges from high μM to mM)[74] because factors such as protein background may mask the ligand signal when the ligand and protein concentrations are similar (a condition required for strong binders whose off-rate is small).

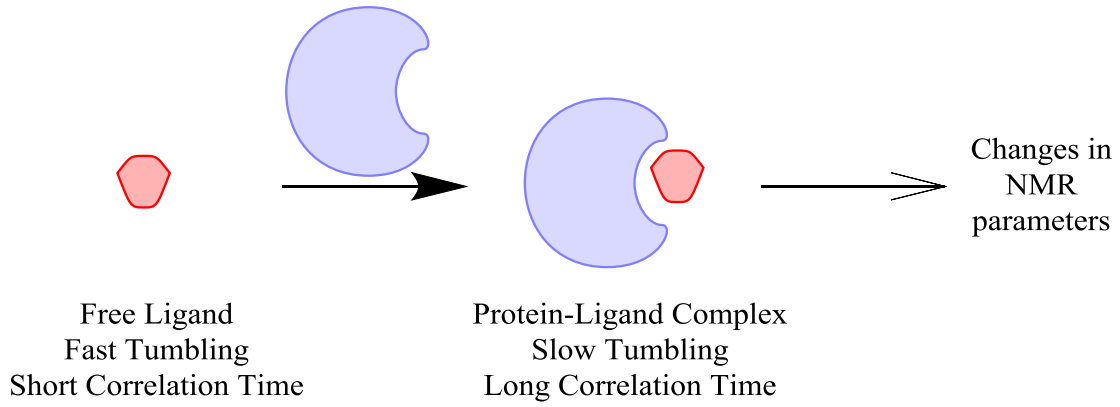

Figure 1.9. Scheme illustrating the principle of direct ligand observation in NMR screening.

1.2.1.2.2. Competition Ligand Screening

Competitive ligand binding experiments are alternatives to direct ligand observation. Perturbation in the binding of the ligand of interest upon addition of a ligand with a known binding site and K_D value indicates that the two compete for the same binding site on the protein (assuming no allosteric regulation). Therefore, monitoring of either the ligand of interest or the competitor may be applied to determine binding parameters **(Figure 1.10)**.[75]

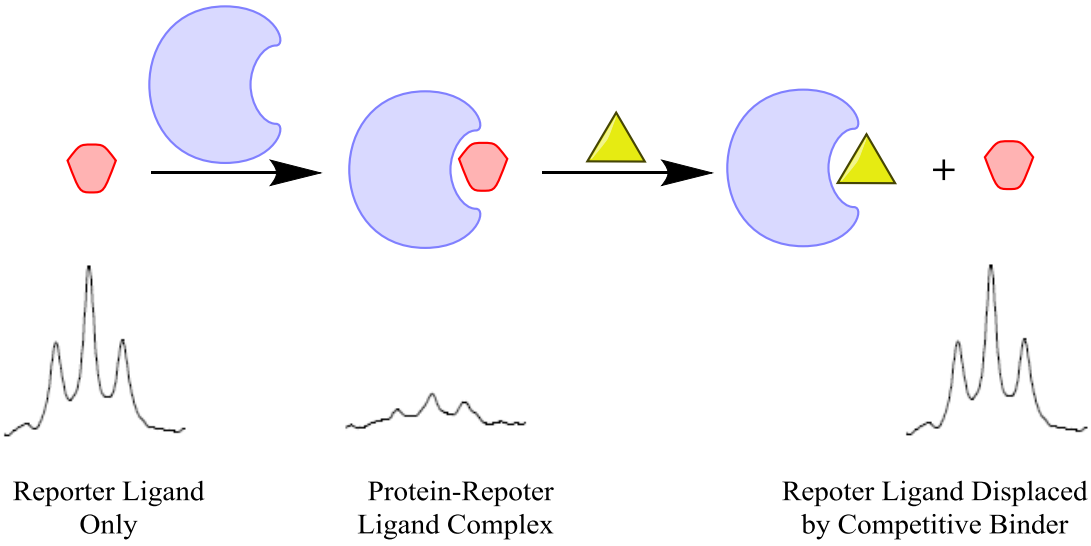

Figure 1.10. Scheme illustrating the principle of reporter ligand displacement method in NMR screening.

By observing changes in the NMR parameters of a reporter ligand, site-specific information about the binding of both high- and low-affinity ligands can be obtained. The choice of the reporter ligand is critical; it is important that it has moderate binding affinity, so that it can be effectively displaced by competing ligands, but should have a strong binding response in the absence of competitors. The presence of the competitor (C) will perturb the dynamic equilibrium between the ligand (L) and the protein receptor (P), leading to a modification of **equation (1.1)** to **equation (1.4)** for single-site binding:[76]

$$P + C \underset{k^{C}_{\text{off}}}{\overset{k^{C}_{\text{on}}}{\rightleftharpoons}} P + C + L \underset{k^{L}_{\text{off}}}{\overset{k^{L}_{\text{on}}}{\rightleftharpoons}} PL \qquad \textbf{(1.4)}$$

A reduced apparent-binding affinity ($K_{D,app}$) for the ligand (L) reflects the reduced availability of the protein to bind the ligand (L) in the presence of a competitor (C) [**equation (1.5)**].

$$K_{D,\,app} = \frac{([P]+[PC])[L]}{[PL]} \qquad \textbf{(1.5)}$$

The apparent K_D equates to the free ligand concentration when half of the protein receptor sites are occupied and will be higher than the true K_D because of the need to compete for the protein binding site(s). If the binding affinity of the competitor is known, K_D values for the ligands of interest can be obtained by titration.[74, 77] However, because this method relies on reporter ligands that bind to specific binding sites, false negative results can occur with compounds which do not compete for the same binding site as the reporter ligand. Another caveat to this technique is that a ligand can bind to a remote site on the protein, leading to displacement of the reporter ligand by allosteric influences, which might lead to false interpretation of the observed displacement. Competitive experiments can also be applied using other nuclei[78] and ^{1}H-edited experiments as described below.

1.2.1.3. CPMG-edited ^{1}H NMR Experiments

Whilst direct observation is advantageous, line broadening can be difficult to discern for ligands with low affinity. Using a small ligand excess (to restrict the concentration of free ligand) can lead to ligand resonances being obscured by that of the protein.[79] Accordingly, it is useful to apply filtering to attenuate the intensities of broad components. It is possible to use Carr-Purcell-Meiboom-Gill (CPMG)-edited ^{1}H NMR spectroscopy to suppress protein resonances, whilst those of the free ligand in solution retain their intensities. Significant attenuation of the resonances of ligands with a high binding affinity will occur with shorter CPMG-spin lock filter times, whilst longer filter times might be needed for lower binding affinity ligands.[80] It is thus important to carefully choose an appropriate filter time, which can range from 10-100 ms depending on the protein-ligand system studied. Peak intensities of CPMG-filtered spectra derived from a titration can then be fitted to determine K_D values for strong binders, providing fast-exchange conditions remain.[79]

1.2.1.4. NOE-based Methods

When ligands bind to proteins, their NOEs undergo major changes leading to the observation of transferred NOEs (trNOEs), which rely on different tumbling times τ_C of free and bound molecules.[81] Low- and medium-molecular-weight molecules have a short correlation time τ_C, and thus exhibit positive NOEs, no NOEs, or very small negative NOEs depending on the compound molecular weight, spectral line shapes, and the spectrometer field strength. However, high-molecular-weight molecules exhibit strongly negative NOEs. When a small-molecule ligand is bound to a larger-molecular-weight protein, it behaves as part of the larger complex, and adopts its NOE properties. Accordingly, binding of a ligand to a protein can be distinguished by looking at the sign and/or size of the observed NOEs.[81-82]

1.2.1.4.1. wLOGSY NMR Experiments

Water-Ligand observed with gradient spectroscopy (wLOGSY) relies on the indirect excitation of the receptor-ligand complex through a selective radiofrequency pulse scheme perturbing the bulk water magnetisation **(Figure 1.11)**.[83] This saturation is transferred *via* NOE processes onto ligands through various magnetisation transfer pathways. Saturated water molecules may transfer magnetisation to the ligand *via* direct NOEs to the receptor-bound ligand and free ligand, spin diffusion *via* the receptor, and *via* direct chemical exchange with labile protons. The observation of negative intermolecular water-ligand NOEs may be explained either by a water shell surrounding the ligand or by protein-bound water proximal to the ligand binding site.[84] It is important to conduct control experiments with the free ligand since the free ligand also experiences water-magnetisation transfer; changes in intensities in the presence and absence of the receptor provide a measure of the direct-water-to-free-ligand enhancement and hence, constitute evidence for ligand binding.[83] Binding does not necessarily show a clear negative response; the response may simply be weaker than in the control sample, or can be completely nulled if the ligand-bound and ligand-free enhancements cancel out. This control is also important to rule out false positives, such as those caused by small-molecule aggregation. wLOGSY experiments are usually conducted in protonated water with ligand excess of 10- to 20-fold, in order to favour the ligand-bound response over the ligand-free response. This approach requires suppression of the water resonance by gradient suppression, and is beneficial for screening low to moderate affinity binders (mM or less), whose off-rate is rapid compared to the ligand-proton-relaxation rates in the bound state.[85]

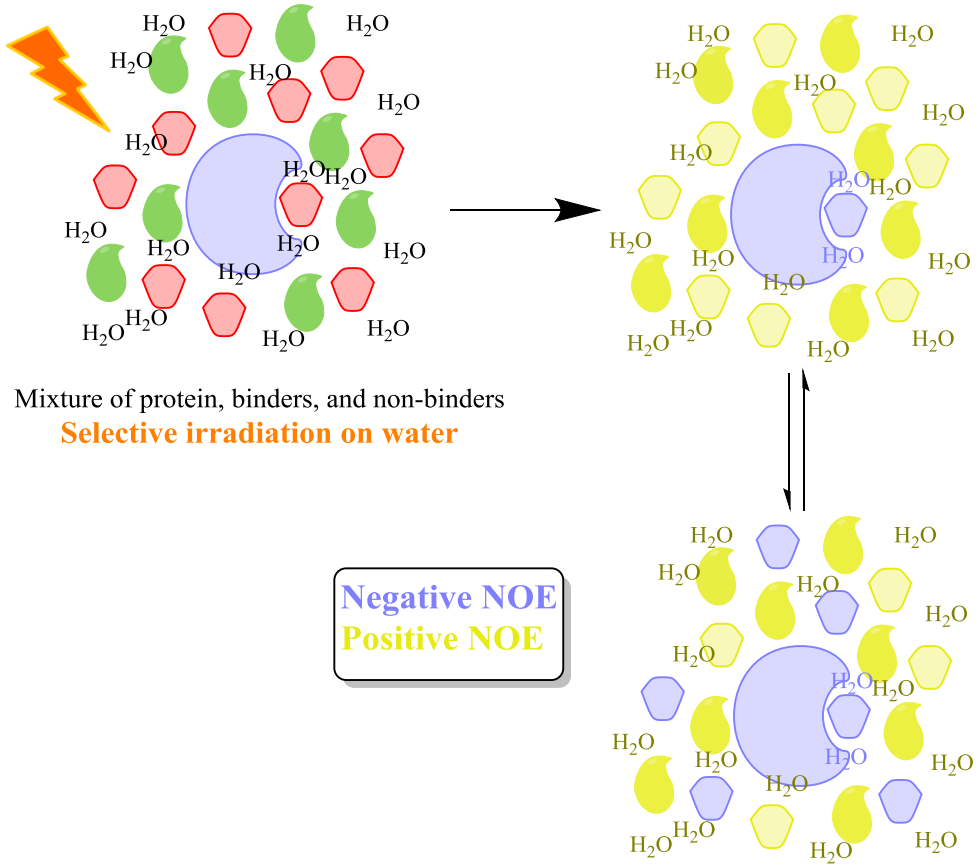

Figure 1.11. Scheme illustrating the principle of water LOGSY. *The transfer of magnetisation between free water, free ligand, protein, bound water and bound ligand leads to a wLOGSY signal which is an average of the positive and negative NOE.*

1.2.1.4.2. Exchange-Transferred NOE

In NOE-based screens, intramolecular NOEs of ligands are observed in 2D-NOESY spectra in the absence and presence of protein receptors. Binding is identified by NOE cross-peaks that change sign upon binding to the receptor. Non-binders show no change in the presence of the receptor, and display either zero or negative cross-peaks with respect to the diagonal. 2D-NOESY relies on short, transient perturbation of magnetisation (100-500 ms), to probe for binding-induced changes of intra-ligand magnetisation transfer. In contrast, wLOGSY is more sensitive mostly because it relies on a long period of intermolecular magnetisation transfer between the ligand and the receptor. 1D NOESY experiments are also

conceivable to reduce acquisition time and constitute an effective screening tool when other screening methods give ambiguous answers. This method is particularly useful in determining the bioactive conformation of weakly binding ligands.[86]

1.2.1.5. 1D Gradient-Selected HSQC

When the ligands and receptors (*e.g.* peptides and proteins) share similar NMR parameters, it can be useful to monitor the displacement of an isotopically labelled reporter. In this case, the resonances of the reporter are not masked by those of similar species in solution, including the competing ligands. ^{13}C labels may be selected for through use of proton-detected isotope-edited techniques, such as 1D gradient-selected HSQC.[87] Only the resonances of the ^{13}C labels will be observed to the limit of ^{13}C-natural abundance, and, hence, unwanted peaks are not detected from the proton spectrum.[88] Since the 1D experiments tend to be acquired with longer free induction decay (FID) acquisition times, either the acquisition times need to be kept short or carbon decoupling has to be removed (hence, yielding $^{1}J_{CH}$ doublets in the ^{1}H spectrum) to avoid undesirable sample heating and/or probe damage.[89]

1.2.1.6. Other Nuclei

NMR active nuclei other than ^{1}H, ^{13}C, or ^{15}N, such as ^{31}P and ^{19}F, can be used to monitor protein-ligand interactions and the activity of proteins, *e.g.* by monitoring the turnover of ATP in the case of kinases. The sensitivity of ^{31}P and ^{19}F detection is lower than for ^{1}H, but both nuclei have large chemical shift window, making chemical shift changes easier to analyse.[90] Since most biologically relevant ligands do not contain ^{31}P or ^{19}F, competitive screening with labelled derivatives is often useful.

1.2.2. Protein-observe NMR Methods

Another approach to track protein-ligand interactions is to monitor protein resonances. Although these experiments (normally) require protein labelling and are usually more laborious and time consuming, they present many advantages over ligand-observe techniques. One particular advantage is that ligand binding sites can be directly determined, whilst important information on protein dynamics and structural changes can be observed.

1.2.2.1. ^{1}H-^{15}N HSQC mapping

Studying the chemical shift perturbations by ^{1}H-^{15}N HSQC NMR requires isotopic labelling of proteins which requires growing cells in isotopically enriched ^{15}N-minimal medium. The need for labelling is often a drawback as not all proteins can be efficiently produced under such conditions. ^{15}N spectrum of labelled proteins yields a peak for the NH backbone amide for each amino acid residue except for proline residues, which have no NH [side chain NH_2 groups (*e.g.* asparagine and glutamine) may also be present in the spectrum]. Well dispersed peaks are indicative of a well-structured protein fold.[91] Ligand binding leads to chemical shift changes in both dimensions (^{1}H and ^{15}N) as a consequence of chemical environment changes at the ligand binding site. In the absence of assigned resonances, HSQC titration experiments can provide a qualitative measure of whether a given ligand is interacting with the protein and can yield a quantitative measurement of the binding affinity. The nature of the changes observed depends on whether the ligand is in a slow- or fast-exchange regime. Similar to ligand-observe techniques, the peaks observed in a fast-exchange system are a weighted-average of both free and bound-species and will move progressively upon increasing ligand concentration.[92] Shift variation can be reported as a scaled geometric average of the chemical shift changes of ^{1}H and ^{15}N, ($\Delta\delta^{1}H$ and $\Delta\delta^{15}N$), as given by **equation (1.6)** so that the contribution from both nuclei is comparable:[91b]

$$\Delta\delta = \sqrt[2]{1/2[(\Delta\delta H)^2 + (0.14\Delta\delta N)^2]} \quad \textbf{(1.6)}$$

In a slow-exchange system, separate resonances will appear for the free- and ligand-bound state; in this case, it may be necessary to re-assign resonances, complicating the analysis.

1.2.2.2. Protein-observe ^{19}F-NMR (PrOF NMR)

^{1}H-^{15}N HSQC is a powerful biophysical method, but it can prove difficult because proton and other resonances overlap to such an extent that the resolution needed to assign a proton peak precisely can be hard to achieve. Hence, efforts have been expanded to develop complementary methods.

1.2.2.2.1. Advantages of PrOF NMR

^{19}F-NMR is being increasingly used to study conformational changes and protein-ligand interactions in solution. ^{19}F-NMR has several advantages: **1)** fluorine is a spin ½ nucleus; **2)** ^{19}F is 100% naturally abundant, which makes it relatively cheap to incorporate in biological systems; **3)** ^{19}F has a gyromagnetic ratio which translates into a high NMR detection sensitivity (83 % that of ^{1}H); **4)** ^{19}F is not found in most biological systems, *i.e.* background resonances, even in highly complex systems, such as cell lysates and whole cells are not an issue; **5)** ^{19}F does not interfere with the water resonance, allowing experiments to be conducted in cheaper, non-deuterated buffers; **6)** ^{19}F is surrounded by 9 electrons what makes its chemical shift highly sensitive to changes in local environment; **7)** the ^{19}F chemical shift spans 400 ppm, much wider than the 15 ppm of ^{1}H, which reduces the problem of peaks overlap even when line broadening occurs; **8)** site-specific labelling with ^{19}F can be achieved to get information about loop dynamics and ligand-binding sites, without the need to assign all of the protein resonances; **9)** relatively quick and simple 1D experiments with ^{19}F can be obtained, which are prone to solvent changes, and, hence, allow for the assessment of solvent isotope effects assessment (H_2O/D_2O), among others; and, **10)** ^{19}F-^{19}F and ^{19}F-^{1}H dipolar

coupling enables NOE and HOE measurements, respectively, to gain further spatial information.[93]

1.2.2.2.2. Labelling Methods

Various methods to incorporate ^{19}F into biological systems have been developed. These can be divided into a biological incorporation and a chemical ligation approaches. A suitable labelling site/approach can be chosen based on the purpose of the experiment, and by looking at the crystal structure of the protein of interest (if one is available).

1.2.2.2.2.1. Biological Incorporation

As the van der Waals radius of fluorine is 1.35 Å [*i.e.* only slightly bigger than that of ^{1}H (1.2 Å)], replacement of a hydrogen atom by fluorine often has little effect on protein structure and, in many cases, activity. To date, fluorinated derivatives of aromatic amino acids (phenylalanine, tryptophan, and tyrosine)[94] have been used to incorporate fluorine into proteins; more recent work has employed fluorinated aliphatic amino acids (*e.g.* fluorothreonine).[95] One method for biological incorporation relies on growing the cells producing the recombinant protein of interest in minimal medium supplemented with the labelled amino acid.[96] Although this method (named fractional labelling) does not guarantee complete labelling of all proteins produced, it does not require sophisticated molecular biology techniques. An alternative is to use a bacterial strain that is auxotrophic for the specific amino acid type, then to add the fluorinated version of the amino acid type before induction.[97] However, whilst this method can give high levels of incorporation of the fluorine label, it is hampered by the lack of suitable bacterial strains. Alternatively, for labelling with aromatic amino acids, cells can be grown in minimal medium in the presence of glyphosate, an aromatic amino acid synthesis inhibitor. The medium is supplemented with the fluorinated aromatic acid type of interest and the other two aromatic amino acid types in unlabelled form;[98] this method can enable efficient labelling, but is often expensive.

All the aforementioned methods lead to labelling of all the amino acids of a specific type. If labelling of a specific amino acid residue is required, selective incorporation can be achieved by using a bioengineered orthogonal-tRNA synthase/tRNA pair;[99] however, this method is labour-intensive and often leads to low protein yields. In certain cases, a trifluoro group (*e.g.* trifluoromethylphenylalanine)[100] has been introduced to proteins in order to enhance the sensitivity of detection, as long as they do not perturb the protein structure.

1.2.2.2.2.2. Chemical Ligation

Chemically modification of amino acid residues after protein production is an attractive alternative to the biological incorporation as it can lead to higher yields of labelled proteins. This approach can involve nucleophilic groups, such as sulphuryl or amino groups, for attachment of the label to the protein.[101] It is often pertinent to incorporate a nucleophilic residue (*e.g.* cysteine) at the appropriate position for labelling using site-directed mutagenesis; it can be necessary to also remove other nucleophilic residues to avoid multiple labelling at sites, although such modifications can lead to changes in protein structure/function. Therefore, the biophysical and structural properties of the labelled protein variants should be validated to ensure they are suitable models of the wildtype protein. 3-Bromo-1,1,1-trifluoroacetone (BTFA) has been used to incorporate fluorine into proteins *via* nucleophilic substitution on cysteines.[113,114] Before NMR analysis, efficient incorporation of the label should be confirmed; preferably by fragment-based MS analyses **(Figure 1.12)**.

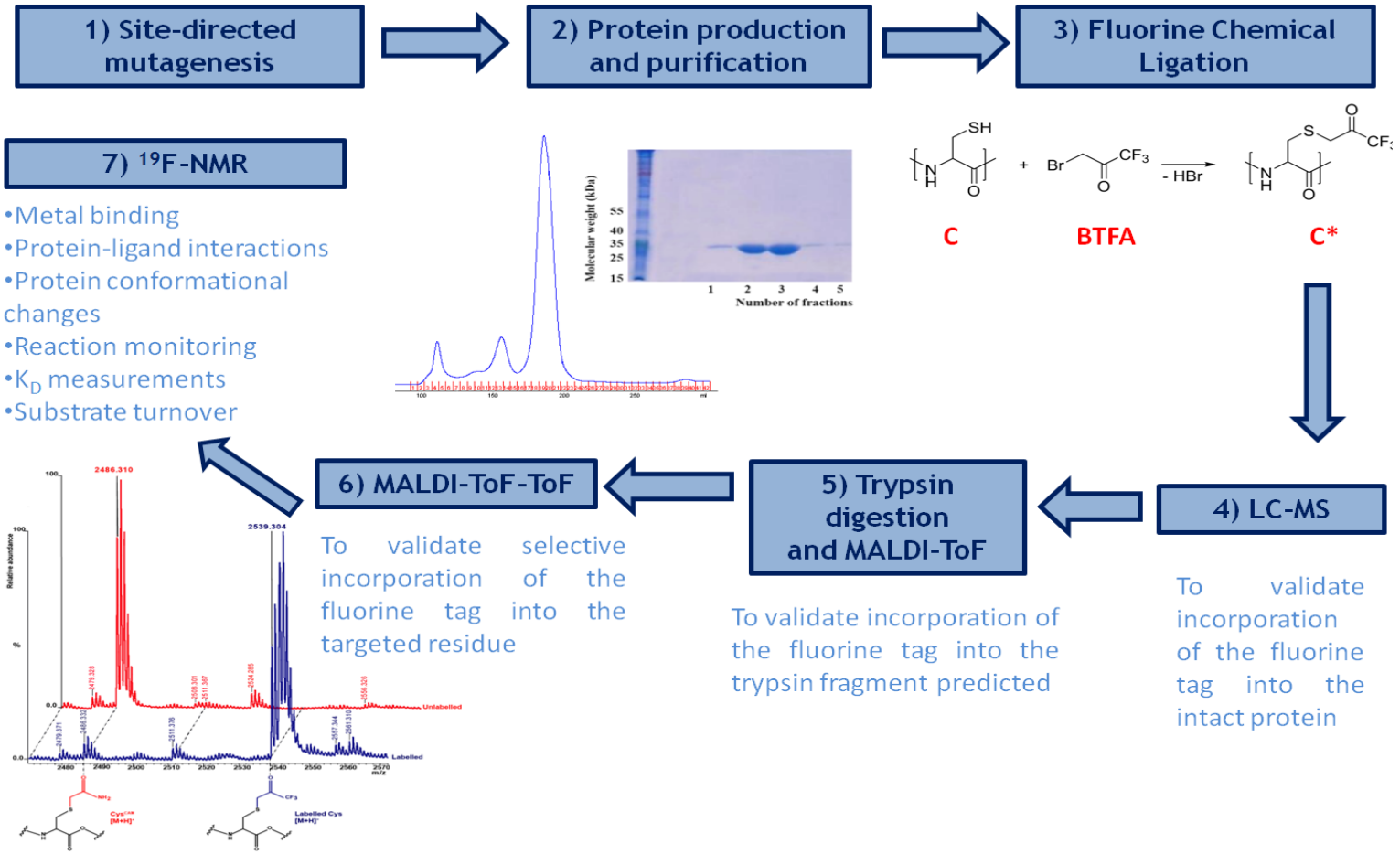

Figure 1.12. Outline scheme of the BTFA-labelling method and the labelling validation steps. *Recombinant proteins are generated by site-directed mutagenesis and produced following a purification method. LC-MS analyses verify the masses of the recombinant proteins which should be in agreement with the calculated masses. The observed mass difference between the unlabelled protein and its labelled counterpart corresponds to the attachment of a single CH_2COCF_3-label per ^{19}F-labelled protein positive ion. The specificity of the labelling method is evaluated by MALDI-ToF-ToF analyses following tryptic digestion.*

1.3. Objectives

The broad aims of the research described in this thesis were:

- Investigations of the substrate selectivity of 2OG-dependent dioxygenases, including the human PHD2 and the *Trichoplax adhaerens* PHD, and studies on the binding interactions with the human pVHL-Elongin B-Elongin C complex.
- Studies on the product release mechanism of PHD2.
- Inhibition studies on PHD2, with particular emphasis on PHD inhibitors in clinical trials.
- Protein-observe ^{19}F-NMR studies on São Paulo metallo β-lactamase (SPM-1), including inhibition and interaction with non-β-lactam inhibitors/substrates.
- Studies on the interaction of a cyclobutanone analogue, a broad-spectrum MBL inhibitor, with SPM-1.
- Investigations of the interactions of avibactam, a non-β-lactam β-lactamase inhibitor, with representatives of class B MBLs.

Chapter 2. Studies on the Substrate Selectivity of PHD2

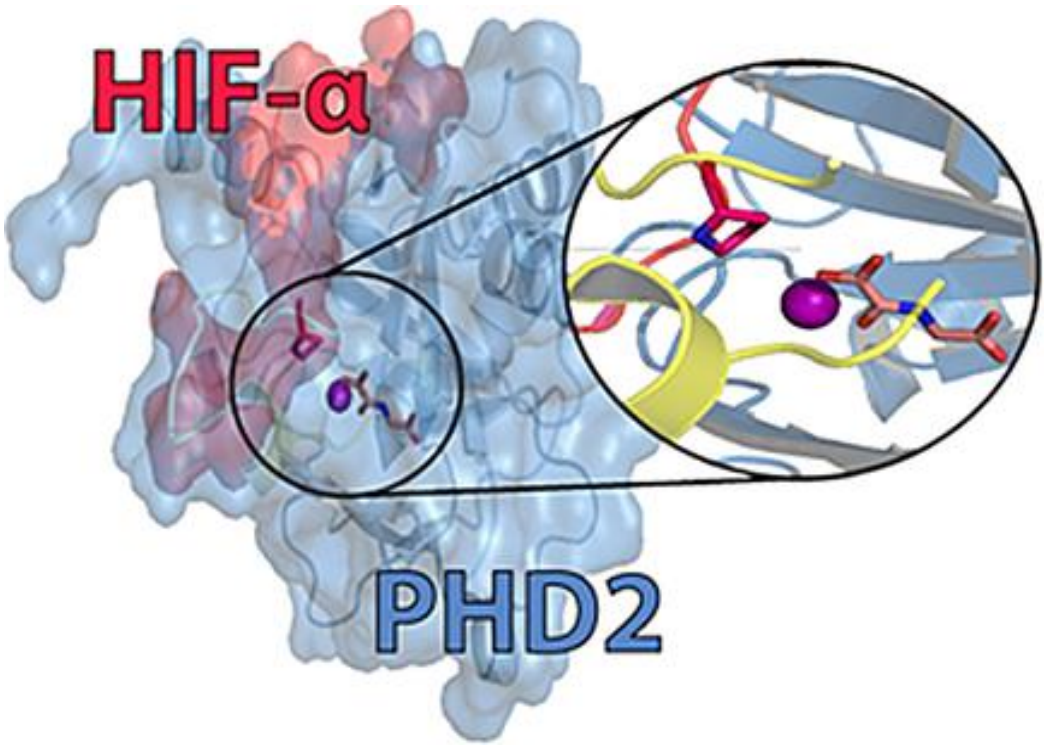

Chapter 2. Contents

2.1. Introduction

The prolyl hydroxylase domain protein (PHD)-catalysed hydroxylation of hypoxia-inducible factor (HIF)-1/2α isoforms occurs in the *N*-terminal and *C*-terminal regions of the oxygen-dependent degradation domain, ODD, (NODD and CODD, respectively).[102] The three human PHDs exhibit different selectivities for NODD and CODD.[103] PHD3 is more selective for CODD than are PHD1/2.[104] The studies described in this chapter focused on PHD2, probably the physiologically most important of the three human PHDs in normoxia.[105] The substrate selectivity of PHD2 towards CODD and NODD was studied using NMR. The resulting preference for the CODD sequence as a substrate seems to be conserved through evolution as shown with studies of the PHD from *Trichoplax adhaerens*, a simpler organism. Another aspect of the work involved analysis of clinically observed variants of PHD2. It was previously reported that heterozygous mutations to PHD2 stabilise HIF-α and are linked to familial erythrocytosis[106] and cancer.[107] Turnover and displacement studies, along with crystallographic analyses, indicate that certain clinical PHD2 variants can be highly selective for CODD or NODD. The findings have implications for future efforts on substrate selective inhibitor design. The work also included biochemical and biophysical studies on reported alternative substrate/binding partners of PHD2 and their interactions with the pVHL-Elongin C-Elongin B (VCB) complex.

2.2. Results

2.2.1. Studies on PHD2 Interactions with ODDs

2.2.1.1. PHD2 Production and Activity Assessment

An *N*-terminal truncated construct of the catalytic domain of PHD2 ($PHD2_{181-426}$) was produced and purified as reported.[108] Previous studies have revealed only small

differences in the catalytic activity, at least in isolated form, between full length PHD2 and $PHD2_{181-426}$.[109] The purity of the recombinant $PHD2_{181-426}$ produced (referred hereafter as PHD2, for simplicity) was assessed by SDS-PAGE analyses and its activity was assessed by monitoring the PHD2-catalysed conversion of 2-oxoglutarate (2OG) to succinate under standard assay conditions using ^{1}H NMR.[110] 2OG decarboxylation was monitored by the decrease in the ^{1}H intensity of the triplet at 2.7 ppm and succinate production was monitored by the increase of the ^{1}H intensity of the singlet at 2.38 ppm **(Figure 2.1)**. 2OG depletion occurs concomitantly with both succinate production and CODD hydroxylation. The results indicate that the recombinant PHD2 produced is active allowing further analyses.

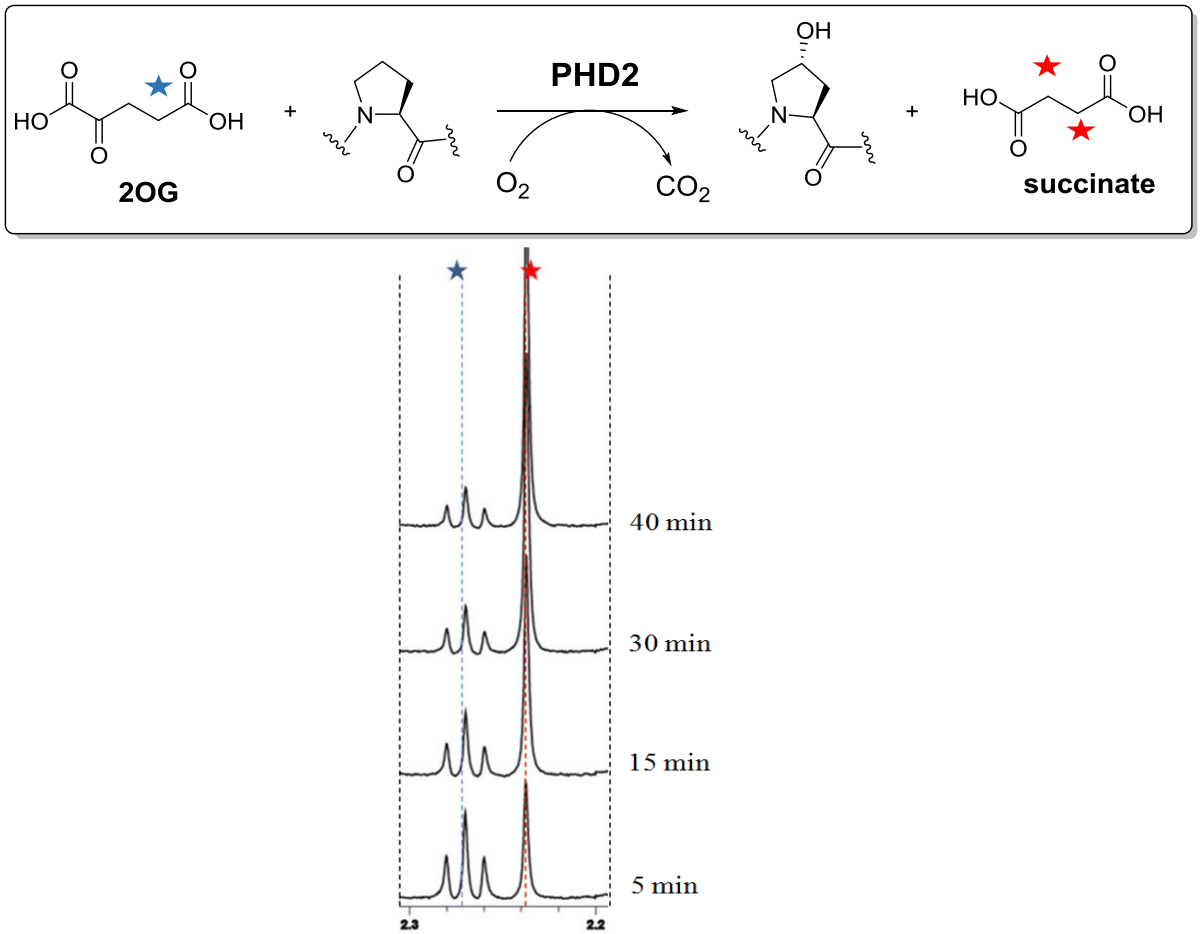

Figure 2.1. PHD2-catalysed 2OG turnover to succinate as monitored by ^{1}H NMR analyses. *Assays mixture contained 20 µM apo-PHD2, 50 µM Fe(II), 400 µM 2OG, 1 mM sodium ascorbate, and 500 µM HIF-1α CODD buffered with Tris-D_{11}, pH 7.5, in 90 % H_2O and 10 % D_2O.*

2.2.1.2. NMR Analyses of PHD2 Interactions with ODDs

NMR was then used to investigate NODD and CODD binding to PHD2. Because there is significant signal overlap between the protein ^{1}H resonances and the ^{1}H resonances from the peptidic substrates, a binding assay was developed using ^{13}C-labelled peptides with monitoring by 1D-Clean In-Phase (CLIP) HSQC with selective ^{13}C-inversion NMR analyses.[111] The ^{13}C-label acts as a handle for spectral editing allowing detection of the free and bound states of the substrates. The 1D ^{1}H-^{13}C HSQC was chosen in favour of direct carbon observation to enhance sensitivity; the experiments were conducted without ^{13}C-decoupling to prevent sample heating during the long acquisition timeframe.[87] A Q3 shaped 180º pulse was applied as the selective pulse; the selective irradiation was applied on C-4 of the 1,2,3,4-^{13}C-labelled 2OG (^{13}C = 30.5 ppm), which was used as a control, and on C-4 of the uniformly ^{13}C-labelled proline ring of the peptides (^{13}C = 24.25 ppm). A proof-of-principle study was first conducted by studying the binding of 2OG and the peptides (CODD and NODD) to PHD2. Check the appendices for CODD and NODD sequences. As expected, when ^{13}C-labelled 2OG, CODD, or NODD are bound to PHD2, almost complete broadening of the ^{13}C resonances is observed, such that the resultant edited spectrum showed near-complete loss of the cosubstrate/substrate signal intensity. Notice the controls with protein and without protein in **Figure 2.2**.

Competition-based assays were then used to compare the relative binding of CODD and NODD to the PHD2.Zn.2OG complex. Zn(II) was used as an Fe(II)-substitute because Zn(II) is diamagnetic, mimics Fe(II), and is not catalytically active.[112] Displacement was assessed based on the intensity observed upon addition of a potential competitor (800 µM, 16-fold excess). Complete displacement corresponds to the same peak intensity as the one observed with the free label control, in the absence of PHD2.

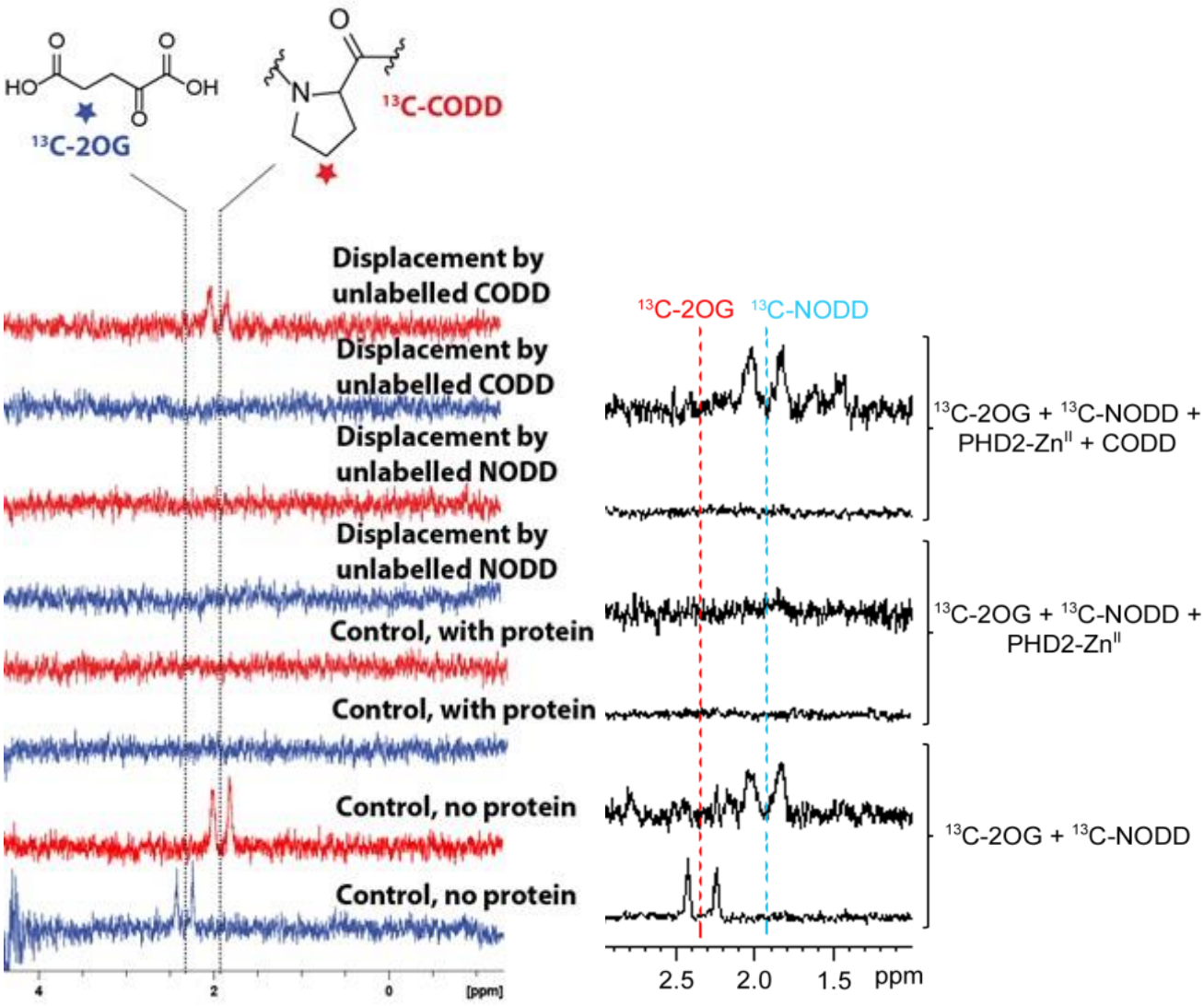

Figure 2.2. NMR studies on the displacement of isotopically-labelled CODD and NODD. *1D ^{13}C-selective Clean In-Phase (CLIP) HSQC NMR spectra for the displacement of ^{13}C-2OG and ^{13}C-CODD (right) or ^{13}C-NODD (left). Assays mixtures contained 50 μM apo-PHD2, 400 μM Zn(II), 50 μM labelled 2OG, 50 μM labelled CODD/NODD (where appropriate) and 800 μM competitor buffered with Tris-D_{11}, pH 7.5, in 90 % H_2O and 10 % D_2O.*[113]

First, ^{13}C-CODD and unlabelled NODD were tested. ^{13}C-CODD was found to bind to the PHD2.Zn.^{13}C-2OG complex without interfering with 2OG binding at a 1:1:1 ratio, PHD2:^{13}C-2OG:^{13}C-CODD, indicating that CODD and 2OG can bind to PHD2 simultaneously, consistent with the proposed mechanism. The addition of unlabelled NODD (800 μM, 16-fold excess) into PHD2.Zn.^{13}C-2OG.^{13}C-CODD did not lead to the

displacement of ^{13}C-CODD from the complex. However, the addition of unlabelled CODD (800 μM, 16-fold excess) into PHD2.Zn.^{13}C-2OG.^{13}C-NODD led to the full displacement of ^{13}C-NODD from the complex. These results indicate that CODD and NODD bind competitively to PHD2.Zn.2OG with a clear preference for CODD over NODD binding. Both CODD and NODD do not interfere with 2OG binding to the PHD2.Zn complex **(Figure 2.2)**.

2.2.1.3. Crystallographic Analyses of PHD2 ODD Selectivity

The preference observed for CODD over NODD binding to PHD2 triggered questions about their binding modes. Both NODD and CODD bind to PHD2 in an extended form. The target prolines (P402/NODD and P564/CODD) adopt both a C^4-*endo* conformation and are deeply embedded in the active site, close to the metal and 2OG. However, comparison of the PHD2.CODD and PHD2.NODD crystal structures (obtained by Dr Rasheduzzaman Chowdhury) reveals differences in the regions involved in NODD/CODD binding, especially in β2/β3 loop and *C*-terminal regions **(Figure 2.3)**.[113]

Crystallographic analyses of the PHD2.CODD structure reveal that CODD binding to PHD2 involves the β2/β3 loop region and the α4 helix (*C*-terminal region) **(Figure 2.3)**. The PHD2 residues 237-254, which adopt a finger-like β2β3 conformation in the uncomplexed PHD2 crystal form (PDB ID: 2G1M),[32] fold to adopt a loop conformation in the PHD2.CODD structure that near entirely encloses the Pro-564$_{CODD}$ region of CODD and the PHD2 active site. Thus, there is a substantial induced fit involved in CODD binding, with the Cα position of Ser-242$_{PHD2}$ differing by 18 Å between the two structures and the Cα position of Lys-400$_{PHD2}$ in the *C*-terminal of α4 helix differing by 2.5 Å between both structures.[24]

An important difference between NODD and CODD binding (in the crystalline state) is that, in contrast to CODD which induces interactions with α4 including *via* salt-bridges

($Asp571_{CODD}$-$Arg396_{PHD2}$), no significant changes were observed in the helix α4 with NODD (*i.e.* α4 adopts similar conformations in the uncomplexed PHD2 crystal form and the PHD2.NODD complex structure). NODD makes more hydrophobic contacts than CODD with the PHD2 *C*-terminal region.[113] These analyses indicate that specific residues/regions are involved in CODD/NODD binding to PHD2. These residues/regions differ amongst the PHD isoforms (see **Chapter 1** for more details); the results thus imply that those residues/regions explain, at least in part, the differences in CODD/NODD selectivity amongst the PHD isoforms.

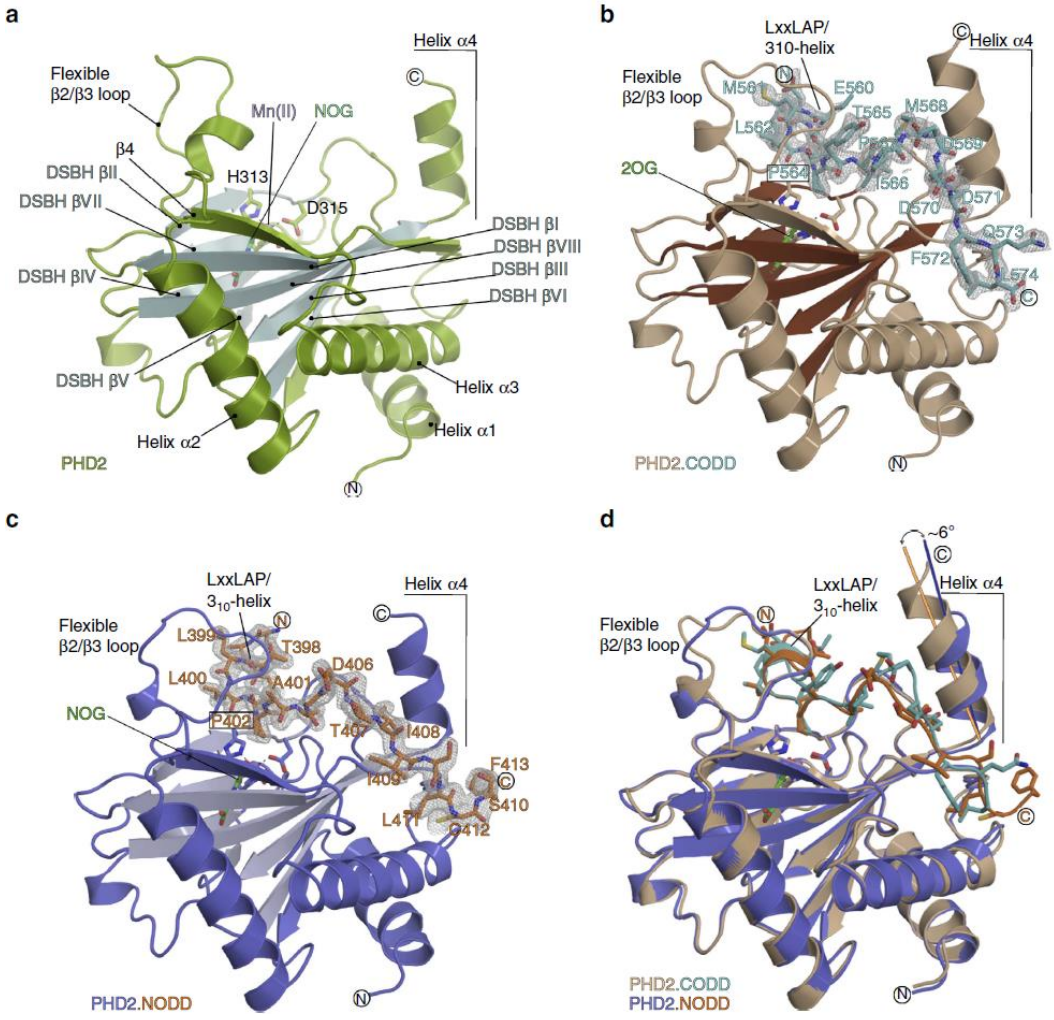

Figure 2.3. Overall binding modes of NODD and CODD to PHD2. *Views from PHD2.NOG (a, PDB: 5L9R), PHD2.2OG.CODD (b, PDB: 5L9B) and PHD2.NOG.NODD complexes (c, PDB: 5L9V) showing secondary structural elements involved in NODD/CODD*

selectivity. (d) Superimposition of PHD2.CODD and PHD2.NODD structures reveals apparently more 'induced fit' in CODD (compared with NODD) binding involving the β2/β3 loop and a4. Figure used with permission from Nature Communications, Nature Publishing Group.[113]

2.2.2. Studies on PHD2 Clinical Variants

In an effort to better understand the substrate selectivity of PHD2, and by implication other PHD isoforms, further studies were conducted with clinically relevant PHD2 variants. PHD2 clinical variants are linked to different phenotypes. The R396T PHD2 variant is linked to breast carcinoma[114] and the P317R PHD2 variant is linked to familial erythrocytosis (an abnormally high red blood count).[115] Interestingly, $Pro317_{PHD2}$ is located two residues away from $Asp315_{PHD2}$, one of the Fe(II)-binding residues, and is located close to the unusually narrow entrance to the PHD2 active site.[24] In order to investigate whether the different phenotypes may correlate with different substrate selectivities, the catalytic activity of PHD2 clinical variants was first studied. The recombinant P317R PHD2 and R396T PHD2 variants were obtained from Dr Rasheduzzaman Chowdhury.

2.2.2.1. 2OG Turnover Analyses with PHD2 Clinical Variants

PHD2-catalysed 2OG turnover to succinate was monitored by ^{1}H NMR under standard conditions. 2OG turnover to succinate is coupled to NODD/CODD proline hydroxylation.[110] Under the assay conditions, similar levels of 2OG turnover to succinate were observed in the presence of NODD with the R396T PHD2 variant and the wildtype (wt) PHD2; however, little turnover was observed in the presence of CODD as a substrate with the R396T PHD2 variant. The P317R PHD variant retained a 2OG turnover rate similar to wt PHD2 in the presence of CODD, but manifested a loss of 2OG turnover with NODD **(Figure 2.4)**. In order to investigate whether the differences observed were due to differential uncoupled turnover with each variant, 2OG turnover to succinate was monitored in the

absence of peptidic substrate **(Figure 2.5)**. The P317R and R396T PHD2 clinical variants displayed similar initial uncoupled turnover rates as wt PHD2 (*i.e.* very slow rates). These findings suggest that the R396T PHD2 and P317R PHD2 phenotype might be, at least in part, linked to the loss of CODD and NODD hydroxylation, respectively.

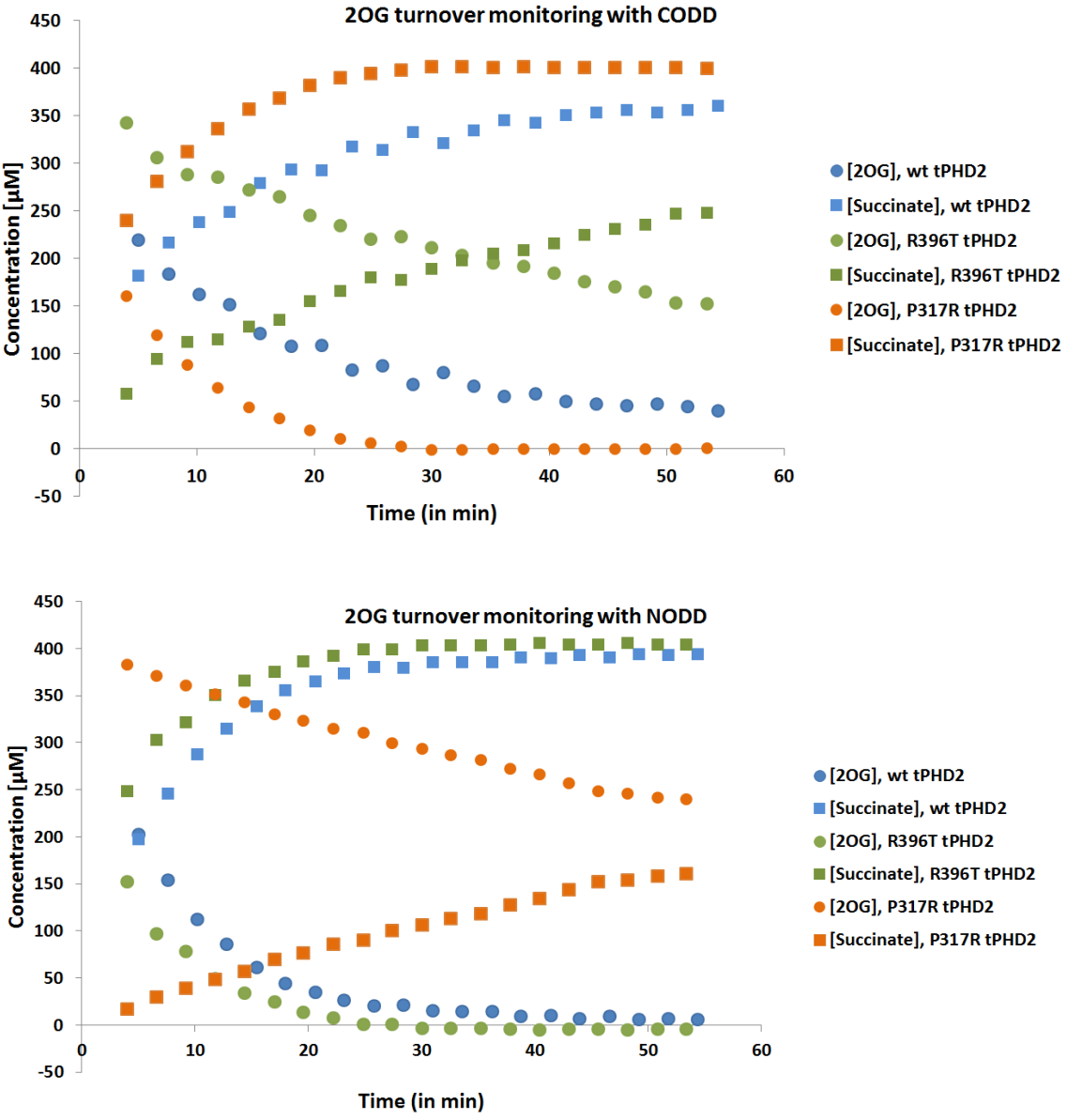

Figure 2.4. 2OG turnover to succinate by PHD2 as monitored by ^{1}H NMR spectroscopy. *The assay mixture contained 20 µM apo-tPHD2, 50 µM Fe^{II}, 400 µM 2OG, 1 mM sodium ascorbate, and 500 µM HIF-1α CODD, in 10 % D_2O and 90 % H_2O buffered with 50 mM Tris-D_{11}, pH 7.5 containing 0.02 % sodium azide.*

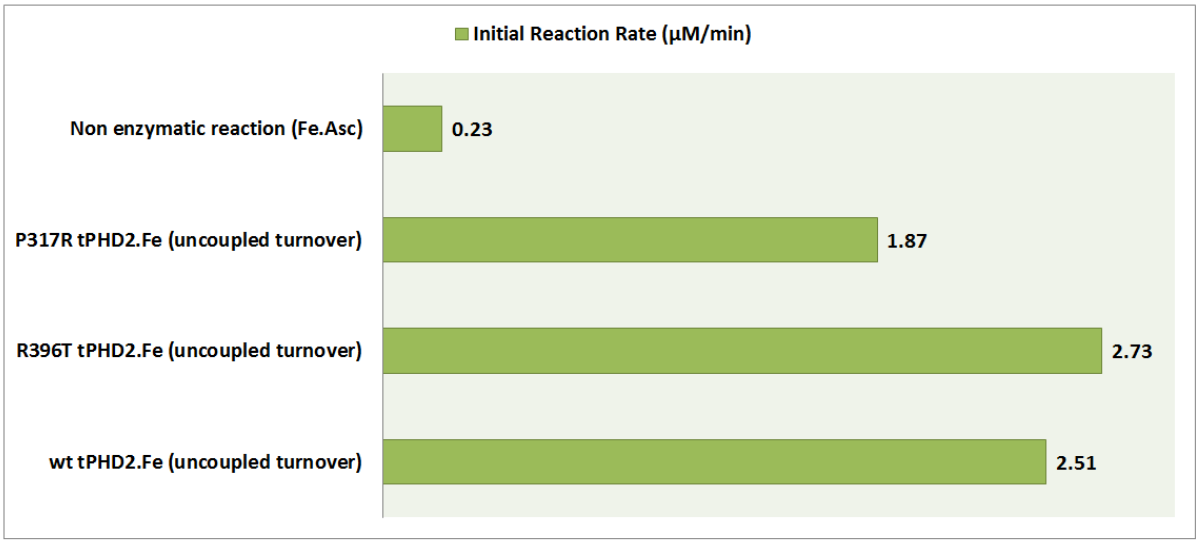

Figure 2.5. Initial rate (µM/min) of 2OG turnover to succinate by PHD2 as monitored by ^{1}H NMR spectroscopy. *The assay mixture contained 20 µM apo-tPHD2, 400 µM 2OG, 1 mM sodium ascorbate, 200 µM Fe(II) in 10 % D_2O and 90 % H_2O buffered with 50 mM Tris-D_{11}, pH 7.5, containing 0.02 % sodium azide.*

2.2.2.2. Crystallographic Analyses of PHD2 Clinical Variants

In order to investigate the structural basis for the differences observed in CODD/NODD hydroxylation by the PHD2 variants, crystal structures of clinical P317R and R396T PHD2 variants were obtained by Dr Rasheduzzaman Chowdhury. Crystallographic analysis of the P317R PHD2 variant structure reveals that Pro317$_{PHD2}$ located on the βII-III loop forms part of a hydrophobic patch binding the ODD LXXLAP-3$_{10}$-helix **(Figure 2.6)**. The P317R structure also reveals Arg317$_{PHD2}$ in 2 conformations, one of which interacts differently with the LXXLAP motif. The lack of reactivity of P317R PHD2 with NODD supports a relatively more important role for Pro317$_{PHD2}$ in binding the LXXLAP residues in NODD than CODD. In the PHD2.CODD structure, Arg396$_{PHD2}$ (α4) salt-bridges with Asp571$_{CODD}$; analyses of the ODD structures imply the R396T substitution disrupts the Asp571$_{CODD}$ interaction, but does not directly impact on NODD binding. Indeed, structures of

R396T with/without NODD suggest how the R396T substitution is tolerated for NODD binding **(Figure 2.6)**.[113]

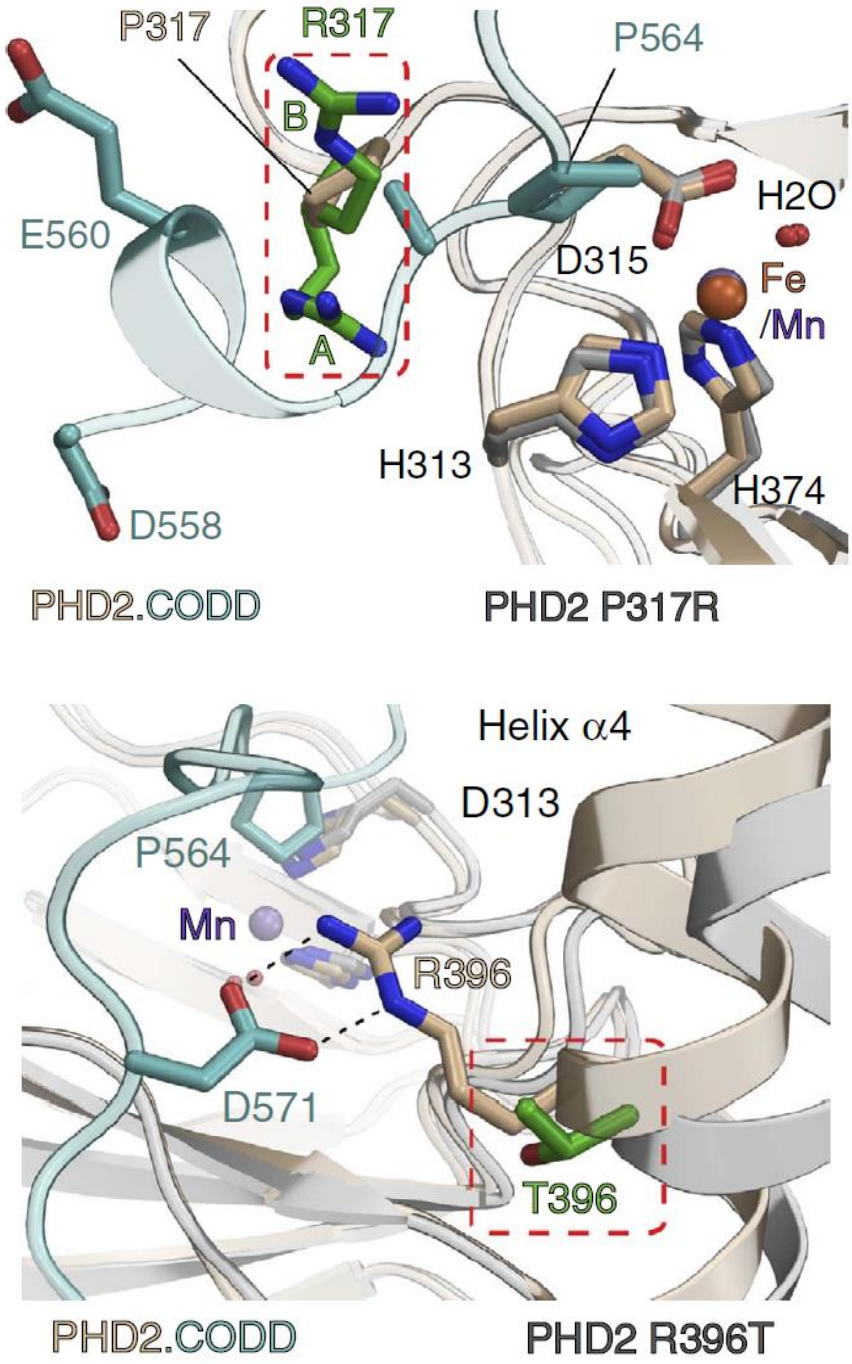

Figure 2.6. Views from PHD2 P317R and R396T crystal structures superimposed with one of PHD2.CODD complex, suggesting substantial impact of the substitutions on substrate binding. *Figure used with permission from Nature Communications, Nature Publishing Group.*[113]

2.2.2.3. Effects of PHD Inhibitors in Clinical Trials

The revelation of differential contributions from specific PHD regions in ODD binding raises the possibility of inhibitors competing differently with NODD or CODD. Accordingly, the displacement of CODD or NODD by PHD clinical inhibitors was studied by 1D-CLIP HSQC NMR analyses (as described in **Section 2.2.1.2**).[111] The inhibitors selected for this study were FG2216 (IOX3),[116] which is used in clinical trials to treat anaemia, and FG4592 (Roxadustat),[116] which is a newer compound in clinical trials for anaemia treatment.

FG2216[116] was observed to displace NODD, but not CODD, from wt PHD2. Analyses of PHD2.FG2216 structures, with and without CODD (PDB ID: 3HQU, 4BQX)[113] suggests this may be because of the relatively greater role of the LXXLAP region in NODD compared to that of CODD binding (with CODD, loss of LXXLAP binding is compensated by interactions involving *C*-terminal regions). In contrast, FG4592[116] efficiently displaces *both* CODD and NODD binding, probably due to its phenoxy-group, which projects into regions binding *C*-terminal residues of both ODDs. Studies on the clinical inhibitors and their mode of binding, including by modelling, are presented in **Chapter 4**.

The effect of the clinical inhibitors on P317R and R396T PHD2 was then studied **(Figure 2.7)**. The results imply that the selectivity of NODD/CODD displacement by the inhibitors is different for the R396T and P317R variants compared to wt PHD2, *i.e.* with R396T, both inhibitors displace NODD less than wt PHD2; for P317R, FG4592 displaces CODD less than wt PHD2. The percentage displacement was calculated according to **equation (2.1)** where I_0 is the intensity of the reporter in the presence of protein without inhibitor, I is the intensity of the reporter in the presence of protein and inhibitor, and I_{blank} is the intensity of the reporter without protein or inhibitor:[112]

$$\%\ \text{Displacement} = \frac{I - I_0}{I_{blank} - I_0} * 100 \qquad \textbf{(2.1)}$$

A 100 % displacement corresponds to a peak intensity similar to the one observed with the free label control, in the absence of protein.

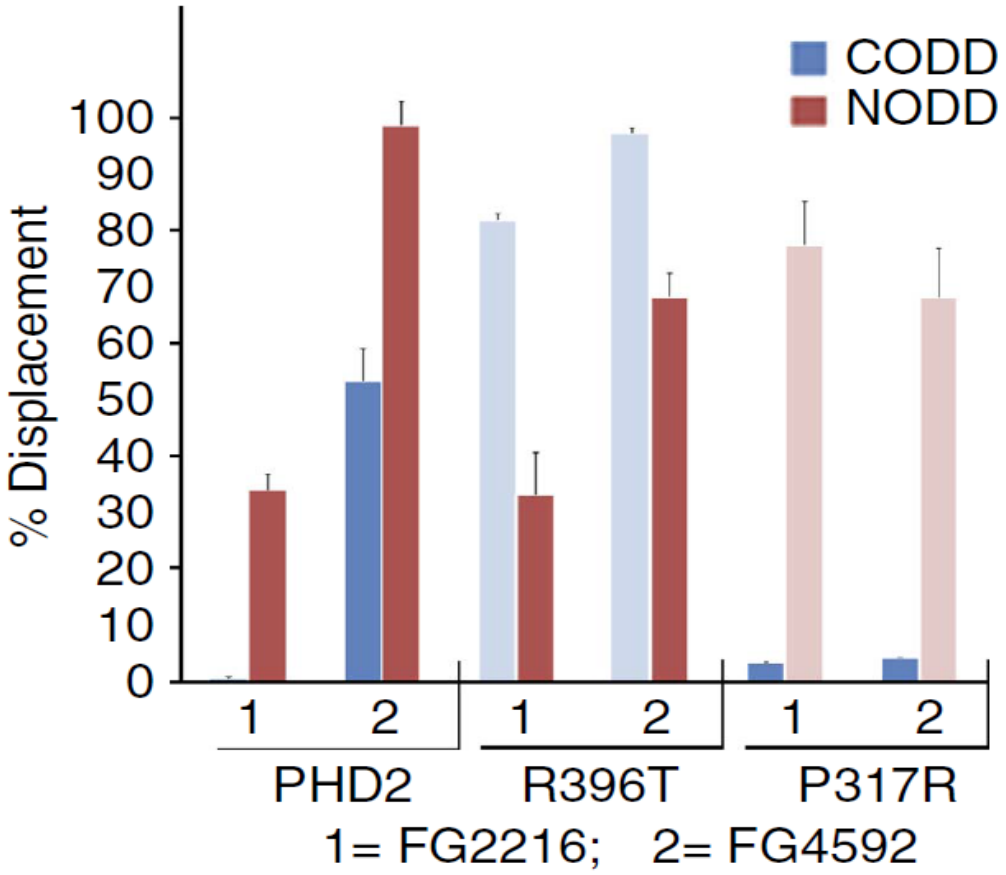

Figure 2.7. One-dimensional ^{13}C-selective clean in-phase (CLIP)–HSQC NMR reveals apparently selective displacement of NODD/CODD from PHD2 wt/clinical variant complexes by using PHD inhibitors (FG2216/ FG4592). *Assays mixtures contained 50 µM apo-PHD2, 400 µM Zn(II), 50 µM 2OG, 50 µM ^{13}C-CODD or ^{13}C-NODD, and 800 µM competitor (FG2216 or FG4592) buffered with Tris-D_{11}, pH 7.5, in 90 % H_2O and 10 % D_2O (n = 5 for wt PHD2 and 2 for variants). Figure used with permission from Nature Communications, Nature Publishing Group.*[113]

Overall, the findings are of interest because they imply that altered PHD2 selectivity may have pathological consequences. The erythrocytosis-associated P317R PHD2 variant has substantially altered ODD selectivity towards CODD, and the breast cancer-associated

R396T PHD2 variant towards NODD. Biophysical analyses employing crystallography and NMR reveal that the molecular basis of PHD isoform and variant selectivity involves enzyme-substrate interactions involving β2/β3 loop residues, the LXXLAP motif, and α3 and α4 regions which display variation between the PHD isoforms. The results thus inform on the substrate selectivities of PHD2 and, by implication, PHD isoforms. The identification of specific interactions determining PHD selectivity for ODDs also opens the way forward to PHD isoform and ODD selective inhibitors useful for the upregulation of specific sets of HIF target genes. The results imply that the development of inhibitors differentially blocking NODD *vs.* CODD binding should be possible

2.2.3. Studies on PHD from Simpler Organisms

In order to better understand the substrate selectivity of the PHDs and their substrate requirements, it was of interest to study the substrate selectivity/requirement of a PHD from a simpler organism. The role of prolyl hydroxylation in protein biosynthesis extends from bacteria to humans and hence studying these proteins is also of interest from an evolutionary perspective.[117] *Trichoplax adhaerens*, the simplest known animal, contains a HIF system and provides evidence for a potential connection of the HIF-PHD-VHL triad in all animals.[118] The *T. adhaerens* HIF-α ODD (taODD) differs substantially from human HIF-1α NODD and CODD (15% and 35% identity over 20 residues, respectively). taODD contains four prolyl residues, but lacks the consensus LXXLAP prolyl-hydroxylation site of HIF-α proteins that have been studied. The progenitor ODD in non-bilateral animals more closely resembles CODD than NODD; thus, NODD was proposed to have evolved after CODD. *T. adhaerens* PHD (taPHD) has similar properties to human PHD2, such as the formation of a stable Fe(II).2OG.PHD2 complex.[118] In order to investigate the substrate requirements of the taPHD and its activity, taPHD-catalysed 2OG turnover to succinate was first monitored in the

presence and absence of taODD as a substrate.[110] Reombinant taPHD and taODD were provided by Kerstin Lippl **(Figure 2.8)**.

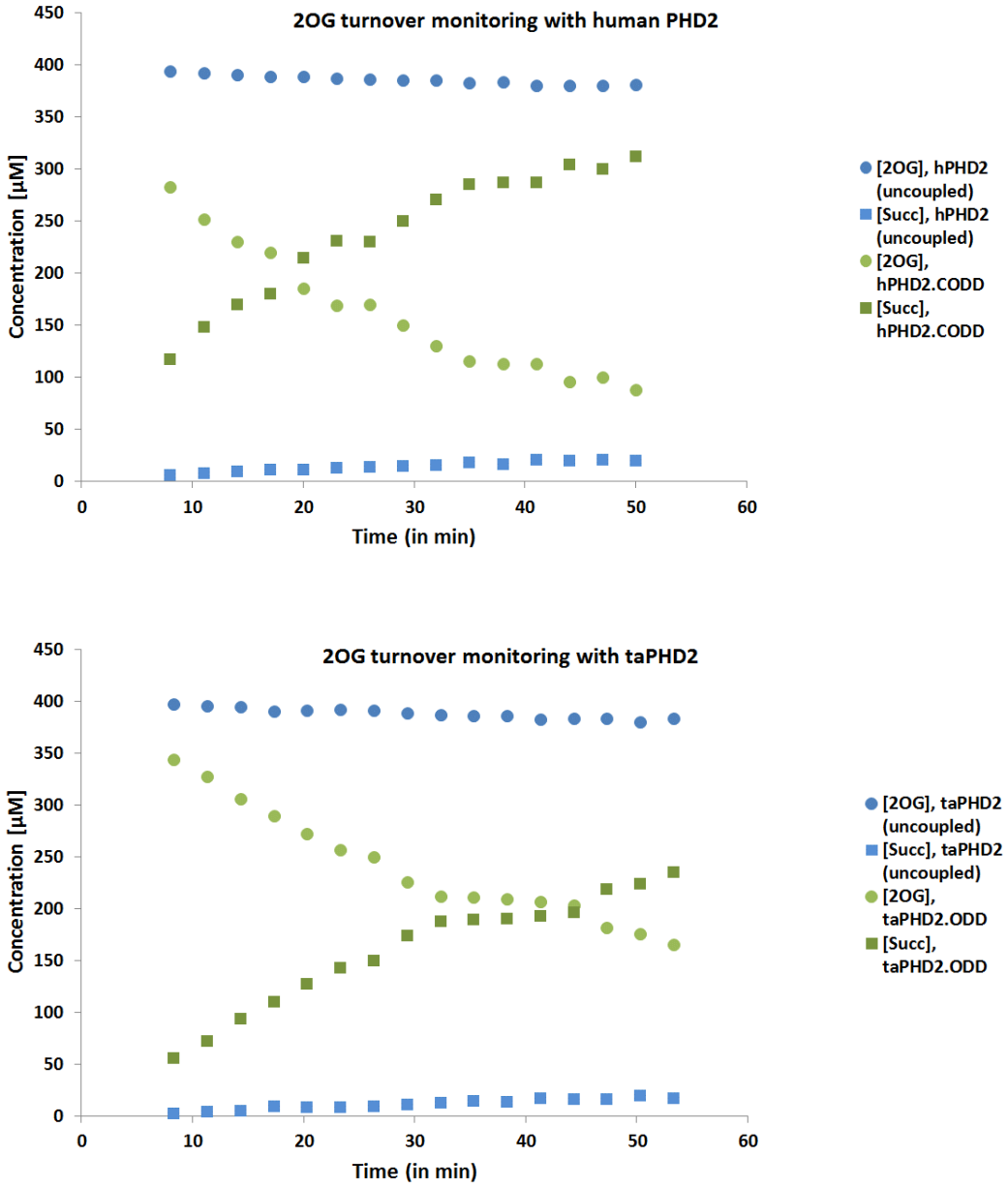

Figure 2.8. 2OG turnover to succinate by hPHD2 and taPHD as monitored by ^{1}H NMR spectroscopy. *The assay mixture contained 20 µM apo-tPHD2, 50 µM Fe^{II}, 400 µM 2OG, 1 mM sodium ascorbate, and 500 µM HIF-1α CODD, in 10 % D_2O and 90 % H_2O buffered with 50 mM Tris-D_{11}, pH 7.5 containing 0.02 % sodium azide.*

It was observed that taPHD efficiently catalyses to 2OG turnover to succinate in the presence of its substrate, taODD. Both taPHD and human PHD2 had similar rates of uncoupled turnover as observed in the absence of their substrates. The binding of human CODD and NODD to taPHD was then investigated by 1D-CLIP HSQC analyses.[111] The results indicate that taPHD discriminates between the binding of CODD and NODD: 42 % of uncomplexed NODD was observed in solution in the presence of a 1:1, taPHD.NODD complex, whilst all of CODD was bound as indicated by complete broadening of its signal upon addition of taPHD **(Figure 2.9)**, consistent with kinetic analyses.[118] The results indicate that CODD is a better binder to taPHD2 than NODD. The studies of taPHD and PHD2 with fragments of HIF-α ODDs imply that the preference of human PHDs for HIF-α CODD over NODD substrates is conserved, supporting the proposal that an ODD more closely related to CODD evolved before NODD.[118]

These results, along with the previous results on PHD2 clinical variants selectivities and the observed greater importance of induced fit in CODD compared to NODD binding to PHD2, suggest a higher conservation of residues correlating with increased CODD than NODD selectivity during the course of animal evolution. There seems to be a preference for conservation of CODD-selective residues during PHD evolution. The results are consistent with clinical/genetic evidence that loss of wt PHD2 cannot be compensated by PHD 1/3[119] and with genetic evidence that PHD2 is the most important PHD isoform in normoxia and that 'CODD-type' hydroxylation likely evolved prior to that of NODD.[120] Overall, the presence of the PHD in *T. adhaerens* suggests that there might be a core set of genes that are hypoxically regulated through the HIF system in all animals. The HIF system and crucial interaction with the PHDs might have helped to enable animal life to respond to metabolic challenges, including the increase in atmospheric oxygen levels on Earth over the course of animal evolution.[118]

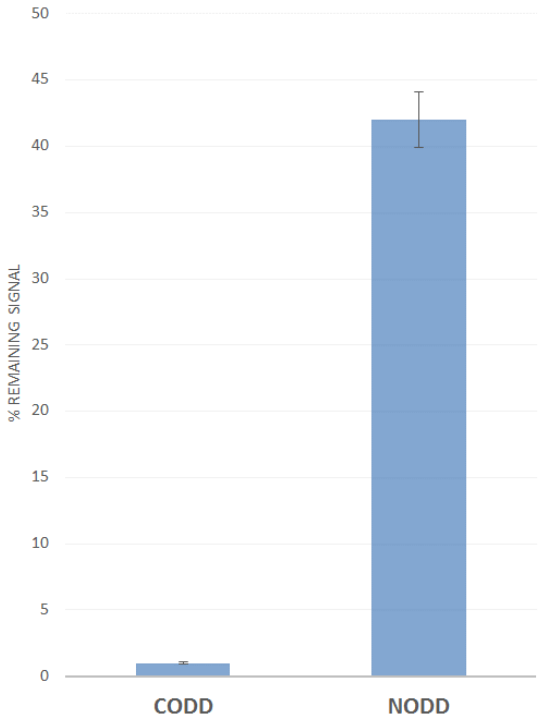

Figure 2.9. NMR analyses of the binding of CODD and NODD to taPHD as observed by 1D CLIP HSQC. *Assays mixtures contained 50 μM apo-taPHD, 400 μM Zn(II), 50 μM 2OG, and 50 μM ^{13}C-CODD or ^{13}C-NODD buffered with Tris-D_{11}, pH 7.5, in 90 % H_2O and 10 % D_2O.*

2.2.4. Studies on PHD2 Alternative Substrates/Interaction Partners

In recent years, there have been multiple reports on PHD substrates other than HIFs.[121] Alternative reported (non-HIF) substrates/interaction partners with PHDs include IκB kinase-β,[122] RNA polymerase II,[123] β_2-adrenergic receptors,[124] and activating transcription factor 4,[125] and others. The physiological roles of these alternative substrates have yet to be determined. It is possible that these alternative substrates compete with HIF-α for PHD binding and thus, impact on the hypoxic response. Validating these reports is of biological relevance given that it will enable better understanding of the PHD-substrate interactions and is of medicinal relevance given that PHD inhibitors are now in the late stage Phase III clinical trials.[126]

Initial work on peptides that contain the putative hydroxylation sites has indicated that the PHDs are much more selective for their well-established substrate HIF. Peptides of reported substrates were screened for their ability to alter the kinetics of HIF-hydroxylation by PHD2 (by Kerstin Lippl) **(Figure 2.10)**.[23] An inhibitory effect of at least two different peptides on PHD2 was observed, suggesting that there is an interaction between the prolyl hydroxylase and these peptides: an inhibitory effect on PHD2 was observed for peptide sequences from the eukaryotic elongation factor 2 (eEF2)[127] and the RNA polymerase II subunit (Rpb1).[123] Both peptides reduced the hydroxylation of NODD in a concentration-dependent manner. In order to investigate the mode of binding and inhibition, NMR studies were carried out and the binding of the two inhibitory peptides, eEF2 and Rpb1, to PHD2 was studied. The binding mode of the peptides was investigated by displacement experiments of ^{13}C-COOD/NODD using 1D-CLIP HSQC analyses.[111] For this aim, PHD2 was first incubated with ^{13}C-labeled HIF-1α CODD or NODD (1:1) that can only be detected in its unbound state. Consistent with the hydroxylation assays, addition of eEF2 and Rpb1 (800 µM, 16-fold excess) led to a full displacement of NODD, but no strong effect on CODD-binding by PHD2 was observed **(Figure 2.11)**.

The binding of the inhibitory peptides to PHD2 was thus confirmed by NMR studies; displacement of HIF-1α NODD by eEF2 and Rpb1 was observed. Altogether, these results provide evidence that the PHDs are selective for HIF as a substrate and that the cellular PHD activity may be influenced by interaction with other proteins.

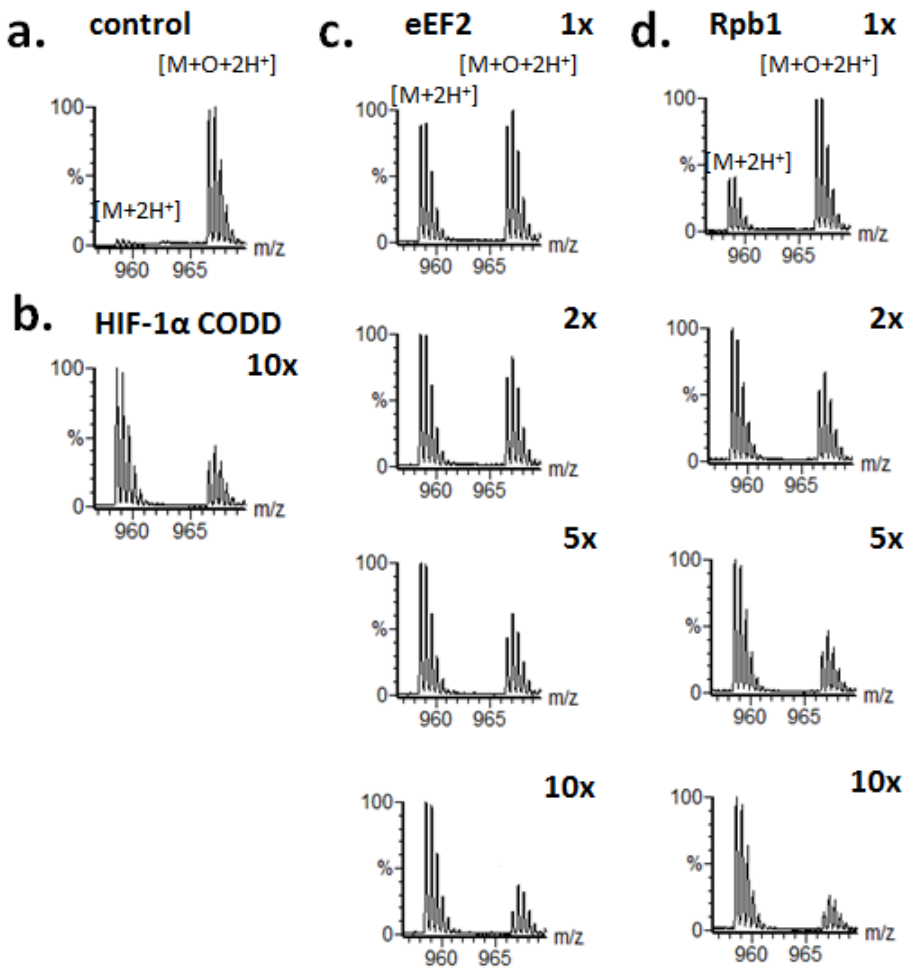

Figure 2.10. Rpb1 and eEF2 compete with HIF-1α NODD hydroxylation. *MS spectra of incubations of a, PHD2 + HIF-1α NODD + random peptide (10x), b, PHD2 + HIF-1α NODD + HIF-1α CODD (10x), c, PHD2 + HIF-1α NODD + eEF2 (1x-10x), d, PHD2 + HIF-1α NODD + Rpb1 (1x-10x), in the relative ratios of PHD2 : HIF-1 α NODD : competitive peptide = 1 : 25 : (25 – 250), corresponding to the 1x, 2x, 5x, and 10x amount of competitive peptide with respect to HIF-1 α NODD. (Competitive hydroxylation assays were conducted by Kerstin Lippl).*

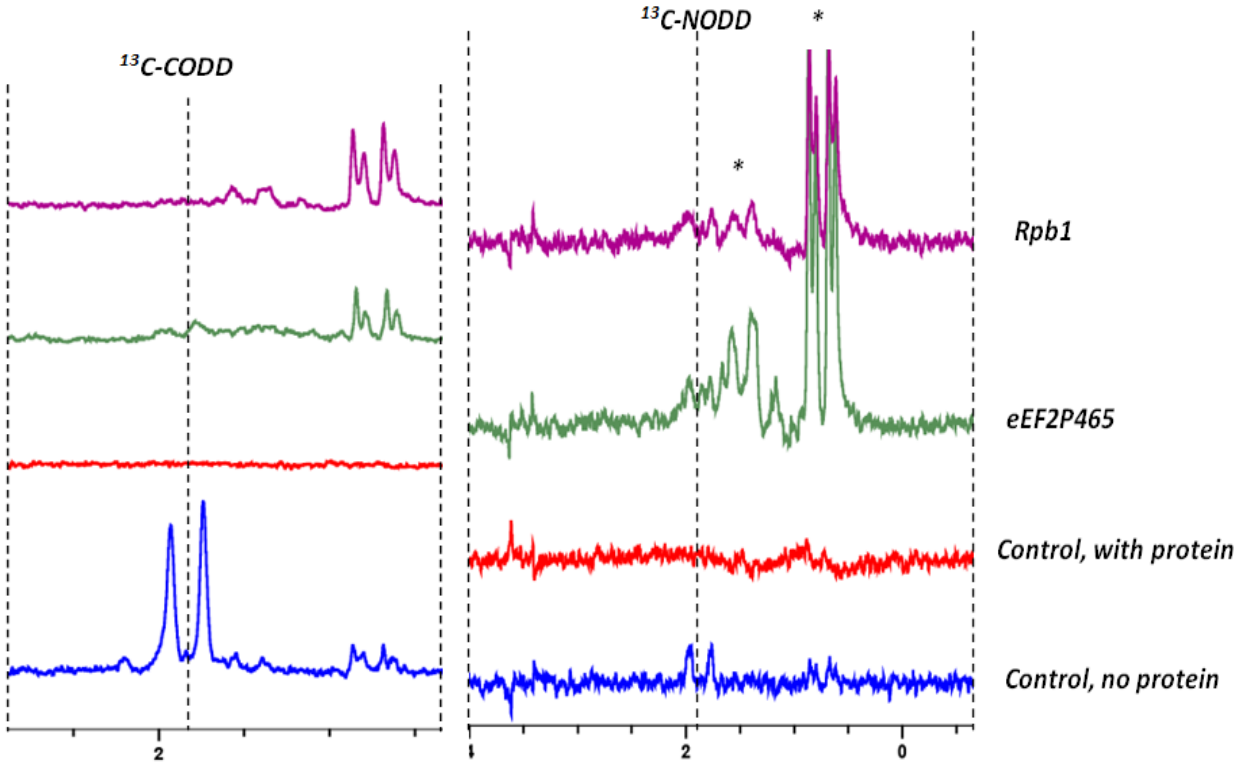

Figure 2.11. Qualitative single concentration screening by ^{13}C-NODD/CODD displacement as monitored by 1D CLIP HSQC with selective ^{13}C-inversion analyses. *The assay mixture contained 50 µM apo-PHD2-$_{181-426}$, 400 µM Zn(II), 50 µM 2OG, 50 µM ^{13}C-CODD/NODD, 800 µM peptide and 50 mM Tris-D_{11}, pH 7.5 in 10 % D_2O and 90 % H_2O. (* denotes intrinsic signals).*

2.2.5. Studies on the VCB complex

A central component of the HIF-mediated response system is the von Hippel Lindau protein (pVHL). Hydroxylated Pro-402 and Pro-564 of HIF-1α bind independently to a single pocket in pVHL, thereby constituting independent proteolysis within the ODD.[28] In normoxia, pVHL mediates hydroxylated HIF-α ubiquitination in the nucleus prior to its export to the cytoplasm for proteasomal degradation.[128] HIF-α hydroxyproline recognition by pVHL is important for downstream cellular signalling; pVHL-Elongin C-Elongin B ubiquitin ligase complex (VCB) along with Cul2, Rbx1 and the related Skp1-Cul1-F-box catalyse polyubiquitination of HIF-α on specific lysine residues (Lys- 532 of HIF-1α, and Lys-467

and Lys-570 of HIF-3α), leading to HIF-α oxygen-dependent proteolysis through proteasomal degradation.[129] However, under hypoxic conditions, HIF-α hydroxylation by PHDs, which are proposed to act as oxygen sensors, is inhibited.[11a] Accordingly, HIF-α subunits are not efficiently recognised by pVHL; they accumulate in the nucleus and dimerise with HIF-β enabling them to bind DNA and activate their target genes.[9] pVHL is also involved in disease. von Hippel Lindau disease is an autosomal dominant cancer syndrome that is characterised by renal cell carcinomas and tumours. The lack of wild type pVHL results in accumulation of HIF in cells and subsequent overexpression of target genes.[130] Accordingly, it is of interest to study pVHL and its interaction with potential binding partners.

2.2.5.1. VCB Expression and Production

pVHL was produced as part of the VCB complex. Human VHL (residues 54 to 213) and full-length human Elongin B were obtained as a dicistronic message into the pGEX-4T-3 plasmid. Human Elongin C (residues 17 to 112) was inserted into a pBB75, a T7-driven expression plasmid that confers resistance to kanamycin. Both plasmids were gifts from Dr Nikola Pavletich. I cotransformed the two plasmids into the BL21(DE3) strain of *E. coli* and subjected them to dual antibiotic selection. Expression of the three genes was carried out at 25°C. The ternary complex was isolated and purified by affinity chromatography using a glutathione Sepharose column. The affinity-purified ternary complex was treated with thrombin at 4°C to cleave the GST fusion protein and was further purified by gel-filtration chromatography and another glutathione Sepharose column to remove the GST-tag from the mixture, as reported.[131] The proteins produced were characterised by MS analyses and the formation of the complex was validated by native gel **(Figure 2.12)**.

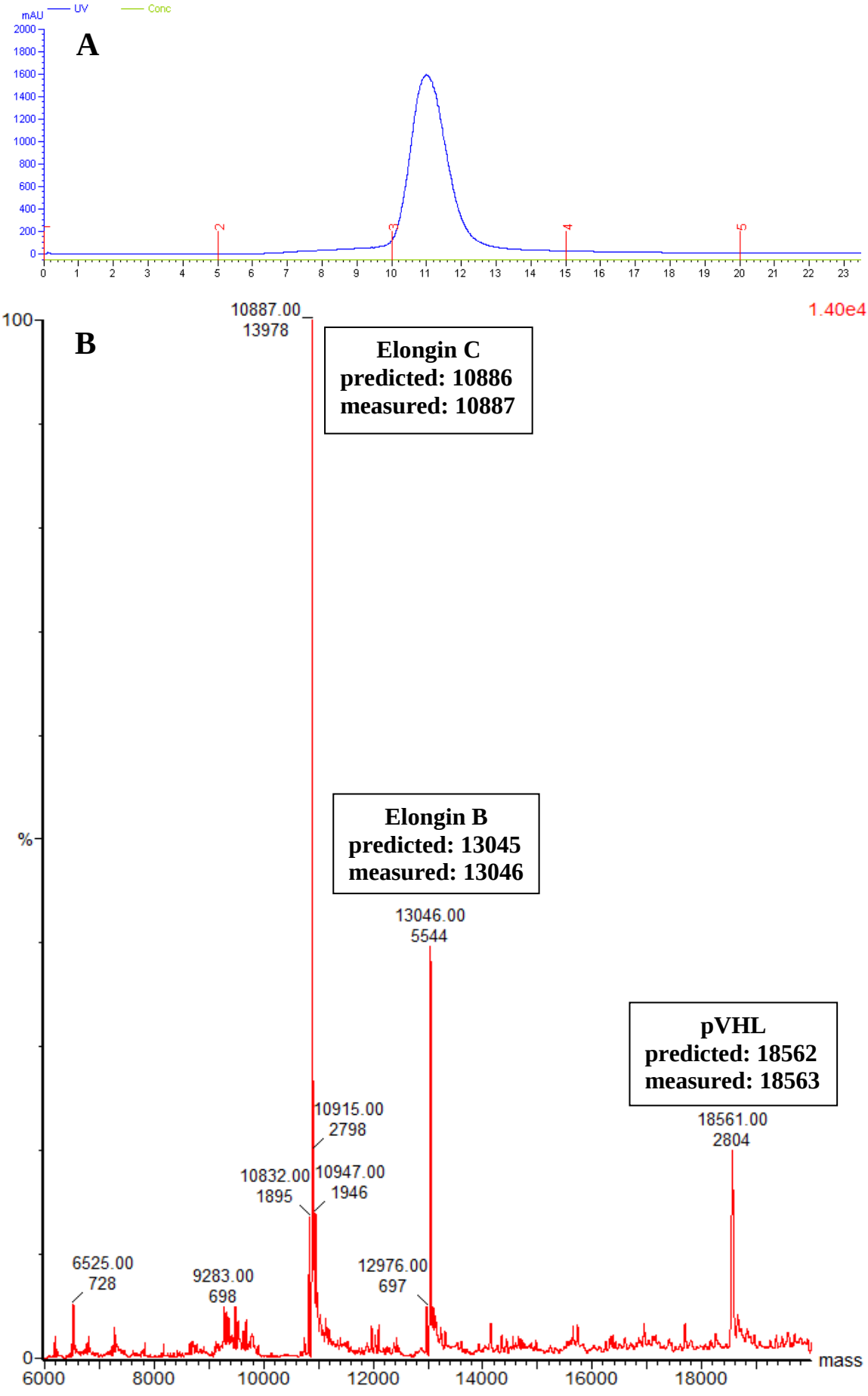
A
mAU
UV
Conc
B
1.40e4
10887.00
13978
Elongin C
predicted: 10886
measured: 10887
Elongin B
predicted: 13045
measured: 13046
13046.00
5544
pVHL
predicted: 18562
measured: 18563
18561.00
2804
10915.00
2798
10832.00
1895
10947.00
1946
6525.00
728
9283.00
698
12976.00
697
%
mass

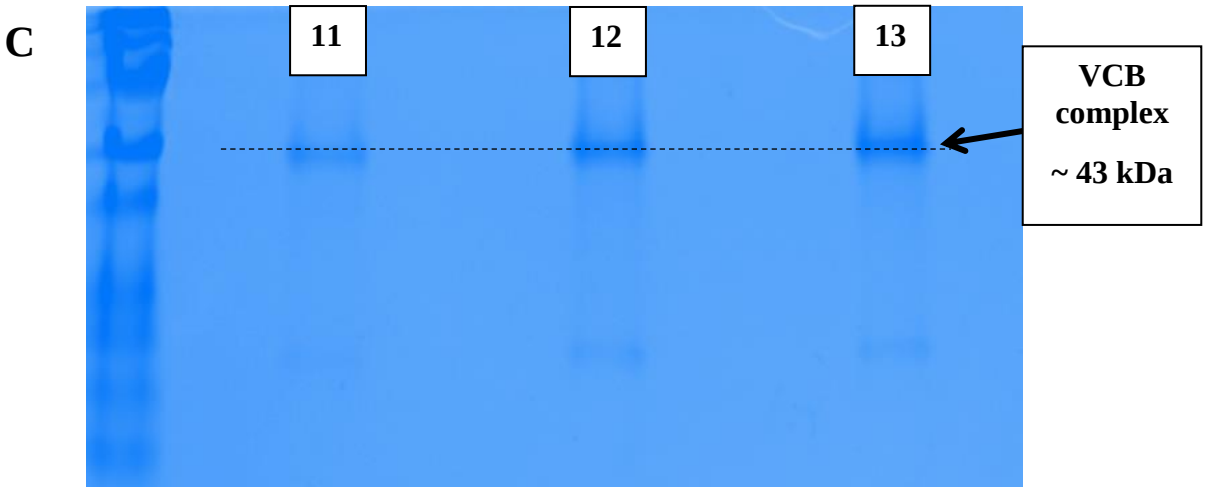

Figure 2.12. VCB production and characterisation. ***(A)*** *Chromatogram trace of VCB after elution from the glutathione S-transferase column.* ***(B)*** *Deconvoluted LC-MS spectrum of VCB in the positive ion electrospray ionisation mode. For experimental details, check section* ***9.2.1.1****.* ***(C)*** *Native gel showing the VCB complex formation. Gel lanes were loaded with samples from fractions 11, 12, and 13 as shown in* ***(A)****. Lane 1 contained a PageRuler Prestained Protein Ladder 10-170 kDa, Thermo Scientific.*

2.2.5.2. Fluorescence Polarisation Assay Optimisation

In order to study the binding of peptides and ligands to VCB, a fluorescence polarisation-based assay was developed and optimised based on that previously reported.[132] Fluorescence polarisation is a technique commonly used for analysing enzyme-ligand interactions. In this case, a fluorescent ligand (tracer) binds to the enzyme and is excited by plane polarised light. The polarisation of the emitted light gives an indication of the extent of binding of the tracer to the enzyme. If the tracer is bound, a larger complex is formed, giving slower tumbling in solution and a high degree of polarisation. Conversely, unbound tracer is smaller and tumbles faster, giving a low degree of polarisation of the emitted light **(Figure 2.13)**.[133]

A hydroxyproline fluorescent peptide (FAMDEALAHyp-YIPD-NH_2), which mimics hydroxylated CODD binding to pVHL, was selected as a tracer fluorescent reporter.[132] A

dose response experiment was first performed to determine the dissociation constant (K_D) for VCB binding to the fluorescent tracer. Several concentrations of tracer were investigated to select the concentration that gives the best signal for use in subsequent experiments. VCB was titrated to fixed concentrations of the fluorescent tracer and the changes in milliporisation units (mP) between the bound samples and the free tracer were plotted using GraphPadPrism. The dose-response curves were fitted to a one-site binding model. After determining the best conditions for the tracer, competitive binding assays were conducted by titrating increasing concentrations of competing ligands to a fixed (optimal) tracer and VCB concentrations. Dose-response curves yielded IC_{50} values. Aqueous DEALA-Hyp-YIPD-NH_2 (hydroxylated CODD of HIF-1α) was used as a positive control. Details are given in the Materials and Methods.

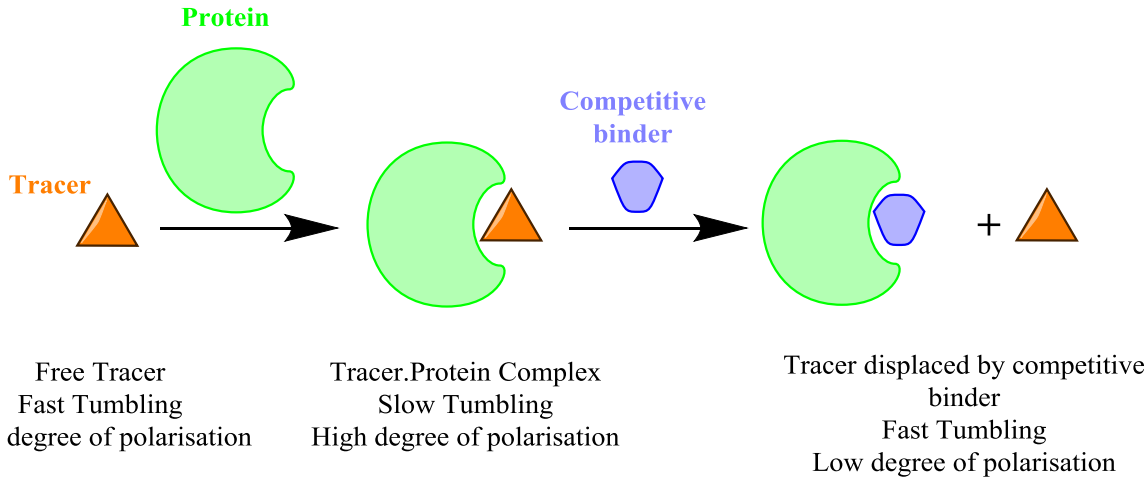

Figure 2.13. Scheme illustrating the principle of competitive binding assays by fluorescence polarisation.

2.2.5.3. Studies on VCB Interactions with PHD2 Binding Partners

The peptides identified as interacting partners of PHD2 (eEF2 and Rbp1) were screened for VCB binding (by Dr Lucia Serran) using the optimised fluorescence polarisation assay described above. The unmodified peptides were identified to be very weak binders to

VCB with IC_{50} > 400 µM. When Rbp1 was hydroxylated on its proline ring, its binding affinity to VCB increased significantly, relative to the unhydroxylated Rbp1, with an IC_{50} of 6 µM, indicating that proline hydroxylation is important for VCB binding. eEF2 contains two proline residues in its sequence, when each proline ring was hydroxylated separately, eEF2 binding affinity to VCB increased relative to the unhydroxylated peptide with an IC_{50} of 84 µM and 74 µM, respectively. Interestingly, when both prolines were hydroxylated, eEF2 binding to VCB was tighter with an IC_{50} of 24 µM **(Figure 2.14)**.

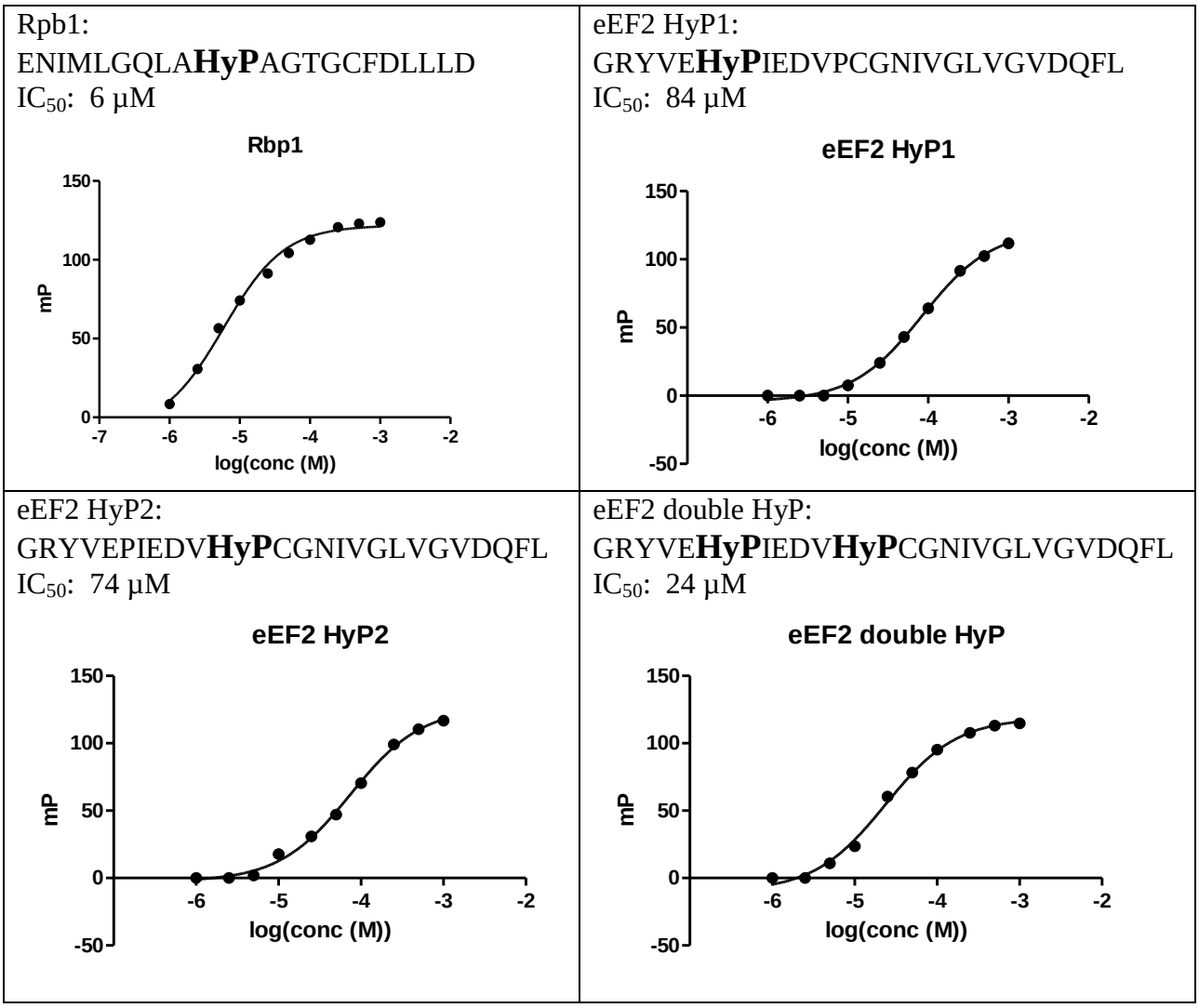

Figure 2.14. IC_{50} plots of the binding of the peptidic binding partners to VCB as assessed by fluorescence polarisation analyses. *Assays were performed by Dr Lucia Serran. Peptides were produced by Kerstin Lippl.*

Crystallographic analyses of VCB in complex with its natural binding partner, hyCODD, structure reveal that HIF-1α residues 561-575 adopt a β-strand-like extended conformation and interact with the β domain of pVHL, making five backbone-backbone hydrogen bonds, in the HIF-1α.VCB complex (PDB IDs: 1LQB/1LM8).[131, 134] The hydroxyproline-564 of HIF-1α (Hyp-564) is almost entirely buried, making multiple van der Waals interactions with Trp-88_{pVHL}, Tyr-98_{pVHL} and Trp-117_{pVHL}.[47] Importantly, Hyp-564 forms hydrogen bonds with the Nδ of His-115_{pVHL} and the OH group of Ser-111_{pVHL} (2.7 A°), both of which appear to be key residues for the strict requirement for hydroxyproline. In the vicinity of Hyp-564, the backbone of HIF-1α is held in place through extensive hydrogen bonds with both backbone and side-chain interaction with pVHL **(Figure 2.15)**.[135] The results suggest that pVHL can interact with other partners beside its natural HIF binding partner. This is of interest because of the in-cell observations with Rpb1[123] and eEF2[127] and their effect on the HIF system-mediated response which is, at least in part, due to their interactions with the PHD as well as pVHL.

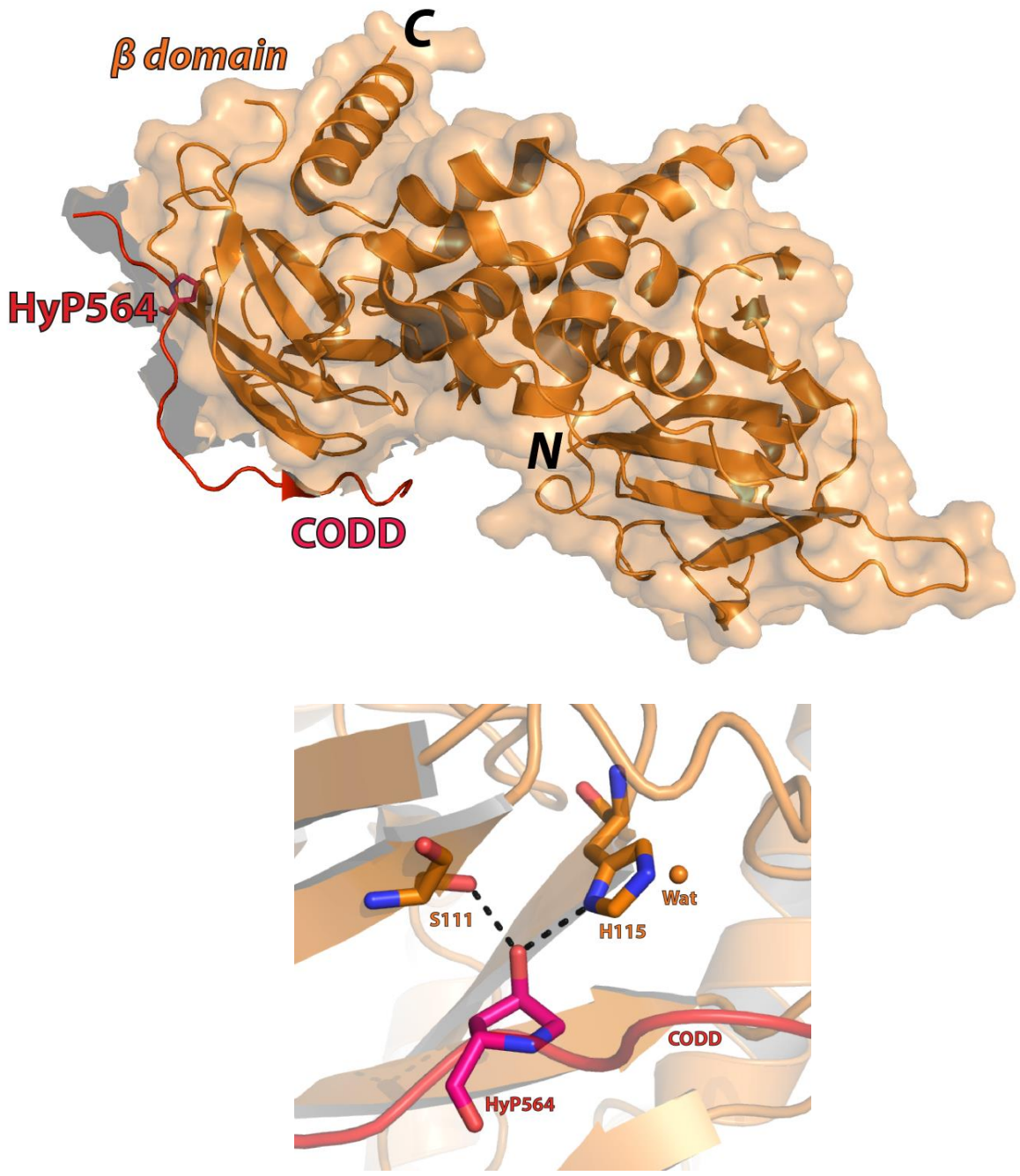

Figure 2.15. View from a crystal structure of pVHL.CODD complex. (PDB ID: 1LM8).[134] *The interactions between the hydroxylated proline of CODD and pVHL are highlighted in a close-up view (lower figure).*[13]

2.3. Summary and Perspectives

Overall, insights into the binding requirements and substrate selectivity of PHD2, and by implication other PHD isoforms, and the VCB complex were obtained. The results presented in this chapter inform on the requirements for PHD2 substrate selectivity. CODD and NODD binding induces different interactions with PHD2 including changes in the β2β3 region and the α3-α4 regions. Since the interaction in the *C*-terminal region differs amongst PHD isoforms, it is possible that isoform-selective PHD inhibition could be achieved. A single substitution, as in the case of P317R PHD2 or R396T PHD2, can alter the selectivity of PHD2 towards its ODD substrate. Those changes are linked to specific disease phenotypes [*i.e.* erythrocytosis (P317R PHD2)[115] or breast cancer (R396T PHD2)[114]]. Wildtype PHD2 is selective towards CODD over NODD, a property conserved in the *Trichoplax adhaerens* PHD. Human CODD was able to bind and be efficiently hydroxylated by taPHD; however, NODD only binds weakly and was a poor substrate for taPHD. This is consistent with previous work[118] and the proposal that CODD might have evolved before NODD. Studies on alternative (non-HIF) partners of PHD2 imply that PHD2 is selective in terms of its substrate requirement; however, peptides (Rbp1 and eEF2) reported by others[123, 127] as PHD substrates were able to bind to PHD2. Such binding might alter PHD2 activity by modulating substrate binding. Interestingly, some of PHD2-interacting partners were able to bind to VCB in their hydroxylated form, indicating that they might interfere with the HIF system at different levels *in vivo*.

2.4. Materials and Methods

2.4.1. Protein Production

The catalytic domain of human PHD2 (residues 181-426) was produced and purified as previously reported.[110] The VCB complex was produced as described in the text.[131]

2.4.2. Competitive Hydroxylation Assays

Competition assays were performed by matrix-assisted laser desorption/ionisation time-of-flight mass spectrometry (MALDI-TOF MS) using a Waters® Micromass® MALDI micro MX™ mass spectrometer. PHD2-$_{181-426}$ (2 μM) was incubated with a 19mer HIF1α NODD or CODD peptide (50 μM, CODD sequence: DLDLEMLAPYIPMDDDFQL-NH_2, NODD sequence: DALTLLAPAAGDTIISLDF-NH_2) in the presence of Fe(II) (50 μM), 2OG (300 μM), ascorbate (4 mM) in 50 mM Tris (pH 7.5) at 37 °C. Reactions were quenched with formic acid (1 % *v*/*v*) at a time-point within the linear region of enzymatic activity. HIF-1α NODD and CODD hydroxylation levels in the presence and absence of putative competitive peptides (500 μM) were quantified using MassLynx™ V4.0.[109-110]

2.4.3. Fluorescence Polarisation Assays

Two-fold serial dilutions of PHD alternative substrates were made in 100% DMSO (1 mM - 1 μM). For polarisation displacement assays, 9 μL of 1 μM VCB (450 nM final), 2 μL of ligands (10% DMSO final), and 9 μL of 278 nM FAM-DEALAHypYIPD-NH_2 were added to a 384 well plate (Corning 3575). The plate was then shaken for 1 minute, and centrifuged for another minute before reading fluorescence polarisation on a PHERAstar FS reader (excitation 485 nm, emission 520 nm). Wells containing VCB, DMSO vehicle (10 % final) and FAM-DEALAHypYIPD-NH_2 served as maximum polarisation (or minimum displacement). Wells containing buffer in place of VCB, DMSO vehicle and FAM-

DEALAHypYIPD-NH_2 served as minimum polarisation (or maximum displacement). Each experiment was conducted in triplicate. Compound dose-response curves were fitted using GraphPad Prism 5 using competitive one-site fitting models.[136]

2.4.4. NMR Experiments

Nuclear Magnetic Resonance (NMR) spectra were recorded using a Bruker AVIII 700 MHz NMR spectrometer equipped with a 5-mm inverse cryoprobe using 5 mm diameter NMR tubes (Norell) or 3 mm MATCH NMR tubes (Cortectnet). Data were processed with Bruker 3.1 software.

2.4.4.1. ^{1}H CPMG NMR Experiments

Typical experimental parameters for Carr-Purcell-Meiboom-Gill (CPMG) NMR spectroscopy were as follows: total echo time, 40 ms; relaxation delay, 2 s; and number of transients, 264. The PROJECT-CPMG sequence as described by Aguilar *et al.* was applied (90°x−[τ−180°y−τ−90°y−τ−180°y−τ]*n*−acq).[137] Water suppression was achieved by pre-saturation. Assay mixtures contained 50 µM *apo*-PHD2 supplemented with 80 µM Zn(II) and 400 µM of peptidic substrate buffered in 50 mM Tris-D_{11} (pH 7.5) and 0.02 % NaN_3 in 90 % H_2O and 10 % D_2O.

2.4.4.2. ^{13}C-2OG and ^{13}C-NODD/CODD Displacement Experiments

2OG was uniformly ^{13}C-labelled and CODD/NODD was uniformly ^{13}C labelled on its proline ring. The CLIP-HSQC sequence was used for 1D HSQC experiments (without ^{13}C decoupling).[111] Relaxation delay was 2 s. The $^{1}J_{CH}$ was set to 160 Hz. A 6.8 ms Q3.1000 180-degree pulse was used and selective irradiation was applied at the selected chemical shift.

2.4.4.3. 2OG Turnover Monitoring

Reaction components (20 µM *apo*-PHD2, 50 µM $(NH_4)_2Fe(SO_4)_2$, 500 µM HIF-1$\alpha_{556–574}$, 500 µM 2OG, and 1 mM ascorbate) were prepared in Tris-D_{11} buffer (pH 7.5, 50 mM). The reaction was carried out at 298 K in a 5 mm diameter NMR tube (Norell), and initiated by addition of 2OG. Spectra were obtained at 150 s intervals and integrated using absolute intensity scaling to monitor changes in the intensity of signals of interest. Synthetic hydroxylated CODD (Severn Biotech) is identical to the enzymatically produced hydroxylated CODD.[27, 110]

Chapter 3. Studies on the Product Release Mechanism of PHD2

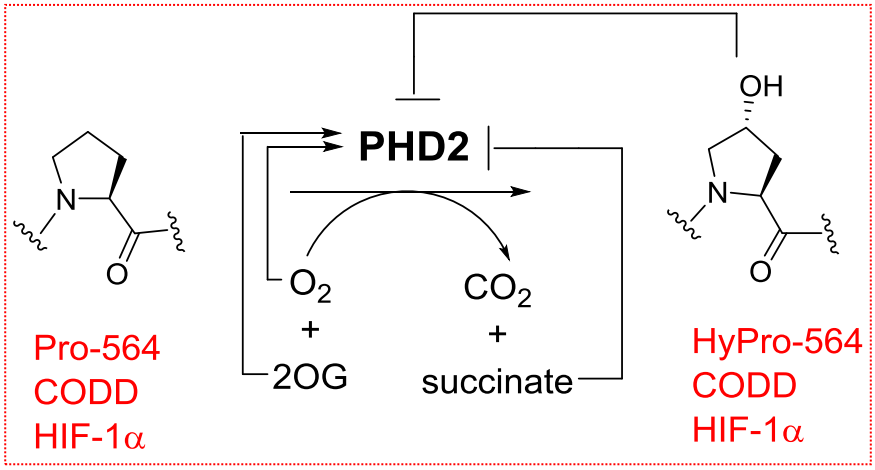

Chapter 3. Contents

3.1. Introduction

The human PHDs are proposed to be biochemically adapted to their roles as hypoxia sensors.[12] However, PHD activity has also the potential to be regulated by 2OG and Fe(II) availability as well as by inhibition by succinate (and related metabolites).[138] Complementary to Fe(II) and 2OG binding, more varied structural elements are involved in substrate binding with PHD2 (and by implication the other PHDs). Substrate binding involves substantial induced fit, including, at least, the β2β3 loop and the *C*-terminal regions **(Figure 3.1)**.[24, 32] Biochemical analyses have revealed that PHD2 reacts unusually slowly with dioxygen[23] and differentiates in the binding of NODD and CODD.[139] It has also been observed that prolyl hydroxylated CODD (hyCODD) is a weak inhibitor of PHD2-catalysed NODD hydroxylation.[139b] Accordingly, it was important to investigate the differential binding selectivity, if any, of CODD and hyCODD to PHD2 and study the hyCODD product release process. The results suggest a new feedback mechanism in the HIF system and raise the possibility that, in some circumstances (*i.e.* when 2OG is limiting), binding of hydroxy-HIF-α to the PHDs may limit HIF-α degradation.

3.2. Results

3.2.1. Protein Expression and Purification

The *N*-terminal truncated catalytic domain of wildtype PHD2 ($PHD2_{181\text{-}426}$) was produced and purified as described in **Chapter 2** and used in most of the assays described in this chapter.[139b] A ^{15}N-labelled *C*- and *N*-terminal truncated construct of the catalytic domain of PHD2 (^{15}N-$PHD2_{181\text{-}402}$) was used for protein NMR studies in order to minimise spectral overlap and to reduce transverse relaxation losses to a minimum. Previous studies have

indicated that there were minimal differences in the catalytic activity between PHD2$_{181\text{-}402}$ and the *N*-terminal truncated PHD2$_{181\text{-}426}$.[110, 139b]

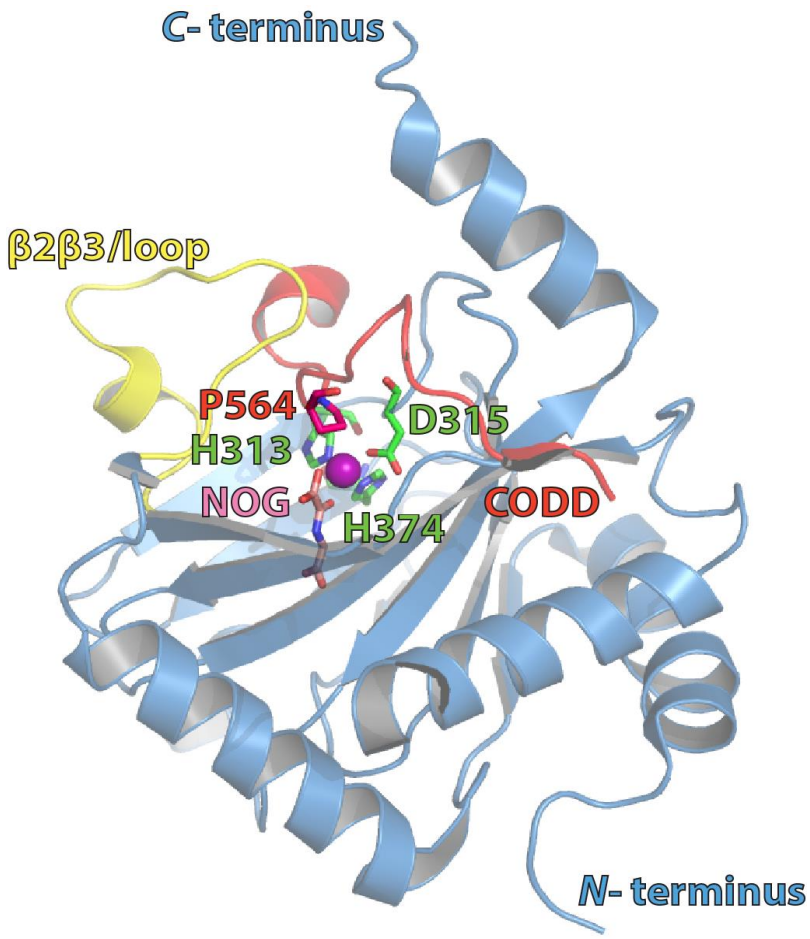

Figure 3.1. View from a crystal structure of PHD2 in complex with CODD (PDB ID: 3HQR).[24]

3.2.2. MS Studies with HIF-1α CODD and hyCODD

The interest in the relative binding of CODD and hyCODD to PHD2 was initially investigated by mass spectrometric analyses. PHD2-catalysed hydroxylation of CODD (HIF-1α$_{556–574}$) can be monitored by electrospray-ionisation mass spectrometry (ESI-MS) under non-denaturing conditions which enable studies on the binding of the substrate, CODD, and cosubstrate, 2OG.[108, 140] Interestingly, the addition of 1 eq. of CODD to 1 eq. of *apo*-PHD2 led to the appearance of *apo*-PHD2.CODD complex. CODD was also observed to bind with a similar affinity to the PHD2.Fe complex. The addition of 1 eq. of 2OG to a mixture of 1:1

apo-PHD2.CODD did not lead to the appearance of an *apo*-PHD2.2OG complex, suggesting that 2OG does not bind *apo*-PHD2 in the absence of the metal, as expected, since 2OG binds to the active site Fe(II) in a bidentate manner for catalysis.[32] When an equimolar mixture of *apo*-PHD2, Fe(II), 2OG, and CODD was analysed, masses corresponding to a ternary complex of PHD2.Fe.hyCODD and a quaternary complex of PHD2.Fe.hyCODD.succinate were observed. The presence of this ternary complex suggests that, aside from CODD, hyCODD also binds to Fe(II)-complexed PHD2 sufficiently tightly to be observed by ESI-MS **(Figure 3.2)**.

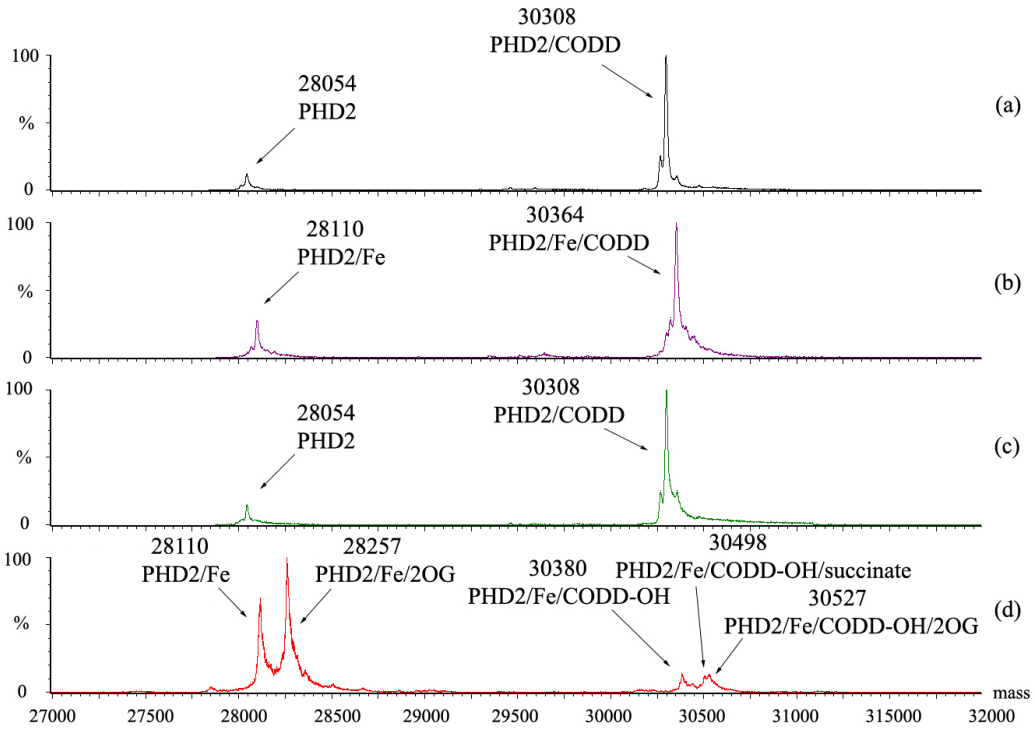

Figure 3.2. Deconvoluted ESI-MS spectra showing substrates and co-factors binding to PHD2. (a) *Black trace: 1:1, PHD2:CODD; (b) purple trace: 1:1:1, PHD2:Fe:CODD; (c) green trace: 1:1:1, (d) PHD2:2OG:CODD; red trace: 1:1:1:1, PHD2:Fe:2OG:CODD. MS experiments were carried out by Dr Jasmin Mecinovic.*

3.2.3. Protein NMR Binding Studies

To investigate substrate and product recognition by PHD2, protein NMR using ^{15}N-labelled PHD2 was used to enable changes in ^{1}H-^{15}N HSQC spectra to be assessed.[113] Firstly, the metal dependence of CODD and hyCODD binding to PHD2 was investigated in the presence and absence of Zn(II), which is a catalytically inactive Fe(II) analogue. Both CODD and hyCODD were able to bind *apo*-PHD2. By contrast, 2OG was only observed to bind in the presence of Zn(II) (PHD2.Zn(II)), consistent with the ESI MS studies. Previous work conducted by Dr Ivanhoe Leung showed that both CODD and hyCODD were observed to saturate *apo*-PHD2 and PHD2.Zn(II) at a 2.7-fold molar excess **(Figure 3.3)**. This finding indicates that the binding affinities of CODD and hyCODD to PHD2 are similar and essentially the same in the presence as absence of the active site metal.

3.2.4. 2OG Discriminates in the Binding of CODD and hyCODD to PHD2

The binding of CODD/hyCODD to PHD2 in the presence of 2OG was then assessed. HyCODD only showed weak binding in the presence of both the metal Zn(II) and 2OG (PHD2.Zn.2OG) as judged by ^{1}H-^{15}N HSQC titration **(Figure 3.3)**. However, under the same conditions, with CODD at a 2.7-fold molar excess, the complex of PHD2.Zn.2OG.CODD was observed as expected based on the crystal structure of PHD2.[24] In a corresponding experiment, it was observed that the ^{1}H-^{15}N HSQC spectra of *apo*-PHD2.hyCODD and *apo*-PHD2.2OG.hyCODD were essentially the same in the presence of excess hyCODD. Because 2OG does not bind to *apo*-PHD2,[27] these results imply that hyCODD binding is blocked by the presence of 2OG at the active site, but that the binding of CODD to PHD2 is not affected by 2OG binding, consistent with anticipated results based on mechanistic grounds.[24, 113]

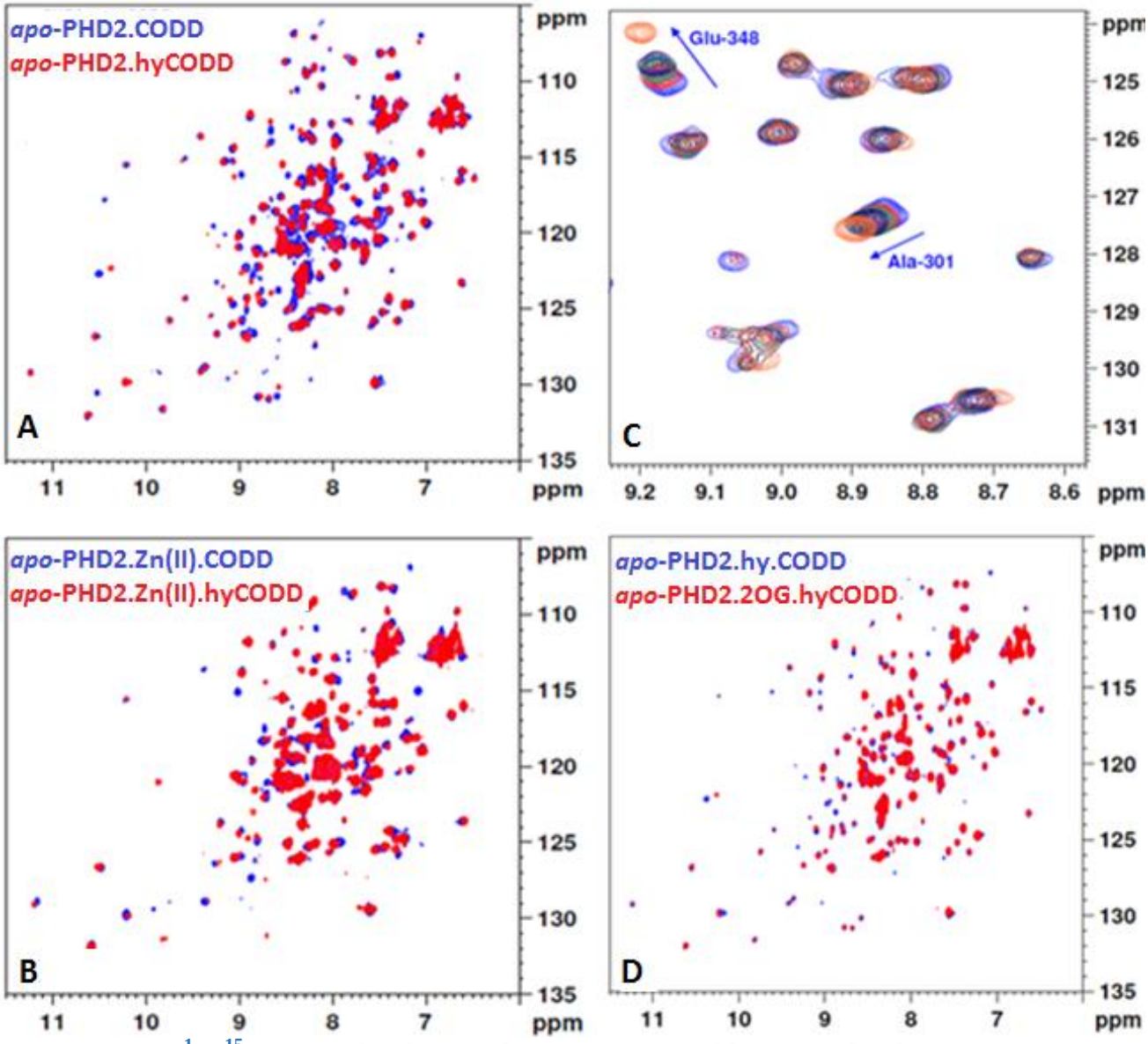

Figure 3.3. ^{1}H-^{15}N HSQC binding studies on CODD and hyCODD binding to PHD2. ***(A)*** *Overlays of the ^{1}H-^{15}N HSQC spectra for apo-^{15}N-PHD2$_{181-402}$.CODD (blue) and apo-^{15}N-PHD2$_{181-402}$.hyCODD (red). Assay mixture contained 150 μM apo-^{15}N-PHD2$_{181-402}$ and 700 μM CODD or 550 μM hyCODD.* ***(B)*** *Overlaying the ^{1}H-^{15}N HSQC spectra for ^{15}N-PHD2$_{181-402}$.Zn.CODD (blue) and ^{15}N-PHD2$_{181-402}$.Zn.hyCODD (red). Assay mixture contained 150 μM apo-^{15}N-PHD2$_{181-402}$, 300 μM Zn(II) and 400 μM CODD/hyCODD.* ***(C)*** *Overlaying a region of the ^{1}H-^{15}N HSQC spectra for ^{15}N-PHD2$_{181-402}$.Zn.2OG with 0 μM hyCODD (blue), 75 μM hyCODD (red), 112.5 μM hyCODD (green) , 150 μM hyCODD (purple) and 300 μM hyCODD (orange).* ***(D)*** *Overlaying the ^{1}H-^{15}N HSQC spectra for an assay mixture of 150 μM apo-^{15}N-PHD2$_{181-402}$ and 400 μM hyCODD (blue), with an assay mixture of 150 μM apo-^{15}N-PHD2$_{181-402}$, 300 μM 2OG and 400 μM hyCODD (red). Samples were buffered with 50 mM Tris-D$_{11}$ at pH 6.6 in 95% H$_2$O and 5% D$_2$O. Protein NMR was carried out by Dr Ivanhoe Leung.*

3.2.5. Fluorescence Polarisation Assay Development

In order to investigate the relative affinities of hyCODD and CODD to PHD2, a fluorescence polarisation assay using an *N*-terminal fluorescein-tagged CODD (CODD*) peptide was developed. A dose response experiment was first performed to determine the dissociation constant (K_D) for PHD2 binding to the fluorescent tracer. Several concentrations of tracer were investigated to select the concentration that gives the best signal for use in subsequent experiments. PHD2 was titrated to fixed concentrations of the fluorescent tracer and the changes in millipolarisation units (mP) between the bound samples and the free tracer were plotted using GraphPadPrism. The dose-response curves were fitted to a one-site binding model **(Figure 3.4)**.

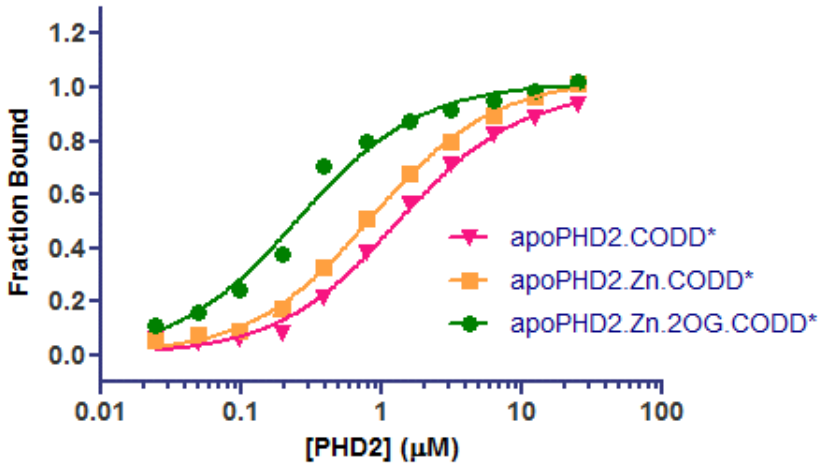

Figure 3.4. Fluorescence polarisation studies of the binding of CODD* to PHD2. *For assay conditions, check Materials and Methods.*

The fraction bound (F) was calculated using **equation (3.1.)**, where *r* is the anisotropy, r_{max} is the maximum anisotropy, r_{min} is the minimum anisotropy, Int_{bound} is the fluorescence intensity in the bound state, and Int_{free} is the fluorescence intensity in the unbound state.[141]

$$F = \frac{r - r_{min}}{R\,(r_{max} - r) + r - r_{min}} \qquad \textbf{(3.1.)}$$

$$R = \frac{Int_{bound}}{Int_{free}} \qquad \textbf{(3.2.)}$$

Anisotropy values were measured across a range of competitor peptide concentrations to calculate their affinities. After determining the best conditions for the tracer, competitive binding assays were conducted by titrating increasing concentrations of competing ligands to a fixed (optimal) tracer.PHD2 concentration. FP assays were conducted with the help and guidance of Dr Tom McAllister. Assay conditions are given in the Materials and Methods section. In the case of *apo*-PHD2.Zn.2OG.CODD near complete competition of the tracer was observed over the concentration range used, indicating tight binding but making EC_{50} determination less reliable. Consistent with NMR data, both CODD and hyCODD were observed to bind *apo*- and metallated-PHD2 equally strongly (within a 2-fold difference). However, in the presence of both Zn(II) and 2OG, hyCODD was observed to bind to PHD2 50-fold less strongly than CODD **(Figure 3.5)**. The assay could be developed and optimised for other PHD isoforms as well as other members of the 2OG-dependent family of oxygenases[142] as it yields important information on substrate competition.

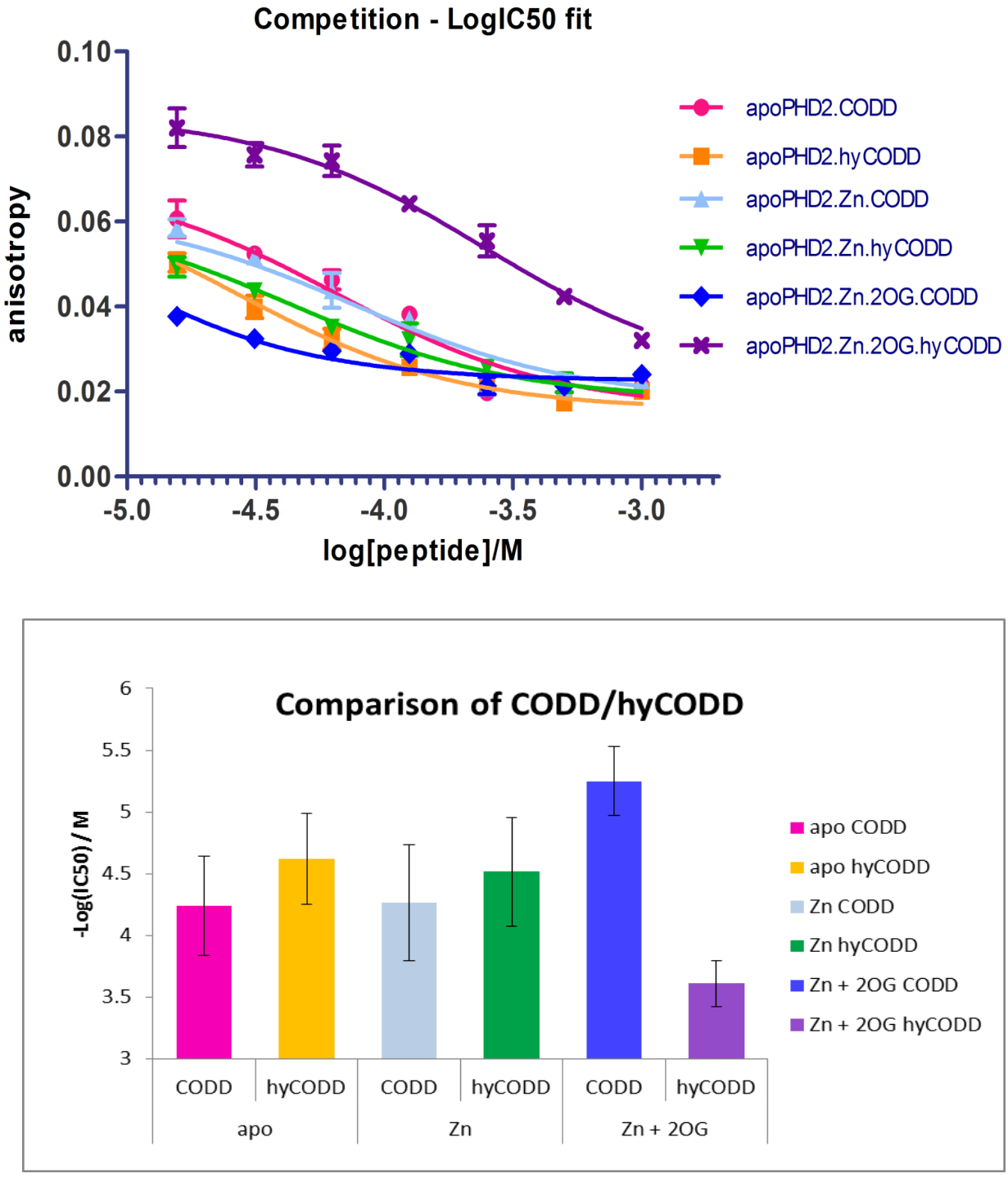

Figure 3.5. Fluorescence polarisation studies of the binding of CODD and hyCODD to PHD2. ***(A)*** *Curves and* ***(B)*** *bar charts showing the changes in CODD and hyCODD binding to PHD2 under various conditions as observed by fluorescence polarisation. For assay conditions, see Materials and Methods.*

3.2.6. Steric Clash Between 2OG and hyCODD

To investigate the competition between hyCODD and 2OG for the same binding site, 2OG displacement studies were conducted by ^{1}H-CPMG NMR.[137] Indeed, hyCODD was observed to displace 2OG under standard screening conditions (10 μM PHD2, 80 μM Zn(II), 10 μM 2OG and 400 μM peptide).[112] Under the same conditions, CODD does not displace 2OG **(Figure 3.6)**, consistent with protein NMR and FP data.

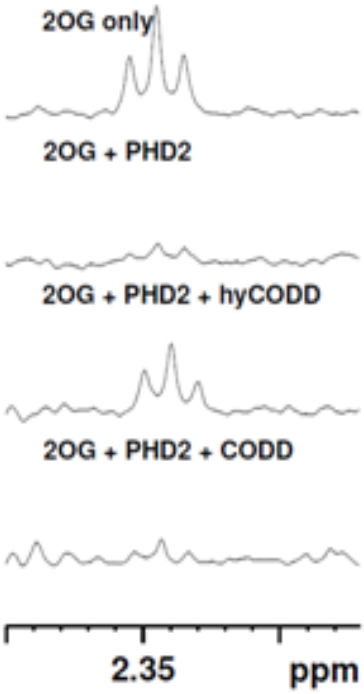

Figure 3.6. Investigations of the binding mode of hyCODD to PHD2 by ^{1}H-edited CPMG reporter displacement analyses in the presence of 2OG. Assay mixture contained 10 μM 2OG; 10 μM PHD2, 80 μM Zn(II) and 400 μM CODD/hyCODD (where necessary), buffered in 50 mM Tris-D_{11}, pH 7.5, in 90 % H_2O and 10 % D_2O.

3.2.7. Investigations on the Binding of the TCA Cycle Intermediates

TCA cycle intermediates were then screened for binding to PHD2. Amongst the screened panel, fumarate and succinate were the only metabolites observed to bind to PHD2. The effect of hyCODD addition to the PHD2.fumarate and PHD2.succinate complexes was then investigated. The binding of fumarate and succinate to PHD2 was only weakly disrupted

by the addition of hyCODD **(Figure 3.7)**, suggesting that the additional carbon of 2OG, compared to fumarate, plays a role in hyCODD displacement. CODD binding did not interfere with neither succinate nor fumarate binding to PHD2. The binding of both succinate and hyCODD to PHD2 is consistent with the quaternary complex observed by non-denaturing MS analysis **(Figure 3.2)**.

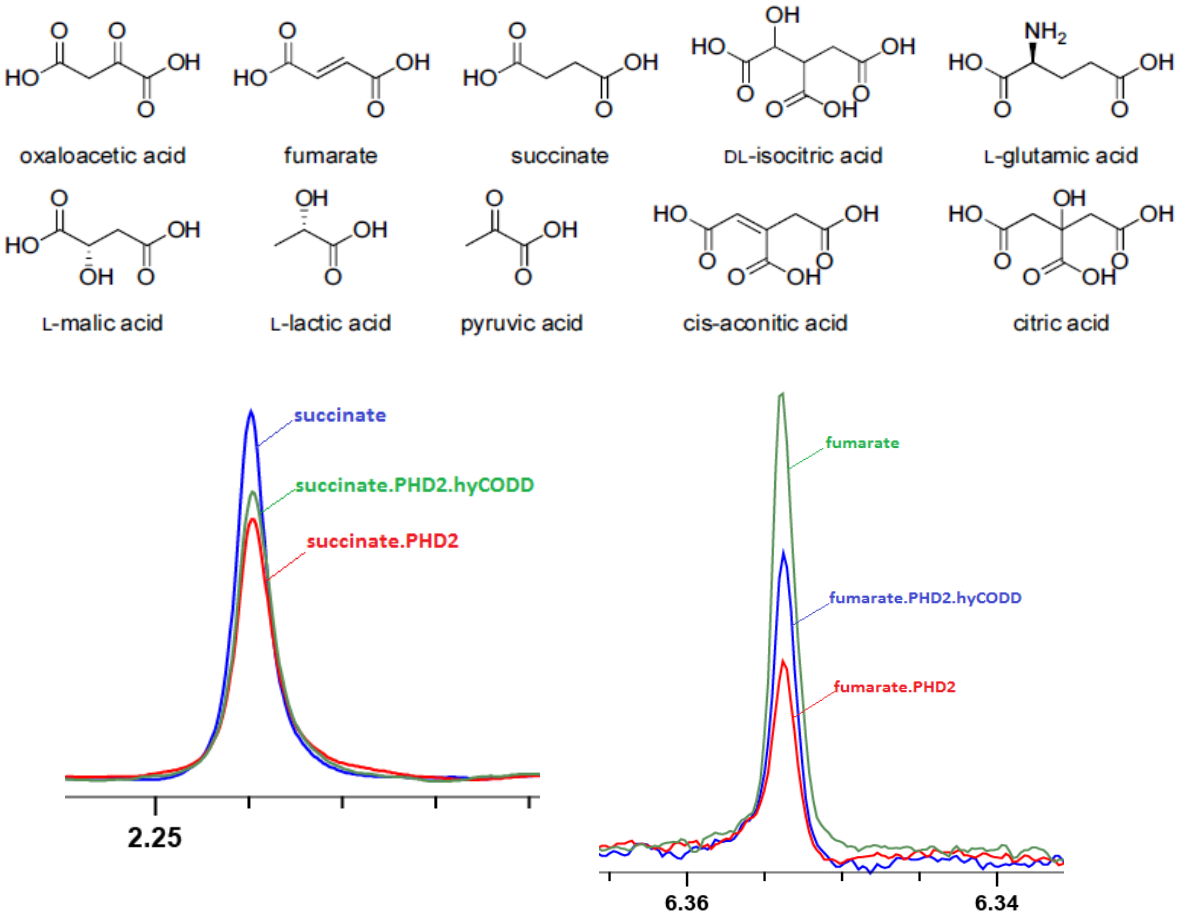

Figure 3.7. Investigations of the role of TCA cycle intermediates on the binding of hyCODD to PHD2. *Assay mixtures contained 10 μM succinate/fumarate (blue), 10 μM PHD2 (red), 80 μM Zn(II) and 400 μM hyCODD (green) buffered in 50 mM Tris-D_{11}, pH 7.5, in 90 % H_2O and 10 % D_2O.*

3.2.8. Studies on the PHD2.NODD Complex

Whether hyCODD competes with either or both 2OG and NODD in the PHD2.Zn.NODD complex was then investigated. 1D CLIP HSQC with selective ^{13}C-inversion NMR analyses were carried out with both ^{13}C-2OG and ^{13}C-NODD.[111] The addition of unlabelled CODD leads to NODD, but not 2OG, displacement, suggesting that CODD binding affinity to PHD2 is tighter that NODD (or less likely the binding of CODD alters the conformation of the protein leading to the displacement of NODD). However, the addition of hyCODD to the mixture leads to the displacement of both 2OG and NODD **(Figure 3.8)**.

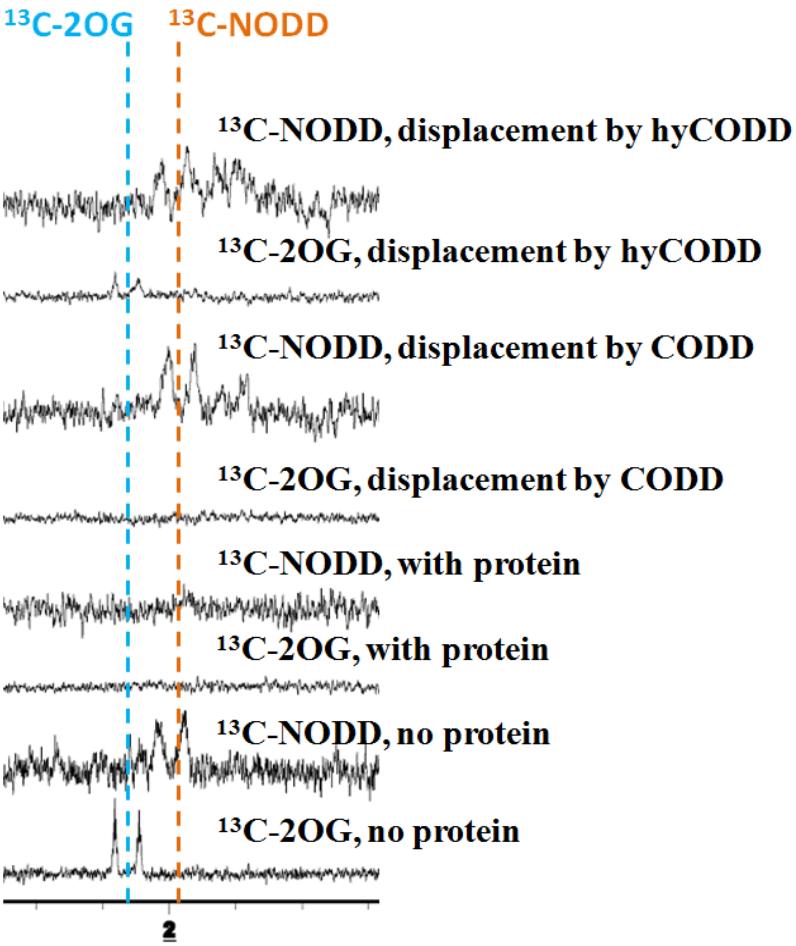

Figure 3.8. 1D-CLIP HSQC with ^{13}C-inversion analyses of the binding of hyCODD to the PHD2.Zn.2OG.NODD complex. *Assay mixtures contained 50 μM 2OG, 50 μM PHD2, 80 μM Zn(II), 50 μM NODD and 400 μM hyCODD (if necessary) buffered in 50 mM Tris-D_{11}, pH 7.5, in 90 % H_2O and 10 % D_2O.*

3.2.9. Inhibition Studies with hyCODD

The effect of hyCODD presence on CODD and NODD hydroxylation was studied by monitoring the PHD2-catalysed 2OG turnover to succinate in the presence of either NODD or CODD as a substrate using ^{1}H NMR.[31] HyCODD was added in around a 5-fold excess to the K_m of the peptidic substrate and pre-incubated for 15 min[139b] in a reaction mixture containing 1 µM *apo*-PHD2, 50 µM Fe(II), 50 µM 2OG, 50 µM peptidic substrate (CODD/NODD) and 500 µM L-ascorbate in 50 mM Tris-D_{11}, pH 7.5. The addition of hyCODD led to 2OG turnover inhibition in the presence of CODD and NODD, with more inhibition being observed with NODD **(Figure 3.9)**.

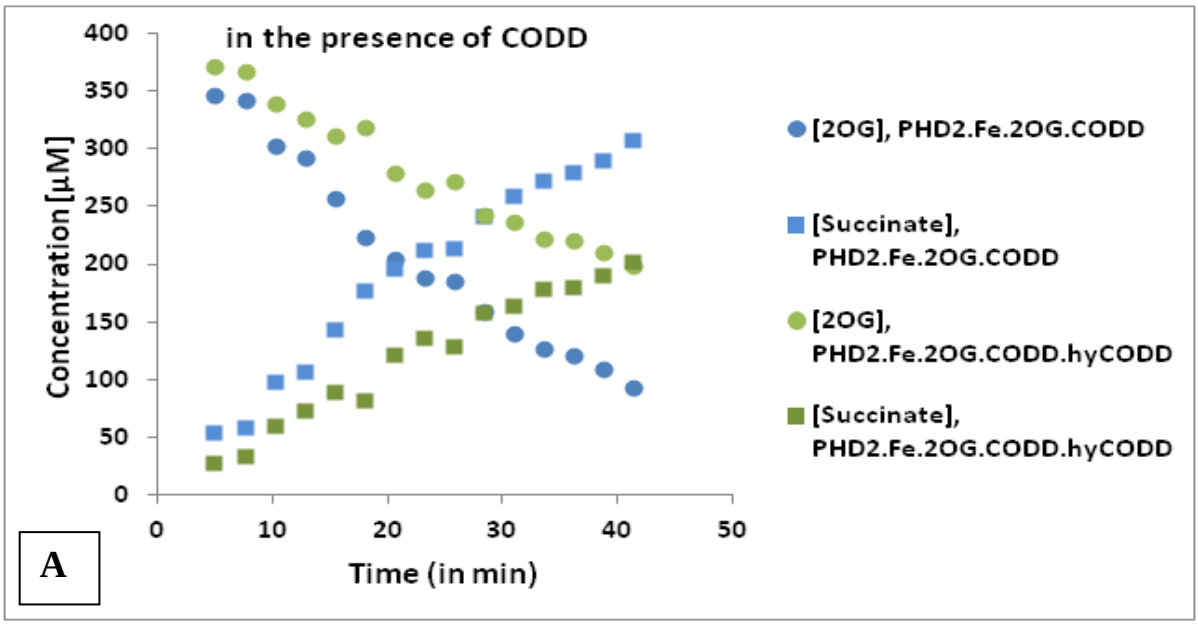

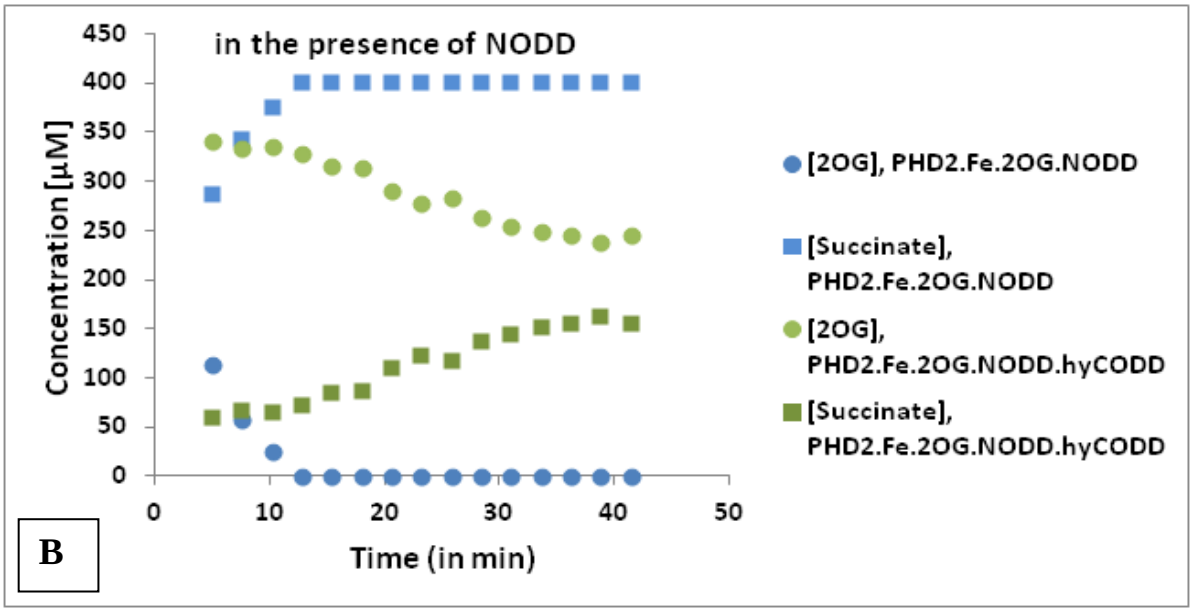

Figure 3.9. 2OG turnover to succinate monitoring in the presence of hyCODD as an inhibitor as observed by ^{1}H NMR in the presence of (A) CODD and (B) NODD as a substrate. *Assay mixtures contained 50 mM Tris-D_{11}, pH 7.5, in 90 % H_2O and 10 % D_2O.*

The overall observations suggest a potential feedback mechanism, in which hyCODD not only competes with CODD/NODD for the peptidic substrate binding site, but also competes with 2OG in the 2OG binding site. It was reported that the affinity of PHD2 to HIF-1$\alpha_{556\text{-}574}$ Pro564 analogues stabilising the C^4-*endo* conformation is five times stronger than for analogues with preference for the C^4-*exo* prolyl conformation.[30] The results obtained here provide a possible mechanism for substrate recognition and product release from PHD2. When CODD is bound to PHD2, the proline residue primarily adopts the C^4-*endo* conformation, possibly due to steric constraints inside the PHD2 active site. This C^4-*endo* conformation is proposed to be required for the reaction of the likely [Fe^{IV}=O] intermediate with the C^4-*trans* prolyl hydrogen atom.[24, 30] However, in *trans*-4-hydroxyproline rings, the stereoelectronic effect arising from the N–C^5–C^4–O *gauche* effect biases the pyrrolidine ring towards the C^4-*exo* conformation in order to maximise delocalisation of electron density

through the σ-bond framework.[30] The adoption of the C^4-*exo* conformation creates a steric clash between hyCODD and 2OG inside the protein active site, which seems capable of disrupting strong protein-protein interactions **(Figure 3.10)**.

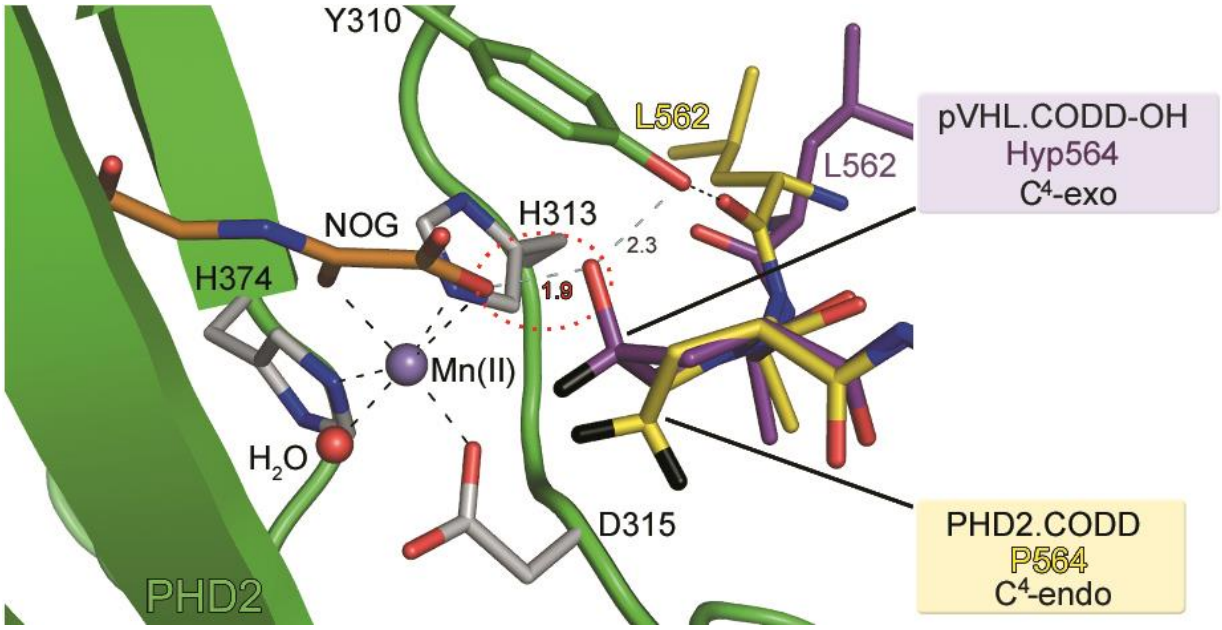

Figure 3.10. View from a crystal structure of PHD2.Mn.NOG.CODD complex (PDB ID: 3HQR)[24] overlaid with hyCODD of pVHL (PDB ID: 1LQB)[135] showing the potential steric clash between NOG and the C^4-*exo* hyPro of CODD-OH. *PHD2 is in green, CODD in yellow, hyCODD in purple, and NOG in orange. Dotted red lines denote steric clash.*

Because both 2OG and Fe(II)/Zn(II) (or other metal ions) bind more tightly to PHD2 than hyCODD (K_D/2OG = 0.9 μM),[112, 143] at a 1:1:1:1 PHD2.metal.2OG.hyCODD complex, hyCODD will be displaced from the protein in the presence of 2OG. However, if there was an accumulation of hyCODD in cell (for instance, due to the blockage of the pVHL in the case of the pVHL disease)[144] or if 2OG availability was limiting (due to isocitrate dehydrogenase (IDH) modifications: IDH1 R132H and IDH2 R172H in the case of glioblastoma for instance),[145] formation of the PHD2.Fe.hyCODD complex may become substantial. The displacement of 2OG might act as a feedback mechanism to limit 2OG availability and HIF hydroxylation. Note an analogous mechanism cannot apply to all 2OG

oxygenases – in the case of the JmjC lysine demethylases, the nascent hydroxylated product (a hemiaminal) is unstable.[146]

3.3. Summary and Perspectives

The results reveal that the presence of 2OG strongly discriminates between the binding of HIF and hyHIF to PHD2. Whilst HIF and hyHIF bind equally strongly to *apo*- and metallated-PHD2, a steric clash with hydroxylated C^4-*endo* proline ring arising from the *gauche* effect can disrupt binding of hyHIF. A fluorescence-based method was developed for tracking peptide binding to PHD2 – the method could be applied to other PHD isoforms and other 2OG dioxygenases.[142] The results suggest a new link with the TCA cycle metabolism and a potential negative feedback mechanism in the HIF system which might be relevant in the case of the VHL disease and IDH1/2 mutations.

3.4. Materials and Methods

3.4.1. Protein Production

For ^{1}H-^{15}N HSQC experiments, a *C*- and *N*-terminal truncated construct of the catalytic domain of PHD2 ($PHD2_{181-402}$) was used in order to minimise spectral overlap and to reduce transverse relaxation losses to a minimum. ^{15}N-enriched PHD2 was produced in glucose-enriched minimal medium (M9 salts). Protein production was induced by addition of 200 μM IPTG when the cell density reached an optical density (OD600) of 0.6–0.8 and left for overnight incubation at 28 °C. Protein purification followed as reported.[23, 32] For all other experiments, the catalytic domain of human PHD2 (residues 181-426) was produced and purified as reported.[110]

3.4.2. Non-Denaturing MS Experiments

For non-denaturing MS measurements, PHD2 solutions were buffer exchanged into 15 mM ammonium acetate buffer (pH 7.5). Spectra were obtained on a Waters Q-TOF mass spectrometer (Q-TOF micro, Micromass) with a chip voltage of 1.70 kV ± 0.2 kV and a delivery pressure of 0.25 psi (1 psi = 6.89 kPa) using a NanoMate HD Robot chip-based nanoelectrospray device (Advion Biosciences). Calibration and sample acquisitions were performed in the positive ion mode in the range of 500–5000 *m/z*. Typically, 15 µM protein samples were sprayed at a cone voltage of 80 V with acquisition/scan times of 10 s/1 s. The pressure at the interface between the atmospheric source and the high vacuum region was 6.60 mbar. Data were processed using MASSLYNX 4.0 (Waters).[24, 147]

3.4.3. NMR Experiments

Nuclear Magnetic Resonance (NMR) spectra were recorded using a Bruker AVIII 700 MHz NMR spectrometer equipped with a 5-mm inverse cryoprobe using 5 mm diameter NMR tubes (Norell) or 3 mm MATCH NMR tubes (Cortectnet). Data were processed with Bruker 3.1 software.

3.4.3.1. ^{1}H CPMG NMR Experiments

Typical experimental parameters for Carr-Purcell-Meiboom-Gill (CPMG) NMR spectroscopy were as follows: total echo time, 40 ms; relaxation delay, 2 s; and number of transients, 264. The PROJECT-CPMG sequence as described by Aguilar *et al.* was applied (90°x−[τ−180°y−τ−90°y−τ−180°y−τ]*n*−acq).[137] Water suppression was achieved by pre-saturation. Assay mixtures contained 50 µM *apo*-PHD2 supplemented with 80 µM Zn(II) and 400 µM of peptidic substrate buffered in 50 mM Tris-D_{11} (pH 7.5) and 0.02 % NaN_3 in 90 % H_2O and 10 % D_2O.

3.4.3.2. ^{13}C-2OG and ^{13}C-NODD/CODD Displacement Experiments

2OG was uniformly ^{13}C-labelled and NODD was ^{13}C labelled on its proline ring. The CLIP-HSQC sequence was used for 1D HSQC experiments (without ^{13}C decoupling).[111] Relaxation delay was 2 s. The $^{1}J_{CH}$ was set to 160 Hz. A 6.8 ms Q3.1000 180-degree pulse was used and selective irradiation was applied at the selected chemical shift.

3.4.3.3. ^{1}H-^{15}N HSQC Experiments

For ^{1}H-^{15}N HSQC experiments, the Bruker sequence *hsqcetfpf3gpsi* was used. Typically, the size of the FID for the ^{1}H dimension was 2048 points, and for the ^{15}N dimension was set as 128, 256 or 1024 points depending on the resolution required. The spectral width was set as 16 ppm (^{1}H) and 40 ppm (^{15}N) respectively, and the centre of the spectrum was set to 4.7 ppm and 120 ppm. $^{1}J_{NH}$ was set to 90 Hz. ^{15}N decoupling was achieved using a 170 μs 90 degree GARP sequence and the high power ^{15}N 90-degree pulse was achieved using a 40 μs GARP sequence. The relaxation delay was 1 second.[113]

3.4.3.4. 2OG Turnover Monitoring

Reaction components (20 μM *apo*-PHD2, 50 μM $(NH_4)_2Fe(SO_4)_2$, 500 μM HIF-1$\alpha_{556–574}$, 500 μM 2OG, and 1 mM ascorbate) were prepared in Tris-D_{11} buffer (pH 7.5, 50 mM). The reaction was carried out at 310 K in a 5 mm diameter NMR tube (Norell), and initiated by addition of 2OG. Spectra were obtained at 150 s intervals and integrated using absolute intensity scaling to monitor changes in the intensity of signals of interest. Synthetic hydroxylated CODD (Severn Biotech) is identical to the enzymatically produced hydroxylated CODD.[27, 110]

3.4.4. Fluorescence Polarisation Assay

Fluorescence polarisation[148] assays used a PHERAstar FS reader (excitation 485 nm, emission 520 nm). Experiments with *apo*-PHD2 were conducted in 50 mM Tris pH 7.5 with 3 µM *apo*-PHD2 and 5% (*v*/*v*) DMSO. For experiments with Zn, 1.5 µM *apo*-PHD2 was used with the addition of $Zn(SO_4)_2.7H_2O$ at a final concentration of 50 µM. For experiments with Zn and 2OG, 0.5 µM *apo*-PHD2 was used with the addition of $Zn(SO_4)_2.7H_2O$ at final concentration of 50 µM and 2OG at a final concentration of 100 µM. Competition assays were used to determine the affinity of CODD and hyCODD for PHD2 using the same buffer conditions and cofactor concentrations as above with the addition of 5% (*v*/*v*) DMSO. A 2-fold dilution series of competitor peptides from 1000 µM to 15.6 µM were used with the following protein concentrations: 3 µM for apoPHD2, 1.5 µM for PHD2.Zn, 0.5 µM for PHD2.Zn.2OG. These data were fitted using a competitive model for the peptides with the top and bottom values of the fit constrained for each condition to be the same for experiments with CODD and hyCODD.

Chapter 4. Inhibition Studies on PHD2

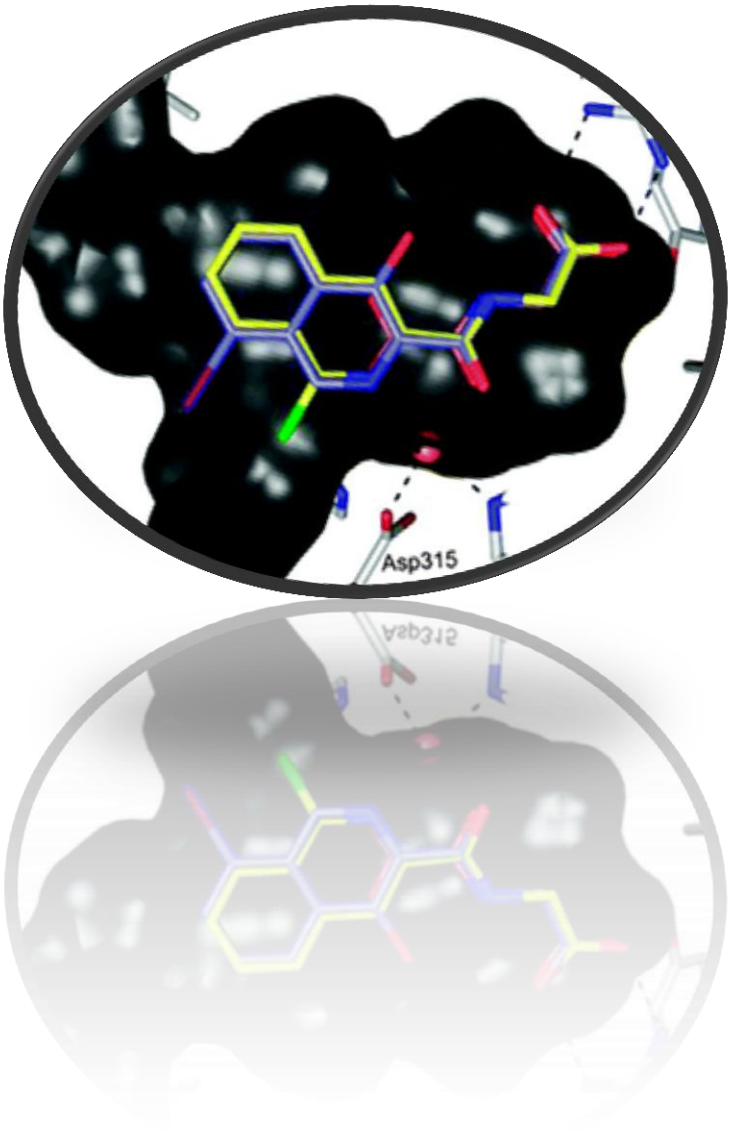

Chapter 4. Contents

4.1. Introduction

PHD inhibition is of interest from the perspective of treating various diseases, including anaemia, ischaemia-related diseases (including coronary heart disease, stroke and diabetic limb ischaemia), gastrointestinal diseases, chondrocytes stabilisation, and wound healing.[13, 126, 149] The first inhibitor to induce HIF-α to be identified was probably (unknowingly) Co(II), which is believed to compete with Fe(II) for binding to the PHDs. However, Co(II) inhibits other 2OG oxygenases as well.[150] A cell permeable (dimethylated) form of *N*-oxalyl glycine NOG (DMOG) was shown to inhibit PHDs, upregulate HIF-α, and promote angiogenesis in animal studies.[151] The available evidence is that small-molecule inhibition of PHD activity is both possible and, at least, not highly toxic over the time period of the current clinical trials.[126] The long-term safety of PHD inhibition is yet to be determined. The specific set of HIF target genes upregulated upon PHD inhibition probably depend on many factors, including the isoforms of HIFs and PHDs present in specific tissues, the relative content of Fe(II), the availability of 2OG, the availability of other TCA cycle intermediates and dioxygen, adaptation processes, and other factors (including pVHL mutations).[138, 144b, 152] In this chapter, studies aim at investigating the mode of inhibition of PHD inhibitors in clinical trials as described.

4.2. Results

Recombinant $PHD2_{181\text{-}426}$ was produced and purified as reported in **Chapter 2**.[109]

4.2.1. Studies on Clinical Metal Chelators

Most of the PHD inhibitors identified to date are bidentate Fe(II) chelators that compete with 2OG for binding at the PHD active site.[126] Some of these inhibitors can chelate iron in solution, and hence their biological effects may be due to iron sequestration.[153]

Deferoxamine (Desferrioxamine DFO) is an iron chelator which is used clinically for the treatment of iron overload and related diseases; DFO has been shown to cause HIF-α stabilisation.[154] Deferasirox (DFR) is a clinical oral iron chelator used to reduce blood iron overload and heavy-metal intoxication.[155] Accordingly, it was of interest to investigate whether HIF-α stabilisation in these cases was PHD2-mediated.

4.2.1.1. PHD2 Inhibition Studies with Deferoxamine and Deferasirox

The inhibition of PHD2 activity by Deferoxamine and Deferasirox was assessed using MALDI-ToF analyses by monitoring the percent hydroxylation of CODD HIF-1α peptide.[109] In a mixture containing 1:1, Fe(II):PHD2 (1 μM), both Deferoxamine and Deferasirox manifest similarly low μM IC_{50} values of 2.38 ± 0.20 μM and 2.44 ± 0.20 μM, respectively. Since Deferoxamine and Deferasirox are iron chelators, their effect on PHD2 activity was assessed using different Fe(II) concentrations. PHD2 inhibition by these compounds was indeed dependent on Fe(II) concentration. At a low Fe(II) concentration (1:1, Fe(II):PHD2), < 10% of the peptidic substrate was hydroxylated by PHD2 in the presence of 100 μM of either Deferoxamine or Deferasirox. However, using higher Fe(II) concentration (75:1, Fe(II):PHD2), around 70 % of CODD was hydroxylated indicating an increased activity of PHD2 and a lower inhibition effect of Deferoxamine and Deferasirox. Accordingly, the IC_{50} of Deferasirox was determined at a higher Fe(II) concentration (25 μM), (IC_{50} = 53.1 ± 12.5 μM), and it was found to be 25-fold higher than the value observed at 1:1, Fe(II):PHD2 **(Figure 4.1).** (Inhibition studies were carried out by Kerstin Lippl). The Fe(II)-dependence of PHD2 inhibition by Deferoxamine and Deferasirox indicates that these compounds act either by sequestering metal in solution and thus inhibiting PHD2-mediated CODD hydroxylation, and/or by chelating to the active site metal and affecting the protein activity. Binding studies of these compounds to recombinant PHD2 were thus conducted.

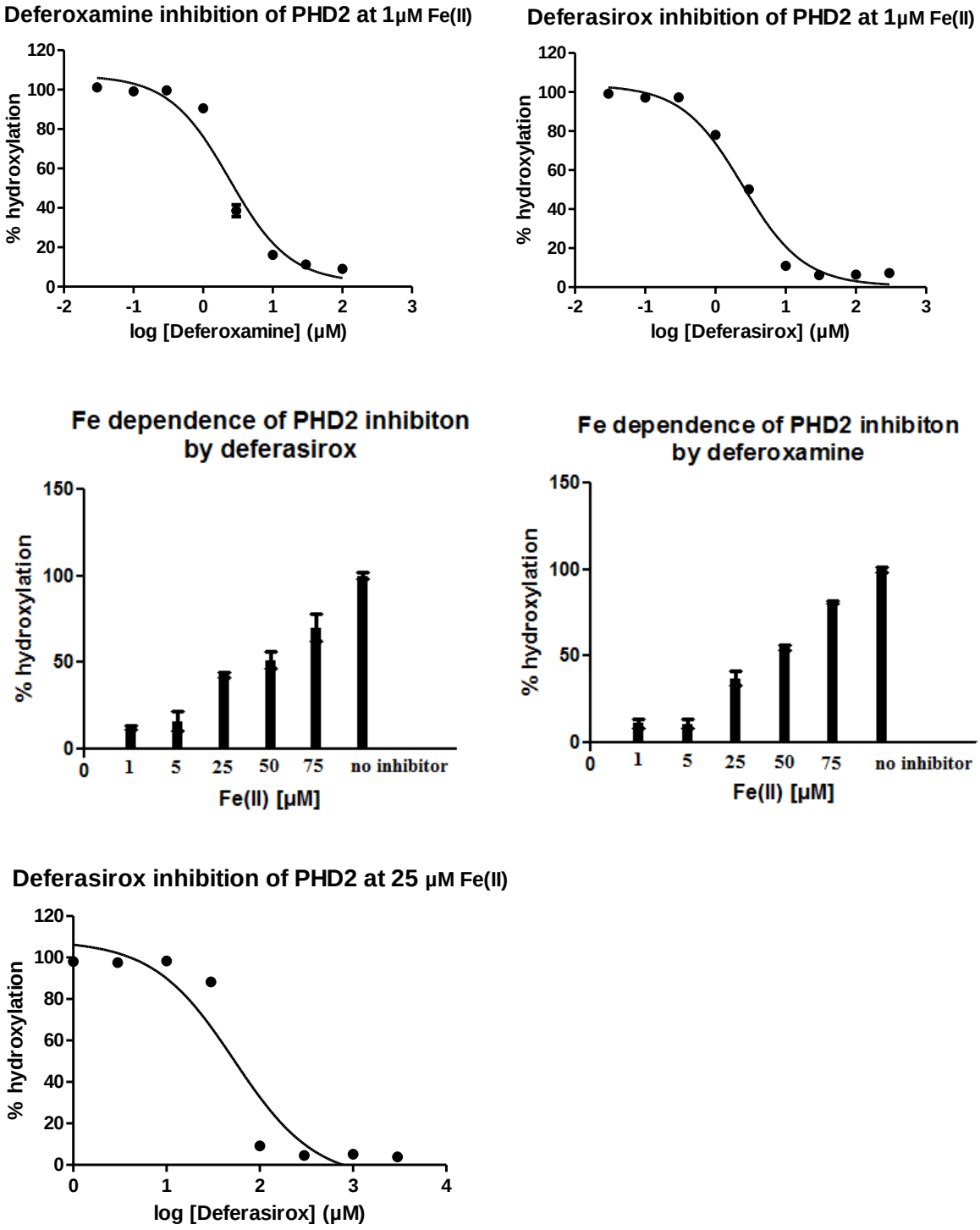

Figure 4.1. Inhibition studies of PHD2-mediated CODD hydroxylation in the presence of Deferasirox and Deferoxamine as monited by MALDI-ToF MS analyses. *For assay conditions, see Materials and Methods.*

4.2.1.2. Investigating the Binding of Deferasirox to PHD2

The binding of Deferasirox to PHD2 was studied by ligand-observe NMR spectroscopy.[74] The addition of PHD2 to a sample of Deferasirox led to line broadening and signal reduction of the Deferasirox peaks as observed by ^{1}H NMR analyses, indicating that Deferasirox binds to PHD2 **(Figure 4.2)**. This obervation is consistent with wLOGSY analyses whereby Deferasirox shares the same NOE sign with PHD2 in a sample containing 400 μM Deferasirox and 20 μM PHD2, suggesting the formation of a protein.compound complex **(Figure 4.5)**.[83] The addition of 2OG, PHD2 cosubstrate, to a mixture of Deferasirox and PHD2 led to some displacement of Deferasirox from its PHD2 binding pocket. Interestingly, the addition of FG-4592,[126] a strong inhibitior of PHD2 currently in clinical trials and a 2OG competitor, did not lead to the displacement of Deferasirox. Both FG-4592 and Deferasirox can bind to PHD2 simultaneously and FG-4592 binding seems to enhance the binding of Deferasirox to PHD2. The metal chelation properties of Deferasirox were then investigated; the addition of 50 μM Zn(II) to a solution containing free Deferasirox led to line broadening of Deferasirox peaks **(Figure 4.3)**. The combined data suggest that Deferasirox is acting through both general metal sequestration and direct binding to PHD2.

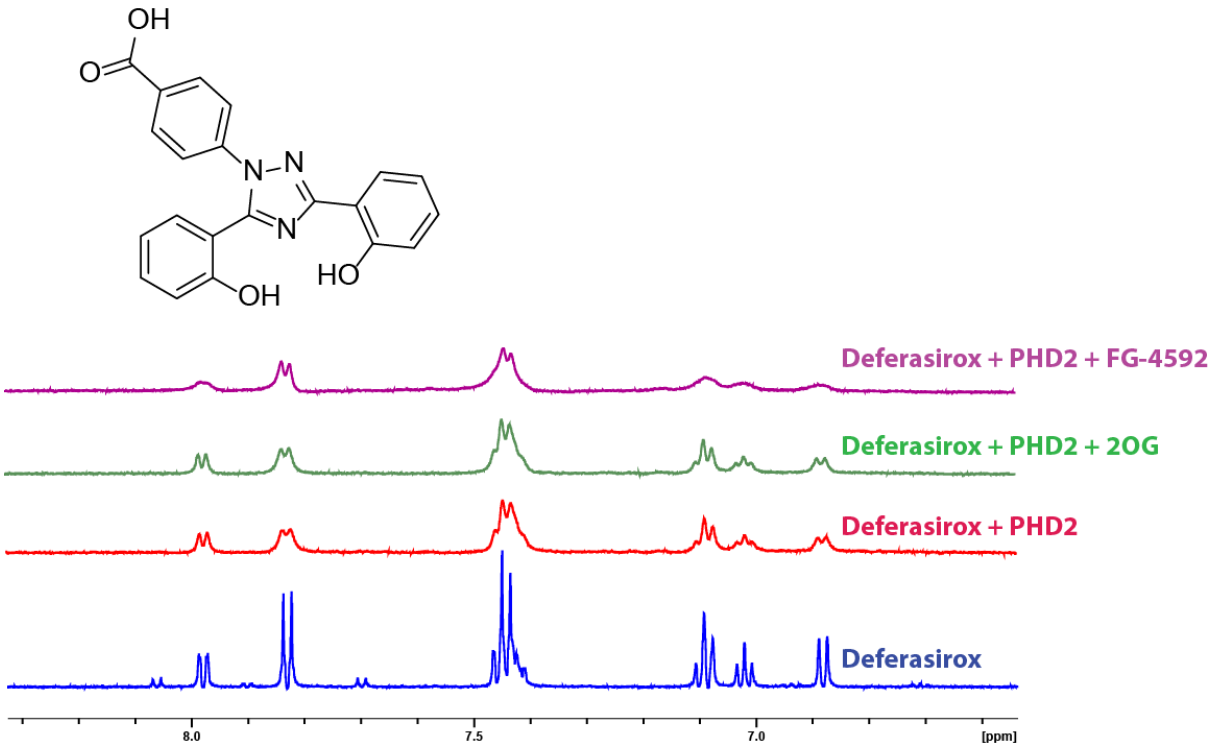

Figure 4.2. ^{1}H excitation sculpting suppression NMR analyses of Deferasirox binding to PHD2. *Blue trace: 400 µM Deferasirox, red trace: 400 µM Deferasirox and 20 µM PHD2, green trace: 400 µM Deferasirox, 20 µM PHD2 and 20 µM 2OG, purple trace: 400 µM Deferasirox, 20 µM PHD2 and 20 µM FG-4592. Assay mixtures were buffered in 50 mM Tris-D_{11}, pH 7.5, in 10 % D_2O and 90 % H_2O.*

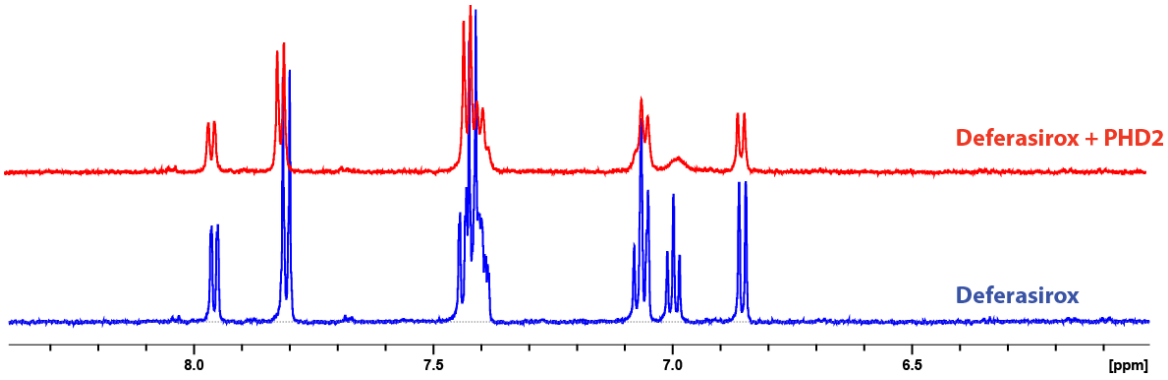

Figure 4.3. ^{1}H NMR analyses of the chelation properties of Deferasirox. Blue trace: 400 µM Deferasirox, red trace: 400 µM Deferoxamine and 50 µM Zn(II). Assay mixtures were buffered in 50 mM Tris-D_{11}, pH 7.5, in 10 % D_2O and 90 % H_2O.4.2.1.3. Investigating the Binding of Deferoxamine to PHD2

4.2.1.3. Investigating the Binding of Deferoxamine to PHD2

The addition of PHD2 to a sample of Deferoxamine leads to little line broadening of the Deferoxamine peaks indicating that Deferoxamine binds only weakly to PHD2 **(Figure 4.4)**. This obervation is consistent with wLOGSY analyses[83] **(Figure 4.5)**, whereby the peaks of Deferoxamine in the presence of PHD2 are less intense than for Deferoxamine alone, suggesting very weak binding. The addition of 50 μM 2OG to a sample containing 400 μM Deferoxamine and 50 μM PHD2 leads to complete signal recovery of Deferoxamine, supporting the proposal that Deferoxamine was only very weakly binding to the PHD2 active site. The small amount of 2OG, relative to the amount of Deferoxamine, capable of displacing Deferoxamine from PHD2 suggests that its weak binding to PHD2 might not be relevant under physiological conditions. In the presence of FG-4592,[126] no Deferoxamine was found to bind PHD2. The combined data suggest that Deferoxamine inhibits PHD2 activity by sequestering metal in solution rather than by direct binding to PHD2.

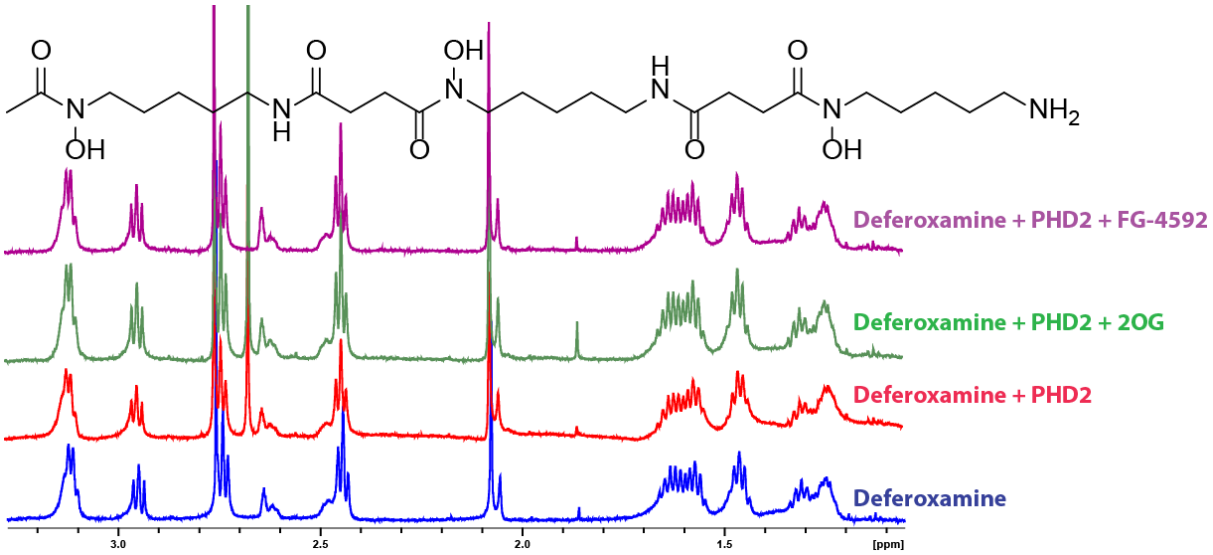

Figure 4.4. ^{1}H excitation sculpting suppression NMR analyses of Deferoxamine binding to PHD2. *Blue trace: 400 μM Deferasirox, red trace: 400 μM Deferoxamine and 20 μM PHD2, green trace: 400 μM Deferoxamine, 20 μM PHD2 and 20 μM 2OG, purple trace: 400 μM Deferoxamine, 20 μM PHD2 and 20 μM FG-4592. Assay mixtures were buffered in 50 mM Tris-D_{11}, pH 7.5, in 10 % D_2O and 90 % H_2O.*

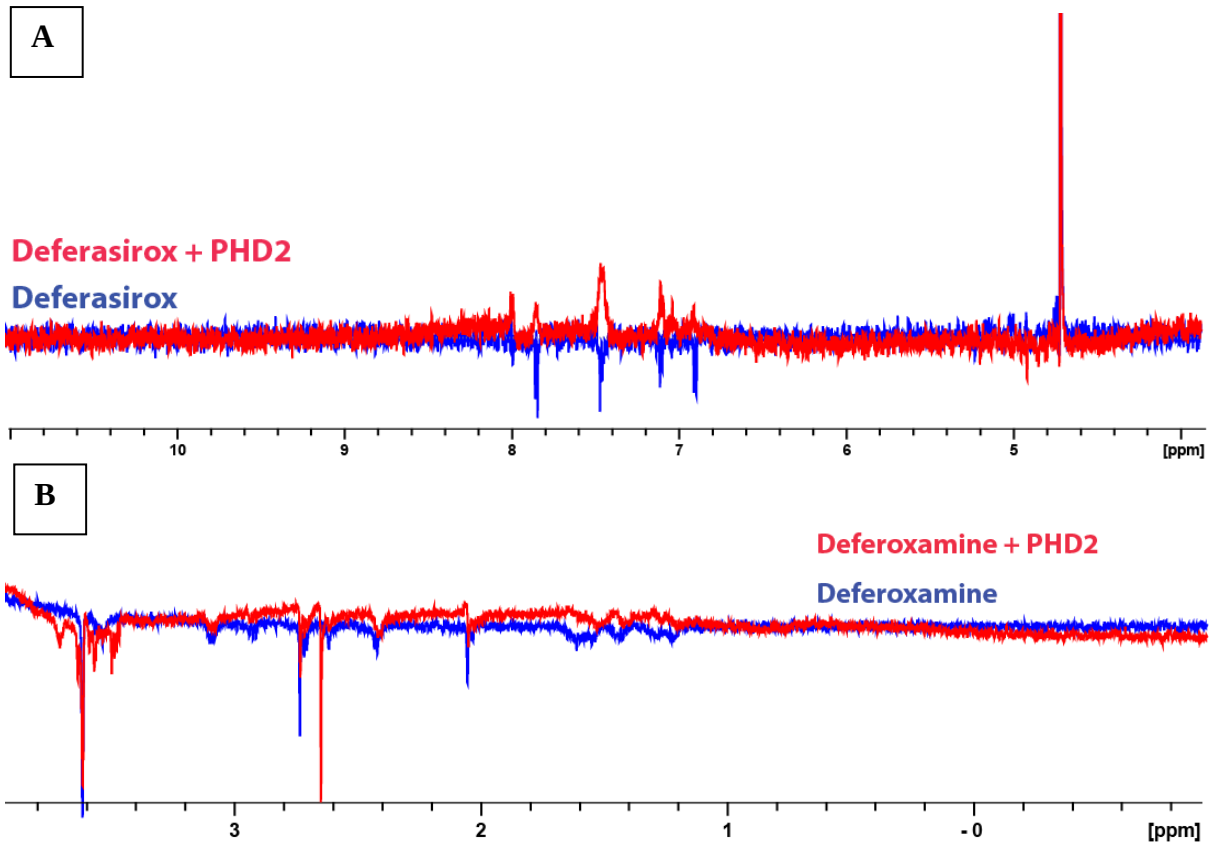

Figure 4.5. wLOGSY NMR analyses of (A) Deferasirox and (B) Deferoxamine binding to PHD2. *Blue trace: 400 μM Deferasirox/Deferoxamine, red trace: 400 μM Deferoxamine/Deferoxamine and 20 μM PHD2.Assay mixtures were buffered in 50 mM Tris-D_{11}, pH 7.5, in 10 % D_2O and 90 % H_2O.*

4.2.2. Studies on Clinical Inhibitors of PHD2

Following studies demonstrating that PHD inhibitors can upregulate HIF-α and hence EPO (and other HIF target genes),[156] pharmaceutical companies have pursued PHD inhibitors as targets for the treatment of anaemia and other hypoxia related diseases.[157] Three PHD inhibitors are now in clinical trials for anaemia treatment.[157b] FG-4592 from FibroGen is currently in phase III, GSK1278863 from GlaxoSmithKline is in phase II, and molidustat from Bayer is in phase II trials.[157d] Given the pleiotropic and complex nature of the hypoxic response and the large number of components involved in the HIF system, it is likely important that clinically used PHD inhibitors are selective as is possible for desired

physiological outcome. Given the differential specificity of the three PHD isoforms over the two prolyl-hydroxylation sites (NODD, Pro-402, and CODD, Pro-564) in HIF-1α,[12] information on NODD/CODD inhibition may shed light on the development of isoform specific inhibitors. Hereafter, comparative studies on the activities and selectivities of PHD inhibitors in clinical trials for anaemia treatment are presented. They partly inform on the mechanism of action of the compounds and will aid in long-term work on the therapeutic manipulation of the natural hypoxic response.

4.2.2.1. Binding Studies on PHD Clinical Inhibitors

FG-4592 was purchased from Selleck Chemicals. FG-2216, IOX-4, GSK1278863, and Molidustat were provided by Dr Marina Demetriades, Dr Cyrille Thinnes, and James Holt-Martyn. FG-2216 is structurally related to FG-4592, sharing the same glycinamide group-side chain and heteroaromatic rings. IOX4 is structurally related to Molidustat. Structures are shown in **Figure 4.6**. Catalytic turnover assays revealed the three clinical compounds (FG-4592, GSK1278863, and Molidustat) to be potent inhibitors of PHD2 in the sub-micromolar range; however, molidustat (and the related compound, IOX4) were approximately ten fold more potent than FG-4592 and GSK1278863 (unpublished data by Dr Tzu-Lan Yeh).

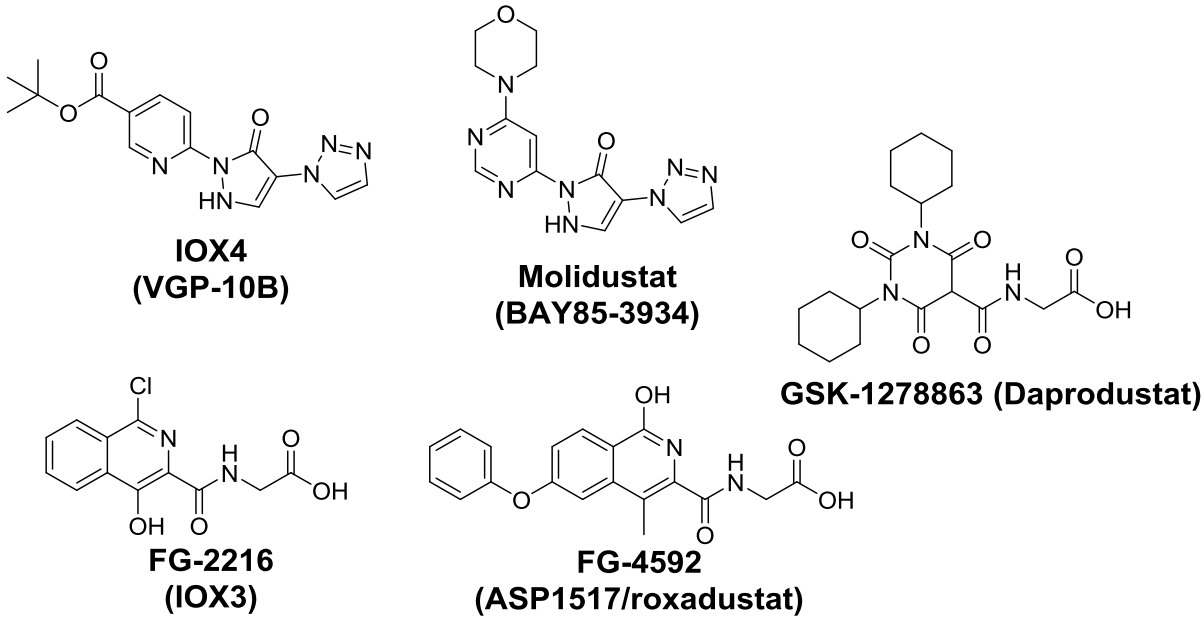

Figure 4.6. Structures of PHD clinical inhibitors and their analogues.

Binding assays using ^{1}H excitation sculpting suppression, ^{1}H CPMG,[137] and wLOGSY[83] methods were used to investigate the modes of inhibitor binding. FG-4592, GSK1278863, Molidustat, and IOX4 were all observed to bind tightly to PHD2 **(Figures 4.7-4.10)**. ^{1}H and wLOGSY NMR analyses were conducted using an excess of ligand to protein, while CPMG analyses were conducted using an equimolar mixture of ligand and protein.

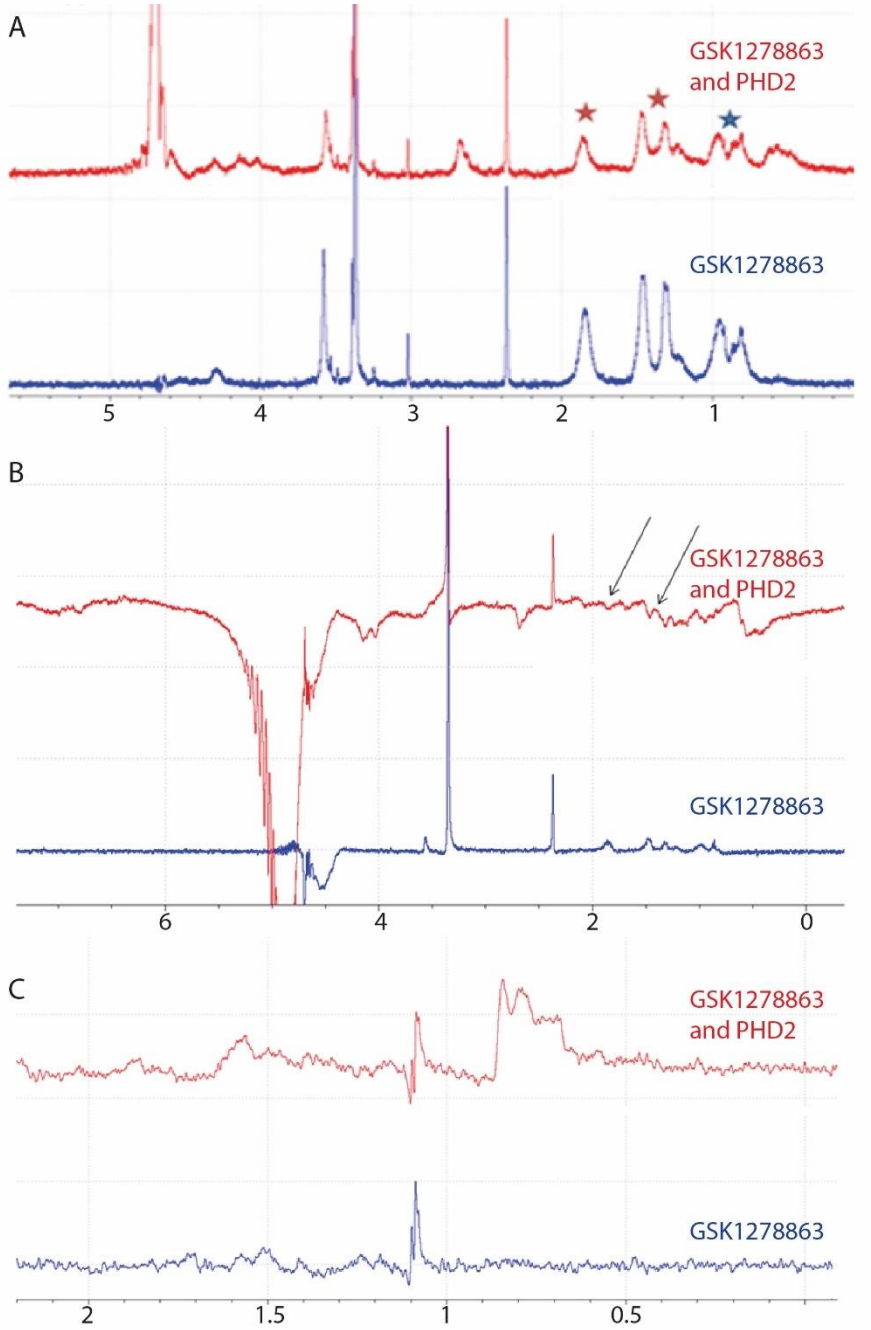

Figure 4.7. NMR analyses of the binding of GSK1278863 to PHD2. *Single-concentration qualitative binding screening of GSK1278863 and PHD2 to PHD2 as monitored by (A) ^{1}H excitation sculpting suppression, (B) w LOGSY, and (C) CPMG NMR analyses. The assay mixture contained either 500 µM GSK1278863 and 50 µM apo-PHD2 (A-B) or an equimolar mixture of apo-PHD2 and GSK1278863 (50 µM) (C), buffered with 50 mM Tris-D_{11} (pH 7.5), 200 µM Zn(II), and 0.02 % NaN_3 in 90 % H_2O and 10 % D_2O.*

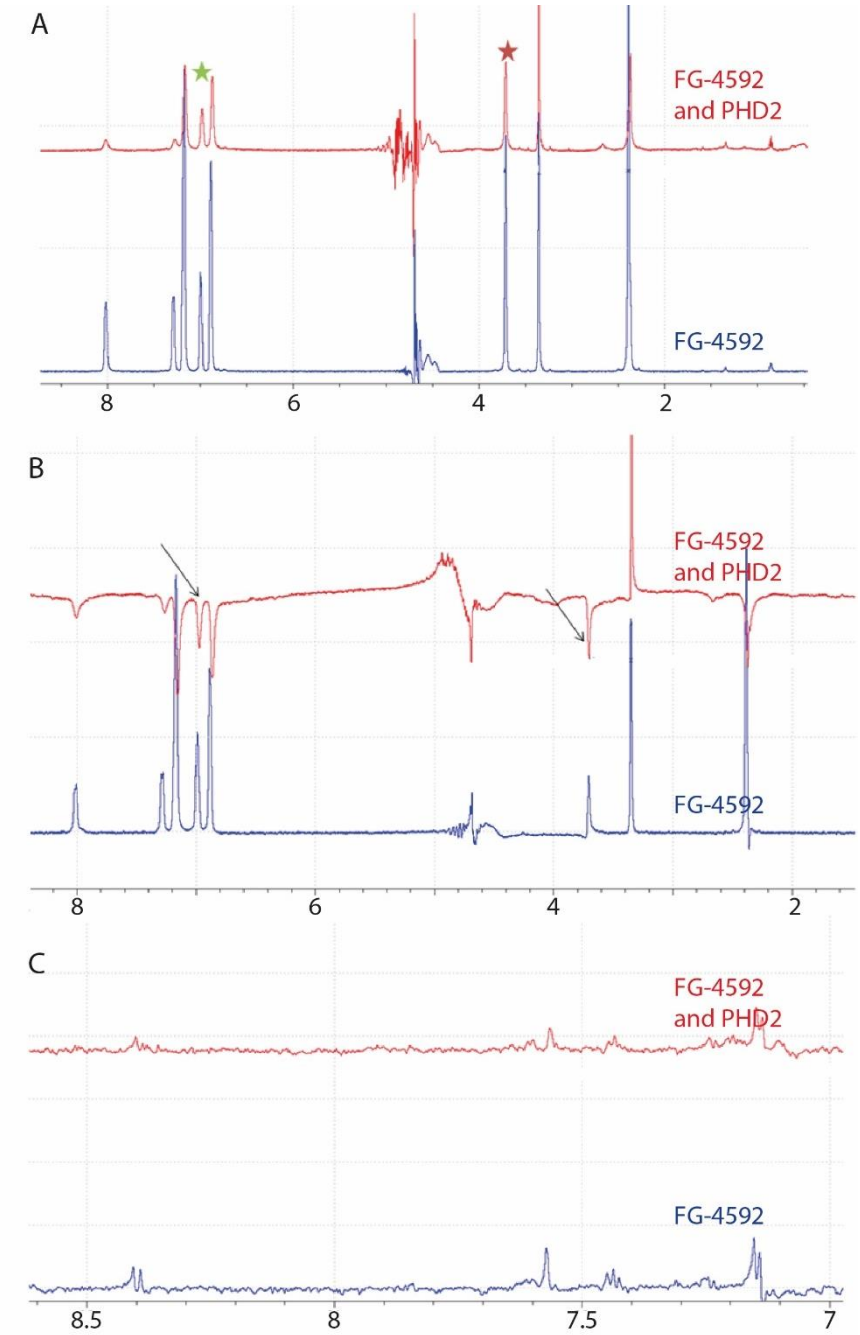

Figure 4.8. NMR analyses of the binding of FG-4592 to PHD2. *Single-concentration qualitative binding screening of FG-4592 and PHD2 to PHD2 as monitored by (A) ^{1}H excitation sculpting suppression, (B) w LOGSY, and (C) CPMG NMR analyses. The assay mixture contained either 500 µM FG-4592 and 50 µM apo-PHD2 (A-B) or an equimolar mixture of apo-PHD2 and FG-4592 (50 µM) (C), buffered with 50 mM Tris-D_{11} (pH 7.5), 200 µM Zn(II), and 0.02 % NaN_3 in 90 % H_2O and 10 % D_2O.*

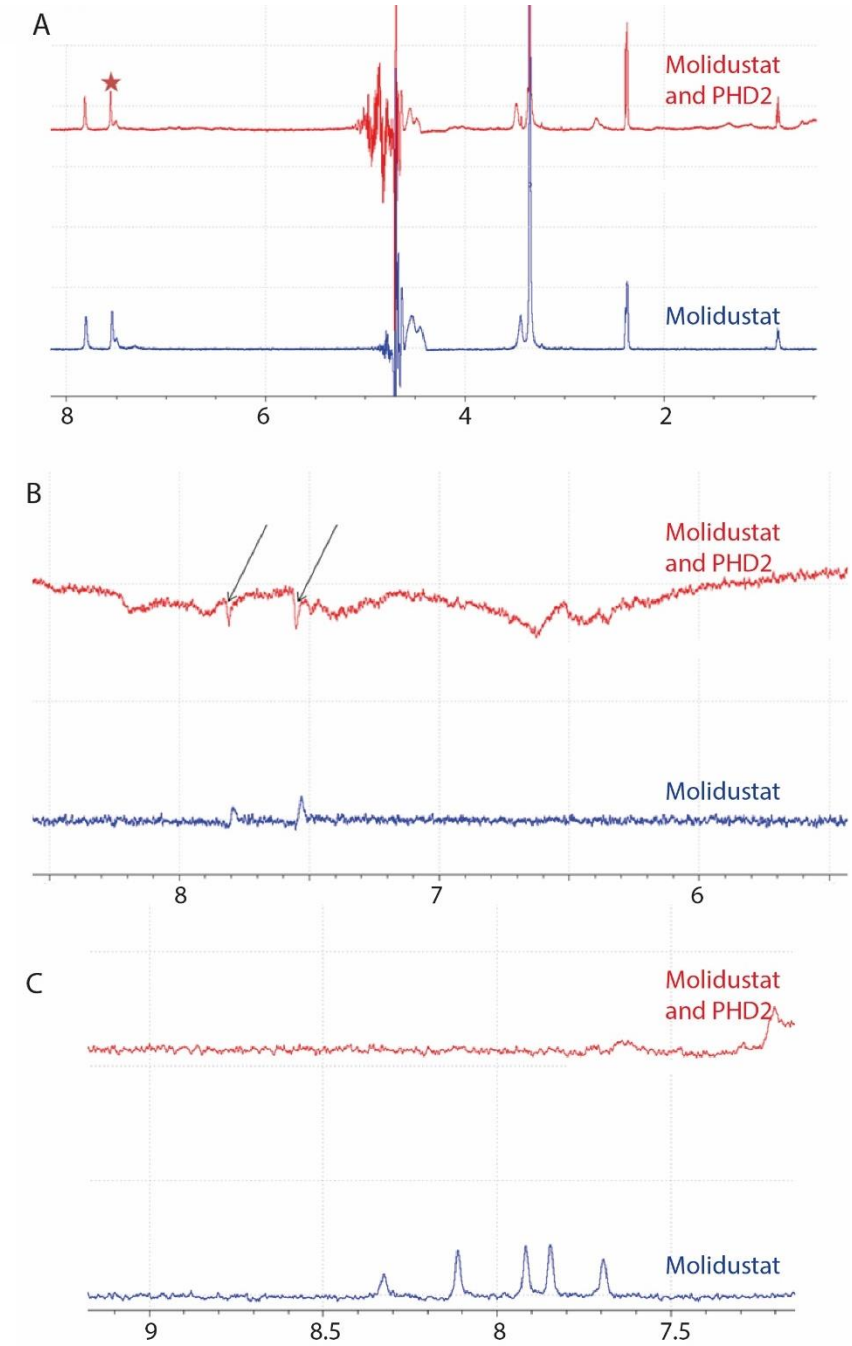

Figure 4.9. NMR analyses of the binding of Molidustat to PHD2. *Single-concentration qualitative binding screening of Molidustat and PHD2 to PHD2 as monitored by (A) ^{1}H excitation sculpting suppression, (B) w LOGSY, and (C) CPMG NMR analyses. The assay mixture contained either 500 µM Molidustat and 50 µM apo-PHD2 (A-B) or an equimolar mixture of apo-PHD2 and Molidustat (50 µM) (C), buffered with 50 mM Tris-D_{11} (pH 7.5), 200 µM Zn(II), and 0.02 % NaN_3 in 90 % H_2O and 10 % D_2O.*

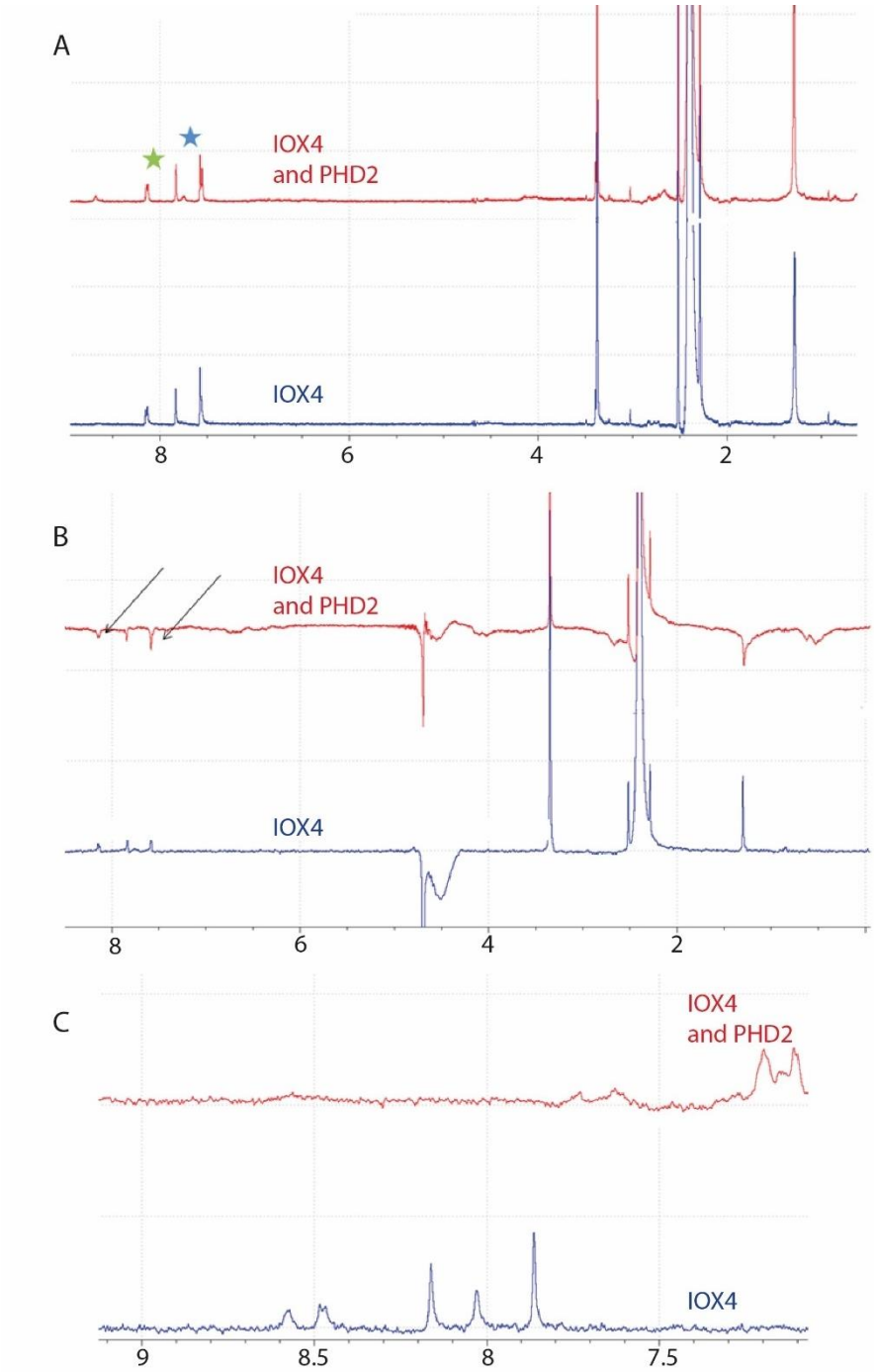

Figure 4.10. NMR analyses of the binding of IOX4 to PHD2. *Single-concentration qualitative binding screening of IOX4 and PHD2 to PHD2 as monitored by (A) ^{1}H excitation sculpting suppression, (B) w LOGSY, and (C) CPMG NMR analyses. The assay mixture contained either 500 µM IOX4 and 50 µM apo-PHD2 (A-B) or an equimolar mixture of apo-PHD2 and IOX4 (50 µM) (C), buffered with 50 mM Tris-D_{11} (pH 7.5), 200 µM Zn(II), and 0.02 % NaN_3 in 90 % H_2O and 10 % D_2O.*

4.2.2.2. Competition Studies with 2OG

In order to investigate the binding mode of the clinical inhibitors, competition assays involving 2OG were carried out utilising ^{1}H CPMG.[112] The results show 100 % 2OG displacement with the clinical inhibitors compared to the control with protein complexed. All four compounds completely displaced 2OG at a concentration of 400 µM with a PHD2 concentration of 10 µM **(Figure 4.11)**, implying they compete with 2OG.

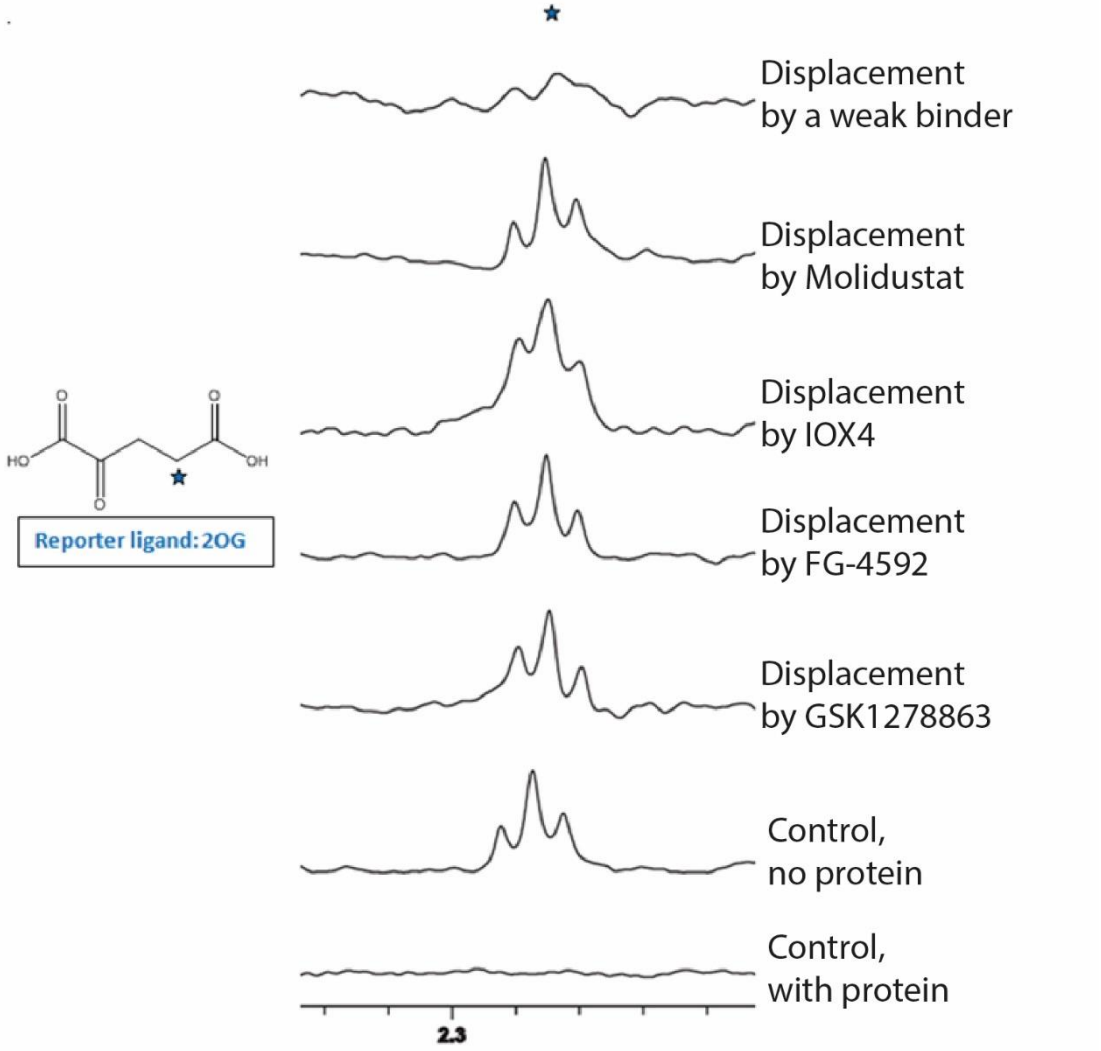

Figure 4.11. Qualitative single concentration screening with various compounds by 2OG displacement as monitored by CPMG-edited ^{1}H analyses. *The assay mixture contained 10 µM apo-PHD2-$_{181-426}$, 60 µM Zn(II), 10 µM 2OG, 400 µM compound and 50 mM Tris-D_{11}, pH 7.5 in 10 % D_2O and 90 % H_2O.*

4.2.2.3. K_D measurements

The dissociation constants K_D of FG-4592, Molidustat, and GSK1278863 to PHD2 were then measured by 2OG displacement using ^{1}H CPMG NMR.[112] The K_D value of IOX4 had been previously measured by Dr Ivanhoe Leung to be 590 ± 250 nM using the water relaxation method[143] (unpublished data). All had a K_D in the sub-micromolar range, consistent with the catalytic activity assays. In the NMR assays, FG-4592 and IOX4 were observed to bind least tightly, and GSK1278863 most tightly of the three clinical compounds, with a rank order of GSK1278863 > Molidustat > FG-4592~IOX4 **(Figure 4.12)**. Surface plasmon resonance would have been a better alternative to measure K_D values because NMR is limited by its low sensitivity (high protein concentration needed) and 80 % displacement was already achieved at low inhibitor concentration. However, attempts at Octet RED were unsuccessful and the assay requires further optimisation.

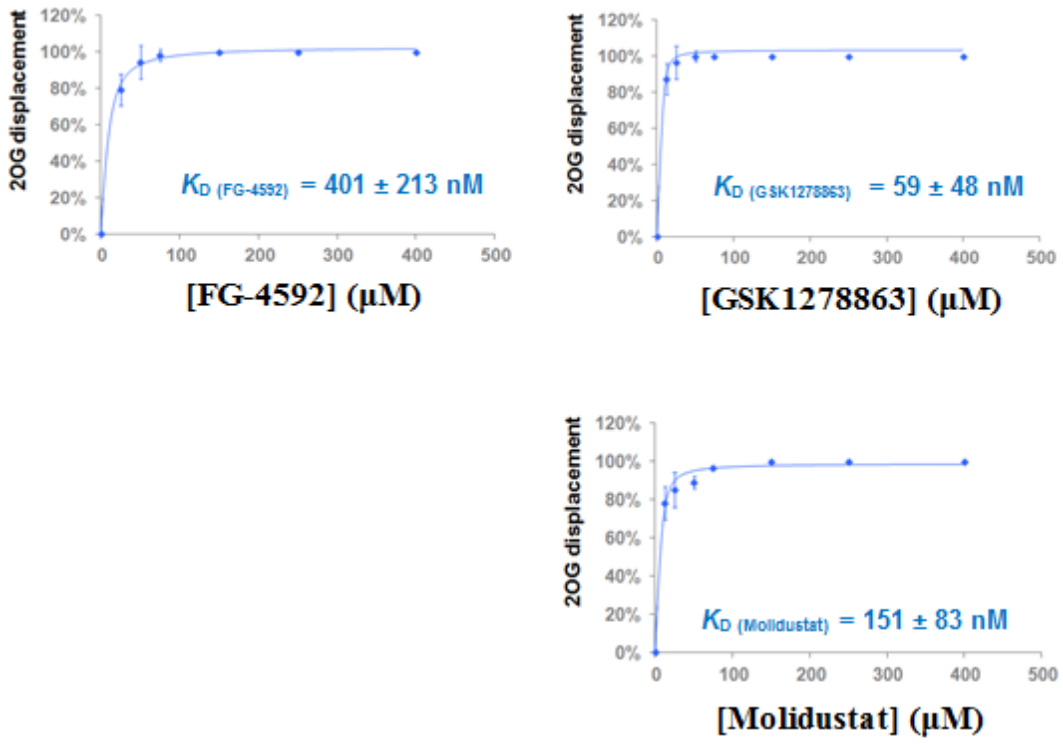

Figure 4.12. K_D fitting for PHD inhibitors as monitored by 2OG displacement using ^{1}H CPMG NMR analyses.

4.2.2.4. Competition Studies with the Peptidic Substrates

Competition assays involving NODD and CODD were then carried out utilising 1D CLIP HSQC NMR with selective ^{13}C inversion experiments.[111] Despite the observation of related binding modes and competition with 2OG, different results were obtained when the effect of compounds on the binding of HIF-1α CODD and NODD was examined.

Notably, of the four compounds tested, only FG-4592 was able to displace both CODD and NODD within the detection limit of the 1D CLIP HSQC with selective ^{13}C inversion NMR assay. (The assay used is previously described in **Chapter 2**). The results show 41 % ^{13}C-CODD displacement on addition of 800 µM FG-4592; this displacement was found to be concentration-dependent as 400 µM FG-4592 displaced 19 % of ^{13}C-CODD **(Figure 4.13)**.

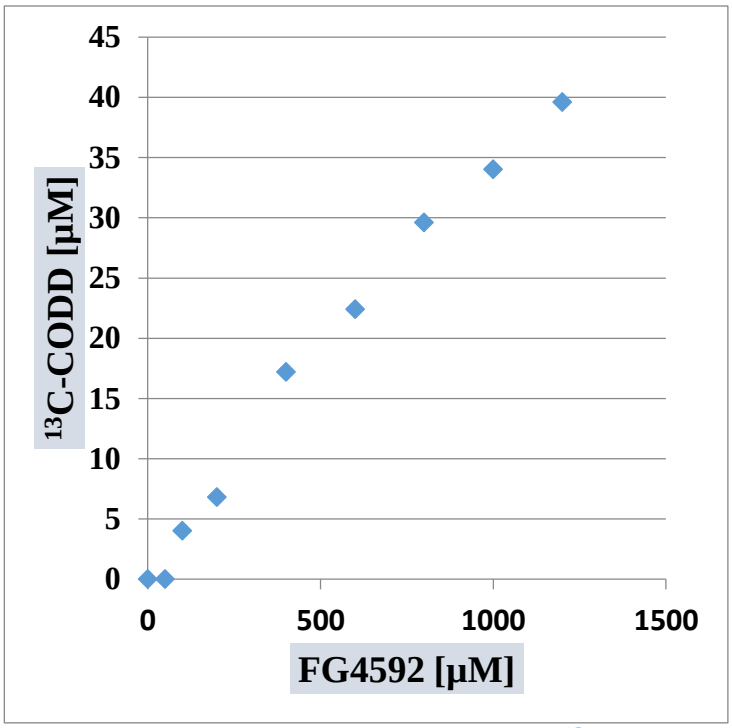

Figure 4.13. Dose-response plot of the displacement of ^{13}C-CODD by FG-4592 as observed by 1D-CLIP HSQC analyses. *The assay mixture contained 50 µM apo-PHD2-$_{181-426}$, 60 µM Zn(II), 50 µM ^{13}C-CODD, increasing concentrations of FG-4592 and 50 mM Tris-D_{11}, pH 7.5 in 10 % D_2O and 90 % H_2O.*

This is notable since compounds closely related to FG-4592, such as FG-2216, would not be expected to, at least completely, displace CODD from PHD2 as revealed by crystallographic analyses.[24, 32] A structure for the PHD2.Mn.FG-2216 complex has been reported and reveals the coordination of the active site metal *via* the glycinamide oxygen (*trans* to PHD2 aspartate 307) and the nitrogen of the isoquinoline (*trans* to PHD2 histidine 374) ring. The carboxylate group of the glycinamide of FG2216 is positioned to form electrostatic interactions with the 2OG C-5 carboxylate-binding residues tyrosine 329 and arginine 383 in PHD2 (in a similar manner to the analogous 2OG carboxylate). It was then of interest to study the binding mode of FG-2216. As expected based on crystallographic evidence,[24, 32] FG-2216 did not displace CODD in solution as observed by 1D-CLIP HSQC NMR analyses. Overlaying the structure of FG-4592 on FG-2216 generates a model for FG-4592 active site interactions with PHD2. The hydrophobic phenoxy group present in FG-4592, but not in FG-2216, projects into the substrate binding region of the active site **(Figure 4.14)**. The docking model was carried out by Dr Rasheduzzaman Chowdhury. The reason for the displacement of CODD by FG-4592 likely, at least in part, results from the presence of its phenoxy group, which projects into the ODD substrate binding region adjacent to the catalytic centre so more efficiently displacing CODD.

However, as shown by experiments with NODD, other factors must be involved. In contrast to the observations with CODD, GSK1278863, FG-4592, and IOX4 all clearly displaced NODD, but the extent of NODD displacement by Molidustat was much less/barely detectable. Data show almost full displacement of ^{13}C-NODD on addition of 800 µM of either FG-4592 or GSK1278863 and around 50 % displacement of ^{13}C-NODD on addition of 800 µM of IOX4 **(Figure 4.15)**.

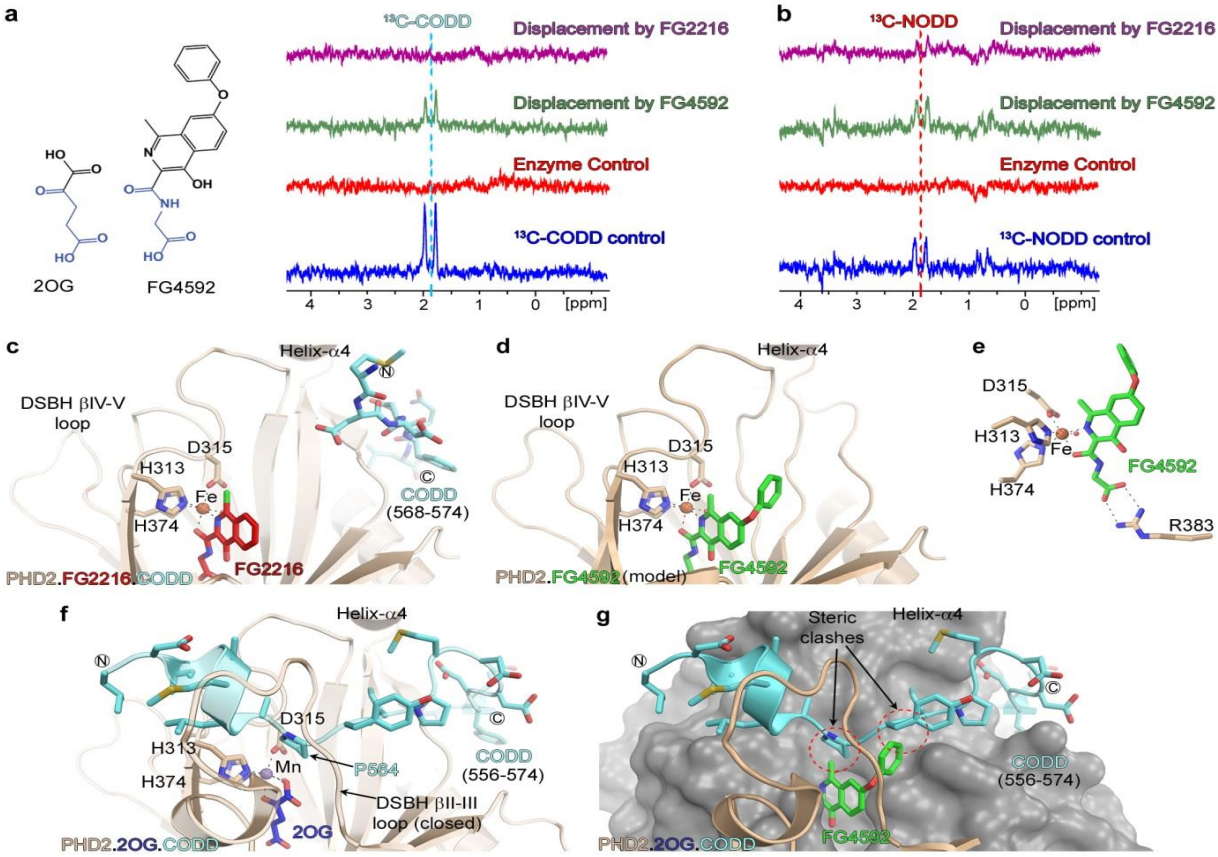

Figure 4.14. Views from PHD2.Fe.FG2216.CODD (PDB: 3HQU) and PHD2.Mn.2OG.CODD (PDB: 5L9B) crystal structures and a PHD2.Fe.FG4592 model. *FG2216 and FG4592 both manifest efficient NODD displacement from PHD2 whereas effective CODD displacement only occurs with FG4592 as evidenced by 1D ^{13}C-selective Clean In-Phase (CLIP) HSQC NMR (a and b). (c) A view from crystal structure of the PHD2.FG2216.CODD complex (PDB: 3HQU) reveals that PHD2 can form a ternary complex with CODD in the presence of FG2216. (d) and (e) show views from a PHD2.Fe.FG4592 model that was generated by using a structure for PHD2.Mn.FG2216 (PDB: 4BQX) and a close-up view from the PHD2.Fe.FG4592 model active site. (f) and (g) show views from a PHD2.Mn.2OG.CODD complex structure (PDB: 5L9B) and a superimposed view of the PHD2.Fe.FG4592 model and the PHD2.Mn.2OG.CODD complex structure indicating how the phenoxy group in FG4592 will overlap with ODD binding. Figure used with permission from Nature Communications, Nature Publishing Group.*[113]

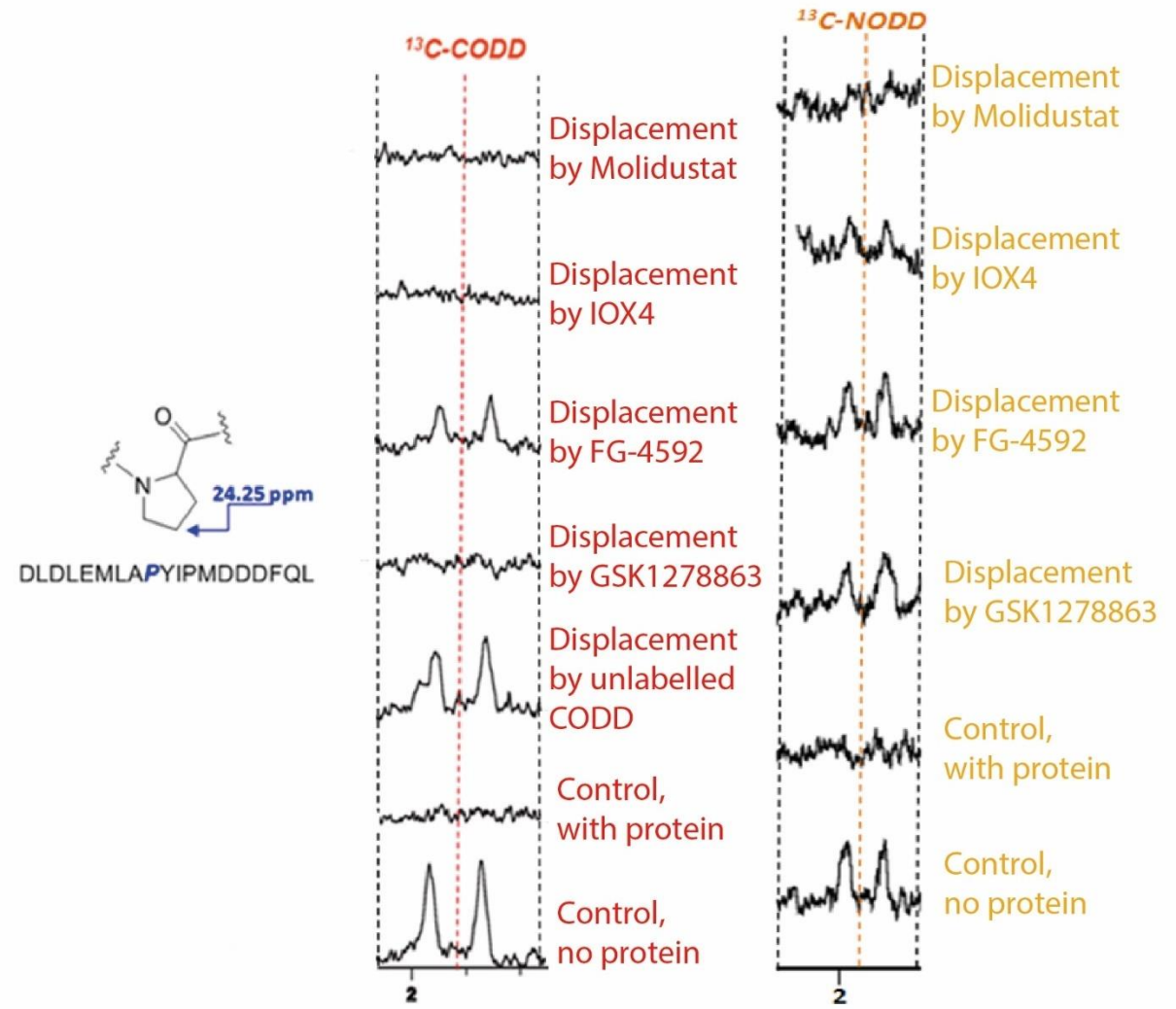

Figure 4.15. Qualitative single concentration screening with various compounds by ^{13}C-CODD/NODD displacement as monitored by 1D CLIP HSQC with selective ^{13}C-inversion analyses. *The assay mixture contained 50 µM apo-PHD2-181-426, 200 µM Zn(II), 50 µM 2OG, 50 µM ^{13}C-CODD/NODD, 800 µM compound and 50 mM Tris-D_{11}, pH 7.5 in 10 % D_2O and 90 % H_2O.*

The combined biophysical analyses reveal that all three of the clinical PHD inhibitors bind to the active site metal and compete with 2OG, but the extent to which they displace NODD or CODD for PHD2 varies. Molidustat is notable in that it can bind without substantially displacing NODD or CODD **(Figure 4.16)**. 2OG displacement by the inhibitors was expected as the compounds are expected to bind to the active site metal in a bidentate manner. The NMR studies revealed differences in the way in which the inhibitors displace

CODD and NODD binding to PHD2. Although all the inhibitors very likely perturb the catalytically productive conformation of HIF-α at the PHD active site,[158] amongst the inhibitors tested, only FG-4592 was able to displace CODD efficiently within the limits of detection using the semi-quantitative NMR assays. FG-2216, which is structurally related to FG-4592, does not displace CODD;[24, 32] this difference likely reflects the presence of an additional phenoxy group on FG-4592, which is predicted to project into the CODD/NODD binding close to the active site iron. However, the situation is more complex than simple steric blockade of substrate binding at the active site, since, *e.g.* one of the cyclohexyl groups of GSK1278863 might be expected to act in a similar manner to the phenoxy group of FG-4592. Further, the results of the NMR-based NODD binding assays, reveal that FG-4592 (100 %), GSK1278863 (100 %), and IOX4 (50 %) all displace NODD at 800 μM, 16-fold excess; however, the level of NODD displacement was barely detectable for Molidustat (5 %).

Overall, these results likely reflect both the induced fit nature of substrate binding to the PHDs and, importantly, imply differences in the binding modes of NODD and CODD to the PHDs, at least when also complexed with inhibitors. Previous solution and crystallographic studies have revealed that binding of CODD and NODD involves substantial induced fit movements, notably involving a loop (β2β3 loop) which folds to near completely enclose the hydroxylated proline and to adjacent residues at the active site.[30] Inhibitors that do not entirely displace the ODD substrates, *i.e.* IOX4 and Molidustat with NODD, and all the inhibitors with CODD, might likely induce different conformations to those completely displacing substrate, *i.e.* GSK1278863 and FG-4592 on NODD. Such differences may possibly reflect the different rank orders in inhibition of catalysis and binding (in particular for GSK1278863).

Studies utilising antibodies specific for the NODD and CODD hydroxylation sites in human VHL-deficient RCC4 cells have validated the ability of FG-4592, GSK1278863, Molidustat, and IOX4 to inhibit PHD activity in cells. Quantification of NODD/CODD hydroxylation levels (using site-hydroxylation specific antibodies) in a cell line manifesting stable HIF-α levels reveals differential effects on NODD/CODD hydroxylation for the different inhibitors. Cell studies were carried out by Dr Tzu-Lan Yeh (data not shown). Although multiple factors are likely operative in cells, it is interesting that the observations on NODD/CODD hydroxylation are in reasonable agreement with NMR NODD/CODD displacement results, *i.e.* FG-4592, the only inhibitor that displaces CODD in the NMR assay, shows the most potent inhibition of CODD hydroxylation; GSK1278863, which only displaced NODD in NMR assay, showed better NODD inhibition over CODD in cells; and Molidustat, does not displace NODD or CODD in NMR assay, had a weaker effect on either hydroxylation site than FG-4592 or GSK1278863 (at 10 μM).

Given the emerging different roles for NODD/CODD and the HIF-α isoforms,[13] the observations on inhibitor effects may be of biological relevance. Differential sequestration of NODD/CODD may have consequences for the activity of inhibitors in cells, *e.g.* by limiting binding of HIF-α to pVHL or by modulating PHD lifetime. The collective results suggest that the development of PHD inhibitors that manifest, at least a degree, of selectivity for NODD/CODD and maybe HIF-1α/HIF-2α should be possible. The latter is of particular interest given that it has been reported that HIF-1α and HIF-2α may have opposing role on the progress of cancer.[159] In this regard the development of inhibitors, including those not binding to the active site metal, which exploit differences in the binding of different substrates to the PHDs is of interest.

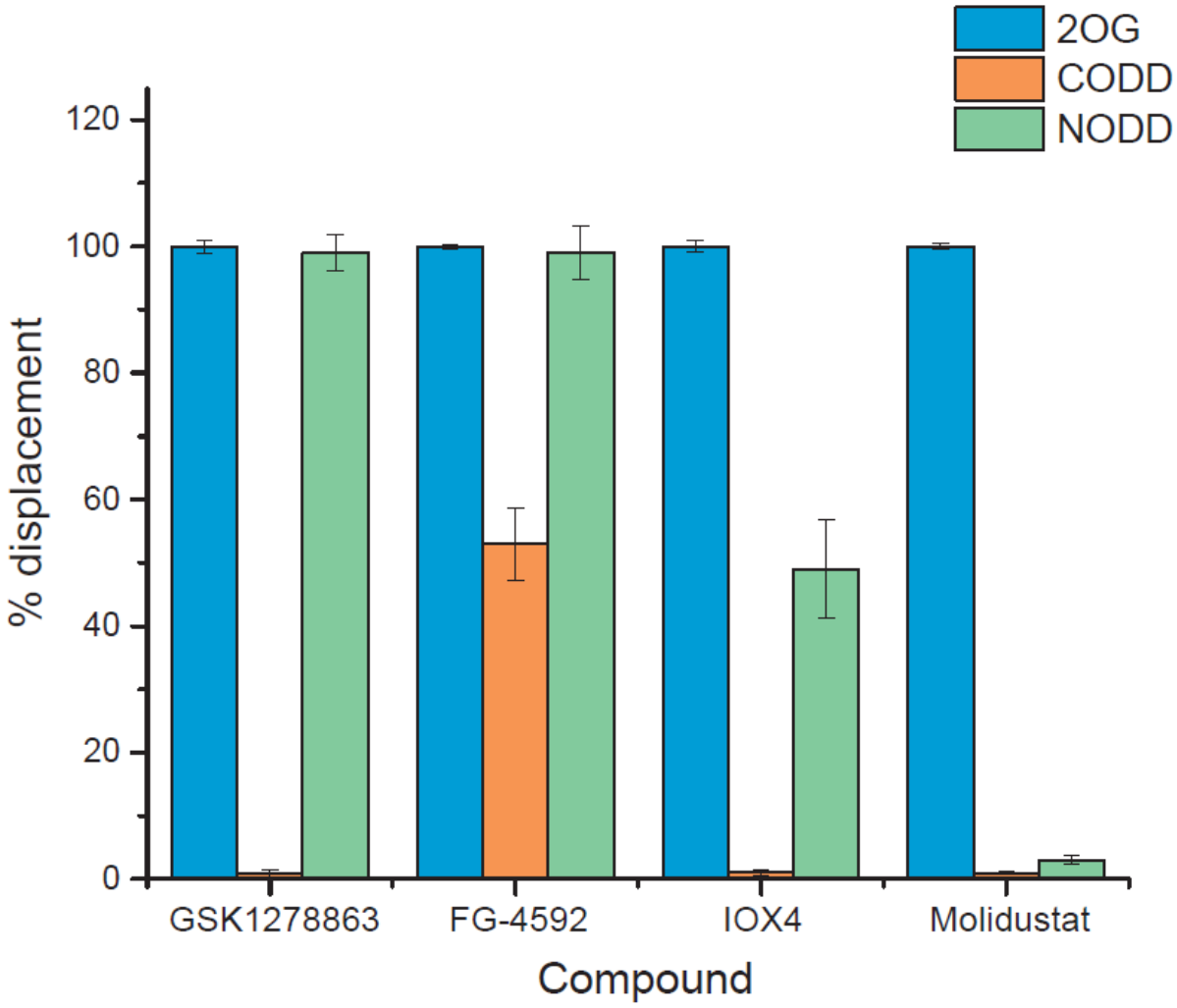

Figure 4.16. Investigations of the binding modes of the various compounds through ^{1}H CPMG monitoring of 2OG displacement and 1D CLIP HSQC with selective ^{13}C-inversion analyses of ^{13}C-CODD displacement and ^{13}C-NODD displacement. *For assay conditions, see Materials and Methods.*

4.3. Summary and Perspectives

In this chapter, work on the inhibition modes of various PHD inhibitors was investigated. Deferoxamine and Deferasirox are both iron chelators used clinically for the treatment of iron overload and heavy metal intoxication.[154a, 155a] Even though they stabilise HIF in cells, they have differential inhibition modes; Deferoxamine sequesters Fe(II) in solution, whilst Deferasirox mostly chelates to PHD2 active site. The results are of interest because they shed light on the possibility of achieving more selective results. Given the differential specificity of PHD isoforms for their HIF substrates, it was important to study the inhibition mode of those clinical inhibitors that may help in the development of isoform selective inhibitors. Comparative studies on the activities and selectivities of PHD inhibitors in clinical trials were presented. Even though all of the clinical inhibitors tested compete with 2OG, it was remarkable that FG-4592 was the only one of the tested inhibitors capable of displacing CODD, whilst Molidustat did not interfere with neither CODD nor NODD binding. The results partly inform on the mechanism of action of the compounds and will aid in long-term work on the therapeutic manipulation of the natural hypoxic response.

4.4. Materials and Methods

4.4.1. Protein Production

For ^{1}H-^{15}N HSQC experiments, a *C*- and *N*-terminal truncated construct of the catalytic domain of PHD2 (PHD2$_{181-402}$) was used in order to minimise spectral overlap and to reduce transverse relaxation losses to a minimum. ^{15}N-enriched PHD2 was produced in glucose-enriched minimal medium (M9 salts). Protein production was induced by addition of 200 μM IPTG when the cell density reached an optical density (OD_{600}) of 0.6–0.8 and left for overnight incubation at 28 °C. Protein purification followed as reported.[23, 32] For all other

experiments, the catalytic domain of human PHD2 (residues 181-426) was produced and purified as previously reported.[110]

4.4.2. NMR Experiments

Nuclear Magnetic Resonance (NMR) spectra were recorded using a Bruker AVIII 700 MHz NMR spectrometer equipped with a 5-mm inverse cryoprobe using 5 mm diameter NMR tubes (Norell) or 3 mm MATCH NMR tubes (Cortectnet). Data were processed with Bruker 3.1 software.

4.4.2.1. NMR Binding Studies

4.4.2.1.1. ^{1}H NMR Experiments

Spectra were typically obtained using 256 scans and a relaxation delay of 1 s. A 2 ms Sinc pulse was used for water suppression. Prior to Fourier transformation, data were multiplied with an exponentional function with 2 Hz line broadening.

4.4.2.1.2. ^{1}H CPMG NMR Experiments

Typical experimental parameters for Carr-Purcell-Meiboom-Gill (CPMG) NMR spectroscopy were as follows: total echo time, 40 ms; relaxation delay, 2 s; and number of transients, 264. The PROJECT-CPMG sequence as described by Aguilar *et al.* was applied (90°x−[τ−180°y−τ−90°y−τ−180°y−τ]*n*−acq).[137] Water suppression was achieved by pre-saturation.

4.4.2.1.2. ^{1}H wLOGSY NMR Experiments

water-Ligand Observed Gradient SpectroscopY (wLOGSY) experiments were conducted using the pulse sequence described by Dalvit *et al.*[83] Typical experimental parameters were as follows: mixing time, 1 s; relaxation delay, 2 s; number of transients, 256. Solvent excitation was achieved using a 16 ms 180 degree selective rectangular shape pulse

with 1000 points (Squa100.1000) set at the H_2O frequency. Water suppression was achieved by a 2 ms Sin pulse (Sinc1.1000) pulse at the H_2O frequency.

4.4.2.2. ^{13}C-2OG and ^{13}C-NODD/CODD Displacement Experiments

2OG was uniformly ^{13}C-labelled and CODD/NODD was uniformly ^{13}C labelled on its proline ring. The CLIP-HSQC sequence was used for 1D HSQC experiments (without ^{13}C decoupling).[111] Relaxation delay was 2 s. The $^1J_{CH}$ was set to 160 Hz. A 6.8 ms Q3.1000 180-degree pulse was used and selective irradiation was applied at the selected chemical shift.

4.4.3. Inhibition Assays

Inhibitor assays were performed by matrix-assisted laser desorption/ionisation time-of-flight mass spectrometry (MALDI-TOF MS) using a Waters® Micromass® MALDI micro MX™ mass spectrometer. Fe(II) dependence was assessed by incubation of PHD2 (1 μM) with increasing concentrations of Fe(II) in the presence of the inhibitor (100 μM), 2OG (10 μM), ascorbate (4 mM) and a 19mer CODD-peptide (10 μM, sequence: DLDLEMLAPYIPMDDDFQL-NH_2) in 50 mM Tris (pH 7.5) at 37 °C. Dose responses were assessed by incubation of PHD2 (1 μM) with increasing concentrations of inhibitor in the presence of Fe(II) (50 μM), 2OG (10 μM), ascorbate (4 mM) and a 19mer CODD-peptide (10 μM, sequence: DLDLEMLAPYIPMDDDFQL-NH_2) in 50 mM Tris (pH 7.5) at 37 °C. Reactions were quenched with formic acid (1 % v/v) at a time-point within the linear region of enzymatic activity. Hydroxylation levels were quantified using MassLynx™ V4.0 and IC_{50} values were determined with GraphPad Prism®.[23]

Chapter 5. Protein-Observe ^{19}F-NMR Studies on São Paulo Metallo β-Lactamase

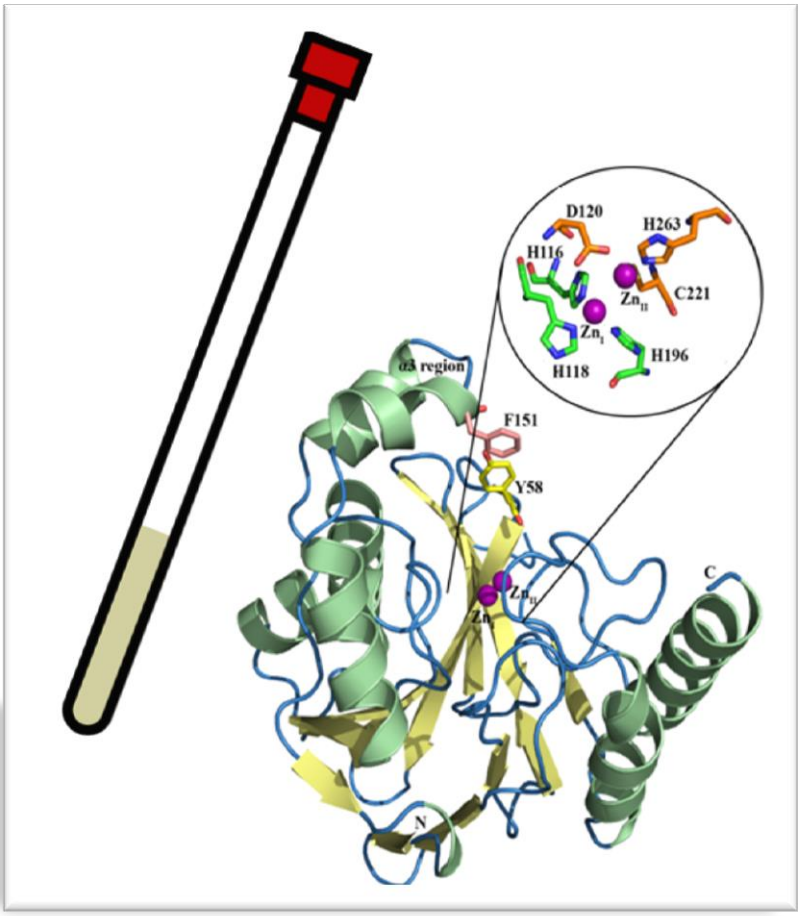

Chapter 5. Contents

5.1. Introduction

Pseudomonas aeruginosa is considered amongst the most virulent and resistant of Gram-negative bacterial pathogens; it can act as an opportunistic, nosocomial pathogen in immunocompromised patients and has the potential to cause septic shock and harmful infections in the skin, blood, pulmonary, urinary and gastrointestinal tracts of healthy individuals.[160] One of its main resistance mechanisms is by the production of the São Paulo metallo β-lactamase 1 (SPM-1). SPM-1 was first identified in San Paulo, Brazil, in 1997 from a 4-year-old leukemic girl.[161] SPM-1 producing *P. aeruginosa* are now endemic in Brazilian hospitals,[160b, 162] and recent reports of SPM-1 mediated resistance in Europe, Asia, and North America imply the global spread potential of SPM-1-mediated resistance.[160c, 163]

SPM-1 is interesting from an inhibition perspective because it has broad substrate selectivity (catalysing penicillin, cephalosporin, and carbapenem hydrolysis) and properties characteristic of both B1 and B2 MBLs.[164] SPM-1 resembles the B1 MBLs in terms of its di-Zn(II) ion requirement and (based on available evidence) with respect to its kinetic properties.[165] However, SPM-1 has unusual second sphere residues[166] and is unique amongst B1 MBLs in terms of the mobile regions around its active site; SPM-1 has an extended 'α3 region' (residues 223-241, BBL numbering) and a relatively short L3 loop (residues 61-66, BBL numbering); these are characteristic features of the B2 MBLs. The 'normal' B1 MBLs typically have a short α3 and a larger L3 loop **(Figure 5.2)**.[164a] SPM-1 is unusual (at least in some regards) amongst MBLs as it is proposed to be a hybrid MBL of the B1 and B2 subclasses. It possesses atypical second sphere residues (S84, G121) which are proposed to give rise to an unusual substrate selectivity.[166] Designing an inhibitor for the hybrid MBL, SPM-1, is a challenge, as it possesses both features of B1 and B2 subclasses. For this purpose, a detailed understanding of its bio/chemical/physical properties, ligand interactions

with its loops, and resistance profile are desirable. As yet, no crystal structure of SPM-1 complexed with a substrate/inhibitor is available, though crystal structures in which the α3 region adopts open[164a] and closed[164b] conformations with respect to its active site have been solved **(Figure 5.1)**.

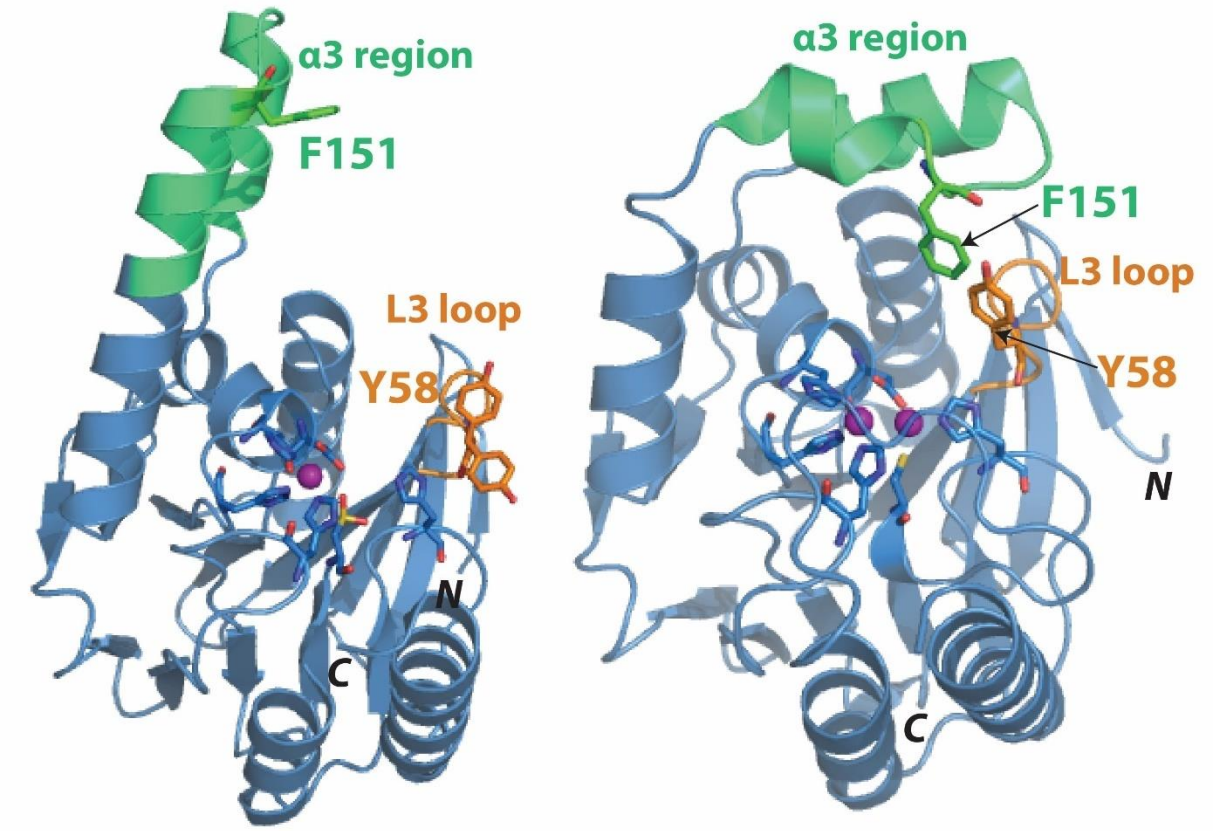

Figure 5.1. Views from SPM-1 crystal structures in the 'open' (PDB ID: 2FHX)[164a] and 'closed' (PDB ID: 4BP0)[164b] conformations of the α3 region. *Note Y58 was refined in two conformations in the former.*[164a] *SPM-1 has a characteristically elongated α3 region (green) and a short L3 loop (orange). Sites of labelling by cysteine alkylation with bromo-1,1,1-trifluoroacteone (BTFA) are highlighted. Note the presence of the active site cysteine (Cys221), which is not labelled by BTFA, likely because it coordinates to Zn(II).*

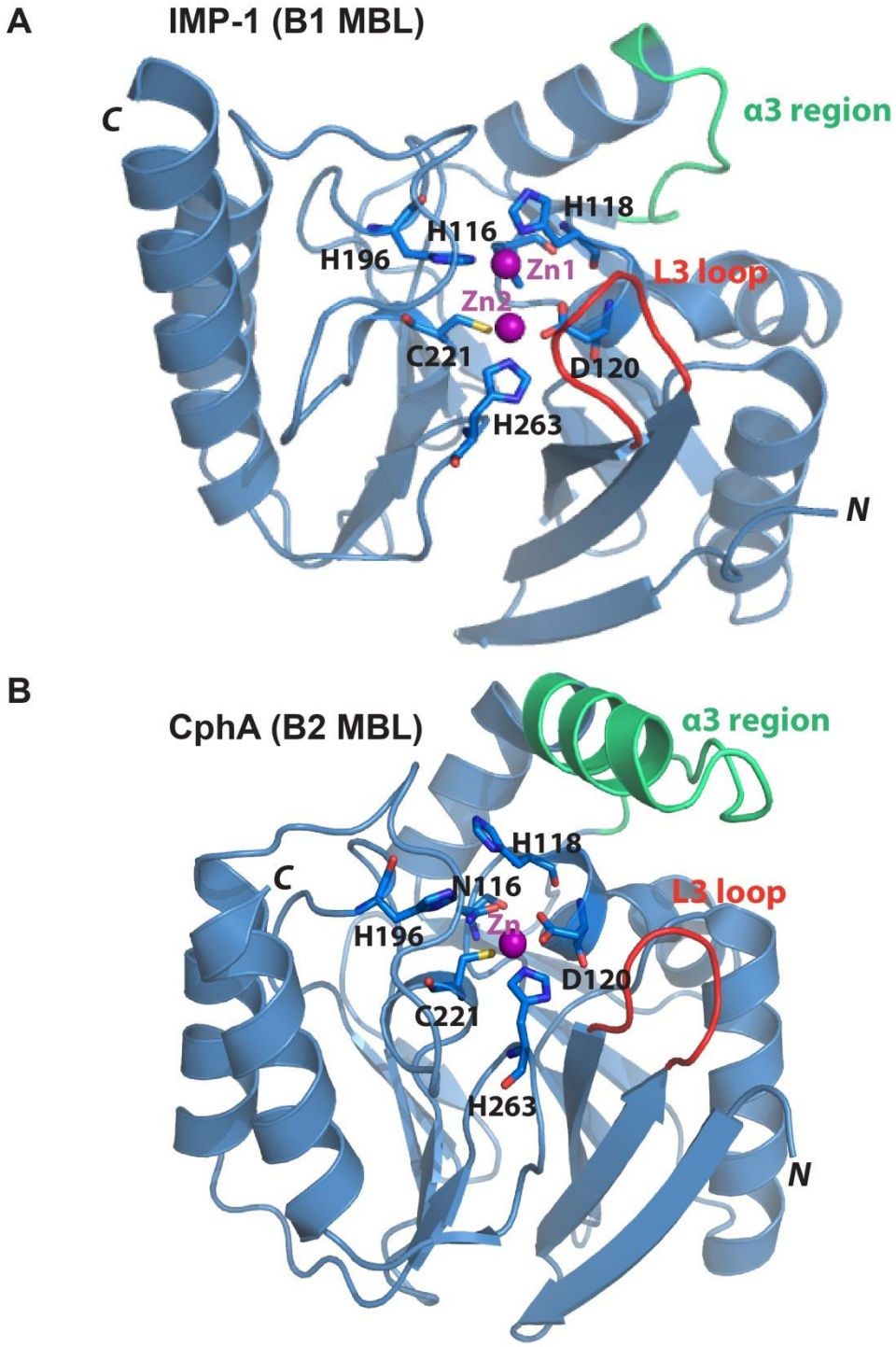

Figure 5.2. Views from MBL crystal structures highlighting potentially mobile regions. *Views of* ***(A)*** *IMP-1 (di-zinc ion B1 MBL, PDB ID: 1JJT)*[167] *and* ***(B)*** *CphA (mono-zinc ion B2 MBL, PDB ID: 1X8I)*[168] *highlighting the different mobile regions (L3 loop (red), and α3 region (green)) that characterise the MBL subfamilies. A longer L3 loop (red) is characteristic of the di-Zn B1 MBLs. The B2 MBLs using mono-zinc ion are characterised by an elongated α3 region (green) and a shorter L3 loop (red).*[56]

^{19}F-NMR is of increasing utility in studying conformational changes and protein-ligand interactions due to its sensitivity, non-overlapping ^{19}F and ^{1}H NMR resonances, and advances in NMR instruments and probe design.[93a, 169] Recently, the use of protein-observe ^{19}F-NMR (PrOF NMR) has been reported to study dynamics in MBL structures, using cysteine-alkylation with 3-bromo-1,1,1-trifluoroacetone (BTFA) as an efficient way of introducing a fluorine label **(Figure 5.3)**.[170] These results revealed the potential of ^{19}F-NMR to monitor MBL loop dynamics. In this chapter, PrOF NMR studies on SPM-1 informing on the importance of the L3 loop and α3 region in binding of different classes of substrates/inhibitors are described. Importantly, the results also reveal that the hydrolysed β-amino acid products of MBL catalysis can bind to SPM-1, in a manner involving the L3 loop. The results have implications for the future design of both MBL inhibitors and β-lactam antibiotics that are resistant to MBL catalysis.

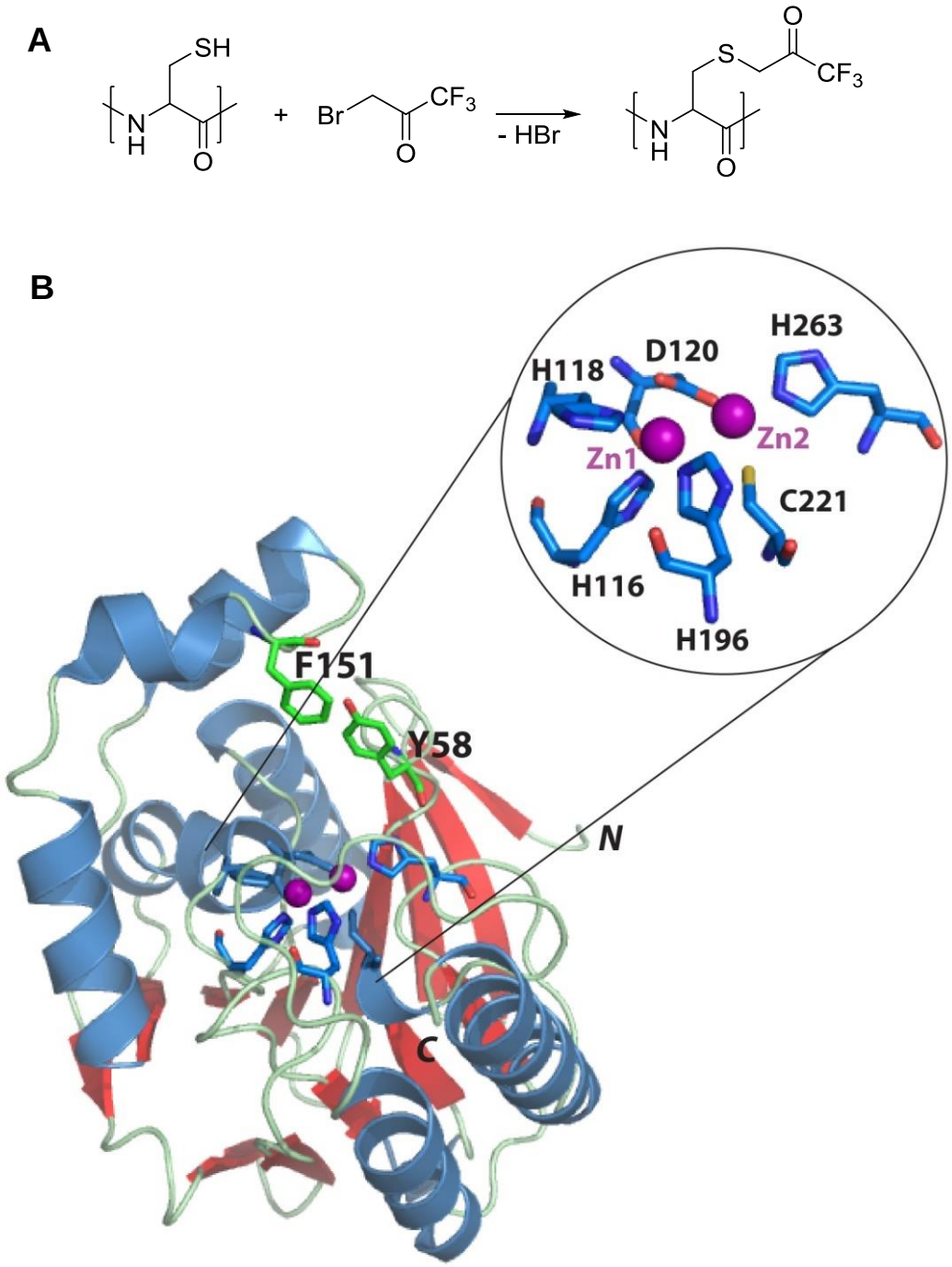

Figure 5.3. Outline reaction of BTFA labelling and an active site view from SPM-1 crystal structure. *PDB ID: 4BP0.*[164b] *The sites of labelling, F151 and Y58, are highlighted in green. Active site residues are shown as sticks in the highlighted circle. Zn1 is coordinated by 3 His residues, H116, H118 and H196. Zn2 is coordinated by D120, H263 and C221. The figure was created using PyMOL.*

5.2. Results

5.2.1. Labelling Site Determination

To use ^{19}F-NMR to study inhibitor/substrate binding to SPM-1, residues in the L3 loop (Tyr58) and α3 regions (Phe151) were selected for labelling with ^{19}F. Previously, Tyr152[164b] had been labelled; I selected Phe151 for further studies because crystallographic analyses reveal that the Phe151 side chain projects closer to the active site zinc ions than that of Tyr152 **(Figure 5.4)**. Y58 and F151 were selected for modification and labeling with ^{19}F. Recombinant SPM-1 variants (Y58C and F151C) were generated by site-directed mutagenesis and produced following a three-step based purification method to more than 95 % purity as judged by SDS-PAGE analyses **(Figures 5.5, 5.6)**. LC-MS analyses verified the masses of the recombinant proteins produced are in agreement with their theoretical masses **(Figure 5.7)**.

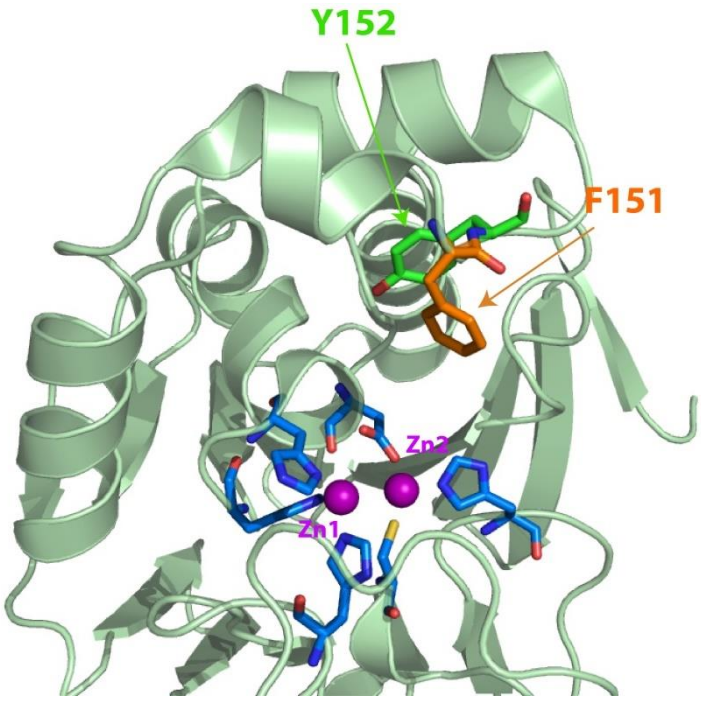

Figure 5.4. View from SPM-1 crystal structure highlighting the difference between residues Y152 and F151 in the α3 region. *PDB ID: 4BP0.*[164b] *The figure was created using PyMOL.*

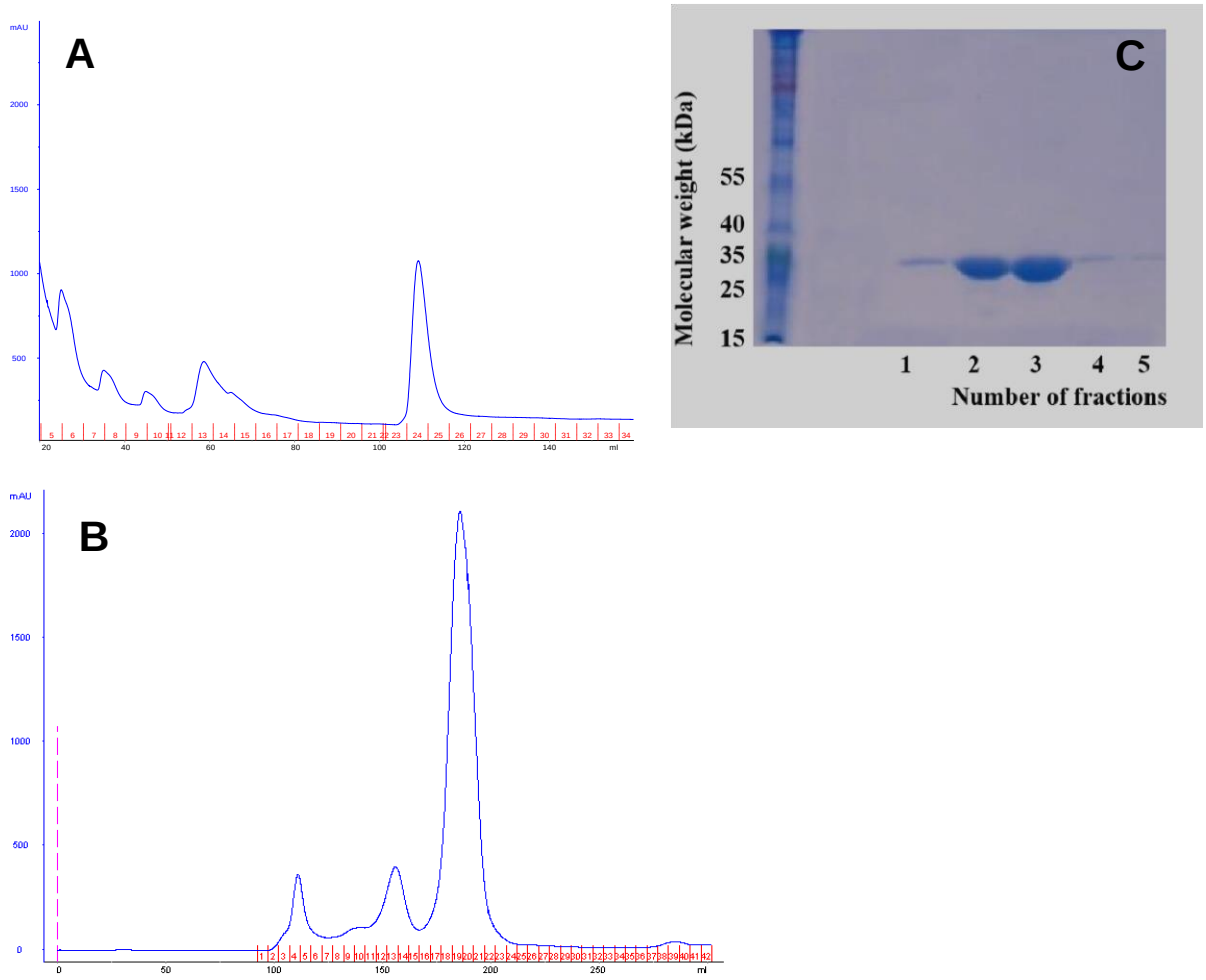

Figure 5.5. Y58C SPM-1 protein purification *by:* ***(A)*** *affinity chromatography (5 mL HisTrap HP column),* ***(B)*** *gel filtration (S75 300 mL preparative column) and* ***(C)*** *SDS-PAGE after His-tag cleavage. The chromatograms show UV absorbance in mAU versus volume eluted in mL. SDS-PAGE – molecular weight markers (PageRuler Prestained Protein Ladder 10-170 kDa, Thermo Scientific).*

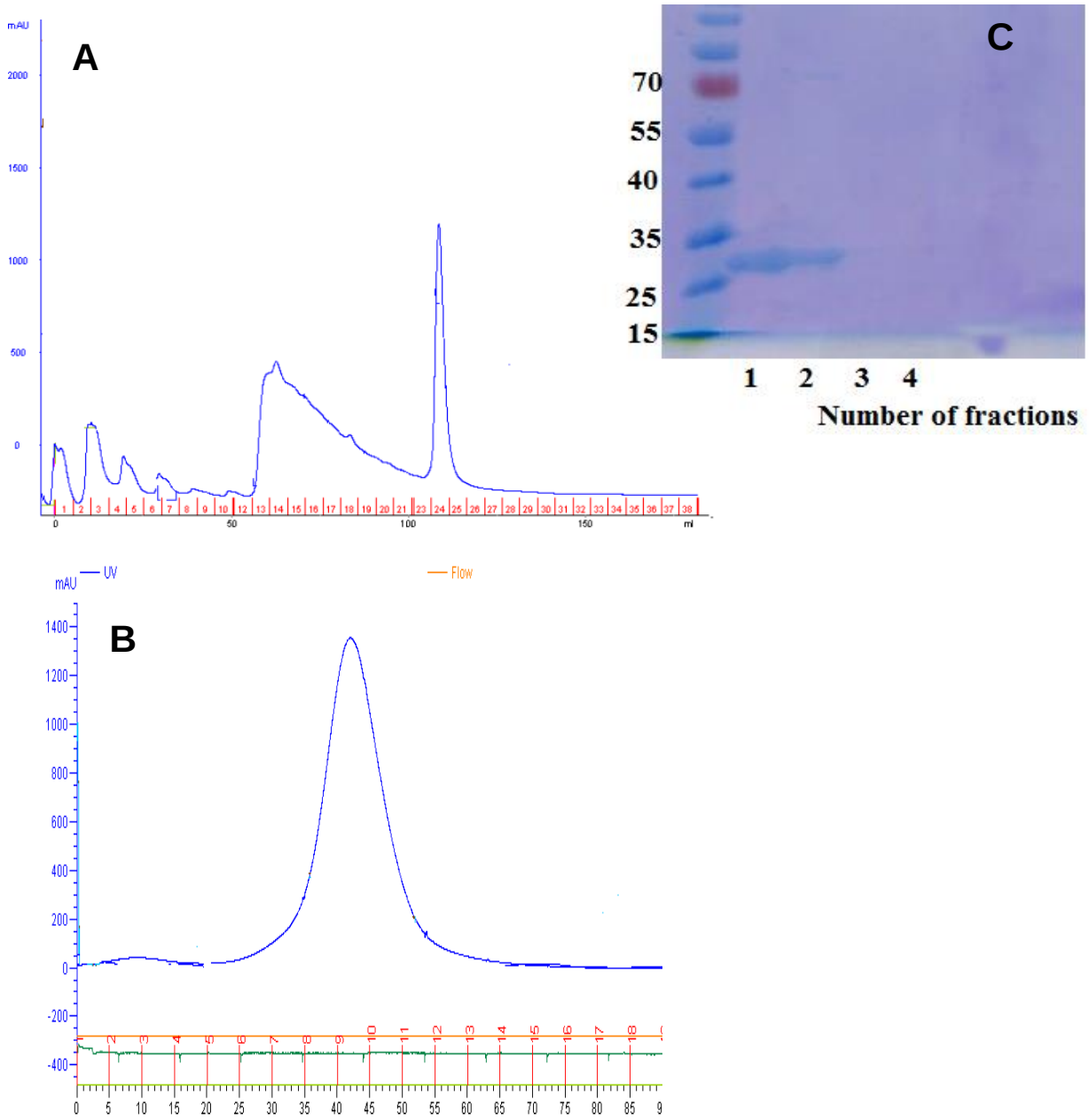

Figure 5.6. F151C SPM-1 protein purification *by:* ***(A)*** *affinity chromatography (5 mL HisTrap HP column),* ***(B)*** *gel filtration (S75 150 mL preparative column) and* ***(C)*** *SDS-PAGE after His-tag cleavage. The chromatograms show UV absorbance in mAU versus volume eluted in mL. SDS-PAGE – molecular weight markers (PageRuler Prestained Protein Ladder 10-170 kDa, Thermo Scientific).*

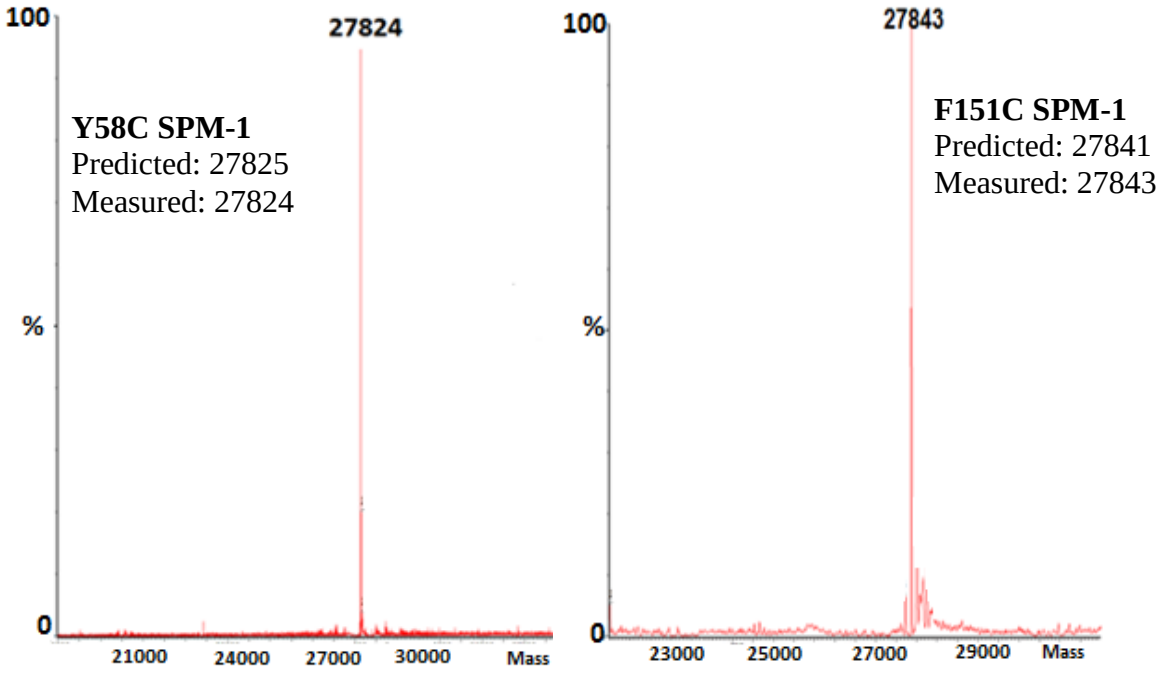

Figure 5.7. MS spectra of Y58C SPM-1 and F151C SPM-1. *Spectra were acquired using a Waters LCT Premier instrument fitted with a ToF analyzer. The positive ion electrospray in the ionisation mode was used. Predicted masses were calculated using ExPASy ProtParam Online tool (http://web.expasy.org/cgi-bin/protparam/protparambased) using the sequence obtained after the site-directed mutagenesis.*

5.2.2. Investigation of the Labelling Specificity

The specificity of the labelling method was evaluated by MALDI-ToF-ToF analyses following tryptic digestion. The observed mass difference between the unlabelled protein and its labelled counterpart corresponds to attachment of a single CH_2COCF_3-label per ^{19}F-labelled SPM-1 positive ion. The labelling reaction is shown in **Figure 5.3A**. Labelling was found to be target-specific as the wildtype (wt) protein cysteine, C221, which coordinates the 'second' Zn(II), was reduced and *S*-carbamidomethylated in all samples while C58 and C151 were labelled using BTFA in Y58C* SPM-1 and F151C* SPM-1, respectively **(Figures 5.8-5.11)**. For simplicity, * denotes the presence of the ^{19}F-label. Initial attempts at trypsin digestion were carried out with the guidance of Dr Inga Pfeffer.

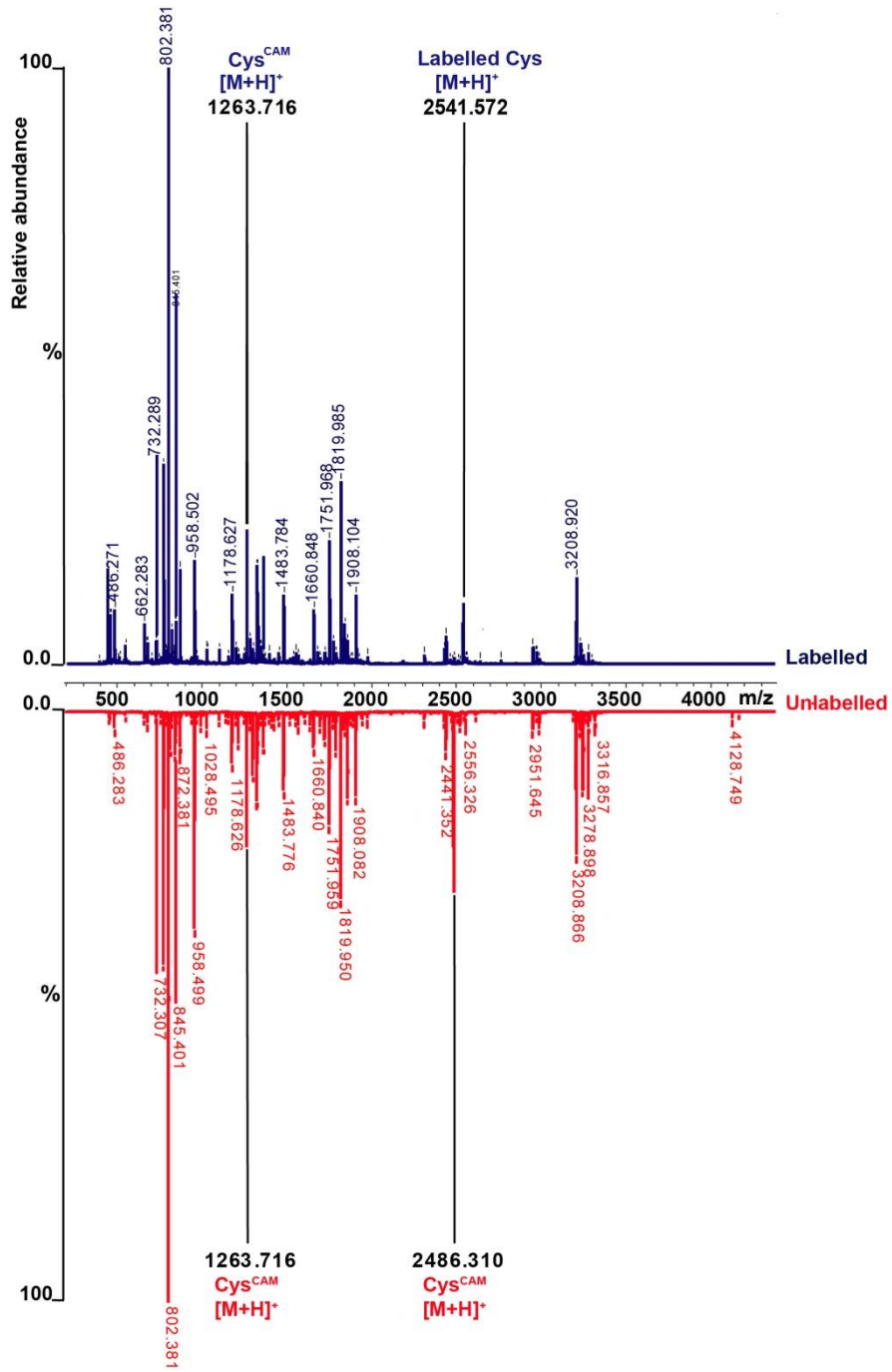

Figure 5.8. MALDI-ToF MS spectra of BTFA-labelled (blue) and unlabelled (red) Y58C SPM-1 digested with porcine trypsin. *The sequence of the peptidic fragment containing Cys221 is LLFGGCMIKPK (m/z = 1206) and that of the peptidic fragment containing Cys58 is IDSDVFVVTDRDFCSSNVLVAK (m/z = 2430). The sample was reduced (DTT) and S-carbamidomethylated (Cys^{CAM}) before digestion. Note that cysteine residue at the active site (Cys221) is unlabelled in both samples (S-cabamidomethylated, m/z = 1263.716), whilst the targeted cysteine (Cys58) is labelled (m/z = 2541.572) in the labelled sample and unlabelled (S-cabamidomethylated) in the control (m/z = 2486.310).*

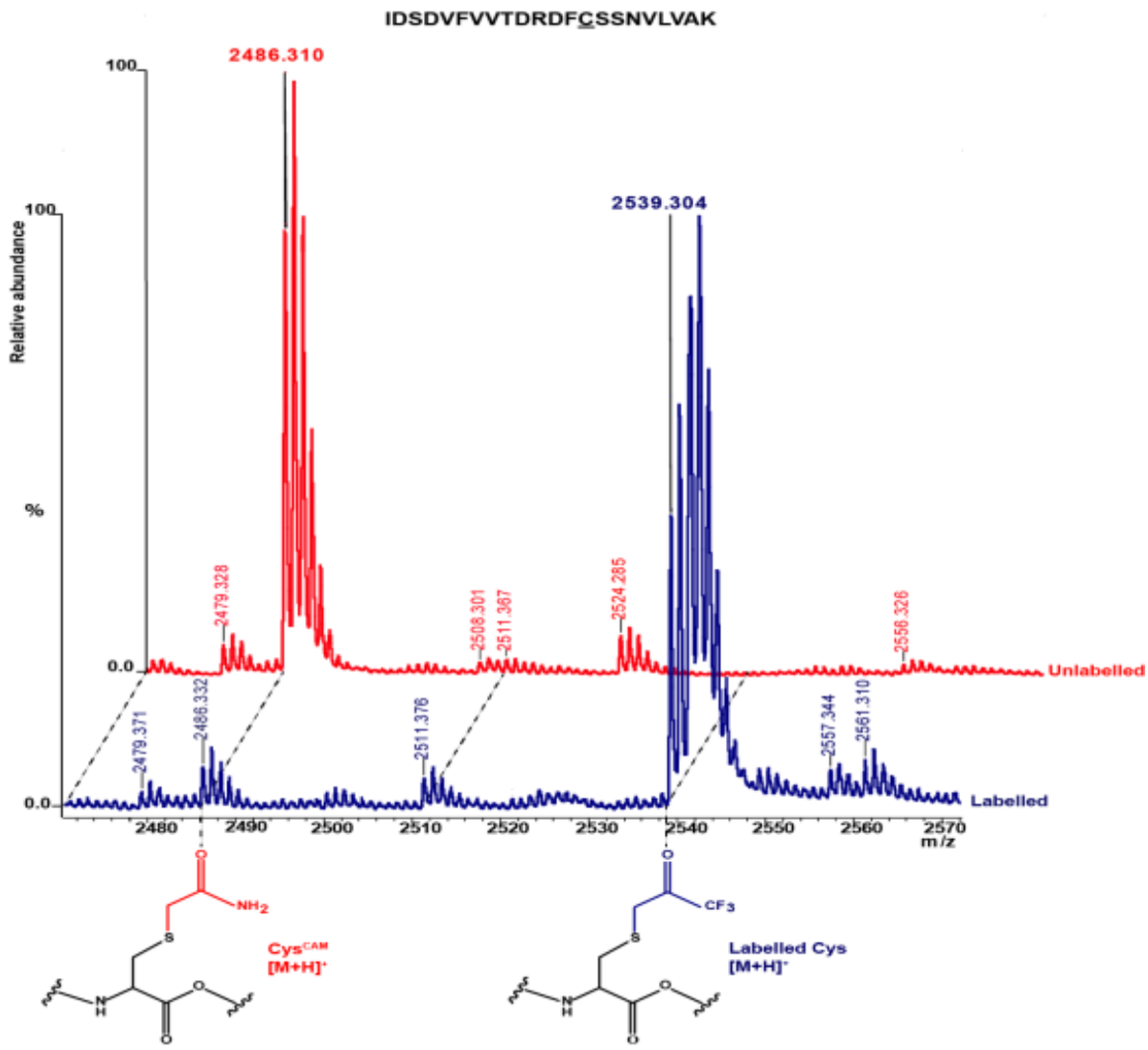

Figure 5.9. MALDI-ToF MS spectra of labelled (blue) and unlabelled (red) Y58C SPM-1 digested with porcine trypsin (Close-up). *The sample was reduced (DTT) and S-carbamidomethylated (Cys^{CAM}) before digestion. Close-up view of the assigned modified peptide (labelled: m/z = 2539.304, S-carbamidomethylated: m/z = 2486.3105). Cys58 was not fluorine-labelled in the control sample (red). Calculation: [2541.572 - (2486.310 – 57)] = 112±2 Da (practical mass corresponding to the incorporation of a CH_2COCF_3-label). The results imply the labelling procedure is efficient (blue).*

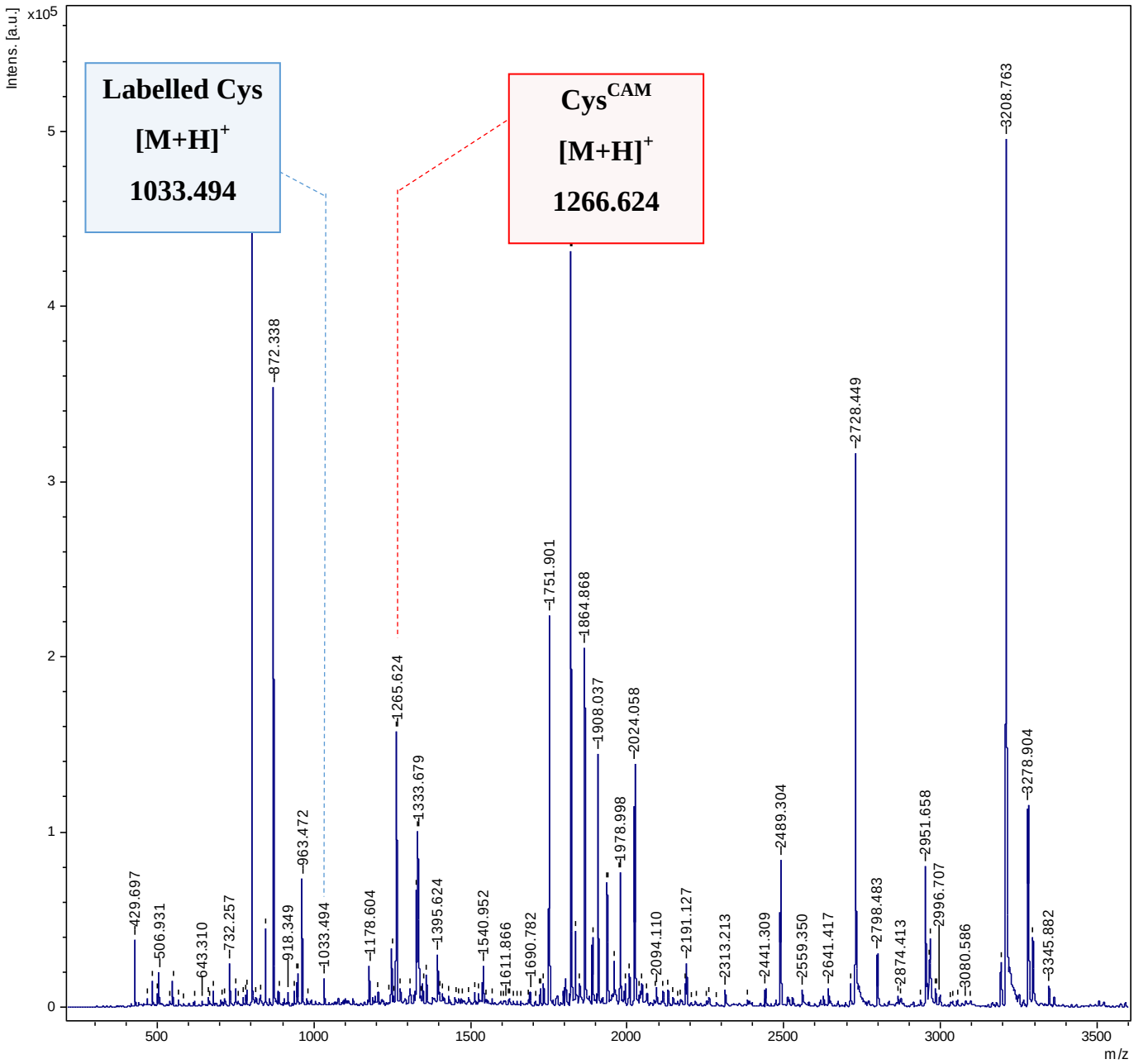

Figure 5.10. MALDI-ToF MS spectrum of BTFA-labelled F151C SPM-1 variant digested with porcine trypsin. *The sequence of the peptidic fragment containing Cys221 is LLFGGCMIKPK (m/z = 1206) and that of the peptidic fragment containing Cys151 is IKAAECYK (m/z = 925). The sample was reduced (DTT) and S-carbamidomethylated (Cys^{CAM}) before digestion. Complete spectrum overview of the digested sample. The cysteine of the active site is unlabelled (S-carbamidomethylated, m/z = 1265.624) while the cysteine of interest (Cys151) was labelled efficiently (m/z= 1033.494).*

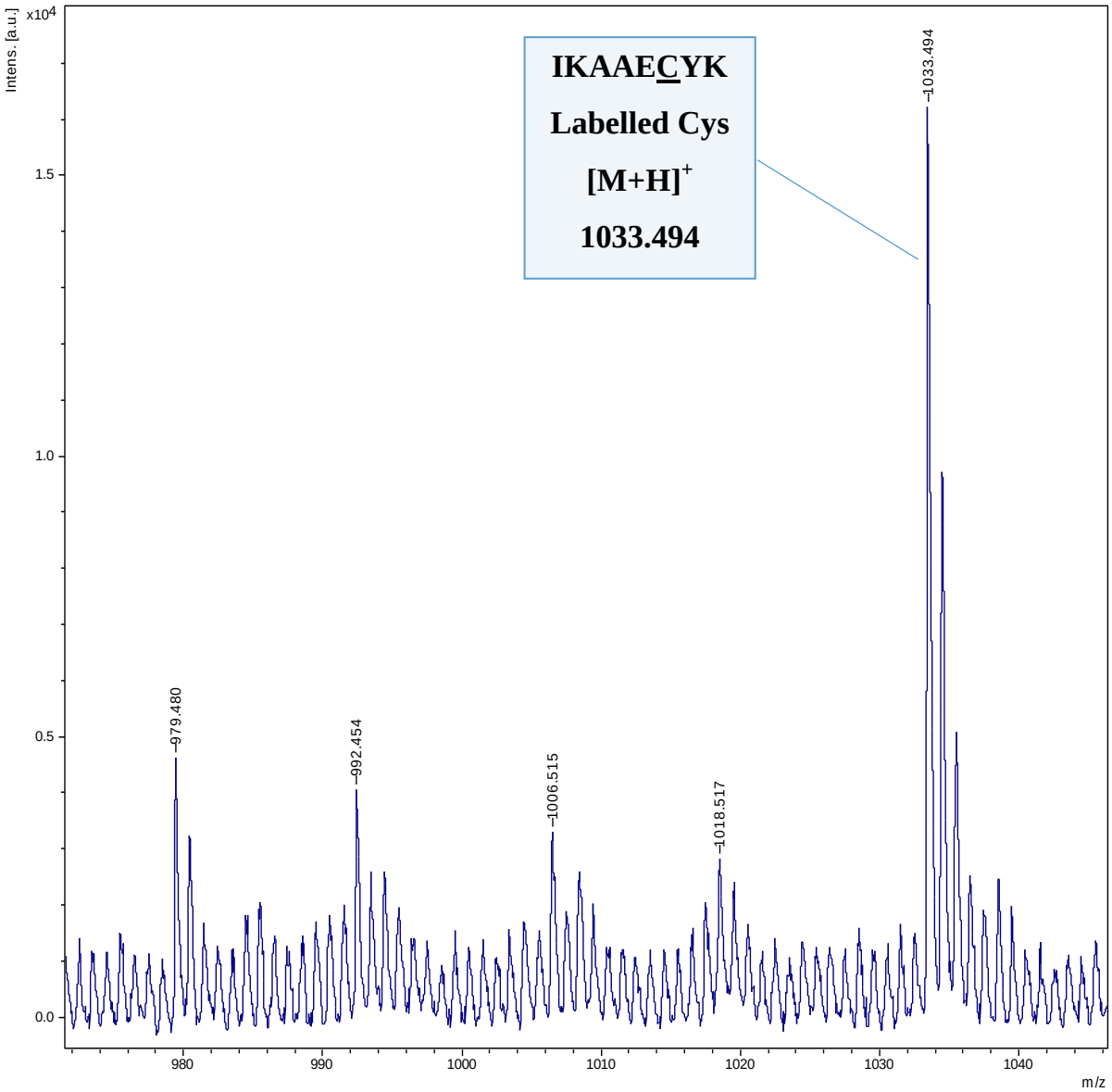

Figure 5.11. MALDI-ToF MS spectra of BTFA-labelled F151C SPM-1 variant digested with porcine trypsin (Close-up). *The sample was reduced (DTT) and S-carbamidomethylated (Cys^{CAM}) before digestion. Close-up view of the assigned modified peptide (labelled: m/z = 1033.494). Calculation: 925 + 110 = 1035 Da (in agreement with the obtained m/z of 1033.494, practical mass corresponding to the incorporation of a CH_2COCF_3-label).*

5.2.3. Structural and Functional Properties of SPM-1* Variants

5.2.3.1. CD Analyses

In order to evaluate the effect of cysteine substitution and fluorination of the SPM-1 variants on the protein secondary structure, circular dichroism (CD) analyses were performed.[63] CD spectra **(Figure 5.12)** for all tested variants were characteristic of well-folded and structured proteins; the β-sheet and α-helical content were in agreement with the crystallographically observed structural features of SPM-1.[164b] The CD spectra of wt SPM-1, Y58C* SPM-1, and F151C* SPM-1 were similar, indicating that cysteine substitutions and fluorination do not substantially affect the overall fold and secondary structure content of SPM-1. CD analyses were carried out with the help of Dr Anne Makena.

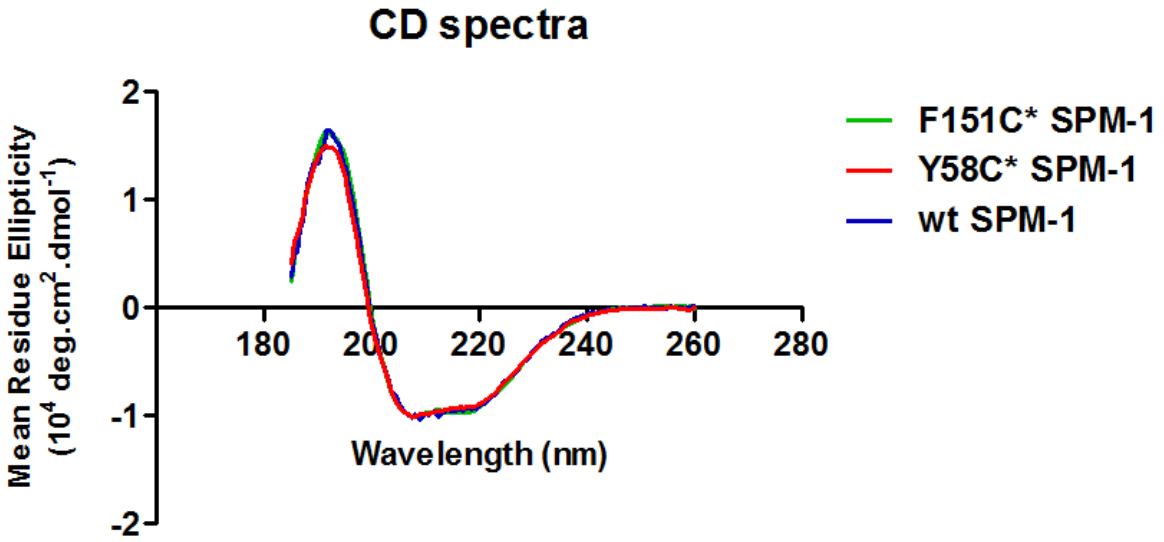

Figure 5.12. CD spectra of SPM-1 variants. *The CD spectra of wildtype SPM-1, Y58C*, and F151C* overlay quite-well, indicating that the secondary content of the proteins tested is comparable. Mean Residue Ellipticity was calculated using the equation:*

$$\theta\ MRE(deg cm^2\ dmol^{-1}) = \frac{\theta(mdeg)}{10^*\ Pathlength(cm)^*[Protein](M)^*\ n\ (no.\ of\ residues)}$$

5.2.3.2. Crystallographic Analyses

In order to investigate whether the cysteine substitution affects the tertiary fold of the protein, a crystal structure of Y58C SPM-1 was obtained by Dr Philip Hinchliffe (resolution 1.75 Å). The results support the proposal that cysteine substitution does not affect the conserved αββα general MBL fold **(Figures 5.13, 5.14)**.

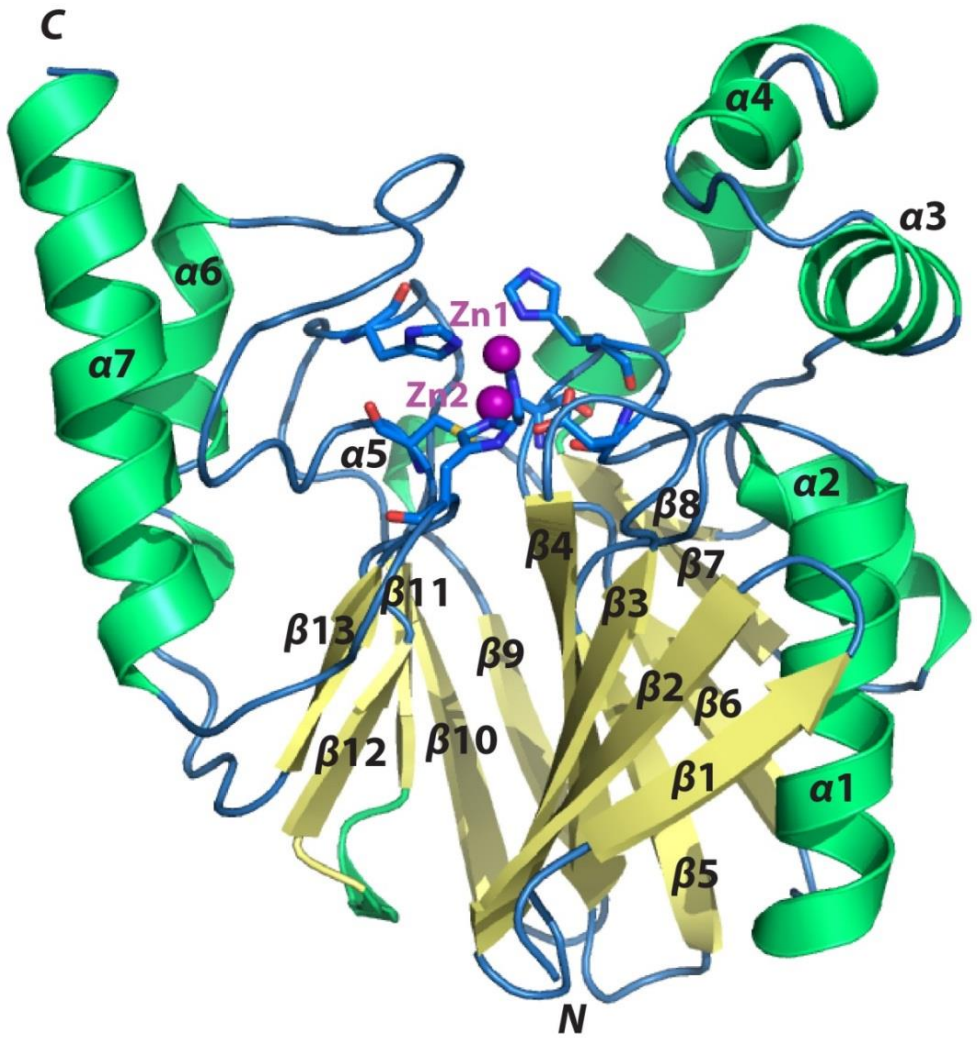

Figure 5.13. View from Y58C SPM-1 variant crystal structure. *(PDB ID: 5LS3). The obtained crystal structure shows that, as expected, Y58C SPM-1 has the conserved αββα general MBL fold.*[164b]

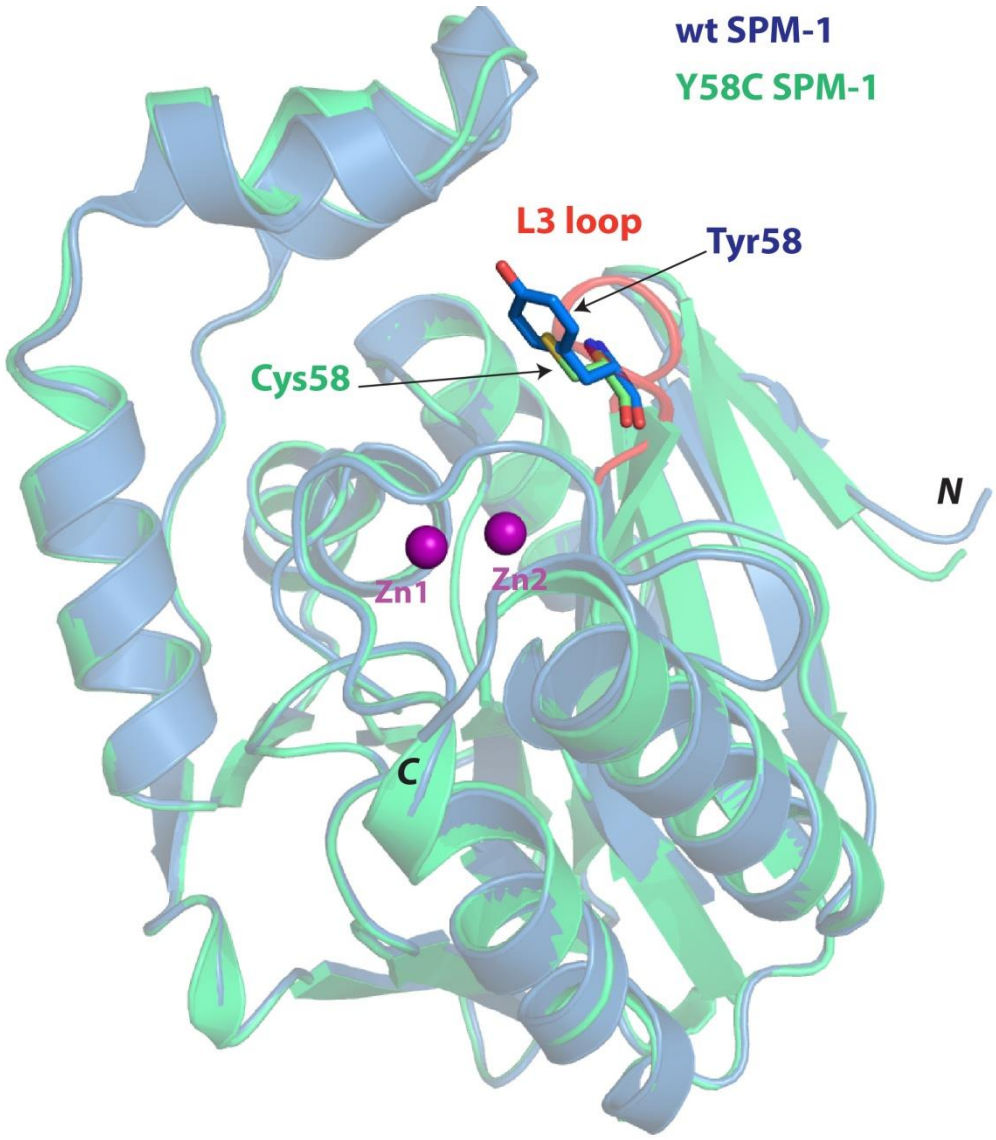

Figure 5.14. Overlay of wt SPM-1 and Y58C SPM-1 variant crystal structures. *The superimposition of both structures shows that tyrosine 58 (in wt SPM-1 structure, PDB ID: 4BP0) and cysteine 58 (in Y58C SPM-1 structure, PDB ID: 5LS3) have the same orientations on the L3 loop.*

5.2.3.3. Kinetic Analyses

In order to investigate the effects of cysteine substitutions and BTFA labelling on SPM-1 activity, kinetic analyses[164b] were conducted using meropenem as a substrate and following the absorbance of its hydrolysed product at 300 nm. The results showed that the introduction of the CH_2COCF_3-label did not significantly alter substrate affinity (*i.e.* similar K_M values were obtained for meropenem with wt, Y58C*, and F151C* SPM-1). A 2.5-fold decrease in the k_{cat} value for meropenem was observed for both Y58C* and F151C* SPM-1, possibly reflecting specific interactions involving the modified residue in enzyme.substrate/intermediate complexes **(Figure 5.15)**.

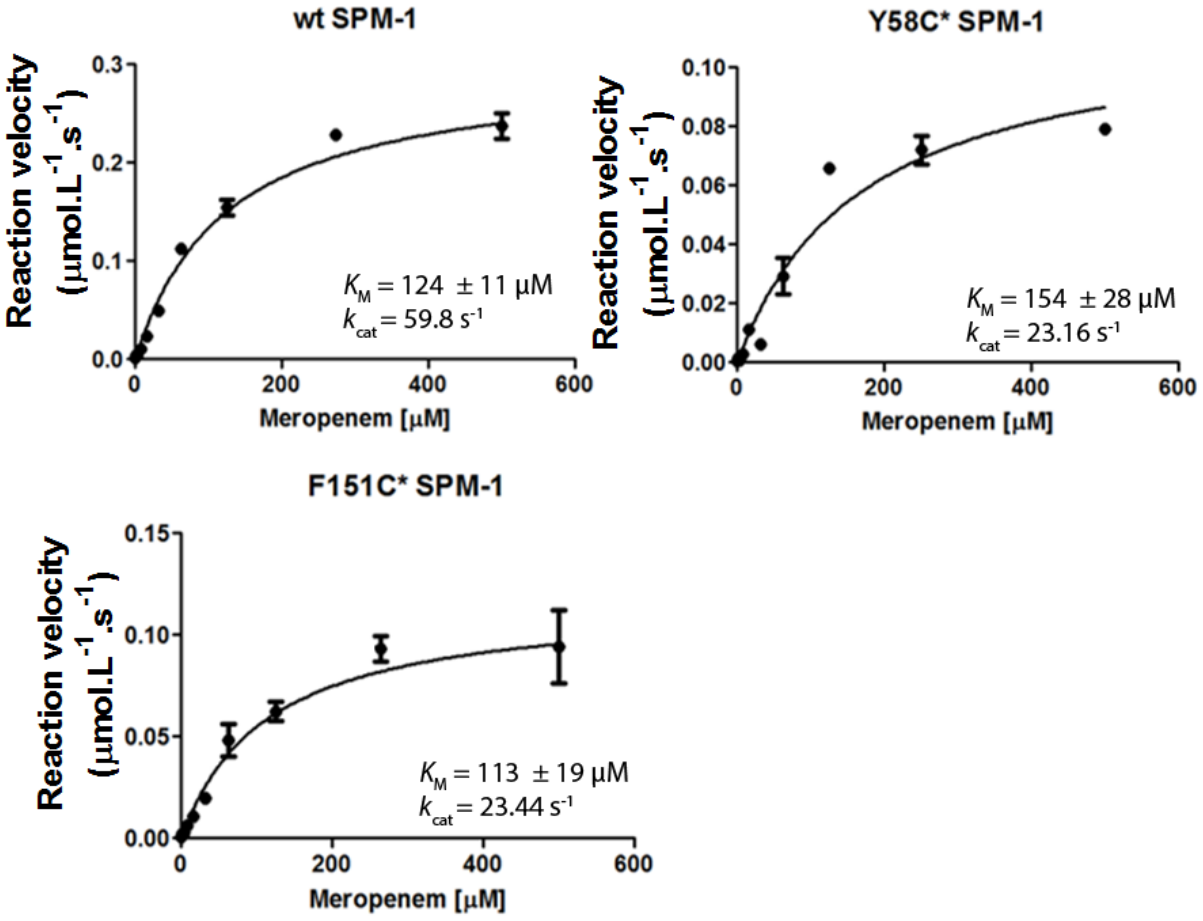

Figure 5.15. Meropenem turnover by wt SPM-1, Y58C* SPM-1 and F151C* SPM-1. Error bars denote SEM, n = 3. Curves were fitted using GraphPad Prism.

Overall, the combined biophysical and kinetic studies demonstrate that the properties of Y58C* and F151C* SPM-1 were sufficiently similar to those of the wt protein, justifying the pursuit of PrOF NMR with them. Together with earlier studies on protein alkylation by BTFA,[171] these results demonstrate that BTFA is a useful reagent for the introduction of a ^{19}F label into proteins by post-translational cysteine alkylation. Hence, ^{19}F-NMR analyses on di-Zn(II) complexes of the Y58C* and F151C* SPM-1 variants were then carried out.

5.2.4. ^{19}F-NMR Spectral Features of SPM-1* Variants

5.2.4.1. Protein-Observe Peaks

The ^{19}F-NMR spectra of the Y58C* and F151C* SPM-1 variants displayed a broader peak than BTFA, consistent with its its incorporation to the large molecule protein system. The increased line width is correlated to the increased molecular correlation time because of the fluorine chemical shift anisotropy contribution to spin-spin relaxation and exchange effects.[93a] Protein-induced fluorine shifts, which were deshielded, can be attributed to van der Waals interactions with the protein tertiary structure and, to a lesser extent, to ring currents, other effects of anisotropic groups in proteins and the effects of electrostatic effects.[90b, 172] The ^{19}F-NMR spectra revealed single major protein-observe resonances at - 83.15 ppm (Y58C* SPM-1) and -84.75 ppm (F151C* SPM-1) indicating that the labelled loops/regions of the variants predominantly existed a single conformation, or, more likely, that the labelled residues are moving rapidly relative to the NMR shift timescale **(Figure 5.16)**. All resonances were reported with respect to the NMR internal standard, trifluoroacetic acid (TFA), whose resonance was calibrated at -75.45 ppm.

5.2.4.2. Variable Temperature Studies

The F151C* variant also displayed broad signals either side of the sharper peak at -84.75 ppm, possibly reflecting conformational motion; however, no changes in the line width and intensity of the signal were observed in variable temperature studies (277 K to 310 K).

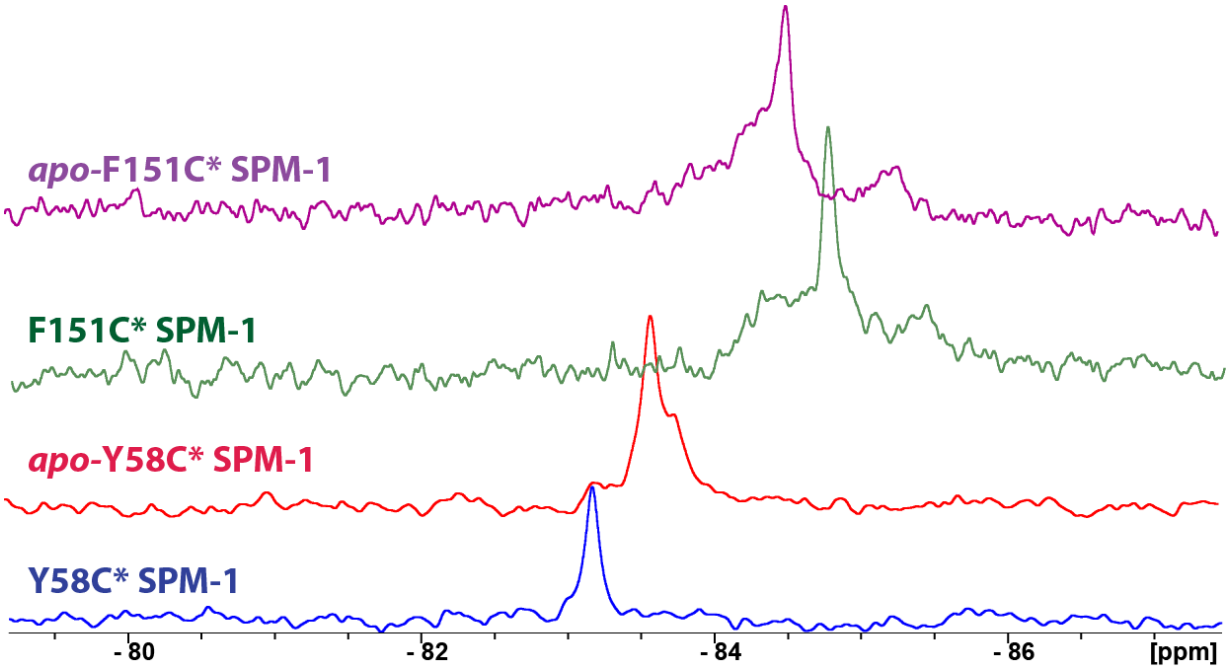

Figure 5.16. PrOF NMR spectra of *apo*- and di-Zn(II)-SPM-1* variants. *The assay mixtures contained SPM-1* variant (40 µM) in 50 mM Tris, pH 7.5, in 90 % H_2O and 10 % D_2O.*

5.2.4.3. Solvent Exposure Studies

Consistent with the crystallographic evidence, solvent isotope exchange studies revealed that F151C*, which is located in the α3 region, is more accessible to the solvent in solution than Y58C*, which is located on the more buried L3 loop **(Figure 5.17)**. Solvent exposure was studied at varied D_2O to H_2O ratio and assessed by comparing the slope of the linear regression fit obtained for the SPM-1* variants to that for the internal standard, TFA.[170, 173]

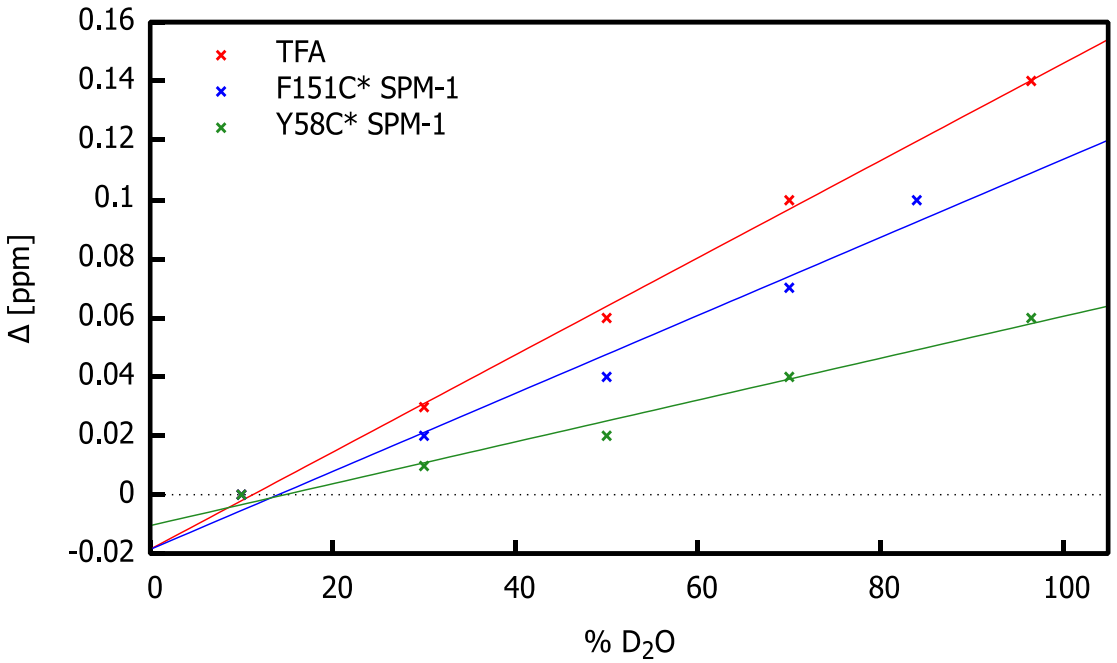

Figure 5.17. Solvent exposure studies of SPM-1* variants by PrOF NMR. *Plot of the chemical shift difference* $\Delta = \delta_{obs} - \delta_0$ *against* D_2O *content for the major protein peak.* δ_0 *refers to the protein chemical shift observed with 10%* D_2O.

Linear regression analyses revealed fitting functions of:

y = 0.00132x-0.018 for F151C SPM-1;*

y = 0.00071x-0.010 for Y58C SPM-1;*

y = 0.00164x-0.018 for TFA.

Red corresponds to TFA, blue to F151C SPM-1, and green for Y58C* SPM-1. The results indicate that F151C* is more exposed to solvent than Y58C*, consistent with crystallographic analyses* ***(Figure 5.14)***.[164b] *The assay mixtures contained SPM-1* variant (40 µM) in 50 mM Tris, pH 7.5, in 90 %* H_2O *and 10 %* D_2O.

5.2.4.4. *Apo*-SPM-1* Variants

Apo-SPM-1* variants were prepared by treating the samples with EDTA overnight. After purification using PD-10 columns, spectra of the *apo*-SPM-1* variants were recorded. They showed different chemical shifts compared to the di-Zn(II)-complexes: - 83.7 ppm for *apo*-Y58C* SPM-1 and - 84.45 ppm for *apo*-F151C* SPM-1 **(Figure 5.16)**. These changes

likely relate to the amphipathic character of fluorine which is linked to its dual propriety to act as a hydrogen bond acceptor or as a hydrophobic moiety. The 'rule of shielding' is proposed to inform on the local environment of fluorine;[174] the type of interaction reflects the local environment of fluorine and thus affects its chemical shift. The shielding observed with *apo*-Y58C* SPM-1 compared to Y58C* SPM-1 suggests that C58* is more involved in hydrophobic interactions in the di-Zn(II)-Y58C* SPM-1 compared to the *apo*-state. In contrast, with *apo*-F151C* SPM-1, a deshielding effect was observed, suggesting that C151* adopts a conformation which is more prone to polar and H-bonding interactions with neighbouring residues in the di-Zn(II) state compared to the *apo*-state of the protein.[174b, 174c]

5.2.4.5. Metal Titration

MBLs are metallo proteins which use either one, or more commonly, two active site Zn(II) ions in catalysis.[175] However, the exact metal content under different conditions and the order of binding to the metal sites is uncertain. Metal binding to SPM-1* was investigated by titrating Zn(II) into *apo*-Y58C* SPM-1 solution. Upon addition of 1 molar equivalent of Zn(II) to *apo*-Y58C* SPM-1, two resonances were clearly observed: one corresponding to the *apo*-Y58C* SPM-1 population at -83.7 ppm and another one at -83.15 ppm which matches with the di-Zn(II)-Y58C* SPM-1 complex resonance. The observation of the resonance at -83.15 ppm could be assigned to the di-Zn(II) complex suggesting that Y58C* SPM-1 is observed in two populations under the experimental conditions (the *apo*- and di-Zn(II) species). This observation is consistent with previous studies on MBLs indicating binding of the first Zn(II) ion promotes binding of the second Zn(II) ion.[176] However, C58* could also adopt the same conformation in both the mono- and di-Zn(II) SPM-1* species leading to the appearance of one averaged resonance. The addition of 2 molar equivalents of Zn(II) led to the appearance of one resonance corresponding to the di-Zn(II)-species **(Figure 5.18)**.

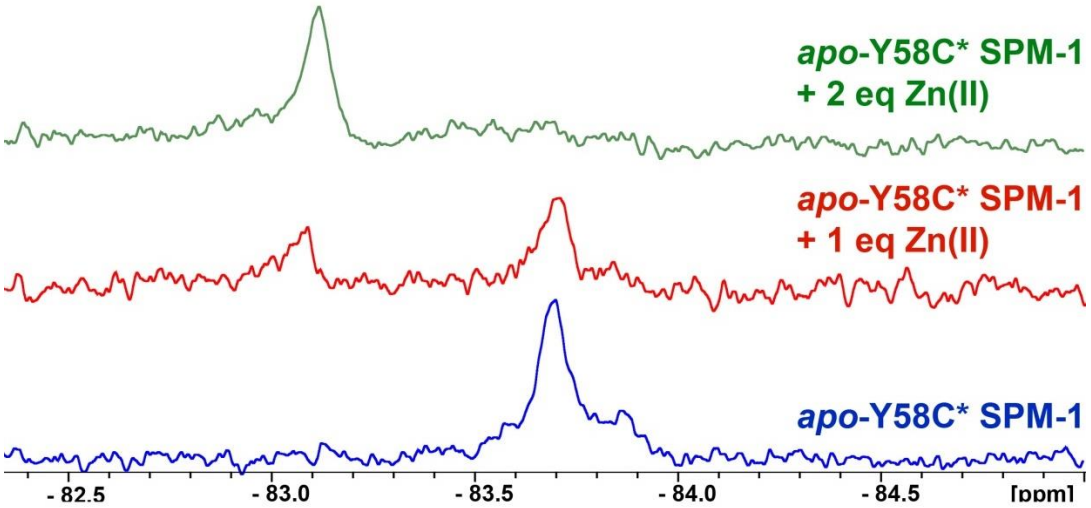

Figure 5.18. Metal titration studies with Y58C* SPM-1 by PrOF NMR. *The assay mixtures contained SPM-1* variant (40 µM) in 50 mM Tris, pH 7.5, in 90 % H_2O and 10 % D_2O.*

In order to further investigate SPM-1 metal content, MS analyses were employed under non-denaturing conditions. Consistent with the NMR data, addition of 1 molar equivalent of Zn(II) led to the apperance of two main peaks: one corresponding to [*apo*-SPM-1 + H]$^+$ (mass: 27875 ± 5 Da) and another one corresponding to [*apo*-SPM-1 + di-Zn(II) + H]$^+$ (mass: 28005 ± 5 Da) (Figure 5.19). However, it cannot be concluded with confidence that the mono-Zn(II)-SPM-1 species does not exist because of potential signal overlaps, detection limits and low resolution. The overall data support a positive co-operativity binding mode of the Zn(II) ions with two states,[176] but cannot confidentially deny the presence of a mono-nuclear state. Previous SPM-1 metal chelation studies have shown that SPM-1 inhibition with chelators fits a biexponential model which consists of one relatively fast step in which a low-affinity zinc ion is removed reasonably quickly and one slower step in which a more tightly bound zinc ion is removed.[165] Accordingly, the mono-nuclear state could be present in solution, and if so, would support a sequential binding mechanism.

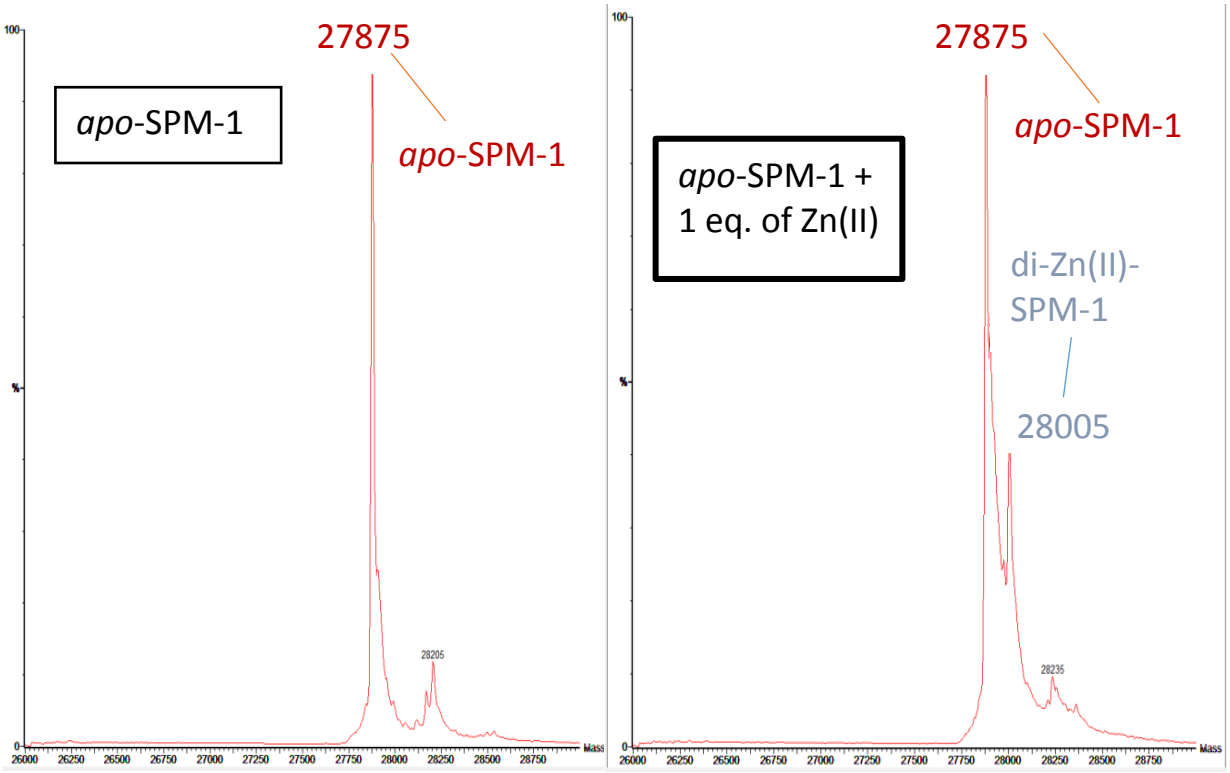

Figure 5.19. Non-denaturing MS analyses of SPM-1 metal content. *The assay mixture contained wt SPM-1 (15 nM) in 15 mM ammonium acetate, pH 7.5.*

5.2.4.6. DMSO Titration

Organic solvents can be used as detection probes of potential binding sites and have been shown to bind in empty cavities of proteins.[177] In order to investigate the effect of DMSO on the SPM-1 active site, a DMSO titration into SPM-1* variants was carried out **(Figure 5.20)**. The change of the chemical shift of the labelled protein peak was measured as a function of increasing concentration of DMSO and normalised to TFA chemical shift changes. The shift of the protein label variants was found to be more sensitive to increasing DMSO concentration than the shift of the TFA signal, indicating that DMSO can weakly bind to the SPM-1* variants. Accordingly, the binding of DMSO to SPM-1* shows that a sulphoxide moiety could be a starting point for the design of SPM-1 inhibitors, and by implication, other MBLs.

DMSO is constantly used to dissolve inhibitors/ligands in binding studies.[177a] It was thus important to study the binding of DMSO to SPM-1* variants as a control experiment, in order to evaluate whether the changes of chemical shift observed upon addition of ligands from DMSO stocks are solely due to DMSO effects.

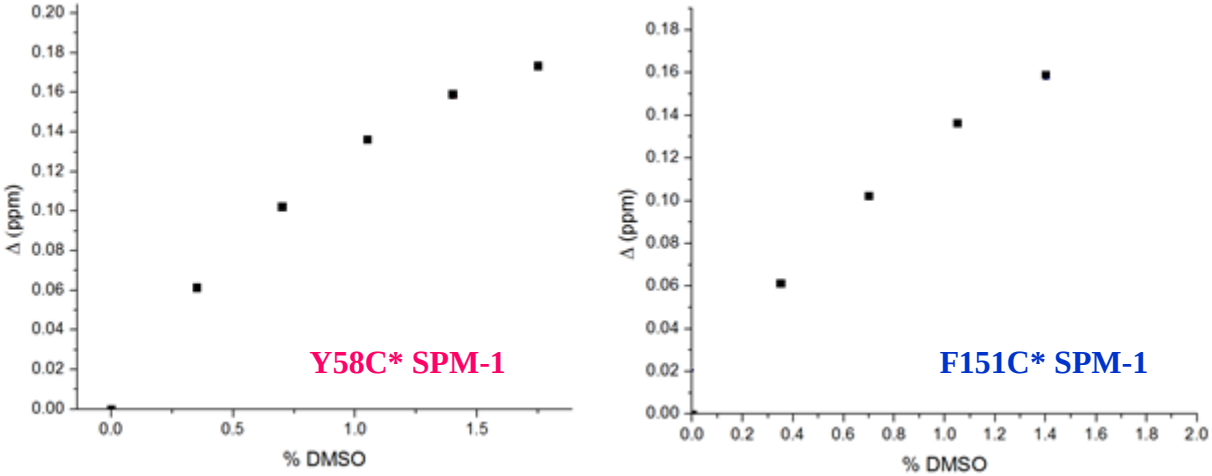

Figure 5.20. Metal titration studies with Y58C* SPM-1 by PrOF NMR. *The assay mixtures contained SPM-1* variant (40 µM) in 50 mM Tris, pH 7.5, in 90 % H_2O and 10 % D_2O. The cut-off limit was set to 0.1 ppm; samples contained 0.8 % DMSO at the highest ligand concentration (400 µM).*

Accordingly, the changes observed hereafter were reported in terms of the chemical shift changes, whereby $\Delta\delta_{max} = \delta_{max} - \delta_0$ represents the chemical shift difference (in ppm) between δ_{max} and δ_0, in which δ_{max} = δ observed in the presence of 400 µM of the ligand added from a 50 mM DMSO stock and δ_0 = δ of the SPM-1* variant in the absence of added ligand and DMSO, δ_0 = - 83.15 ppm for Y58C* SPM-1 and δ_0 = - 84.75 ppm for F151C* SPM-1 (reference: trifluoroacetic acid, TFA, δ_{TFA} = - 75.45 ppm). For $\Delta\delta_{max} < 0.1$ ppm, which was used as a cut-off value, observations were considered insignificant and were denoted as 'no substantial changes', mostly due to DMSO effects (0.8 % DMSO). Assignment of slow/fast exchanges and peaks corresponding to protein.inhibitor complexes should be regarded as probable and relative to the chemical shift time scale.

5.2.5. Protein-Ligand Interactions by PrOF NMR

PrOF NMR was then used to investigate the binding of representative MBL ligands to the Y58C* and F151C* SPM-1 variants. The protein-ligand interactions were also monitored by ^{1}H NMR spectroscopy as a secondary screening assay; however, ^{1}H NMR data are only shown wherever they add value to the PrOF NMR analyses. The NMR observations are summarised in **Table 5.1**.

5.2.5.1. Interactions with Representative MBL Inhibitors

5.2.5.1.1. Interactions with a metal chelator, 1,10-o-phenanthroline

Initially, reported zinc chelating MBL inhibitors were tested to validate SPM-1* variants for investigating ligand binding.[165] On addition of the zinc chelator, 1,10-*o*-phenanthroline, new NMR peaks in a slow exchange system relative to the chemical shift timescale[90b] were observed with both the Y58C* and F151C* SPM-1 variants **(Figures 5.21, 5.22)**. These peaks are the same as those observed for *apo*-SPM-1* spectra, this is consistent with anticipated Zn(II) chelation in solution by 1,10-*o*-phenanthroline.[165] 1,10-*o*-Phenanthroline was not observed to bind to *apo*-Y58C* SPM-1. These results thus reveal the utility of PrOF NMR in detecting metal chelation/binding in solution and/or to the protein, which is not always readily trivial in studies on metallo enzyme inhibition.

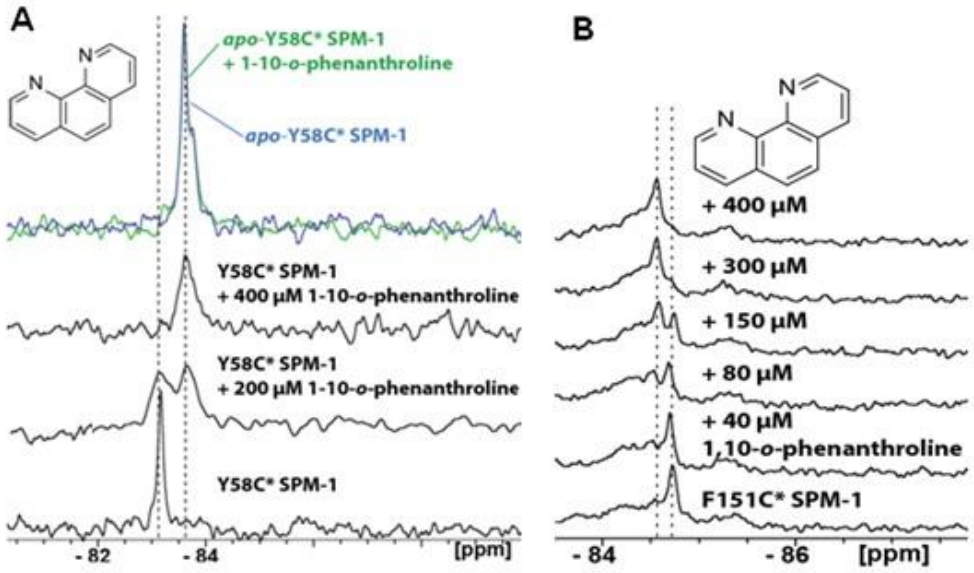

Figure 5.21. ^{19}F-NMR spectra of the interactions of 1,10-*o*-phenanthroline with (A) Y58C* SPM-1 and (B) F151C* SPM-1. *The assay mixtures contained 40 µM SPM-1* in 50 mM Tris, pH 7.5, 90 % H_2O and 10 % D_2O.*

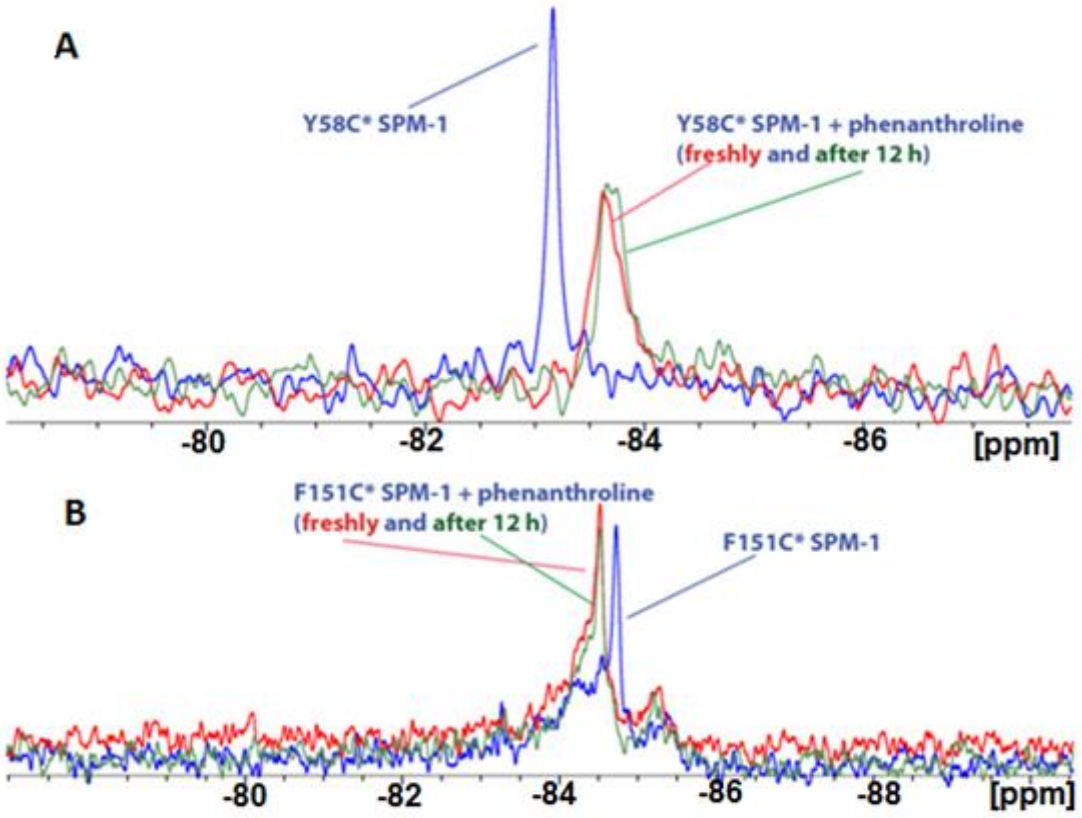

Figure 5.22. ^{19}F-NMR time-course spectra of SPM-1* variants with 1,10-o-phenanthroline. *The assay mixtures contained 40 µM Y58C* SPM-1* ***(A)*** *(blue trace) or F151C* SPM-1* ***(B)*** *and 400 µM ligand (freshly: red trace, repeated after 12 hours: green) in 50 mM Tris, pH 7.5, in 90 % H_2O and 10 % D_2O.*

5.2.5.1.2. Interactions with ML302/ML302F

ML302 (and its hydrolysed product, ML302F) is a broad-spectrum MBL inhibitor.[178] ML302 and ML302F were provided by Dr Klaus-Daniel Umland. The rhodanine, ML302, and thioenolate, ML302F (produced by enzyme- or non-enzyme-catalysed hydrolysis of ML302), gave rise to the appearance of new peaks shielded relative to the uncomplexed Y58C* SPM-1 at -83.75 ppm, indicative of a slow exchange on the chemical shift timescale. Time-course analysis with Y58C* SPM-1 shows a stable inhibitor-protein complex over time: ML302 appears to be bound to the protein after 12 h; most probably in its ML302F form as ML302F in complex with Y58C* SPM-1 peak shares the same chemical shift. Moreover, the interactions of the rhodanine compounds with F151C* SPM-1 led to the appearance of a new peak at -84.40 ppm, in a slow exchange fashion **(Figure 5.24)**. This peak might correspond to a new conformation adopted by the α3 region upon rhodanine binding, which is stable over time. These observations are consistent with the likely hydrolysis of ML302 to give ML302F under the incubation conditions **(Figure 5.23)**. These results are in agreement with the similar inhibition potencies of ML302 and ML302F observed with SPM-1.[179] Furthermore, these results indicate interactions between the α3 region and the inhibitors, and thus have potential implication as a target for inhibitor design.

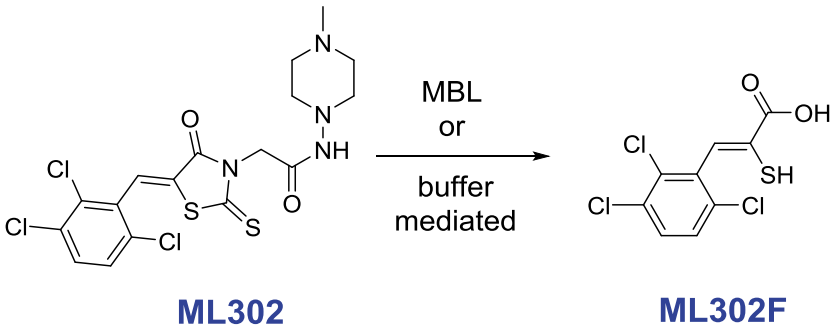

Figure 5.23. Scheme showing the structures of ML302 and ML302F.

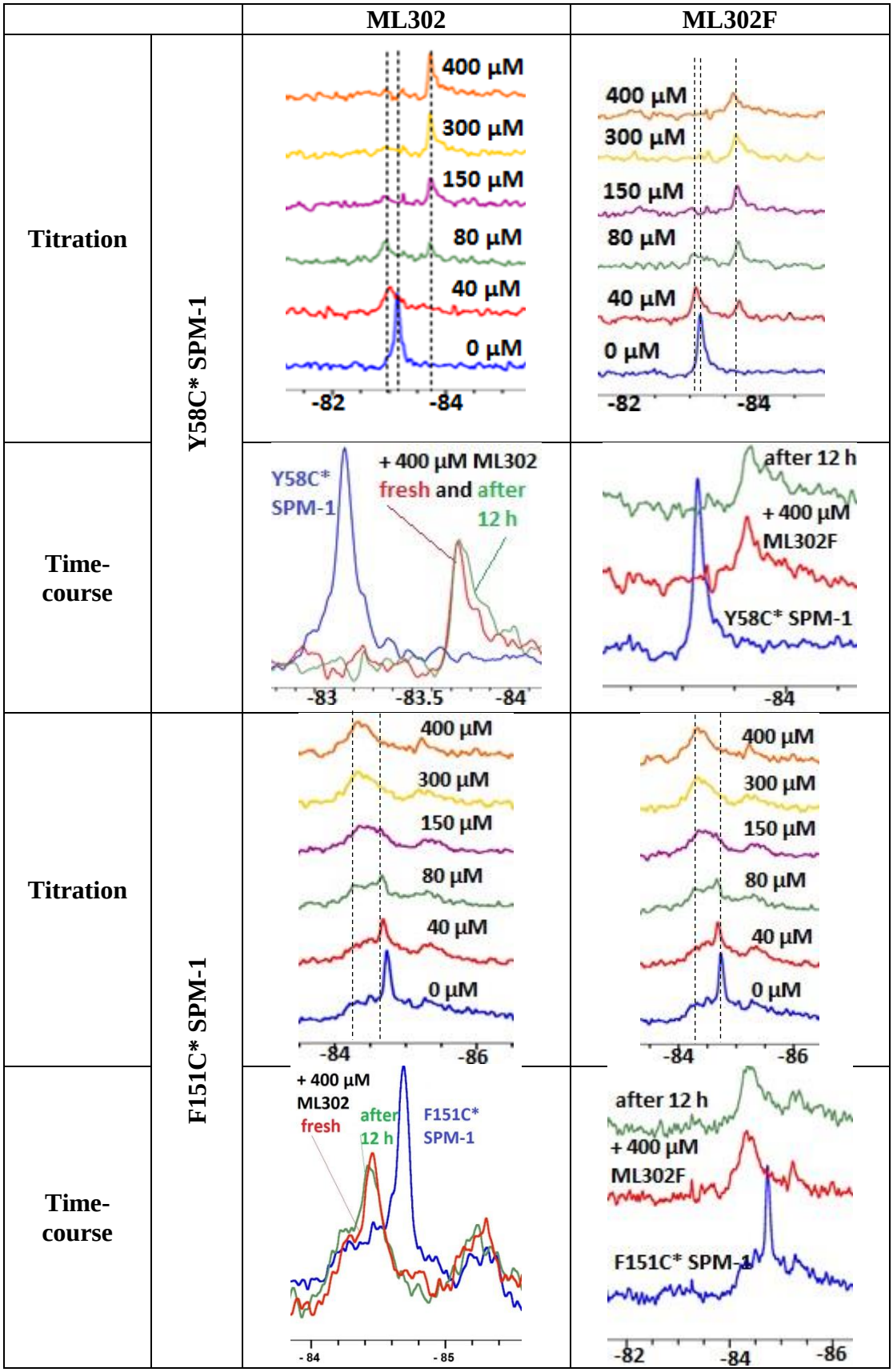

Figure 5.24. PrOF NMR analyses of ML302 and ML302F with SPM-1* variants. *The assay mixtures contained 40 µM SPM-1* in 50 mM Tris, pH 7.5, in 90 % H_2O and 10 % D_2O.*

5.2.5.1.3. Interactions with a weak inhibitor, L-captopril

In contrast, L-captopril, which is reported as a good inhibitor of B1 MBLs,[180] but a very poor inhibitor for SPM-1 (IC_{50} > 500μM)[181] and class B2 MBLs,[180, 182] did not manifest substantial changes in the ^{19}F spectrum for either of the SPM-1* variants **(Figure 5.25)**. SPM-1 is a hybrid B1 and B2 MBL, the observation that SPM-1 is not inhibited/does not interact with L-captopril, a class B1 inhibitor, suggests that SPM-1 might be more similar to B2 MBLs rather than B1 MBLs in terms of its inhibition requirements.

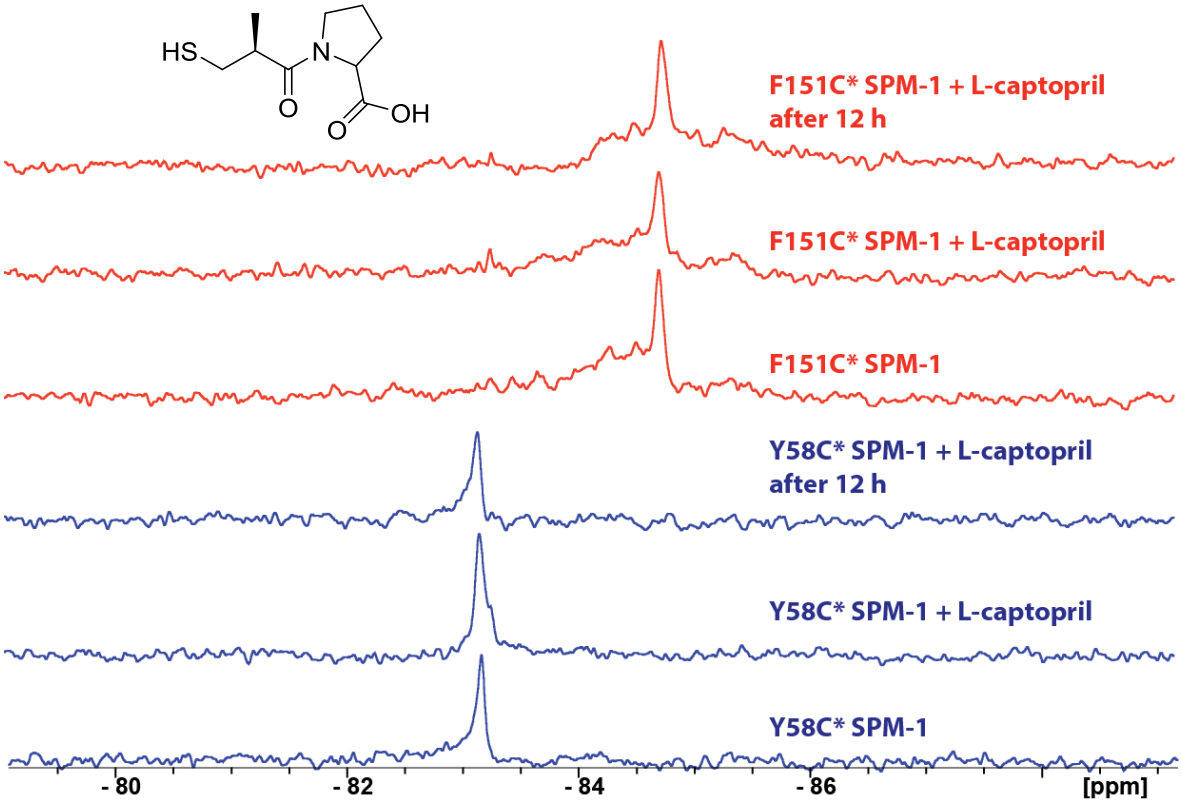

Figure 5.25. ^{19}F-NMR spectra of L-captopril with SPM-1* solutions. *No substantial changes are observed upon addition of 400 μM L-captopril to SPM-1* solutions, including after 12 h. The assay mixtures contained 40 μM SPM-1* in 50 mM Tris, pH 7.5, in 90 % H_2O and 10 % D_2O.*

5.2.5.1.4. Interactions with an isoquinoline derivative, a new binding mode

Isoquinoline derivatives have been reported as MBL inhibitors,[183] but their binding mode is currently unknown. To investigate isoquinoline binding **(Figures 5.26, 5.27)**, a

known isoquinoline MBL inhibitor **5.1** (provided by Dr Anna Rydzik) was titrated into Y58C* SPM-1 solution; significant line broadening upon complex formation was observed, which is typical for an intermediate exchange system.[93a] The addition of ML302F into a sample containing Y58C* SPM-1 and the isoquinoline derivative **5.1** led to the appearance of a peak characteristic of the ML302F bound complex and a new peak, at 1.1 ppm higher than Y58C* SPM-1 peak, suggesting **5.1** can bind in the presence of ML302F **(Figure 5.26A)**. Isoquinoline **5.1** was also found to interact with F151C* SPM-1, inducing broadening and chemical shifts upon its addition **(Figure 5.26B)**. Moreover, the isoquinoline derivative **5.1** was observed to bind to *apo*-Y58C* SPM-1 suggesting that it might potentially have an unprecedented inhibition mode which does not involve metal chelation.

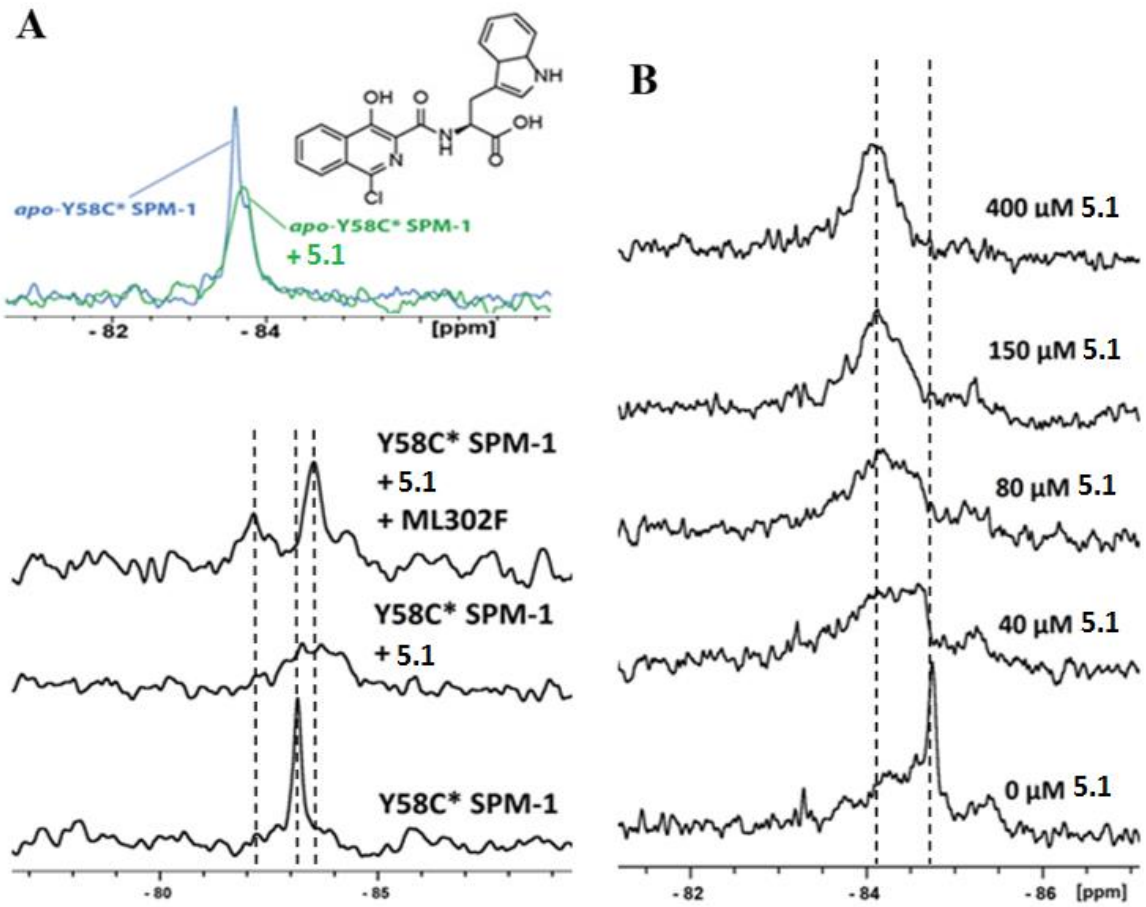

Figure 5.26. ^{19}F-NMR spectra of the interactions of isoquinoline 5.1 with (A) Y58C* SPM-1 and (B) F151C* SPM-1. *Assay mixtures contained 40 µM SPM-1* in 50 mM Tris, pH 7.5, 90 % H_2O and 10 % D_2O.*

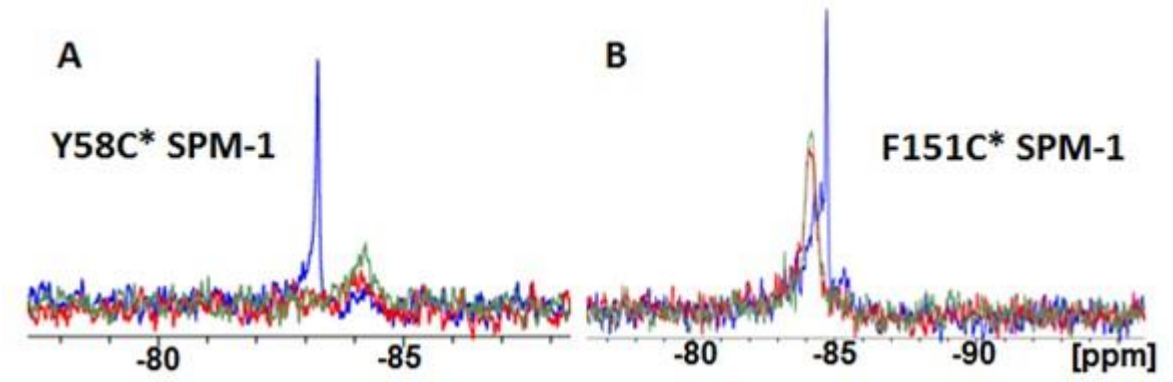

Figure 5.27. ^{19}F-NMR time-course spectra of SPM-1* variants with the isoquinoline derivative 5.1. *The assay mixtures contained 40 µM Y58C* SPM-1* **(A)** *(blue trace) or F151C* SPM-1* **(B)** *and 400 µM isoquinoline derivative* ***5.1*** *(freshly: red trace, after 12 hours: green) in 50 mM Tris, pH 7.5, in 90 % H_2O and 10 % D_2O.*

5.2.5.1.5. Interactions with a poor substrate, avibactam

The applicability of the ^{19}F-NMR method to monitor binding of weak SPM-1 inhibitors was then tested, exemplified by avibactam **(Figure 5.28)**, which inhibits class A, C, and some D β-lactamases.[184] A chemical shift was observed on addition of avibactam into the Y58C* SPM-1 variant, while no substantial changes were observed with the F151C* SPM-1 variant **(Figure 5.29)**. With Y58C*, a shift back to the original protein peak was observed after 12 h incubation; this may be related to the slow hydrolysis of avibactam known to be catalysed by SPM-1.[40, 185] Indeed, addition of fresh avibactam to the reacted solution shifted back the peak towards that arising originally observed on addition of avibactam to Y58C* SPM-1 . The results show avibactam binding induces changes in the L3, but not α3, region. In the time-course, the changes observed are likely due to the slow SPM-1 catalysed avibactam hydrolysis.[185]

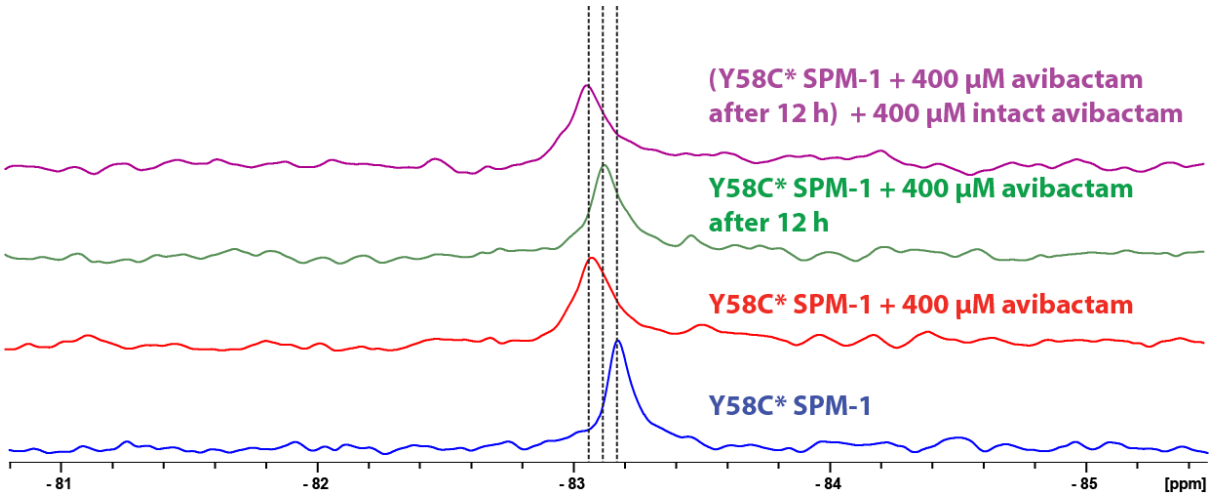

Figure 5.28. ^{19}F-NMR spectra of avibactam with Y58C* SPM-1. *The assay mixtures contained 40 µM SPM-1* in 50 mM Tris, pH 7.5, in 90 % H_2O and 10 % D_2O.*

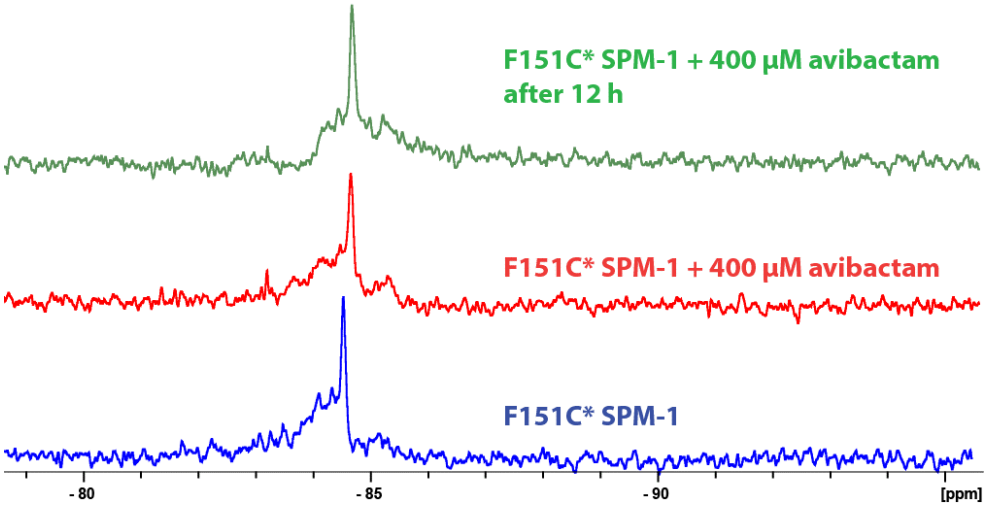

Figure 5.29. ^{19}F-NMR spectra of avibactam with F151C* SPM-1. The assay mixtures contained 40 µM SPM-1* in 50 mM Tris, pH 7.5, in 90 % H_2O and 10 % D_2O.

5.2.5.2. Interactions with β-Lactam Substrates

The results of adding β-lactam substrates (a carbapenem - meropenem, a penicillin - piperacillin, and mechanism-based inhibitors of class A β-lactamases, tazobactam and clavulanic acid) to the Y58C* and F151C* SPM-1 variants were then investigated. Addition

of all these β-lactams to the Y58C* or F151C* variants led to clear observations of broadening and chemical shift changes for Y58C*, but not for F151C* (within detection limits). The changes observed in the ^{19}F-NMR of the Y58C* variant may reflect the close vicinity of its side chain to the active site,[164a] and its likely role in catalysis as revealed by previously assigned MBL-intermediate structures with other MBLs.[55]

5.2.5.2.1. Interactions with meropenem

Meropenem treatment (400 μM) with SPM-1* leads to a 0.95 ppm chemical shift of the Y58C* SPM-1 peak and a line broadening, which are characteristics of a fast to intermediate exchange system on the chemical-shift time scale **(Figure 5.30A)**.[186] No substantial changes, under the experimental conditions, were observed with the F151C* SPM-1 variant indicating no interactions with the mobile α3 region **(Figure 5.30C)**. A time course analysis with meropenem and Y58C* SPM-1 showed the formation of a stable complex over time indicating that hydrolysed meropenem was still bound to Y58C* SPM-1 after 12 h **(Figure 5.30B)**. The presence of the hydrolysed species was observed by ^{1}H NMR analyses **(Figure 5.31)**. The binding of hydrolysed carbapenem has been previously observed with NDM-1, a B1 MBL.[55] Analysis of NDM-1 crystal structure in complex with hydrolysed meropenem **(Figure 5.34)** shows the vicinity of the binding site of hydrolysed meropenem to the L3 loop (Y58 residue) and further emphasises important interactions between the hydrolysed species and the conserved L3 loop region amongst B1 MBLs.

To investigate the binding of hydrolysed meropenem to SPM-1, the *Bacillus cereus* BcII MBL[187] was used to catalyse its hydrolysis. BcII was removed out of the solution mixture using a PD-10 column and the purity of the hydrolysed meropenem was assessed by NMR. Addition of the hydrolysed meropenem to Y58C* manifested a similar peak at -82.95 ppm **(Figure 5.33)**. The binding of hydrolysed meropenem to SPM-1 was further confirmed by ^{1}H and wLOGSY analyses **(Figure 5.32)**.

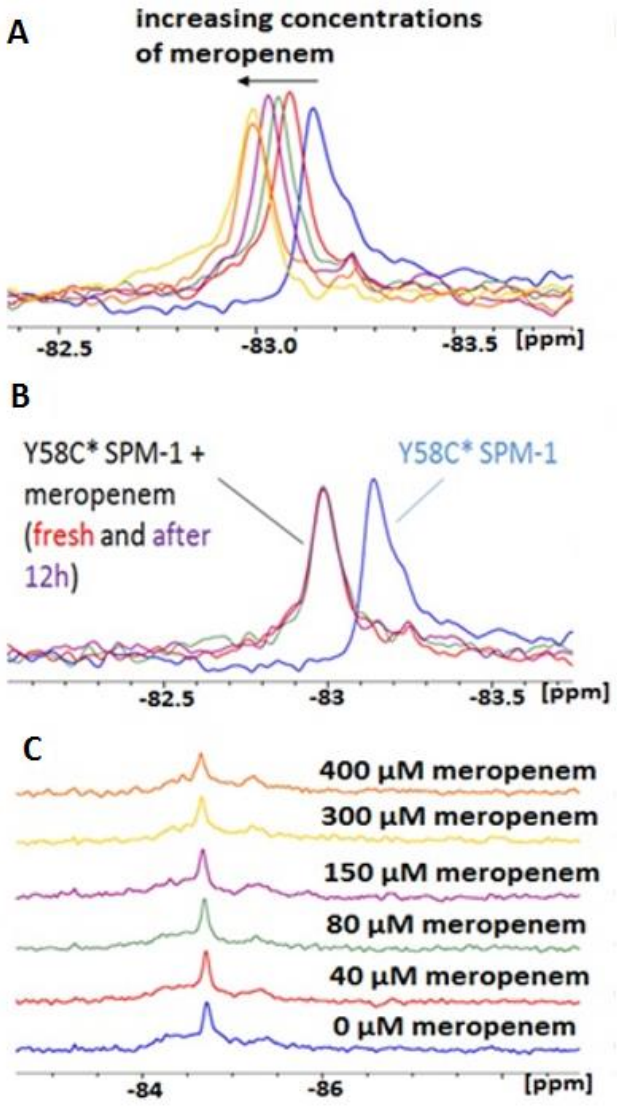

Figure 5.30. Interactions of hydrolysed meropenem with SPM-1* variants by PrOF NMR. *Titration of (A) meropenem into a solution of Y58C* SPM-1 reveals interactions with the L3 variant. Time-course analyses (after 12 h) with (B) meropenem with Y58C* SPM-1 variant are consistent with a stable protein.product peak. Titration of (C) meropenem into a solution of F151C* SPM-1 show no substantial changes. Assay mixtures contained 40 µM SPM-1* variant and increasing ligand concentrations (up to 400 µM) in 50 mM Tris, pH 7.5, in 90 % H_2O and 10 % D_2O.*

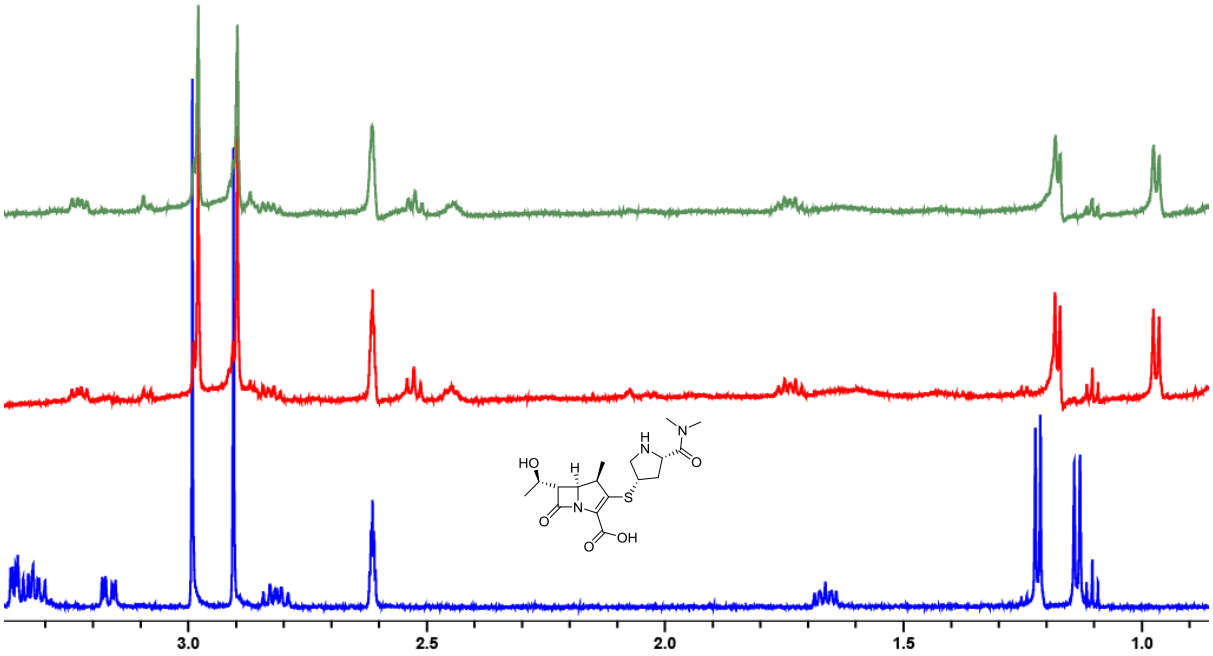

Figure 5.31. ^{1}H CPMG NMR spectra of meropenem with SPM-1 variants. *The assay mixture contained 400 µM meropenem (blue trace), in the presence of 40 µM Y58C* SPM-1 (red trace) or 40 µM F151C* SPM-1 (green trace) after monitoring the reaction for 10 min in 50 mM Tris-D_{11}, pH 7.5, in 90 % H_2O and 10 % D_2O.*

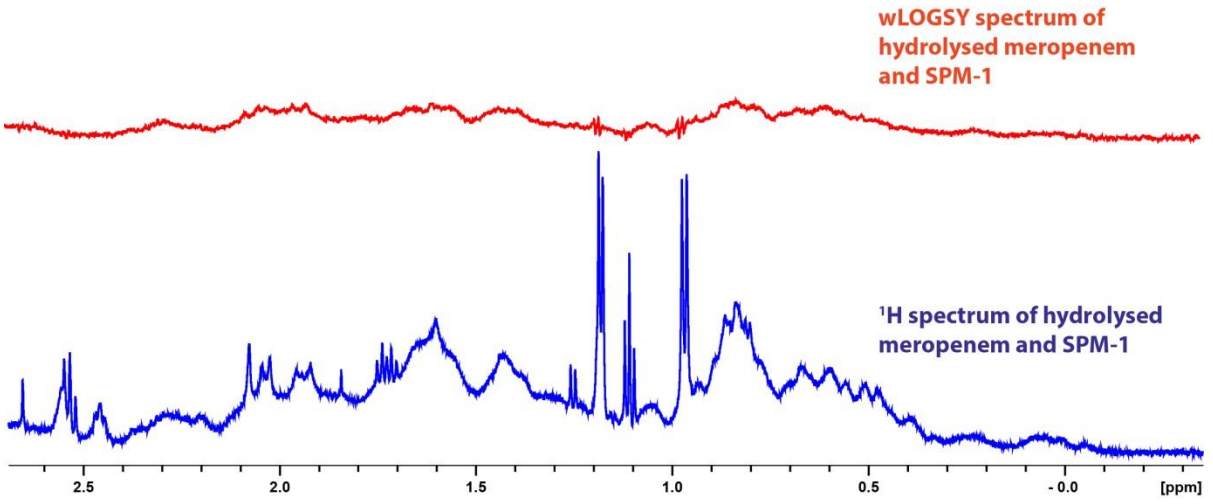

Figure 5.32. Monitoring the binding of hydrolysed meropenem to SPM-1 by ^{1}H and wLOGSY NMR. *The assay mixture contained 400 µM hydrolysed meropenem produced by BcII-mediated catalysis with 40 µM SPM-1 in 50 mM Tris-D_{11}, pH 7.5, in 90 % H_2O and 10 % D_2O.*

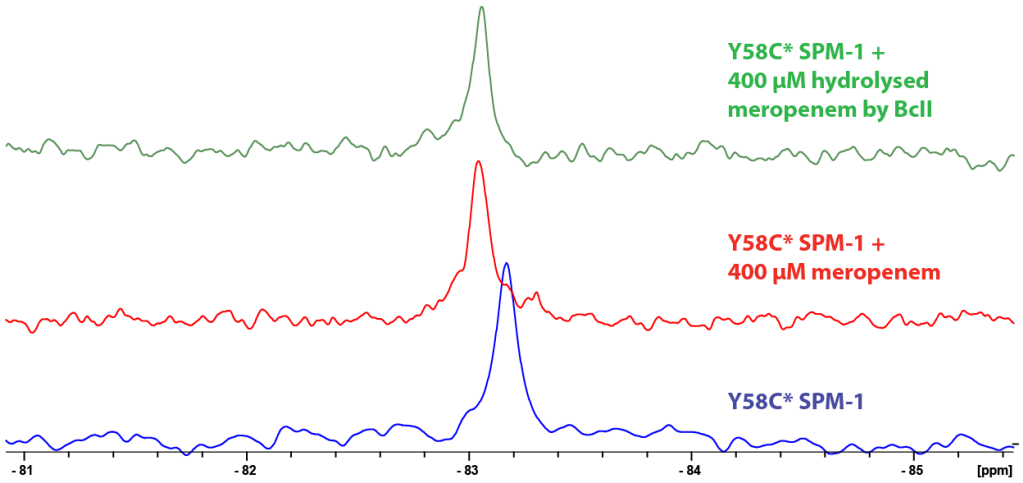

Figure 5.33. ^{19}F-NMR of Y58C* SPM-1 interaction with hydrolysed meropenem. *The assay mixtures contained 40 µM Y58C* SPM-1 (blue trace) and 400 µM added ligand in 50 mM Tris, pH 7.5, in 90 % H_2O and 10 % D_2O.*

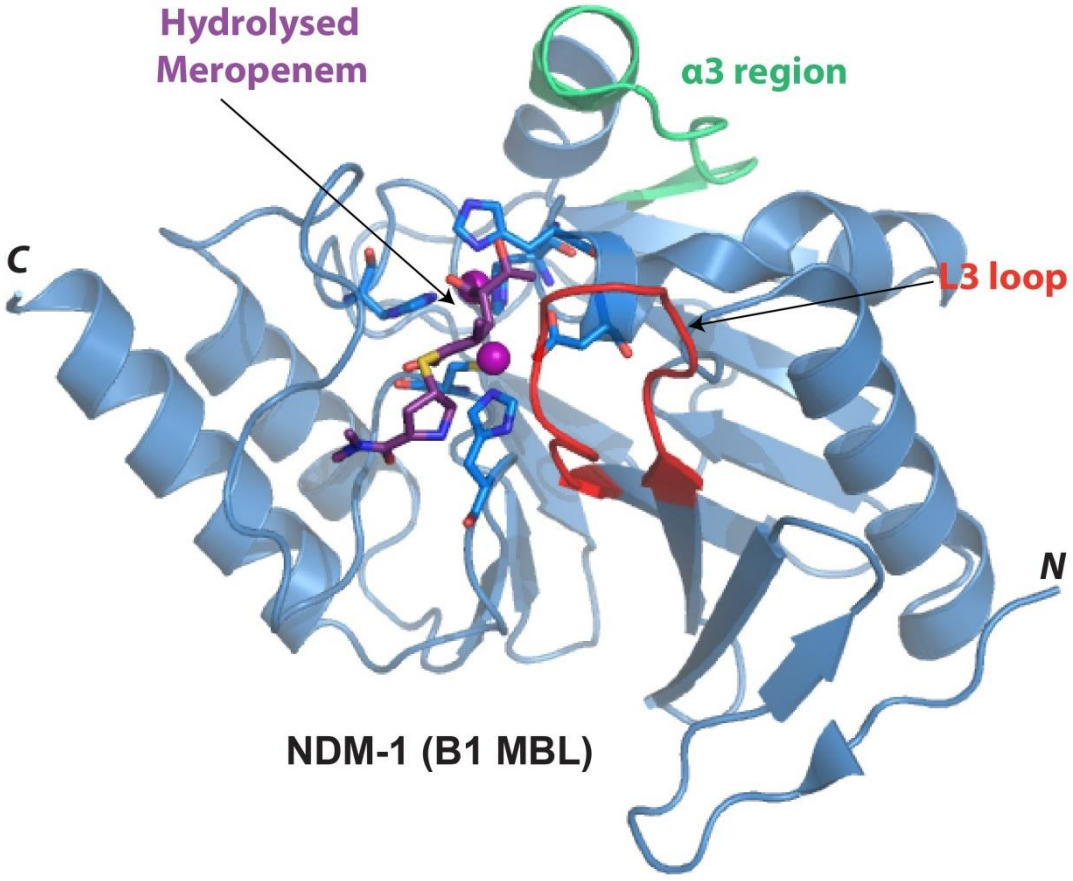

Figure 5.34. View from NDM-1 crystal structure in complex with hydrolysed meropenem. *(PDB ID: 4EYL).*[55] *Hydrolysed meropenem binds to the active site of New Delhi MBL-1 (NDM-1), a B1 subfamily MBL, in close proximity to the L3 loop.*

5.2.5.2.2. Interactions with piperacillin

As shown in **Figure 5.35A**, the addition of 400 µM piperacillin to free Y58C* SPM-1 led to a 0.95 ppm downfield chemical shift of the free Y58C* SPM-1 peak from -83.8 ppm to -82.85 ppm; these observations are characteristic of a fast to an intermediate exchange system on the NMR timescale.[90b] No substantial changes, under the same experimental conditions, were observed with the F151C* SPM-1 **(Figure 5.35C)**. These findings are consistent with reported kinetic data that show that SPM-1 hydrolyses piperacillin in a similar range to B1 MBLs (NDM-1 and BcII)[188] and emphasise the importance of the L3 loop for substrate hydrolysis. A time-course analysis with Y58C* SPM-1 shows an additional 0.2 ppm downfield (-82.65 ppm) chemical shift with further line broadening of the enzyme-product peak, indicating the presence of a new species in solution **(Figure 5.35B)**.

Previous work has revealed that the product of piperacillin hydrolysis can bind to penicillin binding proteins, with the 'epimerised' (5*S*)- penicilloic acid (PA) product binding preferentially to the initially formed (5*R*)-penicilloic acid.[189] ^{1}H NMR was thus used to evaluate the time dependent hydrolysis of piperacillin in the presence of SPM-1 **(Figure 5.36)**. The results imply that SPM-1 catalyses piperacillin hydrolysis to give the (5*R*)-penicilloic acid ((5*R*)-PA) which epimerises more slowly to (5*S*)-PA, likely through a non-enzyme-catalyzed pathway. To investigate binding of the (5*S*)- and (5*R*)-PAs to SPM-1, the *Bacillus cereus* BcII MBL[187] was used to produce PA from piperacillin, the product was subsequently purified **(Figure 5.37)**. Addition of the hydrolysed (5*S*)/(5*R*)-PA mixture to Y58C* manifested a similar peak at -82.57 ppm, as was observed in the piperacillin time course **(Figure 5.38)**. ^{1}H and water LOGSY analyses were then used in a qualitative study of (5*S*)/(5*R*)-PA binding to SPM-1; the results implied binding of both (5*S*)- and (5*R*)-PA to SPM-1 **(Figure 5.39)**.

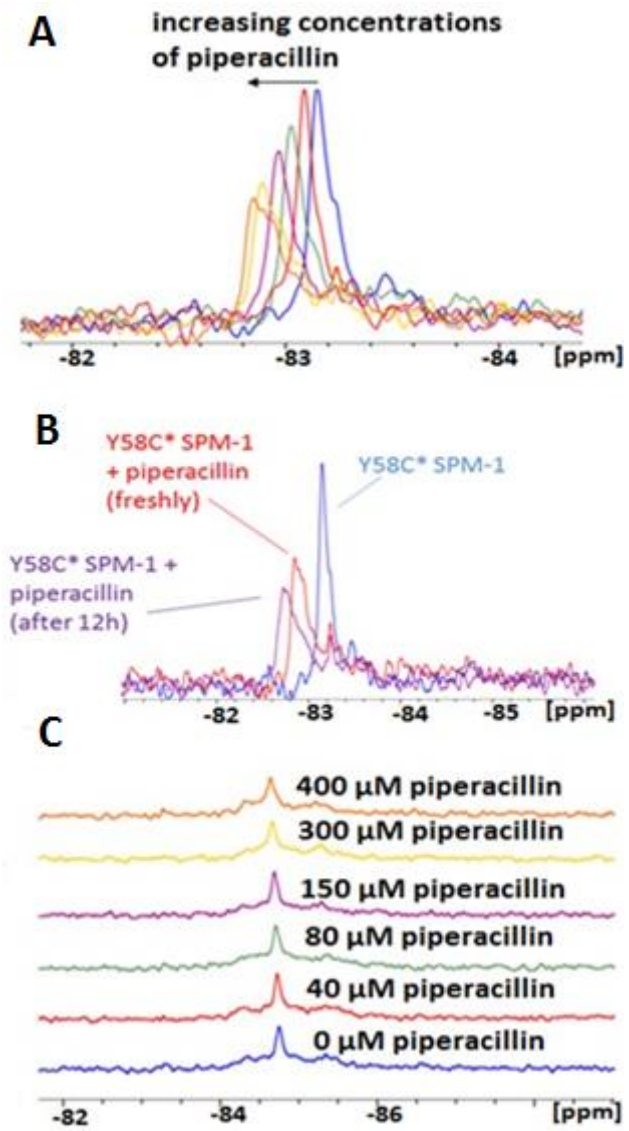

Figure 5.35. Interactions of hydrolysed piperacillin with SPM-1* variants by PrOF NMR. *Titration of (A) piperacillin into a solution of Y58C* SPM-1 reveals interactions with the L3 variant. Time-course analyses (after 12 h) with (B) piperacillin with Y58C* SPM-1 variant are consistent with a stable protein.product peak with an additional shift, indicating the presence of a new species in solution. Titration of (C) piperacillin into a solution of F151C* SPM-1 show no substantial changes. Assay mixtures contained 40 µM SPM-1* variant and increasing ligand concentrations (up to 400 µM) in 50 mM Tris, pH 7.5, in 90 % H_2O and 10 % D_2O.*

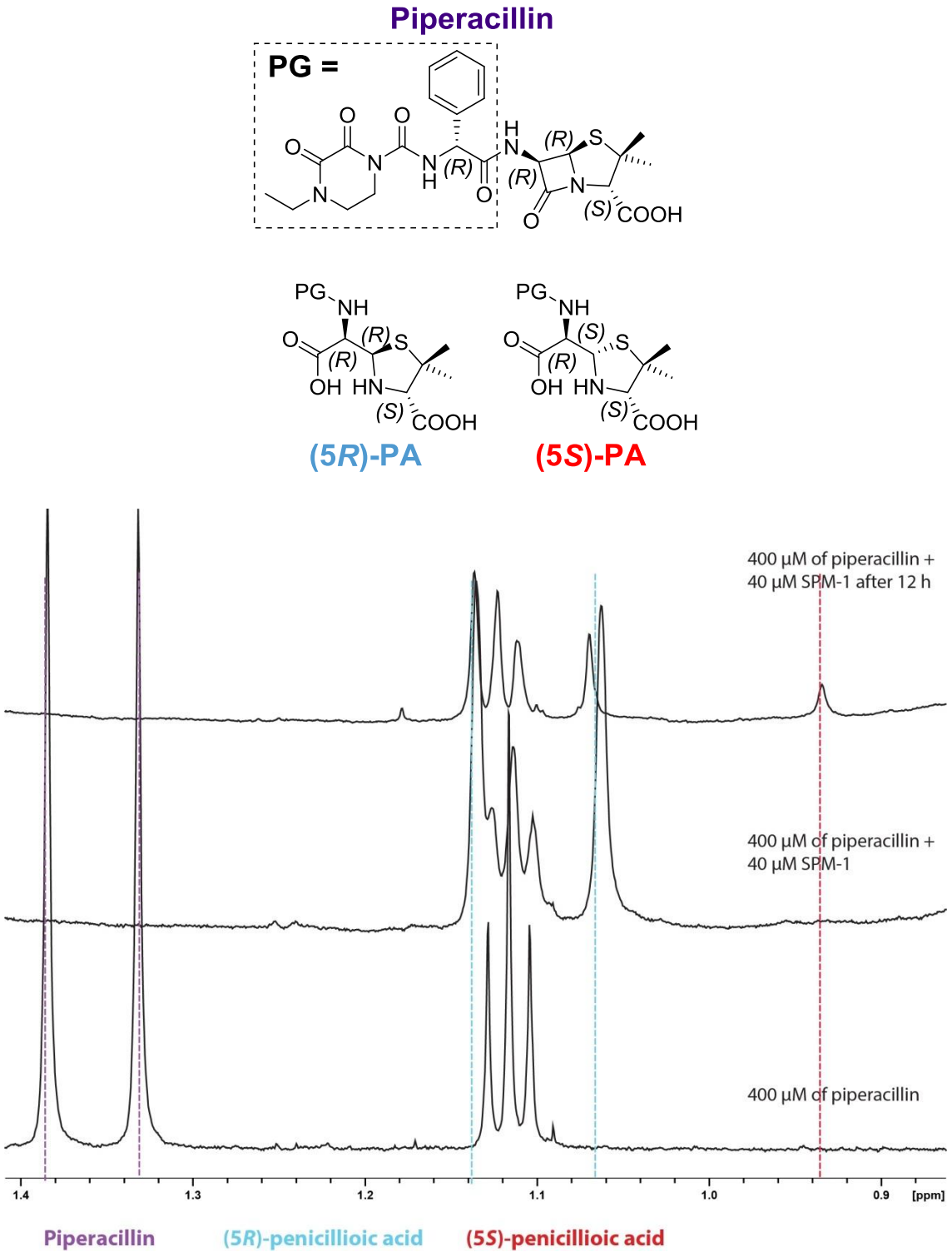

Figure 5.36. Monitoring the reaction of piperacillin with SPM-1 after 12 h. *The assay mixture contained 400 µM piperacillin with 40 µM SPM-1 in 50 mM Tris-D_{11}, pH 7.5, in 90 % H_2O and 10 % D_2O.*

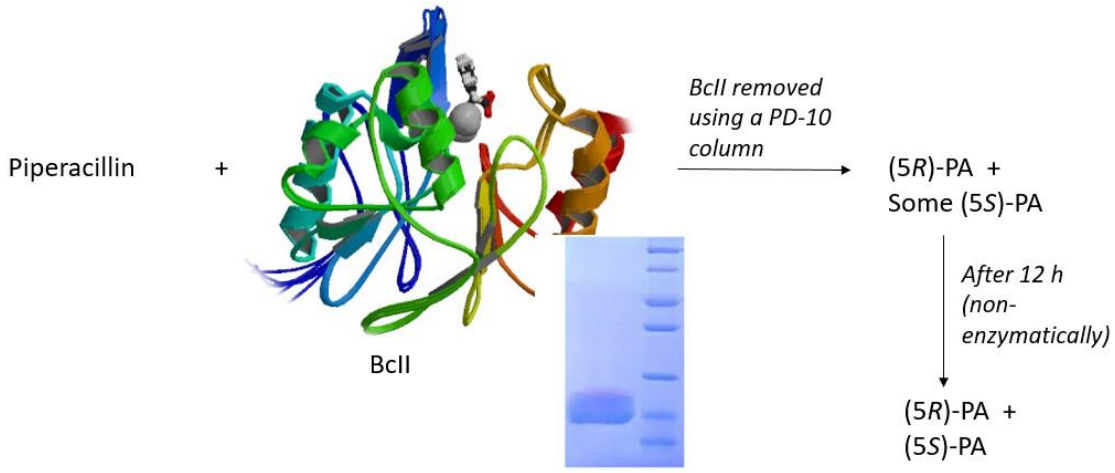

Figure 5.37. Scheme illustrating the production of hydrolysed piperacillin products. *The reaction was monitored by NMR. BcII was removed from the mixture using a PD-10 column. Details in Materials and Methods.*

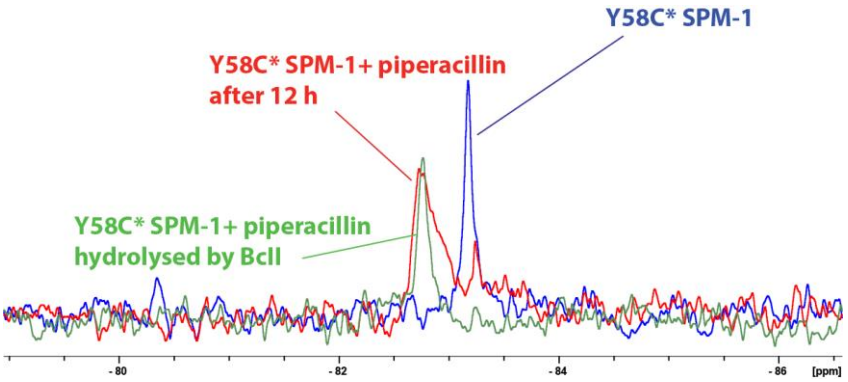

Figure 5.38. ^{19}F-NMR spectra of Y58C* SPM-1 interaction with hydrolysed piperacillin. *Assay mixtures contained 40 µM Y58C* SPM-1 and 400 µM added ligand in 50 mM Tris, pH 7.5, in 90 % H_2O and 10 % D_2O.*

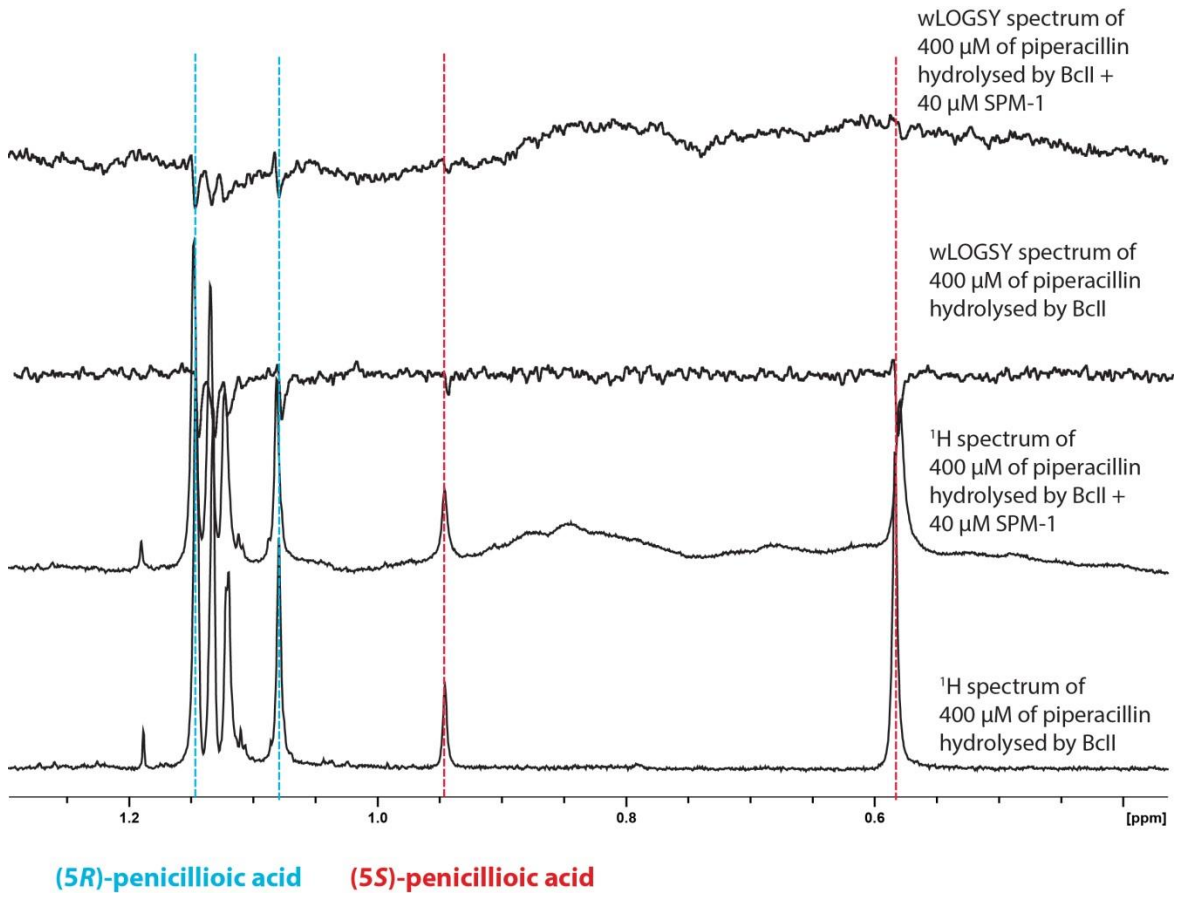

Figure 5.39. Monitoring the binding of hydrolysed piperacillin to SPM-1 by ^{1}H and wLOGSY NMR. *The assay mixture contained 400 µM hydrolysed piperacillin (by BcII)*[189] *with 40 µM SPM-1 in 50 mM Tris-D_{11}, pH 7.5, in 90 % H_2O and 10 % D_2O.*

The PrOF NMR work with penicillin/carbapenem substrates reveals shifts in the resonances for the protein complexes, which likely rise from binding of the hydrolysed β-lactam products. Notably, binding of both (5*S*)- and (5*R*)-PA to SPM-1* was observed, further emphasising the utility of ^{19}F-NMR for revealing subtle differences, in this case the binding of different stereoisomers. The observation of penicilloic acid and hydrolysed meropenem binding to SPM-1 is of potential clinical relevance. Previous studies have shown that penicilloic acids are competitive inhibitors of serine β-lactamases[190] and MBLs.[191] Although the levels of inhibition by penicilloic acids are much less than those for the intact β-lactams, penicillins are sometimes used at very high dose (up to 24 g/day for piperacillin),

and therefore, it is possible that β-lactamase binding by PA is relevant. These results are of interest from the perspective of identifying novel inhibitor scaffolds for SPM-1, and by implication other MBLs. They may lay a foundation for the design of non-β-lactam inhibitors that are not susceptible to β-lactamase hydrolysis and/or β-lactams/β-lactam analogues whose hydrolysed products bind/inhibit MBLs.

5.2.5.2.3. Interactions with class A SBL inhibitors

The interactions with the class A SBL inhibitors, clavulanic acid and tazobactam, both of which are substrates for SPM-1[164a] were then investigated. In both cases, resonance line broadening and a chemical shift from -83.15 to -83.02 ppm for tazobactam **(Figure 5.40A)** and from -83.15 to -82.98 ppm for clavulanic acid **(Figure 5.42A)** were observed in the ^{19}F Y58C* spectra, with no substantial changes evident after 12 h **(Figures 5.41, 5.43)**. No such effects were observed for F151C* SPM-1 **(Figures 5.40B, 5.42B)**. The propensity of clavulanic acid and tazobactam to undergo complex fragmentations[192] (as is the case when they inhibit SBLs) precluded identification of the species that give rise to these shifts – in the case of clavulanate/tazobactam, ^{1}H NMR studies indicated formation of multiple products, as exected on the known mechanistic information **(Figure 5.44)**.

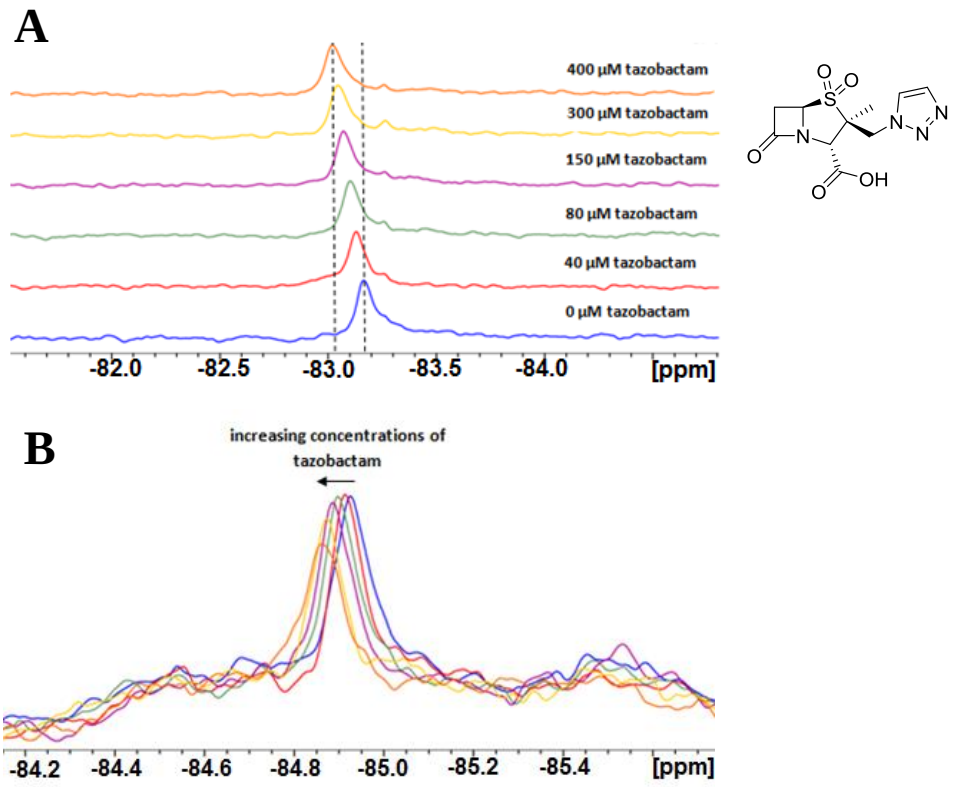

Figure 5.40. ^{19}F-NMR spectra of the titration of tazobactam into (A) Y58C* SPM-1 and (B) F151C* SPM-1 solution. *The assay mixtures, to which tazobactam was titrated, contained 40 µM SPM-1* in 50 mM Tris, pH 7.5, in 90 % H_2O and 10 % D_2O.*

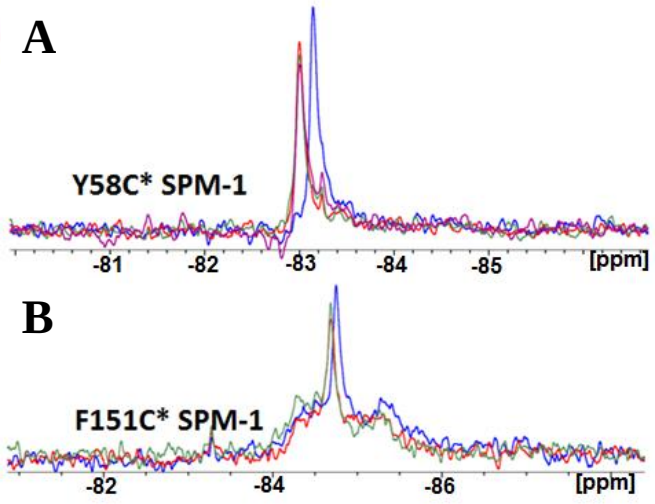

Figure 5.41. ^{19}F-NMR time-course spectra of SPM-1* variants with tazobactam. *The assay mixtures contained 40 µM Y58C* SPM-1* **(A)** *or F151C* SPM-1* **(B)** *(blue trace) and 400 µM tazobactam (freshly: red trace, after 12 hour in duplicate: green and purple traces) in 50 mM Tris, pH 7.5, in 90 % H_2O and 10 % D_2O.*

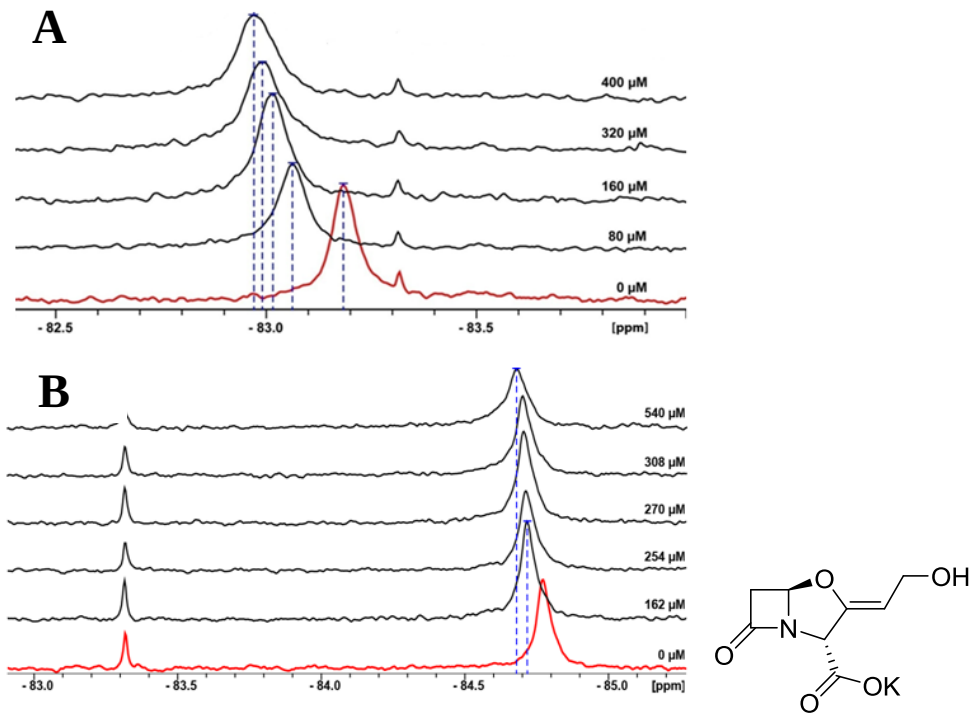

Figure 5.42. ^{19}F-NMR spectra of the titration of clavulanic acid into (B) Y58C* SPM-1 and (B) F151C* SPM-1 solution. *The assay mixtures contained 40 µM SPM-1* in 50 mM Tris, pH 7.5, in 90 % H_2O and 10 % D_2O.*

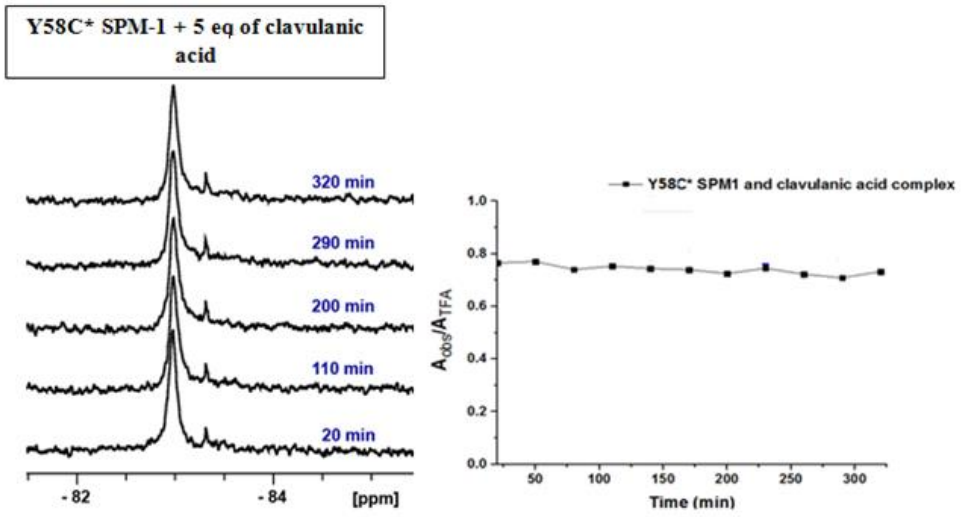

Figure 5.43. ^{19}F-NMR time-course spectra of Y58C* SPM-1 variant with clavulanic acid. *Y58C* SPM-1 appears to form a stable complex on reaction with sodium clavulanate (or fragments thereof, left). The peak intensity of the complex and its integrative area remained similar over the time course as shown (by comparison to the internal standard, TFA (right). The assay mixture contained 40 µM SPM-1* in 50 mM Tris, pH 7.5, in 90 % H_2O and 10 % D_2O.*

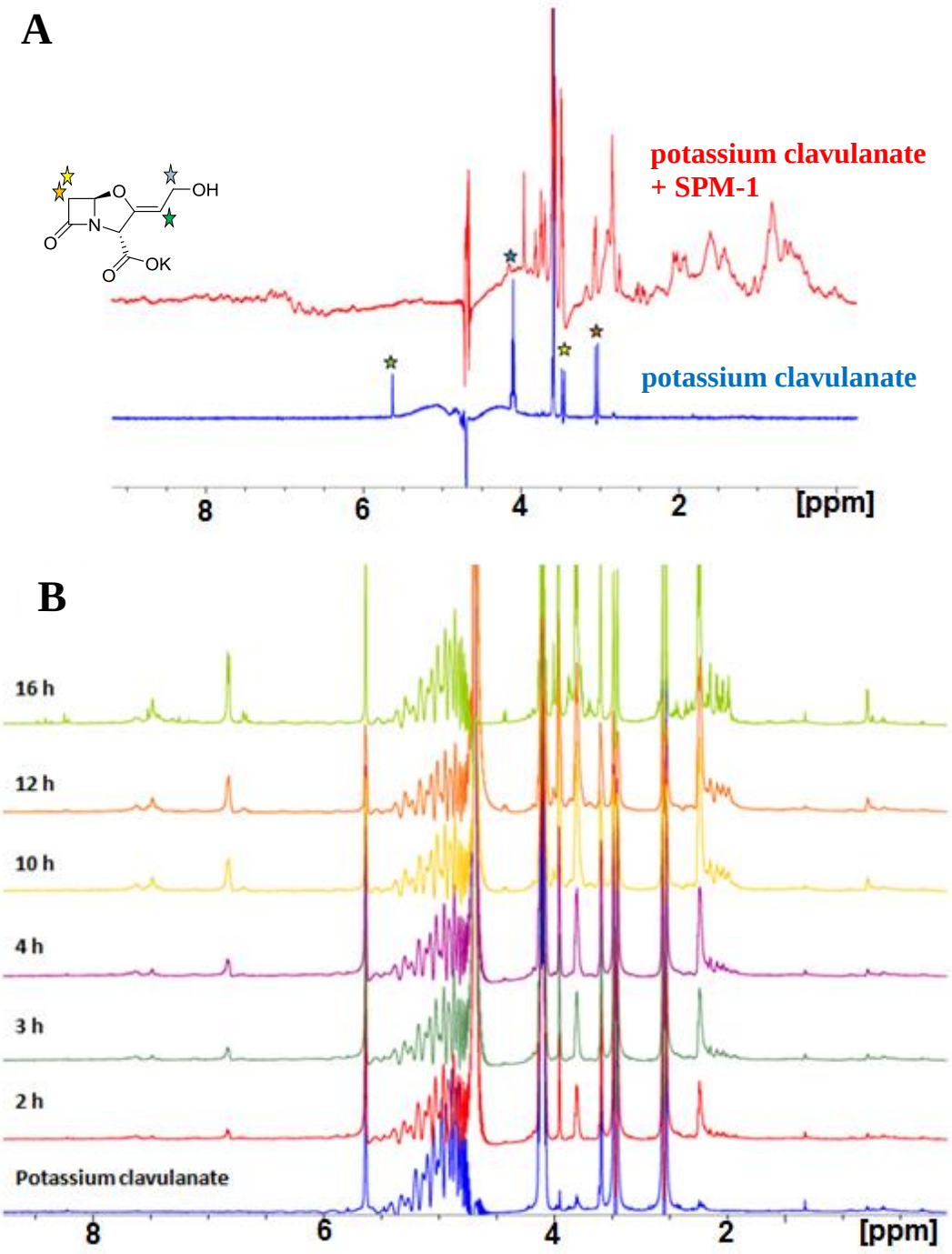

Figure 5.44. ^{1}H NMR spectra of the reaction of clavulanic acid with SPM-1. *Binding with SPM-1* ***(A)*** *and time course reaction monitoring* ***(B)*** *by ^{1}H NMR. The assay mixture contained 400 µM potassium clavulanate (blue trace), in the presence of 40 µM SPM-1 (red trace) after monitoring the reaction for 10 min in 50 mM Tris-D_{11}, pH 7.5, in 90 % H_2O and 10 % D_2O. The products of clavulanate hydrolysis were difficult to assign due to complex fragmentations.*[192]

Table 5.1. Table summarising the NMR observations with SPM-1. Note, $\Delta\delta_{max} = \delta_{max} - \delta_0$ represents the chemical shift difference (in ppm) between δ_{max} and δ_0, in which δ_{max} = δ observed in the presence of 400 µM of the ligand and δ_0 = δ of the SPM-1* variant in the absence of added ligand, δ_0 = -83.15 ppm for Y58C* SPM-1 and δ_0 = -84.75 ppm for F151C* SPM-1 (reference: trifluoroacetic acid, TFA, δ_{TFA} = -75.45 ppm). For $\Delta\delta_{max}$<0.1 ppm, which was used as a cut-off value, observations were denoted as 'no substantial changes'. Assignment of slow/fast exchanges and of peaks corresponding to protein.inhibitor complexes should be regarded as probable and relative to the chemical shift time scale.

	Summary of PrOF NMR analyses of SPM-1*				**Other Observations**
	Ligand titration analyses		**Time-course monitoring (12 h)**		
	Y58C* SPM-1 (L3 variant)	**F151C* SPM-1 (α3 variant)**	**Y58C* SPM-1 (L3 variant)**	**F151C* SPM-1 (α3 variant)**	
1,10-*o*-Phenanthroline 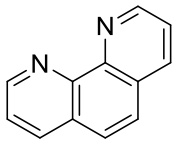	Signal reduction on increased concentrations of the ligand and appearance of a new peak	• Appearance of a new peak • $\Delta\delta_{max}$ = 0.3 ppm •	Stable protein-inhibitor peak at -83.8 ppm	Stable protein-inhibitor peak at -84.45 ppm	• Binding of 1,10-*o*-phenanthroline to SPM-1 was studied using ^{1}H CPMG. • The fluorine peaks observed in the presence of 1,10-*o*-phenanthroline are consistent with *apo*-SPM-1* peaks. • 1,10-*o*-phenanthroline does not induce changes in *apo*-Y58C* SPM-1 spectrum.

ML302 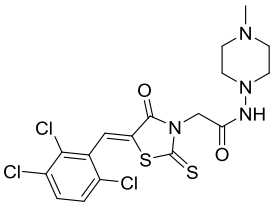	• Appearance of a new peak • Chemical shift, $\Delta\delta_{max}$ = 0.6 ppm • Slow-exchange	• Appearance of a new peak • Chemical shift, $\Delta\delta_{max}$ = 0.35 ppm • Slow-exchange	Stable protein-inhibitor peak observed at -83.75 ppm	Stable protein-inhibitor peak observed at -84.4 ppm	Binding of ML302 to SPM-1 was monitored (^{1}H CPMG).
ML302F 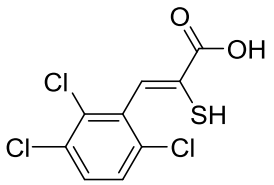	• Appearance of a new peak • Chemical shift, $\Delta\delta_{max}$ = 0.6 ppm • Slow-exchange	• Appearance of a new peak • Chemical shift, $\Delta\delta_{max}$ = 0.35 ppm • Slow-exchange	Stable protein-inhibitor peak observed at -83.75 ppm	Stable protein-inhibitor peak observed at -84.4 ppm	Binding of ML302F to SPM-1 was monitored (^{1}H CPMG).
L-Captopril 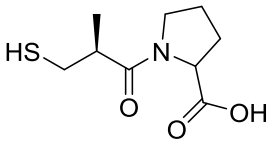	No substantial changes	No substantial changes	No substantial changes	No substantial changes	No/very weak binding of *L*-captopril to SPM-1 was observed by ^{1}H CPMG.

Isoquinoline derivative 5.1 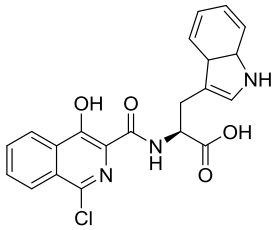	Significant line broadening and disappearance of the signal within the baseline (even at low ligand concentrations)	• Line broadening • $\Delta\delta_{max}$ = 0.75 ppm • Fast-exchange	Very broad peak close to the baseline	Stable protein-inhibitor peak at -84 ppm	• Binding of the isoquinoline **5.1** to SPM-1 was studied using ^{1}H CPMG. • Addition of ML302F to Y58C* SPM-1 led to some displacement of isoquinoline **5.1** with the ML302F.Y58C* SPM-1 complex peak appearing and a new peak observed ($\Delta\delta_{max}$ = 0.95 ppm). • Isoquinoline **5.1** was observed to bind to *apo*-Y58C* SPM-1.

Avibactam 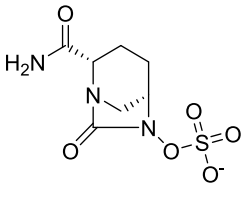	• Line broadening • $\Delta\delta_{max}$ = 0.1 ppm • Fast-exchange	No substantial changes	The peak shifts back towards original protein peak position	No substantial changes	• Weak binding of avibactam to SPM-1 and slow hydrolysis were monitored (CPMG)[185]. • Hydrolysed products do not bind to SPM-1 (wLOGSY)[185]. • Addition of intact avibactam after 24 h led to shifting the equilibrium back to the avibactam.Y58C* SPM-1 complex peak.
Meropenem 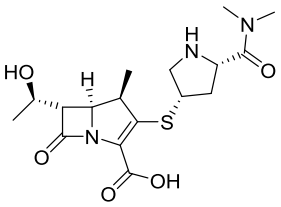	• Line broadening • $\Delta\delta_{max}$ = 0.20 ppm • Fast-exchange	No substantial changes	Stable protein-product peak observed at -82.95 ppm	No substantial changes	• Binding of meropenem to SPM-1 and its hydrolysis were monitored by ^{1}H NMR. • Meropenem was hydrolysed by BcII and its product was observed to bind to SPM-1 (wLOGSY and PrOF).

Piperacillin 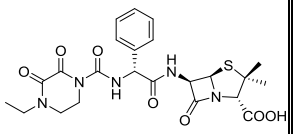	• Line broadening • $\Delta\delta_{max}$ = 0.40 ppm • Fast-exchange	No substantial changes	Additional downfield shift ($\Delta\delta$ = 0.18 ppm) and line broadening	No substantial changes	• Binding/hydrolysis of piperacillin with SPM-1 reveals time-dependent (5*R*)-PA epimerisation of the product to (5*S*)-PA. • Piperacillin was hydrolysed by BcII and PA products were observed to bind to SPM-1 (^{1}H, wLOGSY and PrOF).
Tazobactam 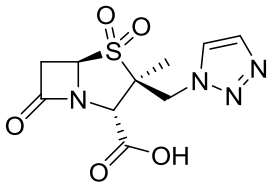	• Line broadening • $\Delta\delta_{max}$ = 0.13 ppm • Fast-exchange	No substantial changes ($\Delta\delta_{max}$ = 0.09 ppm)	Stable protein-product peak observed at -83.02 ppm	No substantial changes	Binding of tazobactam to wt SPM-1 and tazobactam hydrolysis/fragmentation were observed by ^{1}H NMR.
Potassium clavulanate 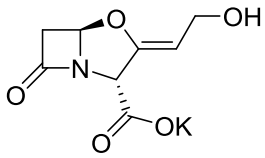	• Line broadening • $\Delta\delta_{max}$ = 0.17 ppm • Fast-exchange	No substantial changes ($\Delta\delta_{max}$ = 0.07 ppm)	Stable protein-product peak observed at -82.98 ppm	No substantial changes	Binding of potassium clavulanate/clavulanate fragments to wt SPM-1 and clavulanate hydrolysis/fragmentation were observed by ^{1}H NMR.

The overall results support dynamic roles for the α3 and L3 regions in ligand binding by SPM-1. They also further validate the use of cysteine-alkylation by BTFA as an efficient post-translational modification method for introducing a ^{19}F label into proteins. The BTFA method is complementary to methods employing the use of fluorinated residues introduced by protein biosynthesis.[93a] The useful application of the BTFA method relies on the selective alkylation of specific cysteines and on the ability of the labelled proteins to mimic that of wt SPM-1.[174a] Both of these properties do not always apply, but are often readily testable. The cost effective and efficient nature of Cys-alkylation by BTFA makes it an attraction option for ^{19}F labelling. In the case of the Y58C* and F151C* SPM-1 variants efficient and selective alkylation of the introduced cysteines was achieved, whilst the wildtype active site cysteine (Cys221) was unmodified, likely due to its 'protection' by Zn(II) chelation. The properties of the Y58C* and F151C* variants were very similar, though not identical to wt SPM-1, consistent with the CD and activity analyses, including crystallographic analyses.

The ^{19}F NMR analyses on the SPM-1* variants revealed interesting differences in the binding of the different ligands tested. Although substantially similar results might have been obtained by ^{13}C/^{15}N labelled protein observe NMR, such methods are more expensive/time consuming, and ^{19}F NMR labelling (of side chains) have the preference to reveal subtle differences in H-bonding and hydrophobic interactions,[174b 172, 193] not readily revealed by other biophysical techniques including crystallography/electron microscopy.[194] The cost effective and efficient nature of Cys-alkylation by BTFA makes it an attractive option for ^{19}F labelling which can be applied to other systems.

One common result arising from the ^{19}F NMR results is that all of the inhibitors tested, including for the Zn(II) chelator, 1,10-*o*-phenanthroline, manifest substantial changes in both the α3 and L3 regions, emphasising on the importance of both regions, and, in particular the α3 region, to inhibitor development. In contrast, the β-lactam substrates

(piperacillin, meropenem, tazobactam, and clavulanate) gave rise to hydrolysis products whose complexes only manifested changes in the L3 region. Although, it is possible that substrate binding involves both the α3 and L3 regions, the latter appears more important in product binding, and hence, likely product release. This proposal is consistent with work indicating that SPM-1 is, at least in some cases, mechanistically closer to the B1 MBLs, this has been evidenced by stopped-flow kinetics[164b] and mutagenesis work involving the deletion of the SPM-1 α3-α4 region which, within detection limits, does not affect β-lactam hydrolysis.[164a] Furthermore, crystallographic studies imply binding of hydrolysed meropenem involves the L3 region of the B1 MBL NDM-1 **(Figure 5.36)**.[195] The overall results support the proposed importance of dynamic roles in the α3 and L3 regions to ligand binding.

The results with inhibitors and substrates further reveal interesting differences and spectral features which illustrate the utility of PrOF NMR for investigating metal chelation, the presence of stereoisomers, and unrecognised binding modes (*i.e.* with the isoquinoline analogue). The overall results are of interest from the perspective of identifying novel inhibitor scaffolds for SPM-1, and by implication other MBLs, either for the design of non-β-lactam inhibitors that are not susceptible to β-lactamase hydrolysis and/or β-lactams/β-lactam analogues whose hydrolysed products bind/inhibit MBLs.

5.3. Summary and Perspectives

The role of MBLs in β-lactam antibacterial resistance is a growing concern. In this chapter, PrOF NMR studies on the SPM-1 from β-lactam resistant *Pseudomonas aeruginosa* were reported. Cysteinyl-variants on the α3 and L3 regions, which flank the di-Zn(II) active site, were selectively ^{19}F-labelled using BTFA. The results reveal roles of the mobile α3 and L3 regions in both inhibitor and β-lactam hydrolysis product binding to SPM-1. They may have implications for the mechanisms and inhibition of MBLs by β-lactams and non-β-

lactams. They illustrate the utility of PrOF NMR for identifying metal chelation, detecting new binding modes, and distinguishing in the binding of a mixture of stereoisomers in solution.

5.4. Materials and Methods

5.4.1. Mutagenesis

The Y58C SPM-1 and F151C SPM-1 variants were generated using the wt pOPINF SPM-1 plasmid obtained from Prof Jean-Marie Frère.[196] The desired point mutations were achieved employing the QuikChange site directed mutagenesis kit (Stratagene) using the following primers:

SPM-1 variant	Primers sequences
Y58C SPM-1	Forward: 5'-cagcacgttggaactgcagaagtcacgatcggt-3' Reverse: 5'-accgatcgtgacttctgcagttccaacgtgctg-3'
F151C SPM-1	Forward: 5'-aggtcttcattcttgtaacattcggccgctttaatgcg-3 Reverse: 5'-cgcattaaagcggccgaatgttacaagaatgaagacct-3'

5.4.2. Expression Trials and Protein Production

Expression trials were performed at different temperatures (18, 30, 37 ºC) using various isopropyl β-D-1-thiogalactopyranoside (IPTG) concentrations (0, 0.1, 0.2, 0.5, 0.7 and 1mM) and different induction times (4, 6, 8 and 20 h). Cells were lysed using the BugBuster kit; preferred conditions for expression were assessed by SDS-PAGE analyses. Recombinant di-Zn(II)-SPM-1 proteins were produced in *E. coli* BL21(DE3) pLysS cells using 2TY medium supplemented with 50 μg/mL ampicillin and 34 μg/mL chloramphenicol. Cells were grown at 37 ºC until they reached OD_{600} = 0.6-0.8; the temperature was then

reduced to 30 ºC for 6 h. Cells were harvested by centrifugation (10 min, 10g), then resuspended in 50 mL lysis buffer supplemented with DNase, lysosyme and EDTA-free protease-inhibitors. The cells were then further lysed by sonication (2 x 7 min); cell debris was then removed by centrifugation (20 g, 30 min). The cell lysates were then loaded onto a 5 mL HisTrap HP column (GE Healthcare Life Sciences, Little Chalfont, UK), with 50 mM Tris pH 7.5, 500 mM NaCl, containing 20 mM imidazole, then eluted with an imidazole gradient (up to 500 mM imidazole). Fractions containing di-Zn(II)-SPM-1 were further purified using a Superdex S200 column (300 mL) equilibrated with 20 mM Tris, pH 7.5, 200 mM NaCl. Eluted SPM-1 fractions were incubated overnight at 4 °C with 3C protease (1:100 w/w) and then purified using a 5 mL HisTrap HP column to give the untagged protein. The purity of the resulting fractions was assessed to > 90% (by SDS-PAGE). Fractions containing purified protein were concentrated by centrifugal ultra-filtration (10 kDa cut-off membrane). The concentrations of the purified proteins were determined using a ND-1000 NanoDrop spectrophotometer, as previously reported.[164b]

5.4.3. Fluorine Labelling

The SPM-1 variants (Y58C and F151C) were incubated on ice with tris-(2-carboxyethyl)phosphine (TCEP, final concentration 2 mM) in 50 mM Tris buffer, pH 7.5, for 30 min. The samples were buffered exchanged into phosphate buffer (50 mM, pH 7.0, 200 mM NaCl) using a PD-10 desalting column (GE Healthcare). A concentrated stock of 100 mM 3-bromo-1,1,1-trifluoroacetone (BTFA) reagent in phosphate buffer was prepared freshly prior to the reaction. SPM-1 variant samples were treated with 35-equivalents of 3-bromo-1,1,1-trifluoroacetone for 10 min at room temperature, prior to buffer exchange into Tris buffer (50 mM, pH 7.5, 200 mM NaCl) using a PD-10 desalting column (GE Healthcare).[170]

5.4.4. *Apo*-SPM-1 Production

Apo-SPM-1 proteins were produced by EDTA treatment of the di-Zn(II)-SPM-1. The di-Zn(II)-SPM-1 variants were incubated with 10,000-equivalents of EDTA at 4 ºC overnight. The treated proteins were further purified using a Superdex S200 column (300 mL) equilibrated with 20 mM Tris pH 7.5, 200 mM NaCl. Fractions containing purified protein were concentrated by centrifugal ultrafiltration (10 kDa cutoffs). The purity of the resulting fractions was ascertained to be > 90% by SDS-PAGE. Concentrations of the purified proteins were determined using a ND-1000 NanoDrop spectrophotometer. Removal of the metal was confirmed by non-denaturing mass spectrometry and activity analyses.

5.4.5. Circular dichroism (CD) Experiments

CD measurements were carried out using a Chirascan CD spectrometer (Applied Photophysics) equipped with a Peltier temperature-controlled cell holder. Experiments were performed at 23 °C in a 0.1 cm path length cuvette using 0.2 mg/mL protein in 10 mM sodium phosphate buffer (pH 8.0) supplemented with 50 mM $ZnSO_4$. Data were recorded from 260 to 185 nm at 0.5 nm intervals; each data point was averaged for 1 s. Spectra were baseline corrected and smoothed using the Savitzky–Golay filter. Data recorded in the 190–240 nm range were analysed using DichroWeb; the CDSSTR deconvolution method was used to estimate secondary structural content using reference set 4. To minimise the effects of differences in protein concentration, the data were normalised at 207 nm.[63, 183]

5.4.6. Crystallisation Conditions

SPM-1 Y58C (20 mg/mL) was crystallised by Dr Philip Hinchliffe using sitting-drop vapor diffusion in 24-well Cryschem plates (Hampton Research). Protein (2 µL) was mixed crystallisation reagent (with 2 µL, 0.1 M mixture of HEPES and MOPS, pH 7.5, 0.03 M NaF, 0.03 M NaI, 0.03 M NaB, 12% PEG3350, 12% PEG1000, 12% 2-methyl-2,4-pentanediol)

and equilibrated against 500 µL. Crystals grew to maximum size in 3 days and were looped directly from the drop and flash-frozen in liquid nitrogen.

Diffraction data were collected at 100 K on beamline I24 (Diamond Light Source, Didcot, UK). The dataset was indexed and integrated using XDS[197] and scaled using Aimless in CCP4.[198] Data were cut at 1.75 Å as completeness dropped significantly at higher resolutions. Phases were determined using molecular replacement in Phaser[199] with 4BP0[170] as the search model (with Y58 mutated to a cysteine). The structure was refined and modelled in Phenix[200] and Coot,[201] respectively. After several rounds of refinement residue 58 was modelled as a cysteine into clearly defined electron density, before undergoing a final round of refinement and model building. Structure validation was assisted by Molprobity[202] and Phenix.

5.4.7. Steady-State Kinetics

The hydrolysis of meropenem was monitored at 25 °C in 50 mM HEPES buffer (pH 7.2) supplemented with 1 µg/mL BSA, 1 mM $ZnSO_4$ and 0.01% Triton X-100. Analyses were carried out in triplicate ($n \geq 3$); the absorbance values were read using a BMG Labtech Pherastar FS plate reader at 300 nm. Extinction coefficients were determined by plotting the absorbance units against decreasing concentrations of the substrate. Kinetic constants (K_M and k_{cat}) were obtained by determining the initial rate of the reaction at different substrate concentrations. The concentration-dependence of the initial rate was fitted and analysed using GraphPad Prism 5.01 software to generate Michaelis–Menten curves.[188]

5.4.8. Production of Hydrolysed β-Lactams

β-Lactamase mediated hydrolysis was used to produce hydrolysed meropenem and piperacillin. Incubation of 5 equivalents of piperacillin and meropenem with *Bacillus cereus* m569/H/9 (BcII) produced (5*R*)-penicillioic acid (PA) [and some (5*S*)-PA] and hydrolysed meropenem, respectively. BcII was removed from the reaction mixture using PD-10 columns.

Subsequent epimerisation of (5*R*)- to (5*S*)-PA was performed under neutral conditions, non-enzymatically, at 4°C, for an overnight. The hydrolysed products were obtained *via* spin filtration using 10 kDa Centricon concentrators. The reaction and the purity of hydrolysed β-lactams were assessed by NMR analyses. BcII was produced and purified as described by Cahill *et al*.[187]

5.4.9. NMR Experiments

Spectra were recorded using a Bruker AVIII 600 with BB-F/^{1}H Prodigy N_2 cryoprobe operating at 298 K using 5 mm diameter NMR tubes (Norell).

5.4.9.1. ^{19}F-NMR Experiments

^{19}F NMR experiments were typically obtained using 256 scans and a recovery delay of 2 s. Data were processed with 5 Hz Lorentzian line broadening using TopSpin 3.1 software (Bruker) and were referenced to the internal 1,1,1-trifluoroacetone standard (10 μM, at -74.45 ppm). Samples contained the SPM-1* variant (40 μM, unless otherwise stated) and added ligand in Tris buffer (50 mM, pH 7.5) supplemented with 10% D_2O.

5.4.9.2. ^{1}H CPMG NMR Experiments

Typical experimental parameters for Carr-Purcell-Meiboom-Gill (CPMG) NMR spectroscopy were as follows: total echo time, 40 ms; relaxation delay, 2 s; number of transients, 64. The PROJECT-CPMG sequence (90°x−[τ−180°y−τ−90°y−τ−180°y−τ]*n*−acq) was applied.[137] Water suppression was achieved by pre-saturation. Data were processed with 0.3 Hz Lorentzian line broadening using TopSpin 3.1 software (Bruker). The assay mixtures contained 40 μM protein and 400 μM of ligand buffered with 50 mM Tris-D_{11} (pH 7.5) and 0.02 % NaN_3 in 90 % H_2O and 10 % D_2O.

5.4.9.3. wLOGSY NMR Experiments

For water-Ligand Observed Gradient SpectroscopY (wLOGSY) analyses,[84] typical experimental parameters were: mixing time, 1 s; relaxation delay, 2 s; number of transients, 256. Solvent excitation was achieved using a 16 ms 180 degrees selective rectangular shape pulse with 1000 points (Squa100.1000) set at the H_2O frequency. Water suppression was achieved by a 2 ms Sinc pulse (Sinc1.1000) at the H_2O frequency. Data were processed with 0.3 Hz Lorentzian line broadening using TopSpin 3.1 software (Bruker). The assay mixtures contained 40 µM protein and 400 µM of ligand buffered with 50 mM Tris-D_{11} (pH 7.5) and 0.02 % NaN_3 in 90 % H_2O and 10 % D_2O.

Chapter 6. Cyclobutanones as Broad-Spectrum β-Lactamase Inhibitors

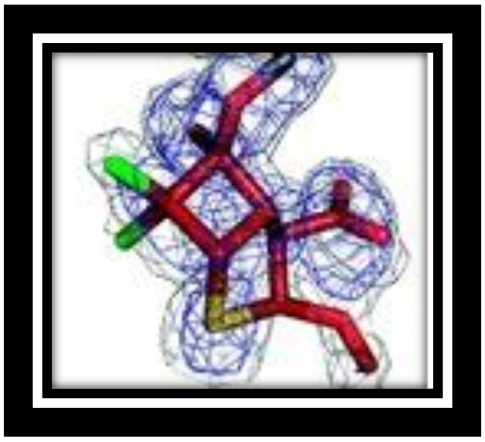

Chapter 6. Contents

6.1. Introduction

Cyclobutanone β-lactam analogues have been explored as both antibiotics and potential β-lactamase inhibitors.[203] Though initial experiments identified cyclobutanones to be only weak inhibitors of class A SBLs and to lack antibiotic activity, the potential of cyclobutanones to act as broad-spectrum β-lactamase inhibitors has recently been re-evaluated **(Figure 6.1)**.[203-204] Although these studies provided direct crystallographic evidence for inhibition of the SBL OXA-10, and by implication other SBLs, by the hydrated form of a cyclobutanone inhibitor bound *via* a hemiketal linkage to the active site serine,[204] no information was available on the mechanism by which cyclobutanones inhibited MBLs. As a consequence, the interaction of cyclobutanones with MBL targets was investigated by NMR with the aim of identifying a model system in which their mode of inhibition can be studied, and hence elucidate the basis for the activity of these compounds against both mechanistic types of β-lactamases.

Previous results have identified the penem cyclobutanone analogue **6.1** (structure in **Figure 6.4**) as the most potent compound tested against the SBLs KPC-2 and GC1 (classes A and C, respectively), and having modest but detectable inhibition of the IMP-1 MBL.[204] The inhibition of a wider range of MBLs by **6.1** was therefore investigated, and SPM-1 was identified as an enzyme against which **6.1** has more potent activity. Cyclobutanone **6.1** was provided by Dr Jarrod Johnson (Dmitrienko laboratory, University of Waterloo). SPM-1 is an MBL with a binuclear zinc center having co-ordination typical of the most clinically important MBL types (NDM, VIM and IMP enzymes).[164a, 165] SPM-1 is widely distributed in South America in clinical strains of the Gram-negative pathogen *Pseudomonas aeruginosa*.[160b, 205]

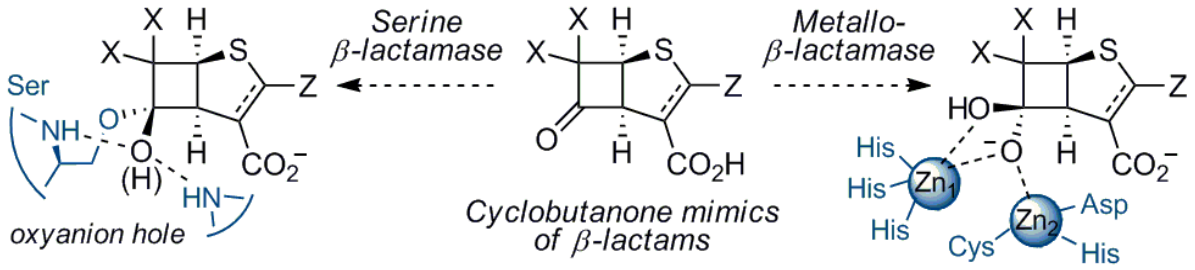

Figure 6.1. Cyclobutanones as potential broad-spectrum β-lactamase inhibitors.[203]

6.2. Results

6.2.1. Binding Studies with SPM-1

To study binding of **6.1** to SPM-1, ^{19}F NMR methods were employed, as described in **Chapter 5**. The SPM-1 active site **(Figure 6.2)** is located in a deep cleft flanked by an extended α-helix (α3) that is expected to undergo extensive rearrangement on small molecule ligand binding, and by additional hydrophobic residues situated on the loops linking secondary structural elements.[164a, 206] Previously, site-directed mutagenesis has been used to introduce a cysteine residue at position 152 on the α3 helix of SPM-1; C152 was then selectively alkylated using 3-bromo-1,1,1-trifluoroacetone (BTFA) to generate a ^{19}F labelled enzyme (Y152C* SPM-1) and studied by PrOF NMR.[206] The ^{19}F NMR spectrum of SPM-1 Y152C* contains two peaks corresponding to closed (-83.2796 ppm) and open (-72.3741 ppm) conformations of the α3 loop. In studies in the previous chapter, addition of small molecule inhibitors to SPM-1* resulted in line broadening and chemical shift changes, indicating that inhibitor binding involves rearrangements within the α3 region. Contrary to the earlier findings in **Chapter 5** with different inhibitors, addition of **6.1** to SPM-1 Y152C* revealed only very subtle effects on the ^{19}F NMR spectrum **(Figure 6.3)**.

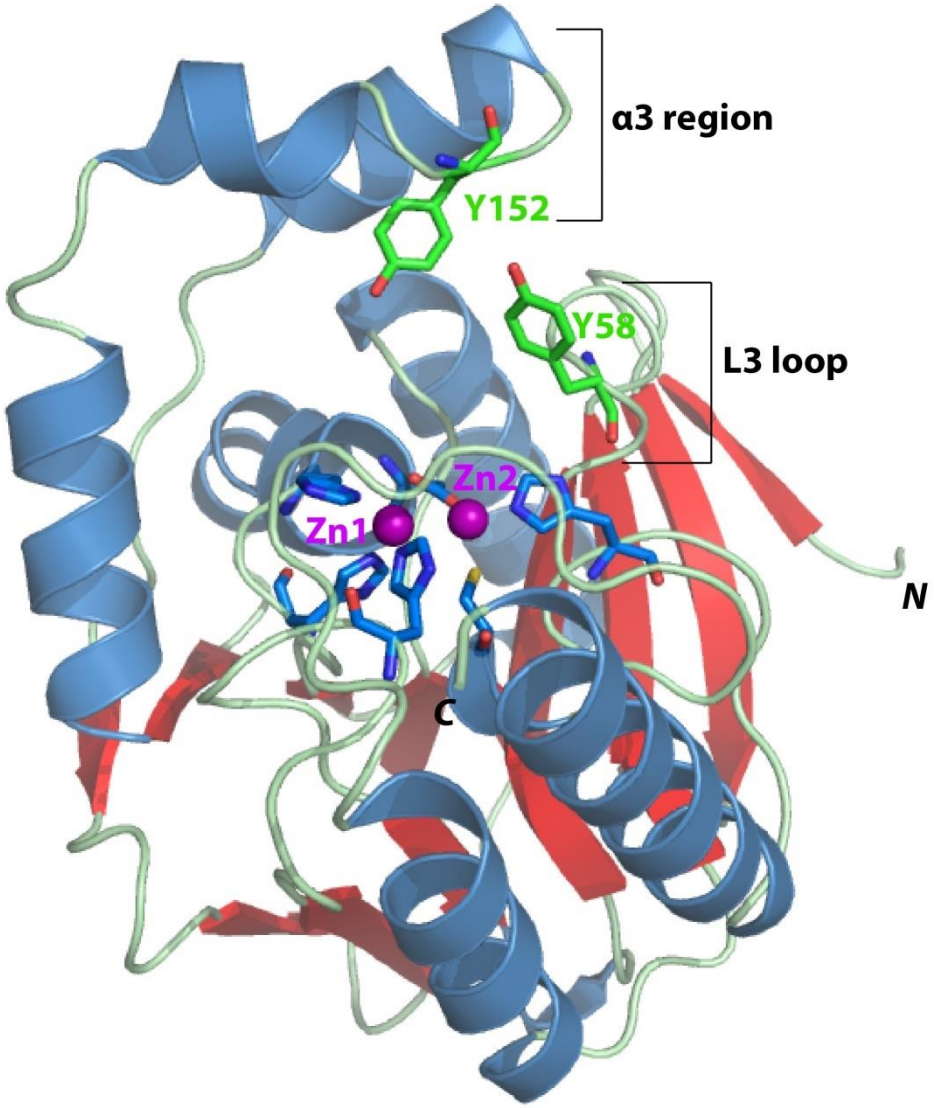

Figure 6.2. View from a crystal structure of the closed conformation of di-Zn(II)-SPM-1. *PDB ID: 4BP0.*[206] *The residues of interest, Y58 and Y152, are in green. The active site residues are sticks. The first Zn(II) is coordinated by 3 His residues, H116, H118 and H196. The second Zn(II) is coordinated by D120, H263 and C221. The figure was created using PyMOL.*

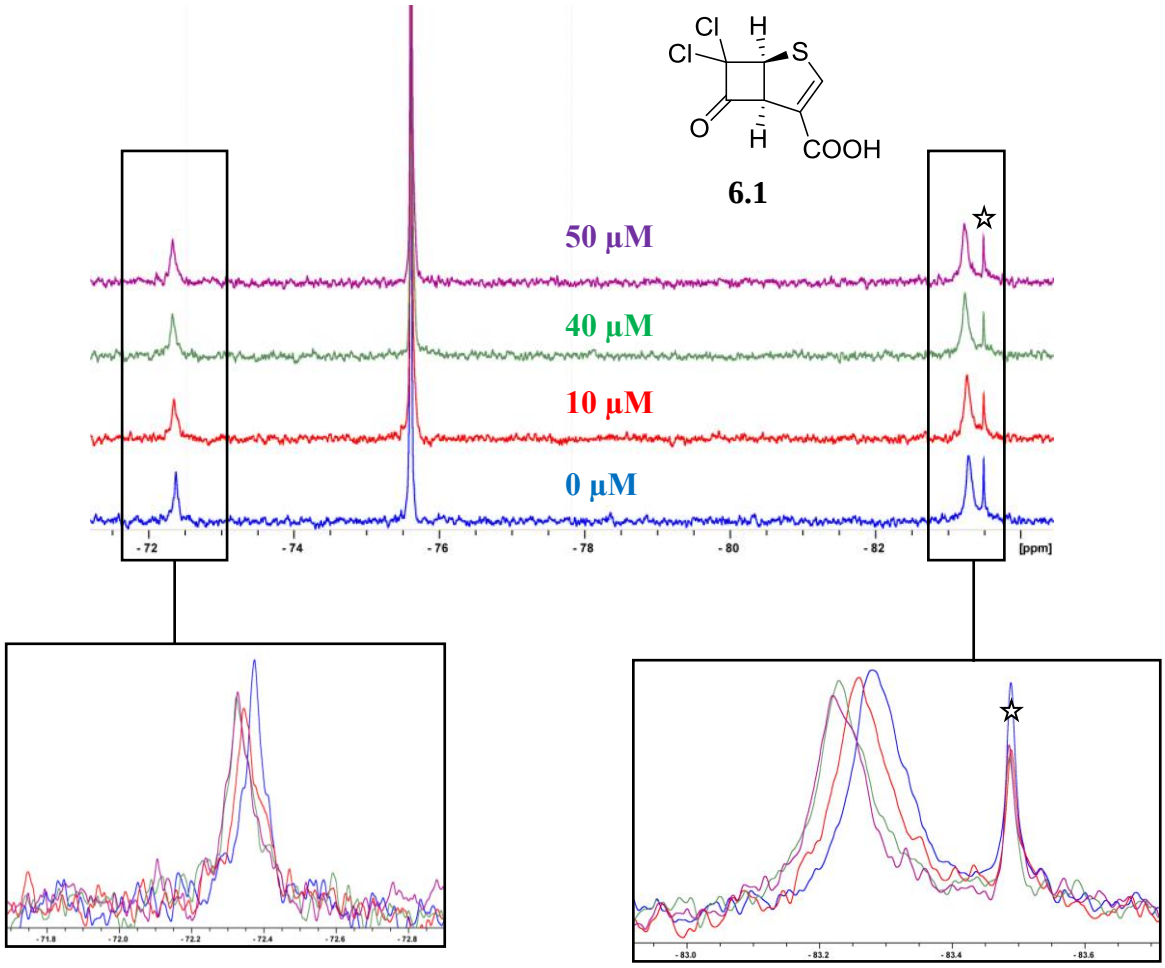

Figure 6.3. ^{19}F NMR spectra of Y152C* SPM-1 with increasing concentrations of the cyclobutanone analogue. *The peaks assigned to the closed of the α3 loop (-83.2796 ppm) and open conformations of the α3 loop (-72.3741 ppm)*[206] *are highlighted in boxes and overlaid with the traces corresponding to increased concentrations of the cyclobutanone analogue. The star denotes the peak corresponding to the residual the labelling reagent (3-bromo-1,1,1-trifluoroacetone). The results imply binding of cyclobutanone analogue to Y152C* SPM-1. The chemical shift changes and line broadening observed indicate that binding of* ***6.1*** *to SPM-1 in the vicinity of the α3 loop led to subtle conformational changes of the loop in a fast-exchange system on the NMR timescale. The assay mixture contained Y152C* di-Zn(II)-SPM-1* variant in Tris buffer (50 mM, pH 7.5) supplemented with 10 % D_2O. Trifluoroacetic acid (10 µM) was used as an internal NMR standard.*

A second BTFA-labelled variant was used. Y58C* SPM-1, which incorporates a ^{19}F label on the L3 loop connecting strands β3 and β4, was then prepared. Interactions between Y58C* with **6.1** were similarly studied by ^{19}F NMR *(the details of its production and characterisation were given in* ***Chapter 5****)*. The L3 loop region of SPM-1, unlike the α3 loop, is not anticipated to undergo gross structural rearrangements upon binding of small molecule ligands.[206] Consistent with this proposal, the ^{19}F NMR spectrum of Y58C* SPM-1 contains a single well defined peak (-83.3326 ppm). Addition of **6.1** (9.9 μM) causes this peak to shift (-83.2146 ppm) and undergo line broadening, consistent with binding to SPM-1 in the vicinity of residue C58 in a system that is in fast-exchange on the NMR timescale **(Figure 6.4)**.[169]

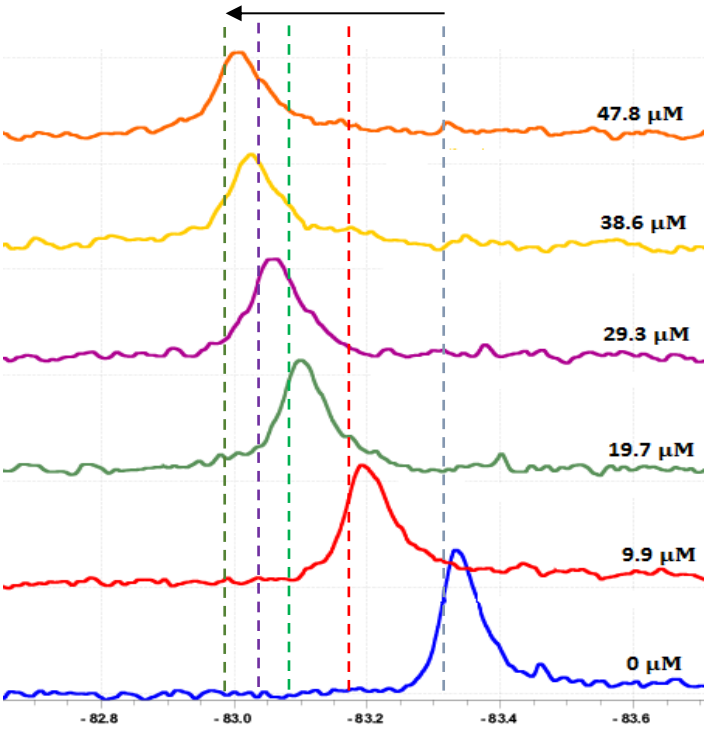

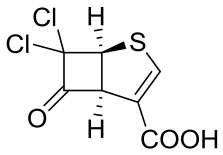

6.1

Figure 6.4. ^{19}F NMR spectra of Y58C* SPM-1 (lower trace, blue) and Y58C* SPM-1 with increasing concentrations of the cyclobutanone analogue. *The results imply binding of the cyclobutanone analogue to Y58C* SPM-1. The peak corresponding to Y58C* SPM-1 was shifted from -83.3326 ppm to -83.2146 ppm on addition of 10 μM* ***6.1****. The chemical shift changes and line broadening observed indicate binding of the cyclobutanone analogue to SPM-1 in the vicinity of the C58 residue in a fast-exchange system on the NMR timescale.*[169] *The assay mixture contained Y58C* di-Zn(II)-SPM-1* variant in Tris buffer (50 mM, pH 7.5) supplemented with 10 % D_2O. Trifluoroacetic acid (10 μM) was used as an internal NMR standard.*

Monitoring the concentration dependence of ^{19}F chemical shift changes on titration of **6.1** into Y58C* SPM-1 enabled the dissociation constant for the inhibitor (K_D) to be estimated as 22.4 ± 6.6 μM **(Figure 6.5)**.

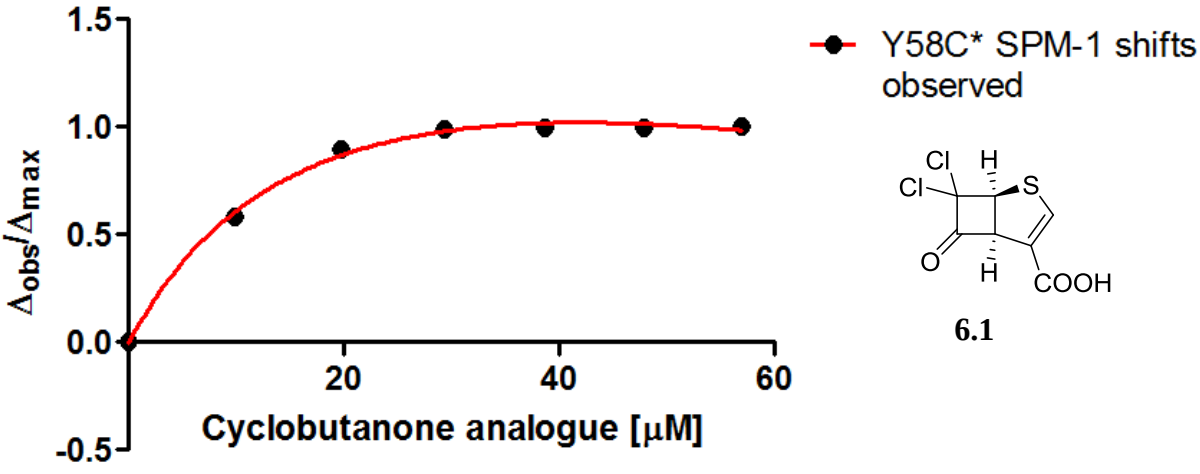

Figure 6.5. K_D fitting for cyclobutanone analogue with Y58C* SPM-1 variant. *The K_D value (i.e. the dissociation constant of cyclobutanone analogue binding) was determined using the equation below, where $[L_0]$ is the total ligand (**6.1**) concentration and $[P_0]$ is the total protein (Y58C* SPM-1) concentration.*[170, 206]

$$y = \frac{([L_0] + [P_0] + K_D) - \sqrt{([L_0] + [P_0] + K_D)^2 - 4[L_0][P_0]}}{2[P_0]}$$

	K_D (in μM)
Y58C* SPM-1	22.43±6.63

Kinetic analyses with wt SPM-1 and its variants are given in **Chapter 5**.

6.2.2. Crystallographic Analysis

A crystal structure of SPM-1 complexed with a ligand was obtained by Dr Philip Hinchliffe, Spencer laboratory, University of Bristol. SPM-1, like other MBLs of B1 subclass MBLs, contains a dinuclear zinc center with one metal ion in a (normally tetrahedral) trihistidine site (Zn1) and another one in a trigonal bipyramidal site (Zn2) comprised of conserved Asp, Cys, and His residues and two water molecules. One of these water molecules, Wat1 'bridges' the two active site zinc ions and is proposed to act as the 'hydrolytic water' **(Figure 6.6A)**.[164a, 206] Previous studies with NDM-1 (Kim Y. *et al*, FASEB, 27(5), pp.1917-1927, 2013) revealed that the distance between both Zn varies from 3.4 to 4.4 Å depending on whether the bridging 'water' exists as a hydroxide ion or a water molecule.

The most notable interactions made by cyclobutanone **6.1** with the SPM-1 active site, as revealed by crystallography, are in the vicinity of the Zn2 site. The C4 carboxylate makes direct interactions with both Zn2 (2.4 Å distance) and Lys219 (2.8 Å), which is involved in substrate binding by B1 MBLs. In contrast, only weak interactions are made with Zn1, with the two C6 oxygen atoms lying 3.4 Å and 4.0 Å away from the metal ion, respectively. The Zn-bridging Wat1 remains, potentially interacting with both C6 oxygen atoms of **6.1** (2.7 Å distance). Inhibitor binding does not exert significant structural effects on the metal center, with little change in Zn - Wat1; Zn1 – Zn2 or Zn:protein ligand distances (when compared to the structure of the native enzyme[206] obtained from the same crystal form) **(Figure 6.6B)**. The most notable difference evident on inhibitor binding is a small (0.5 Å) displacement of the Zn2 metal ion into a more solvent-exposed position in the active site cavity.

In addition to interactions with the metal center, **6.1** is positioned to make hydrophobic contacts with residues adjacent to the active site. SPM-1 is distinguished from

other B1 MBLs in possessing a 'wall' of hydrophobic residues,[164a] including Phe57 and Tyr58 on the L3 loop, Phe79 on the loop connecting β5 and α1, Phe151 and Tyr152 on the kinked α3 helix of the 'closed' form, and an additional Tyr at position 228 on the opposite side of the active site cleft **(Figure 6.6C)**.[207] Binding of **6.1** involves several of these residues, with the inhibitor bicyclic scaffold effectively sandwiched between the aromatic rings of Tyr58 and Tyr228, and making additional edge-face interactions with Phe79. The side chain of Tyr152 lies more distant, with its OH group 6.7 Å (chain A) or 10.9 Å (chain B) away from the C7 atom of **6.1** **(Figure 6.6D)**. Indeed, despite the clear presence of bound inhibitor in both active sites, the conformation of the α3 loop differs substantially between the two molecules in the asymmetric unit, and compared to the rest of the structure this region is relatively flexible [B-factors = 77 $Å^2$ (chain A) and 59 $Å^2$ (chain B)]. In contrast, no conformational change in the L3 loop was observed by crystallography on inhibitor binding **(Figure 6.6C)**. The larger ^{19}F NMR chemical shift changes observed on binding of **6.1** to Y58C* SPM-1, compared to Y152C* SPM-1 **(Figures 6.3, 6.4)**, would then be explained by the closer proximity of residue 58 to the inhibitor binding site, notwithstanding the more extensive conformational changes that are observed in the α3 region.

Although an increasing number of structures describe binding of hydrolysed β-lactams to MBLs,[55] progress in this area has been hampered by the continuing absence of structures describing interactions of the MBL active center with intact substrates. However, the SPM-1:**6.1** complex structure presented here serves as the closest analogue of an intact β-lactam for which an MBL complex structure is available, and thus offers insights into the possible modes of β-lactam binding. Notably, the results highlight the importance of interactions between the Zn2 ion, residues adjacent to the MBL active site (Lys219), and the C4 carboxylate group of the cyclobutanone analogue to the binding of **6.1** to SPM-1 **(Figure 6.6B)**. Such interactions also feature in binding of hydrolysed β-lactams by MBLs.[55] This

structure supports their involvement in binding intact β-lactam substrates, and possible formation of early-stage complexes in the hydrolytic reaction.

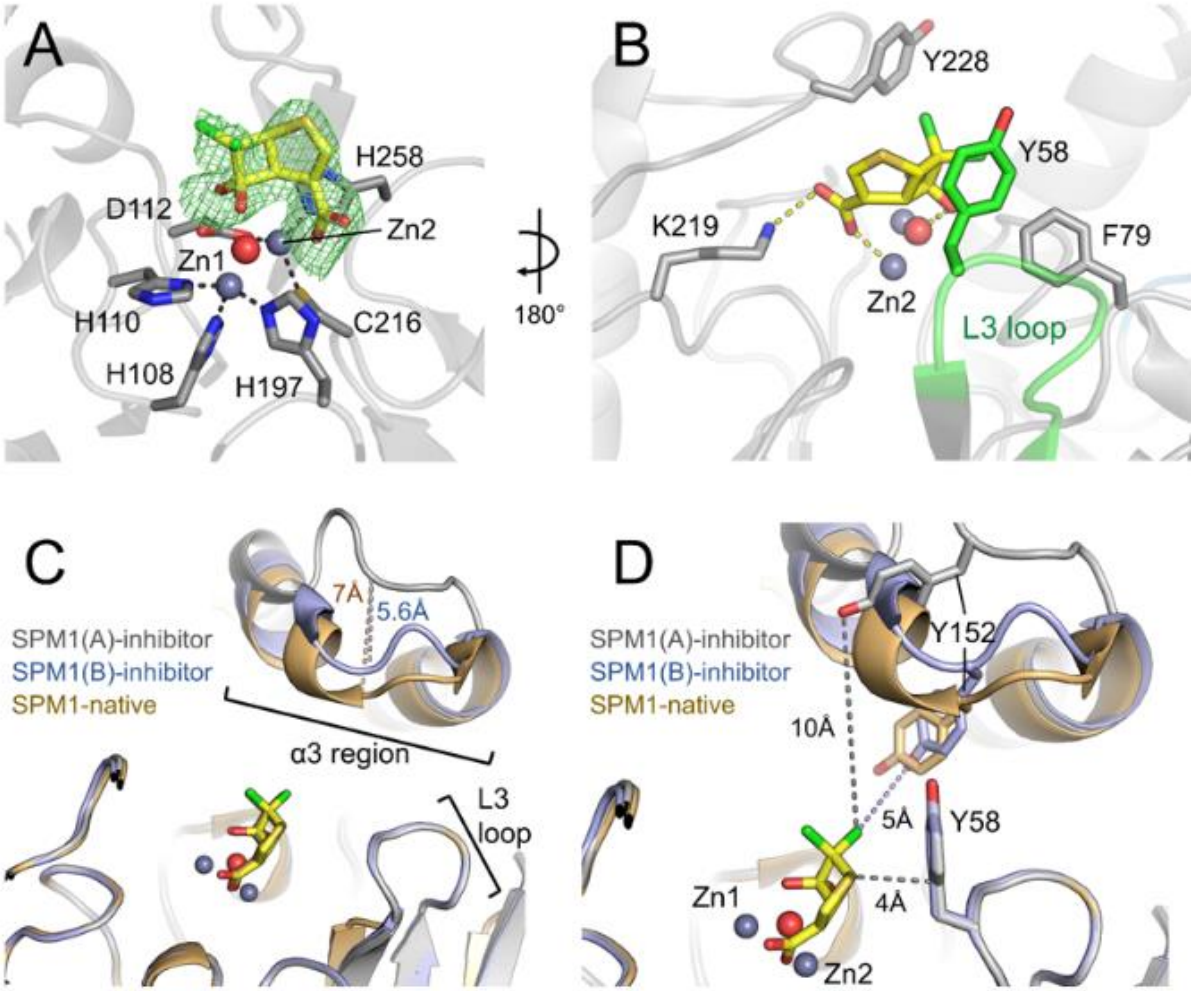

Figure 6.6. Crystallographic analyses of cyclobutanone 6.1 binding to SPM-1. *Cyclobutanone **6.1** is represented as sticks (yellow). Zinc ions (Zn1, Zn2) and the bridging water, Wat1, are shown as gray and red spheres, respectively. **(A)** Cyclobutanone binding to the di-zinc SPM-1 active site of chain B (gray ribbon). F_o-F_c density (green) is calculated from the SPM-1 model in the absence of ligand. Zn-interacting residues are labelled and shown as sticks. **(B)** Interactions between SPM-1 and cyclobutanone (yellow dashes). **(C)** Superposition of native SPM-1 (orange) with chain A (gray) and B (blue) of the SPM-1:cyclobutanone complex. **(D)** Positions and movement of Tyr58 and Y152 in unliganded and cyclobutanone-bound SPM-1. The crystallography was conducted by Dr Philip Hinchliffe.*

It is also notable that the SPM-1:**6.1** complex does not feature direct interactions between the C6-bound oxygen atoms with Zn1. The Zn1 site has been proposed to polarise the β-lactam amide prior to attack of the Wat1 nucleophile, and to be important for activation of Wat1 for this process. As such, binding of an intact β-lactam could trigger dissociation of Wat1 from Zn2 to generate a terminal nucleophile on Zn1; the tetrahedral species formed on attack of Wat1 on the β-lactam C6 would be stabilised by Zn1 binding. In a hydrated cyclobutanone the C6 oxygen atoms are expected to be protonated, reducing its affinity for Zn1 and instead favoring interaction with Wat1. Furthermore, approach of the uncharged C5 of **6.1** to Zn2 will be disfavored compared to that of a β-lactam amide nitrogen. β-Lactam binding will differ from that of **6.1** in these two aspects, and that together they may limit the potency of current cyclobutanones against MBLs.

6.2.3. Determination of the Bound Species

Previous work concluded that cyclobutanone **6.1** exists predominantly in the hydrated form (as per NMR and crystallographic analyses).[203-204] The hydrated species was also observed to be predominant, in aqueous solution, in studies involving cyclopropanone analogues.[208] On this basis, **6.1** was refined as its hydrated form in the crystal structure described above. However, test refinements modelling **6.1** as the ketone yielded statistics very similar to those for the hydrate, indicating that crystallographic data alone cannot definitively identify the form of **6.1** present in the SPM-1 active site. Accordingly, NMR spectroscopy was used to investigate the behavior of **6.1** in solution and in the presence of SPM-1. For these experiments a derivative of **6.1** in which the C6 (ketone) and adjacent C7 dichlorinated carbon atoms were labelled with ^{13}C was provided by Dr Anthony Krismanich (Dmitrienko's group, Waterloo). Under buffer conditions similar to those employed in the binding studies, this compound was found to exist (almost) entirely as the hydrate, as indicated by the ^{13}C chemical shift (102 ppm) for C6. A coupling constant of ^{2}J = 38 Hz was

observed between C7 (98.7 ppm), indicating that the C6-C7 bond remains intact in the compound under these conditions. Addition of SPM-1 to the sample yielded no change in the chemical shifts of either the C6 or C7 peaks, with specifically no appearance of a peak at 190 ppm that would be considered indicative of a ketone at C6 **(Figure 6.7)**.[203, 208] Binding of **6.1** to the enzyme under these conditions was confirmed and indicated binding in the hydrated, rather than the ketone, form.

Cyclobutanone inhibition of SBLs involves formation of a hemiketal linkage to the active site serine nucleophile,[204] exploiting the 'oxyanion hole' that stabilises tetrahedral oxyanionic species formed on addition of serine to the β-lactam amide **(Figure 6.1)**. In contrast, MBLs are proposed to preferentially stabilise ring-opened intermediates present after addition of the Wat1 nucleophile to the amide carbonyl carbon but before proton transfer to the amide nitrogen. Interaction of Zn2 with the anionic nitrogen of such species is proposed to be the main mechanism for stabilisation.[203-204] This work, however, suggests that the SPM-1 active site can bind with reasonable affinity to a compound, *i.e.* the hydrated cyclobutanones, whose tetrahedral carbon (C6) atoms make them analogous to a β-lactam oxyanion. Taking into consideration the known activity of cyclobutanones against all classes of SBLs,[204] these results indicate that structures replicating the tetrahedral oxyanion deserve investigation as starting points for inhibitors effective against both mechanistic classes of β-lactamases.

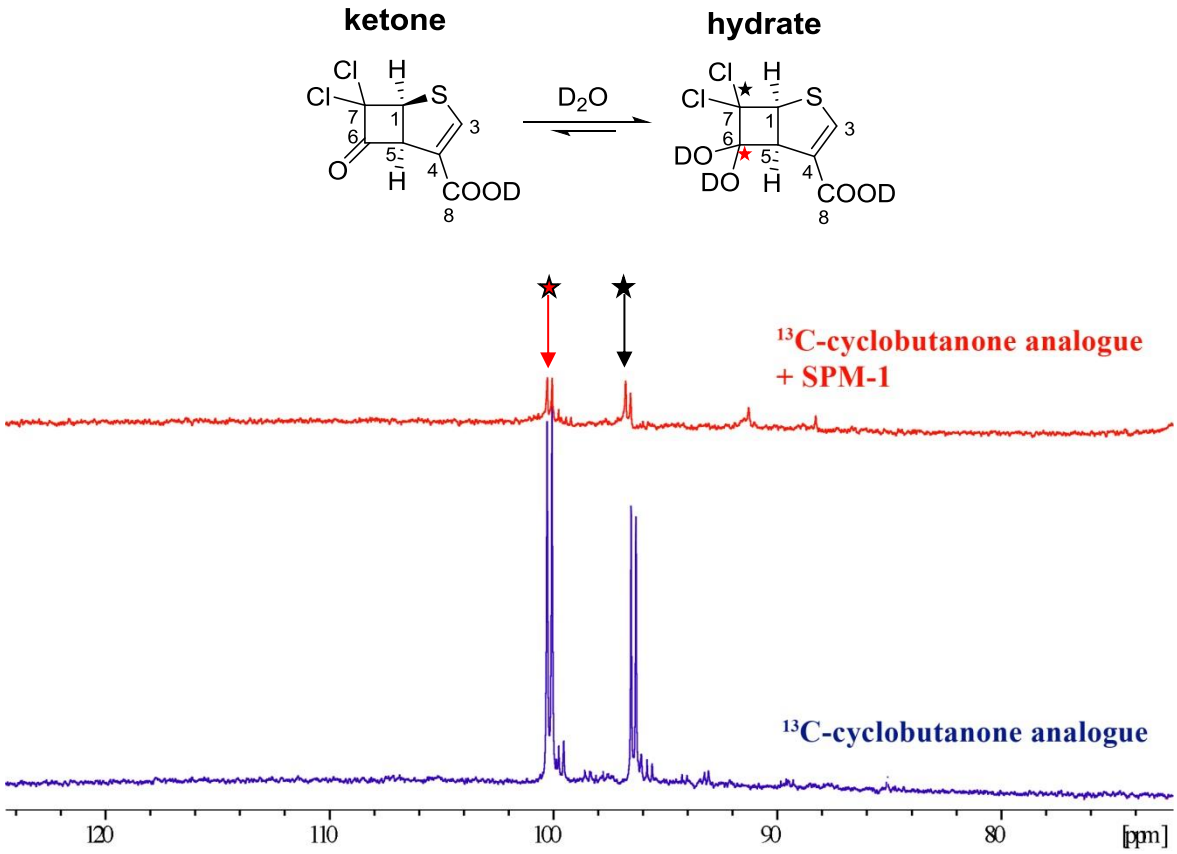

Figure 6.7. ^{13}C-NMR spectra of wildtype (wt) SPM-1 with ^{13}C-labelled cyclobutanone analogue. *The peak at 102.156 ppm corresponds to the carbon of the hydrated form of* ***6.1****[203, 208] (red star) and that at 98.669 ppm corresponds to the di-chlorinated carbon (black star). They are vicinal carbons with a coupling constant ^{2}J of 38 Hz. Upon addition of SPM-1 (red trace), the peaks corresponding to the compound (blue trace) were strongly attenauted, indicating a binding event. Under the experimental conditions, in aqueous buffer, cyclobutanone analogue was found to be in its hydrated form bound to SPM-1. The assay mixture contained wt SPM-1 (0.84 mM) and ^{13}C-labelled cyclobutanone analogue (4.2 mM) in Tris-D_{11} buffer (50 mM, pH 7.5) supplemented with 0.02 % NaN_3 and 10% D_2O.*

6.3. Summary and Perspectives

This chapter describes work on the interaction of the cyclobutanones, β-lactam analogues known to inhibit all three classes of serine β-lactamases,[160b] with SPM-1, a member of the zinc-dependent MBL enzyme family. ^{19}F-NMR of a fluorine-labelled SPM-1 variant reveals cyclobutanone binding to the enzyme with micromolar affinity, in a manner which causes perturbation of a loop, L3, adjacent to the active site. Cyclobutanone binding causes a smaller effect on more distant helical elements that define the active site cleft. A crystal structure of the SPM-1:cyclobutanone complex shows binding of a hydrated cyclobutanone *via* interactions with one of the two active-site zinc ions, stabilisation of the hydrate by hydrogen bonding to zinc-bound water, and hydrophobic contacts with aromatic aside chains adjacent to the active site. ^{13}C-NMR of a labelled cyclobutanone derivative supports assignment of the bound species as the hydrate, rather than the ketone, form. These results reveal a possible mode by which MBLs bind tetrahedral oxyanionic species and support investigation of similar analogues as effective inhibitors against multiple β-lactamase classes.

6.4. Materials and Methods

Y58C* SPM-1 and wt SPM-1 were produced, purified, characterised, and/or crystallised as described in **Chapter 5**. Y152C* SPM-1 was provided by Dr Jürgen Brem.[206]

6.4.1. NMR Experiments

NMR spectra (^{1}H and ^{19}F) were recorded using a Bruker AVIII 600 MHz NMR spectrometer equipped with a BB-F/^{1}H Prodigy N_2 cryoprobe using 5 mm diameter NMR tubes (Norell)

6.4.1.1. ^{1}H Excitation Sculpting Suppression NMR Experiments

Spectra were typically obtained using 252 scans, a relaxation delay of 1 s, and a pre-scan delay of 10 μs. A 2 ms sinc pulse was used for water suppression. Data were processed with a line broadening of 0.3 Hz using TopSpin 3.1 software (Bruker). Samples contained wt di-Zn(II)-SPM-1 complex (355 μM) and the cyclobutanone analogue (2.5 mM) in Tris-D_{11} buffer (50 mM, pH 7.5) supplemented with 10% D_2O.

6.4.1.2. ^{19}F NMR Experiments

Spectra were typically obtained using 512 scans and a relaxation delay of 4 s. Samples contained the ^{19}F-labelled di-Zn(II)-SPM-1 complex (45 μM) in Tris buffer (50 mM, pH 7.5) supplemented with 10% D_2O, unless otherwise stated.The cyclobutanone analogue was titrated in the assay mixture from a DMSO stock. Trifluoroacetic acid (10 μM) was used as an internal NMR standard.[170, 206] Data were processed with a line broadening of 5 Hz using TopSpin 3.1 software (Bruker).

6.4.1.3. ^{13}C NMR Experiments

NMR experiments were recorded with 4000 scans using a Bruker AVIII 700 spectrometer equipped with an inverse TCI cryoprobe optimised for ^{1}H observation and installed with Topspin 3.1 software (Bruker). The assay mixture contained wt SPM-1 (0.84 mM) and ^{13}C-labelled cyclobutanone analogue (4.2 mM) in Tris-D_{11} buffer (50 mM, pH 7.5) supplemented with 0.02 % NaN_3 and 10% D_2O.

6.4.2. Characterisation of the Cyclobutanone Analogue by NMR

Ketone: ^{1}H NMR (500 MHz): δ 5.21 (d, $J_{5,1}$ = 10.1 Hz, 1H, H_5), 5.56 (dd, $J_{1,3}$ = 1.8 Hz, $J_{1,5}$ = 10.1 Hz, 1H, H_1), 7.73 (d, $J_{3,1}$ = 1.8 Hz, 1H, H_3). ^{13}C NMR (125 MHz): δ 60.5, 72.5, 94.7, 123.0, 149.0, 165.4, 192.4. **Hydrate**: ^{1}H NMR (500 MHz): δ 4.45 (d, $J_{1,3}$ = 1.4

Hz, $J_{1,5}$ = 10.1 Hz, 3H, H_5), 4.88 (d, $J_{1,5}$ = 10.1 Hz, 1H, H_1), 7.63 (d, $J_{3,1}$ = 1.4 Hz, 1H, H_3). ^{13}C NMR (125 MHz): δ 61.6, 62.7, 97.6, 101.5, 126.6, 149.9, 166.9.

Chapter 7. Interaction of Avibactam with MBLs

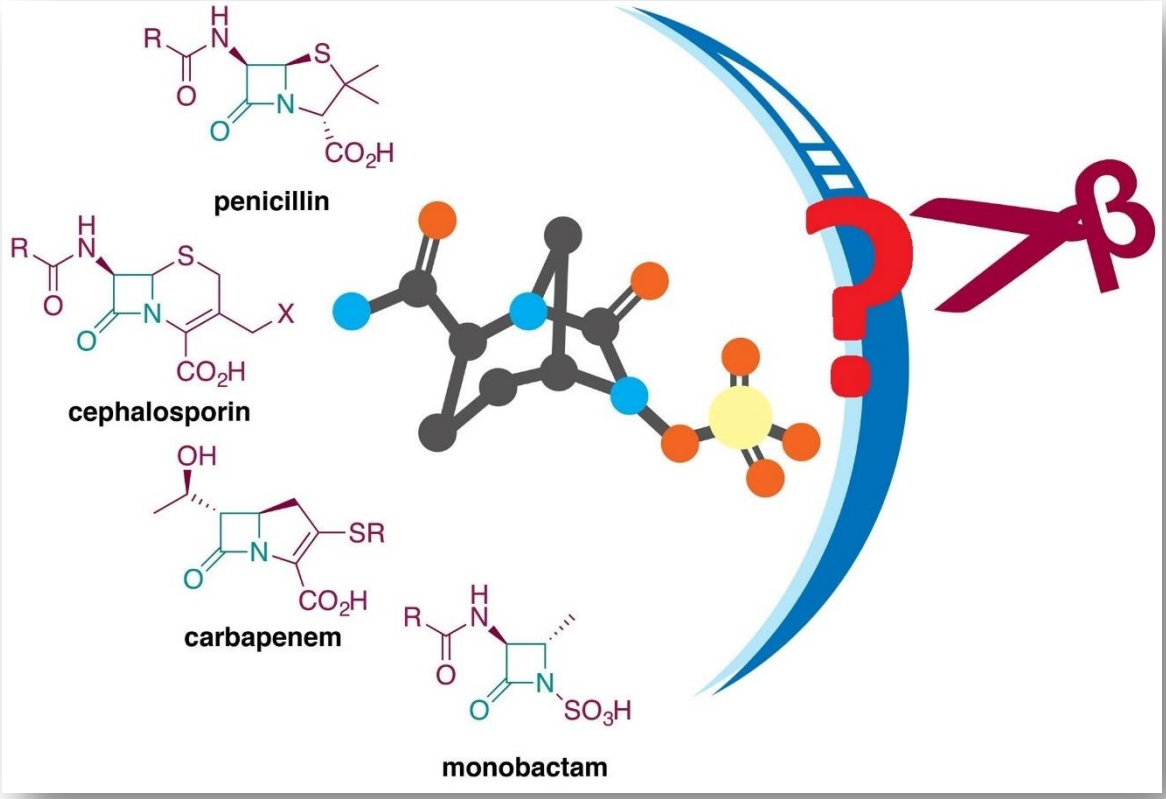

Figure created by David Wang.

Chapter 7. Contents

7.1. Introduction

Avibactam (previously, NXL104 or AVE1330A) is the first non-β-lactam based β-lactamase inhibitor to reach the market (in combination with ceftazidime, it is branded as Avycaz).[40, 209] Avibactam contains a diazabicyclooctane (DBO) core. Avibactam is a potent broad-spectrum inhibitor of class A, class C, and some class D serine-β-lactamases (SBLs).[40, 60] Like the β-lactam antibiotics, avibactam has a core heterocyclic system ring which is subject to inhibition by SBLs *via* covalent interaction with their catalytically active site serine residue.[184] In contrast to β-lactams which react irreversibly with SBLs, avibactam has been shown to react reversibly with SBLs *via* recyclisation of its core ring.[60, 210] Accordingly, avibactam is more efficient than β-lactams in terms of the number of molecules required to inhibit each serine β-lactamase; it requires only 1-5 avibactam molecules per β-lactamase compared with 10s-100s molecules of SBL inhibitors per β-lactamase.[184, 211] Avibactam also forms a long-lived complex with its SBL target ($t_{1/2}$ > 7 days).[60, 211a] As the first clinically useful non-β-lactam β-lactamase inhibitor, avibactam represents a major breakthrough in the β-lactamase/penicillin binding protein antibacterial field.[212] The susceptibility of avibactam to MBL catalysed hydrolysis has not yet been reported. This is an important issue since MBLs are becoming more widespread,[213] and MBL-catalysed avibactam hydrolysis by an overproduced MBL might impair the potency of the cephalosporin-avibactam combinations against strains that produce both an MBL and one or several SBLs. The work reported in this chapter shows that avibactam is not an MBL inhibitor and a poor substrate of most members of the three suclasses of MBLs tested. In some cases, it undergoes hydrolysis of its urea carbonyl followed by loss of CO_2, in a process different from studied SBLs as suggested in **Figure 7.1**.

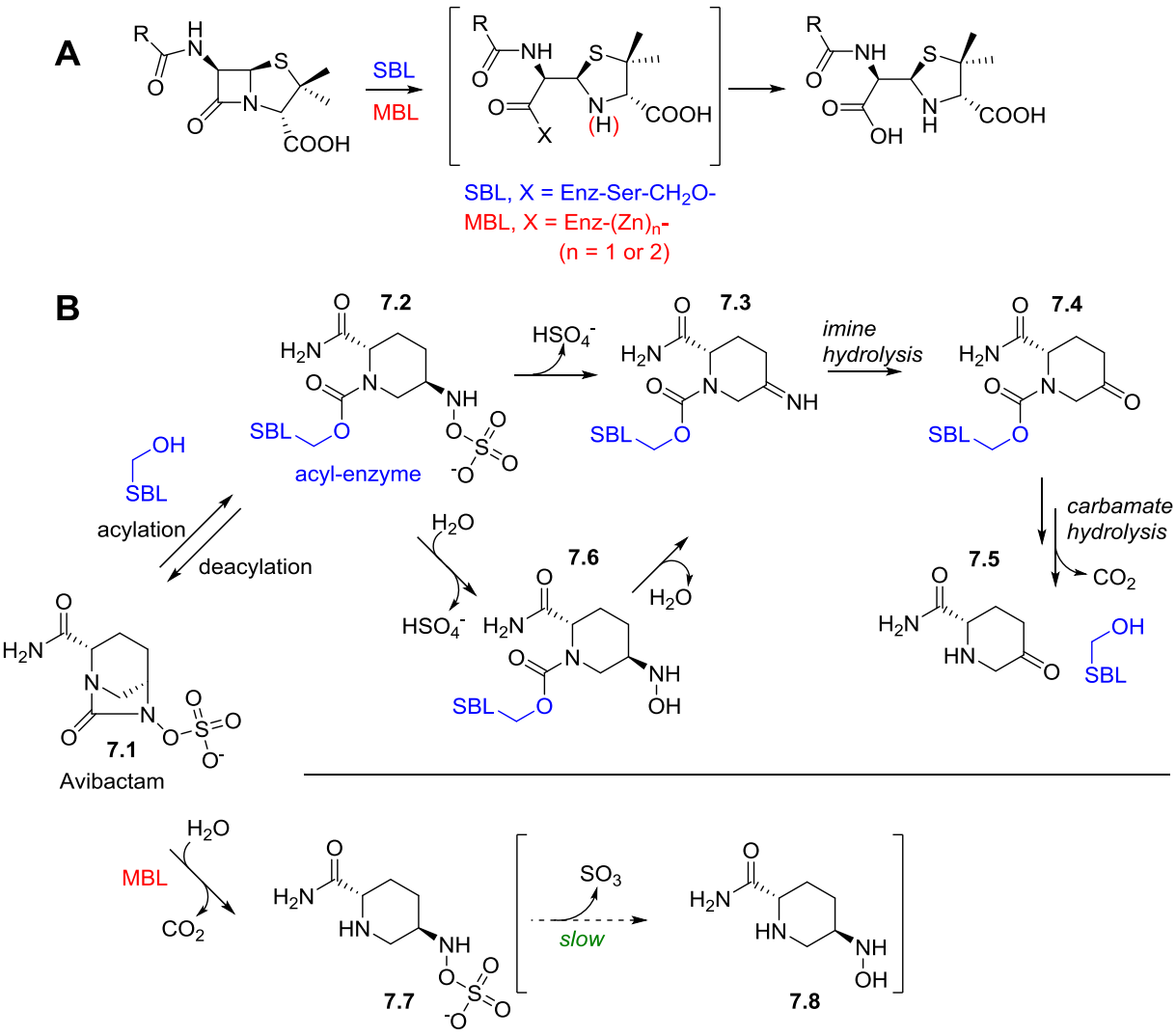

Figure 7.1. β-Lactamase catalysis and inhibition of avibactam. ***(A)*** *Reactions catalysed by serine (SBLs) and metallo β-lactamases (MBLs), outlining the proposed intermediates.*[46b] ***(B)*** *The reactions of avibactam with SBLs and MBLs differ. With SBLs, the available evidence is that hydrolysis of the acyl-enzyme complex proceeds via elimination to give an imine.*[184] *In the case of the MBLs, hydrolysis without elimination and imine hydrolysis can occur.*

7.2. Results

7.2.1. Protein Production and Purification

In order to study the interaction of avibactam with MBLs, representative of the 3 different MBL subfamilies were selected. The differences and similarities between the MBL subclasses are highlighted in **Chapter 1, Table 1.1**. NDM-1, SPM-1, BcII, VIM-2 and VIM-4 were selected as representatives of B1 MBLs, CphA as a representative of B2 MBLs, and FEZ-1 as a representative of B3 MBLs. I produced the selected MBLs (NDM-1, SPM-1, BcII, VIM-2, and FEZ-1) in *Escherichia coli* as previously reported.[188, 214] The purity of the recombinant proteins produced was assessed by SDS-PAGE analyses, as exemplified with NDM-1 in **Figure 7.2**. VIM-4 and CphA were produced by Dr Jürgen Brem.

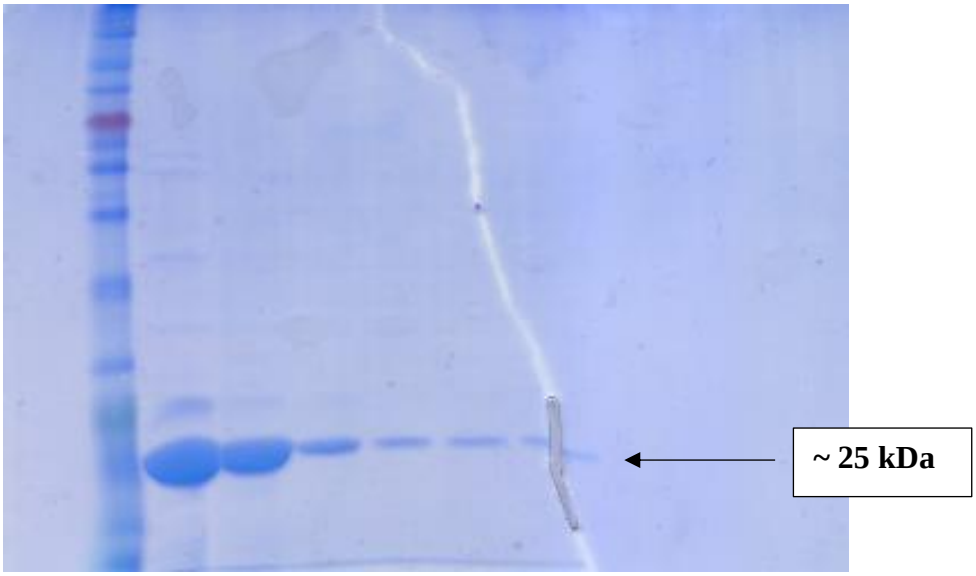

Figure 7.2. SDS-PAGE analysis of the purification of recombinant NDM-1. *Molecular weight markers (PageRuler Prestained Protein Ladder 10-170 kDa, Thermo Scientific).*

7.2.2. Binding Studies

In order to study the binding of avibactam to MBLs, ligand-observe NMR spectroscopy methods were first used as outlined in **Table 7.1**. To assay for binding of avibactam to MBLs, representatives of the 3 different MBL subfamilies (NDM-1, SPM-1, BcII, VIM-2 and VIM-4 B1 MBLs, CphA B2 MBL, and FEZ-1 B3 MBL) were used. All the tested MBLs use a di-zinc active site except for CphA, which is a mono-zinc MBL.[215]

Table 7.1. Summary of the predicted observations of ligand binding to proteins as observed by ligand-observe NMR methods.

NMR method	Predicted observations on binding *(within detection range)*
^{1}H NMR	line broadening
^{1}H CPMG NMR	intensity reduction
wLOGSY NMR	change of the NOE intensity in the presence of the receptor

The ^{1}H CPMG[137] results with NDM-1, VIM-2, VIM-4, SPM-1, and FEZ-1, all indicated weak binding of avibactam **(Figure 7.3)**. In the case of the model B1 MBL from *Bacillus cereus* BcII,[49a] no binding was observed by ^{1}H CPMG under the standard conditions. However, evidence for binding of avibactam to BcII was accrued using the sensitive wLOGSY[84] NMR method, implying avibactam is a (very) weak binder of BcII **(Figure 7.4)**. Further analyses were carried out on SPM-1 because it has structural elements of both B1 and B2 subfamilies;[164a, 165] all the NMR methods used [^{1}H,[216] CPMG,[137] and wLOGSY[84] **(Figure 7.5)**] indicated that avibactam is a weak binder to SPM-1. Avibactam hydrolysis was then assayed using NMR. For BcII only very low levels of hydrolysis were observed, consistent with the very poor binding observed by NMR; SPM-1-catalysed hydrolysis was also slow **(Figure 7.6A)**. The results of time-course wLOGSY[84] analyses with SPM-1 implied that

whilst avibactam itself binds to the protein, the observed products of avibactam hydrolysis did not: the hydrolysed species manifested NOE values which are characteristics of a free ligand in solution while the intact avibactam shared the same NOE sign with SPM-1 **(Figure 7.6B)**. For NDM-1 and VIM-4, more efficient hydrolysis (though still slow by normal β-lactamase standards) was observed to give an apparently stable product (> 4 hours after a 4-hour incubation for VIM-4). Controls without enzyme did not lead to detectable product levels; avibactam hydrolysis is MBL-mediated.

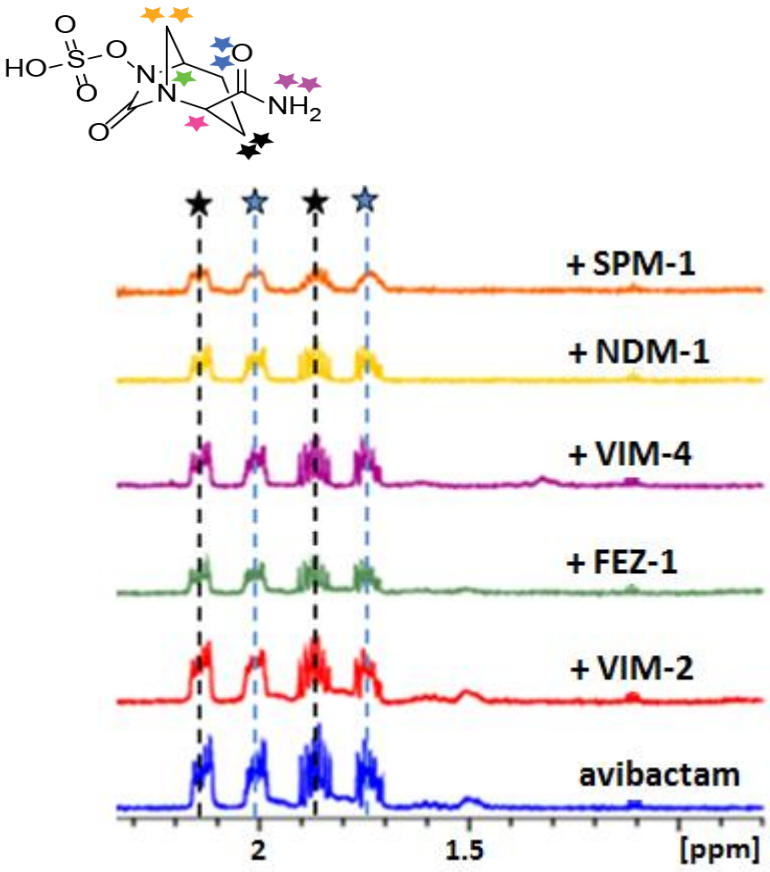

Figure 7.3. Studies of the binding of avibactam to MBLs using ^{1}H CPMG NMR. *^{1}H CPMG analyses of avibactam with selected MBLs reveal that avibactam is a weak binder. The assay mixtures contained 80 µM MBL and 4 mM avibactam in 90 % H_2O and 10 % D_2O, 50 mM Tris-D_{11}, pH 7.5.*

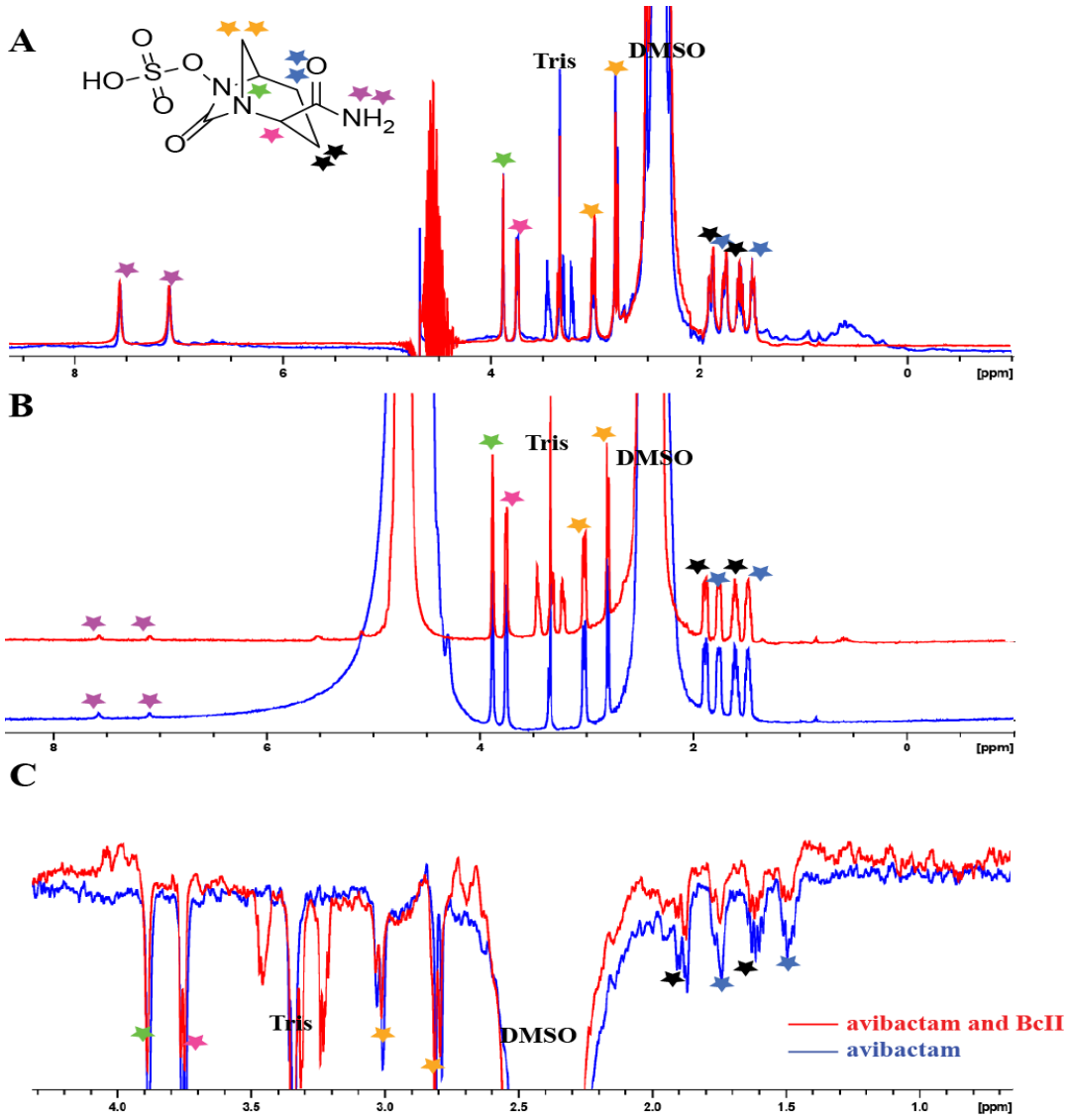

Figure 7.4. NMR assays for binding of avibactam to BcII. ***(A)*** *^{1}H NMR spectra of avibactam (blue trace) and BcII mixed with avibactam (red trace).* ***(B)*** *^{1}H CPMG NMR spectra of avibactam (blue trace) and Bc-II mixed with avibactam (red trace).* ***(C)*** *wLOGSY NMR spectra of avibactam (blue trace) and Bc-II mixed with avibactam (red trace). The wLOGSY results indicate weak binding of avibactam to BcII. The assay mixtures contained 80 µM di-Zn(II)-BcII and 4 mM avibactam in 90 % H_2O and 10 % D_2O, 50 mM Tris-D_{11}, pH 7.5.*

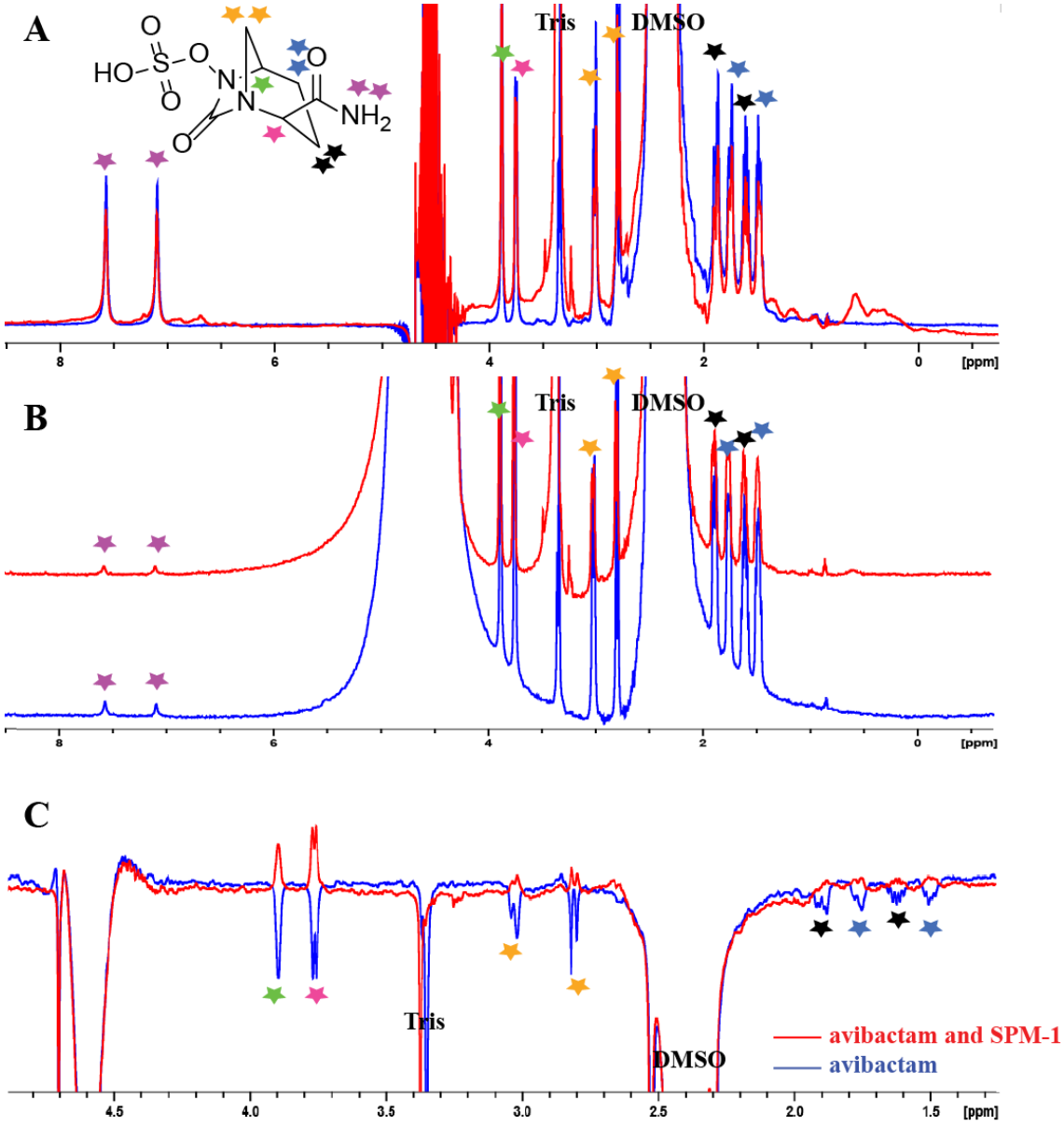

Figure 7.5. NMR assays for binding of avibactam to SPM-1. ***(A)*** *^{1}H NMR spectra of avibactam (blue trace) and SPM-1 mixed with avibactam (red trace).* ***(B)*** *^{1}H CPMG NMR spectra of avibactam (blue trace) and SPM-1 mixed with avibactam (red trace).* ***(C)*** *wLOGSY NMR spectra of avibactam (blue trace) and SPM-1 mixed with avibactam (red trace). The results imply weak binding of avibactam to SPM-1. The assay mixtures contained 80 µM di-Zn(II)-SPM-1 and 4 mM avibactam in 90 % H_2O and 10 % D_2O, 50 mM Tris-D_{11}, pH 7.5.*

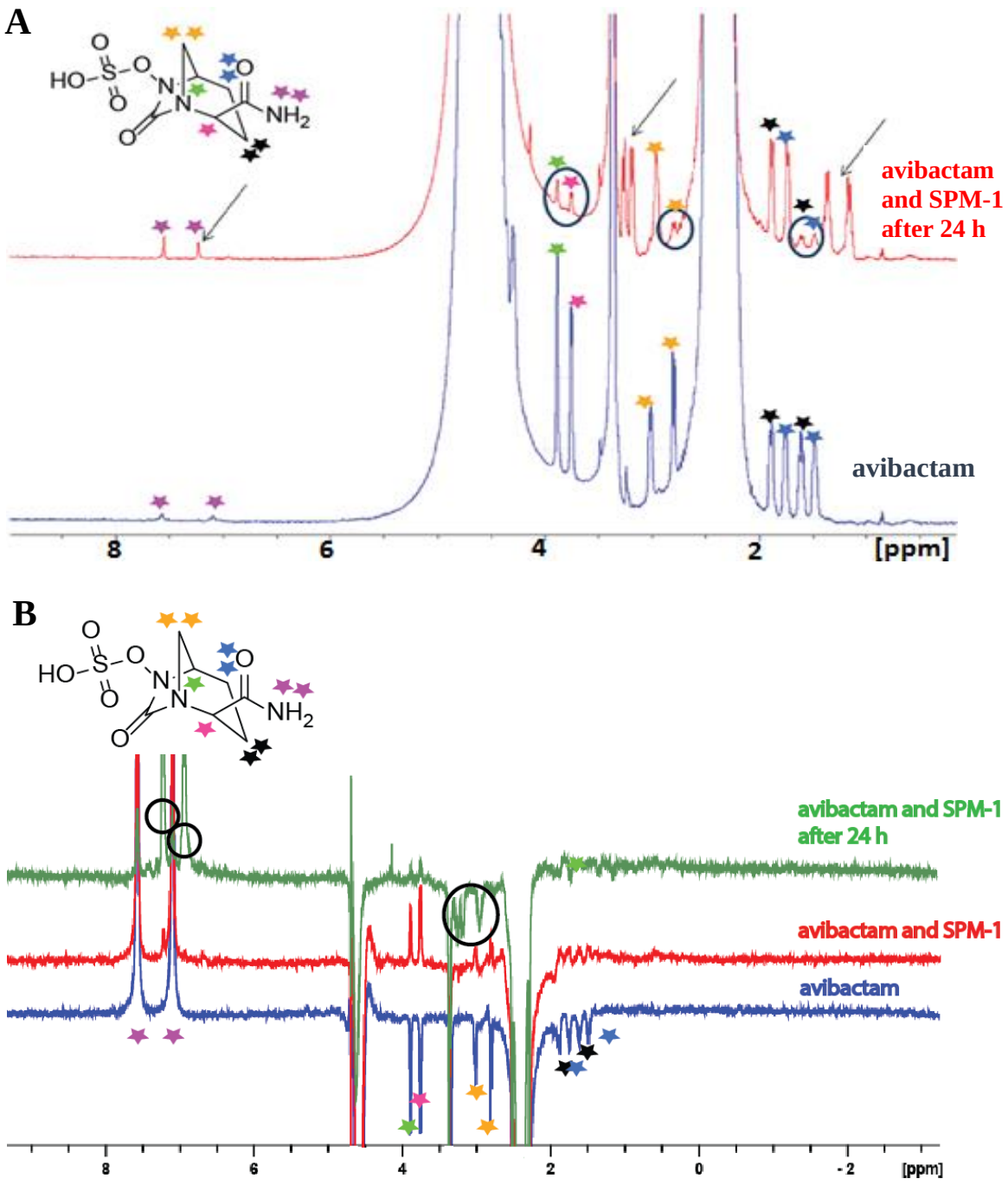

Figure 7.6. Time-course NMR spectra of the reaction of SPM-1 and avibactam. ***(A)*** *^{1}H CPMG NMR spectra.* ***(B)*** *wLOGSY NMR spectra. The results imply avibactam hydrolysis is catalysed slowly by SPM-1. Peaks corresponding to new species are highlighted with arrows. Reductions in the major signal intensities of the intact avibactam peaks are highlighted in circles. Peaks corresponding to the new species are highlighted with arrows; no evidence for binding of this new species to SPM-1 was accrued. In contrast, the results imply intact avibactam binds weakly to SPM-1. The assay mixture contained 80 μM di-Zn(II)-SPM-1 and 50 molar equivalents of avibactam (4 mM from a DMSO stock) in Tris-D_{11} buffer (50 mM, pH 7.5) supplemented with 10 % D_2O.*

7.2.3. Kinetic Analyses

A reported spectroscopic assay for monitoring avibactam hydrolysis[184] was first employed to assess whether MBLs hydrolyse avibactam. Comparison of the UV-visible spectra indicated that the hydrolysed product exhibits a decreased absorbance relative to avibactam with the highest variation in the 220-230 nm area (ε_{230} = 910 $M^{-1}.cm^{-1}$). Monitoring the changes in absorbance at 230 nm, the results give the following order of avibactam hydrolysis efficiency in both HEPES and cacodylate buffers: VIM-4 > FEZ-1 > IMP-1 ~ NDM-1. The inhibitory potency of avibactam on MBL catalysis was assessed by carrying out assays using ceftazidime as a substrate.[217] For all the MBLs tested, the residual MBL-mediated cetazidime hydrolysis activity was observed to be > 50 % in the presence of 1 mM avibactam. Consequently, the results indicate that MBL 'protection' by the ceftazidime is not an important factor in the analysis of the results. Kinetic analyses were carried out by Prof Jean-Marie Frère.

Table 7.2. Residual activity at ceftazidime (30 µM) in the presence of 1 mM avibactam (HEPES buffer). *For assay conditions, see Materials and Methods.*

Enzyme	Residual activity (%)
VIM-2	91 ± 4
VIM-4	85 ± 5
NDM-1	90 ± 5
IMP-1	60 ± 6
FEZ-1	71 ± 2

The results imply that avibactam binds to the tested MBLs weakly and that, at least some, MBLs are capable of inefficiently/slowly catalysing avibactam hydrolysis. These findings suggest that the evolution of new MBLs that efficiently catalyse avibactam hydrolysis should be anticipated. It is therefore of interest to develop variants of avibactam that are either resistant to MBL catalysed hydrolysis and/or which are MBL inhibitors. Aztreonam, a monobactam, is the only clinically used β-lactam which is not an MBL substrate.[218] By comparing the structures of avibactam and aztreonam **(Figure 7.7)**, there is likely scope for decreasing MBL-catalysed hydrolysis of avibactam by modifying its RN–OSO_3^- group. Interestingly, avibactam protects aztreonam from hydrolysis by SBLs even in the presence of MBLs; thus, it would seem important to preserve and build on the apparent advantage of the aztreonam-avibactam combination.[217b, 218-219]

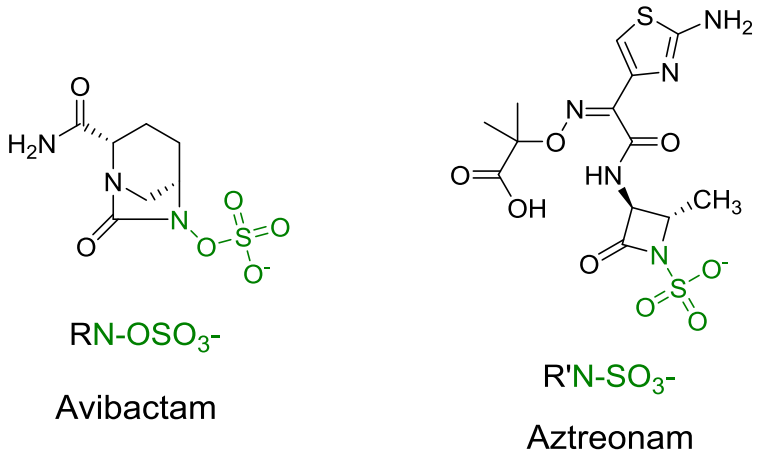

Figure 7.7. Structures of avibactam and aztreonam. *Both aztreonam and avibactam have an –SO_3^- group. For the β-lactam aztreonam* ***4.11****, the –SO_3^- group is directly linked to the nitrogen of the acylating heterocycle. In the case of avibactam* ***4.1****, the –SO_3^- group is linked to the cyclic urea via an O atom (i.e. an RN-OSO_3^- group). Thus, there may be scope for decreasing MBL catalysed hydrolysis of the avibactam core by modifying its RN-OSO_3^- group.*

7.2.4. Characterisation of MBL-mediated avibactam hydrolysed product(s)

7.2.4.1. NMR Analyses

^{1}H NMR, COSY, HMBC and HSQC NMR analyses implied the product (from SPM-1 and VIM-4 catalysis) had lost the C7 C=O group of avibactam but had retained the N1 and N6 atoms **(Figures 7.8, 7.9)**. The nitrogen of the CO-NH_2 side-chain could not be detected because of proton exchange with the solvent. Based on NMR analyses solely, it was not possible to tell whether the N-OSO_3^- group had been cleaved. My work with SPM-1 and that of Dr Christian Damblon with VIM-4 revealed similar chemical shifts/product(s) are derived from MBL-catalysed avibactam hydrolysis as outlined in **Table 7.3**.

Table 7.3. Assigned chemical shifts (ppm) of the potential products of avibactam VIM-4 and SPM-1 mediated hydrolysis, indicating similar hydrolysed product(s).

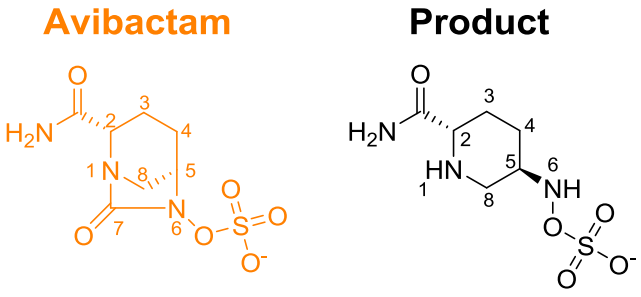

	Avibactam			Hydrolysed product(s)		
Atom	**C**	**H**	**N**	**C**	**H**	**N**
1			78.4			41.6
2	60.3	4.0		57.1	3.7	
3	18.0	2.1 1.9		26.0	2.2 1.7	
4	19.8	2.0 1.7		25.1	2.0 1.5	
5	59.9	4.1		54.2	3.3	
6			184.2			163.4
7	169.3					
8	47.1	3.3 3.0		45.4	3.5 2.8	
$CONH_2$	174.7			173		

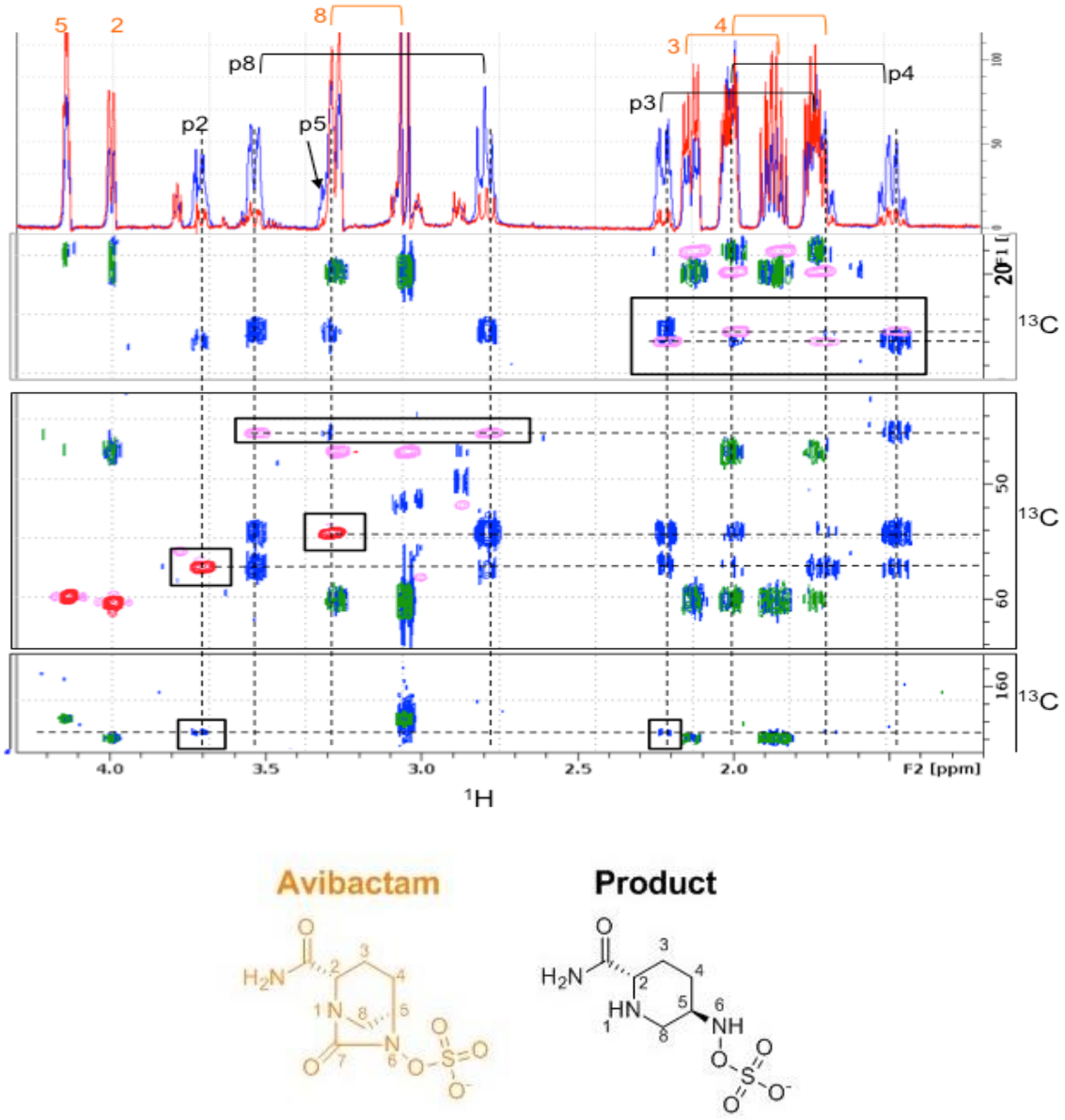

Figure 7.8. Analyses of the hydrolysis reaction of avibactam with selected MBLs by NMR. *2D ^{1}H-^{13}C correlation analysis of a mixture of 50 % avibactam and 50 % avibactam hydrolyzed products. Edited HSQC: CH (red) CH_2 (pink). HMBC: avibactam pure (green), hydrolysis-avibactam reaction mixture 50/50 (blue). Hydrolysis product signals are in black box in the 2D ^{1}H-^{13}C correlation. The 1D ^{1}H spectrum displayed at the top of the 2D plane corresponds to avibatam (red) and the hydrolysis-avibactam reaction mixture 50/50 (blue). The black labels correspond to the hydrolysed product(s). Orange labels correspond to avibactam.*

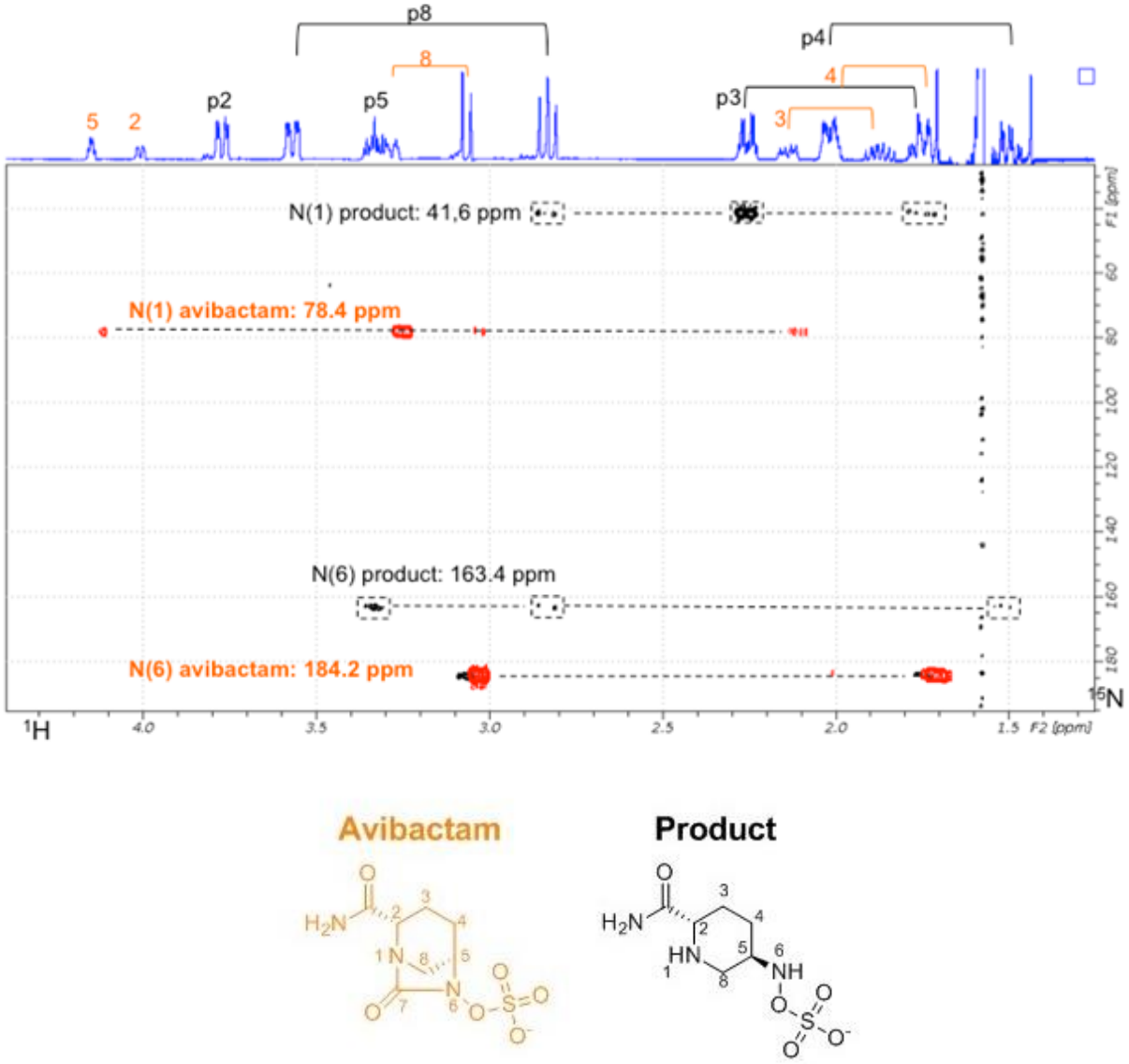

Figure 7.9. Characterisation of VIM-4 mediated avibactam hydrolysis. *The 1D ^{1}H spectrum at the top of the 2D plane corresponds to the hydrolysed-avibactam reaction mixture 50/50 (blue). Black labels correspond to the hydrolysis product. 2D ^{1}H-^{15}N HMBC correlation experiment of the ~1:1 mixture of avibactam and the assigned avibactam hydrolysed product(s) (black). 2D ^{1}H-^{15}N HMBC correlation experiment of avibactam is in red. Orange labels correspond to avibactam.*

7.2.4.2. Raman Analyses

Due to the described limitations of using NMR to detect the potential loss of the SO_3 moiety following avibactam hydrolysis by MBLs, Raman spectroscopy was employed in an effort to detect the free sulphate (by collaborators at the University of Liege). Under the working conditions, free sulphate yields a sharp band just below 1000 cm^{-1}. A comparison of the spectra of VIM-4 with avibactam taken after 240 min of incubation with that of the same sample to which an identical volume of Na_2SO_4 had been added **(Figure 7.10)**. The amount of sulphate in the unspiked reaction mixture (blue trace) is very low; it can be concluded that the proportion of product that has lost the SO_3 moiety does not significantly exceed 15 %. Thus, the major product from VIM-4 catalysed hydrolysis retains the intact N-OSO_3^- group. Overall, these results imply that hydrolysis of avibactam by VIM-4, and by implication other MBLs, predominantly proceeds *via* 'simple' hydrolysis of the avibactam cyclic urea, rather than the more complex mechanism of hydrolysis operating for KPC-2.[184]

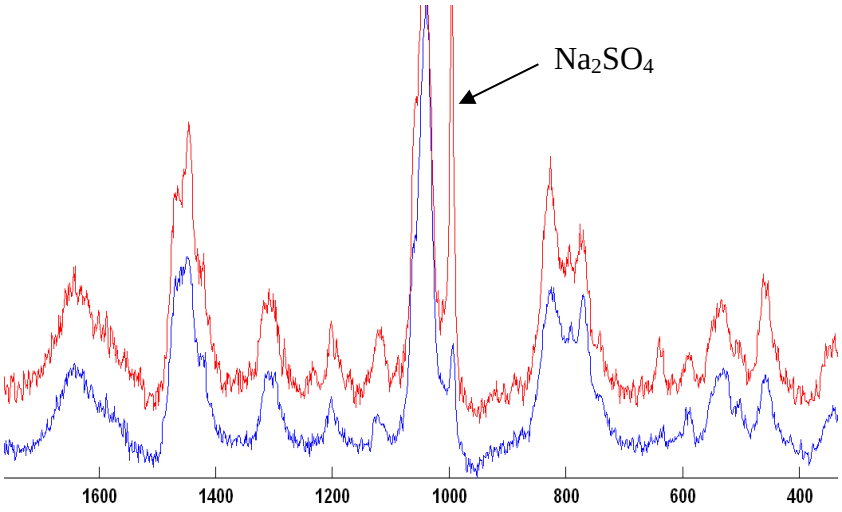

Figure 7.10. Raman analyses of the reaction of VIM-4 and avibactam. *Blue trace: VIM-4 and avibactam after 240 min, red trace: same sample spiked with Na_2SO_4 (the arrow corresponds to Na_2SO_4). For assay conditions, see Materials and Methods.*

The combined NMR and Raman studies imply that, at least in the cases studied in detail, MBL-catalysed avibactam hydrolysis proceeds *via* 'simple' hydrolysis of the acyl urea **(Figure 7.1B)** to give an unstable carbamate which deacylates to give a stable product **7.7**. By MS, low levels of a product implying further hydrolysis of the RN–OSO_3^- to give the RNHOH were detected **7.8**; however, this was a low level product and it cannot be confirmed it results from enzyme catalysis.[185] In contrast, with SBLs, avibactam reacts with the nucleophilic serine reversibly to give an acyl-enzyme complex **7.2**.[60] The available evidence (with KPC-2)[184] is that this complex undergoes initial β-elimination to give an imine **7.3** prior to hydrolysis of the acyl-enzyme complex ester. The imine may be hydrolysed to the ketone **7.4** before or after acyl-enzyme complex hydrolysis.[184] Thus, pathways for β-lactamase catalysed avibactam hydrolysis are different for the tested SBLs and MBLs. (Check **Figure 7.1B** for reaction schemes).

7.3. Summary and Perspectives

Avibactam binds weakly to most of the representatives from all the 3 MBL subfamilies B1, B2 and B3 tested, respectively. In some cases, avibactam undergoes hydrolysis of its urea carbonyl followed by loss of CO_2, in a process different from studied SBLs. The results suggest that whilst the evolution of MBLs that more efficiently catalyse avibactam hydrolysis should be anticipated, the development of dual action SBL and MBL inhibitors based on the diazabicyclooctane of avibactam may be productive.

7.4. Materials and Methods

7.4.1. Protein production and purification

Recombinant forms of the Δ42-NDM-1, VIM-2, VIM-4, SPM-1, FEZ-1, CphA, IMP-1 and BcII MBLs were produced in *Escherichia coli* as described.[188, 214]

7.4.2. NMR binding experiments

For FEZ-1, VIM-2, VIM-4, CphA, NDM-1, SPM-1 and BcII, NMR spectra were recorded using a Bruker AVIII 600 MHz NMR spectrometer equipped with a BB-F/^{1}H Prodigy N_2 cryoprobe using 5 mm diameter NMR tubes (Norell) or 3 mm MATCH NMR tubes (Cortecnet). Data were processed using TopSpin 3.1 software (Bruker). Samples contained the MBL (80 μM) and 50 molar equivalents of avibactam (4 mM final from a DMSO stock) in Tris-D_{11} buffer (50 mM, pH 7.5) supplemented with 10 % D_2O, unless otherwise stated.[185] More details about the NMR sequences are stated below.

7.4.2.1. ^{1}H CPMG NMR experiments

Typical experimental parameters for CPMG NMR spectroscopy were: total echo time, 40 ms; relaxation delay, 2 s; and number of transients, 264. The PROJECT-CPMG sequence ($90°x–[\tau–180°y–\tau–90°y–\tau–180°y–\tau]_n–acq$) was applied.[137] Water suppression was achieved by presaturation. Prior to Fourier transformation, the data were multiplied with an exponential function with 0.3 Hz line broadening.

7.4.2.2. ^{1}H NMR experiments

For ^{1}H excitation sculpting suppression with perfect echo NMR experiments, spectra were typically obtained using 252 scans, and a relaxation delay of 1 s. A 2 ms Sinc pulse was used for water suppression. Prior to Fourier transformation, data were multiplied with an exponential function with 2 Hz line broadening.

7.4.2.3. wLOGSY NMR experiments

For wLOGSY analyses, typical experimental parameters were: mixing time, 1 s; relaxation delay, 2 s; number of transients, 256. Solvent excitation was achieved using a 16 ms 180 degrees selective rectangular shape pulse with 1000 points (Squa100.1000) set at the

H_2O frequency.[83] Water suppression was achieved by a 2 ms Sinc pulse (Sinc1.1000) at the H_2O frequency.

7.4.3. Hydrolysis of Avibactam Followed by UV-VIS Spectroscopy

To a 1 mM solution avibactam (1 mL) in 5 mM HEPES buffer, pH 7.5 containing 35 µM $ZnCl_2$ was added VIM-4 (8 µg). A spectrum was then immediately recorded between 210 and 280 nm. After 20 hrs at 20°C, another spectrum was then recorded; the appearance of this spectrum was not modified after further incubation. The rate of avibactam hydrolysis was estimated by monitoring the decrease in absorbance at 230 nm ($\Delta\varepsilon$ = 910 $M^{-1}.cm^{-1}$). Two buffers were used: 5 mM HEPES, pH 7.5 and 50 mM cacodylate, pH 7.0, both containing 20µM $ZnCl_2$. The MBL (8-75 µg, depending upon the activity) was added to a 600 µL sample of 1 mM avibactam in buffer and the absorbance was monitored for 40 to 240 min at 30°C. Due to the low activity observed with NDM-1, incubation was continued overnight (20 hrs).[184] Assay performed by Prof Jean-Marie Frère.

7.4.4. Inhibition of Ceftazidime Hydrolysis by Avibactam

Ceftazidime inhibition assays were performed in 5 mM HEPES buffer pH 7.5 containing 20 µM $ZnCl_2$. The initial rate of ceftazidime hydrolysis (30 µM) was monitored at 260 nm and 30°C in the presence or absence of 1 mM avibactam.[212a] Assay performed by Prof Jean-Marie Frère.

7.4.5. Analyses of Avibactam Hydrolysis Products

7.4.5.1. NMR Analyses

NMR spectra (^1H, 2D COSY, ^1H-^{15}N/^1H-^{13}C HSQC and HMBC) were recorded using a Bruker Avance I 500 MHz equipped with a TCI cryoprobe. Avibactam (1 mg/mL, 1 mL) in 10 mM sodium phosphate pH 7.5 in D_2O was added to 20 µg of VIM-4/SPM-1 enzyme.

7.4.5.2. Raman Spectroscopy

Raman analyses were conducted by colleagues at the University of Liege as follows.[185] Six hundred µL of 1 mM avibactam in 5 mM HEPES pH 7.5 containing 20 µM $ZnCl_2$ were mixed with 12 µg of VIM-4. After 240 min at 37°C, changes in the absorbance at 270 nm indicated that ~ 70 % of avibactam had been hydrolysed. Samples (2 µL) were withdrawn after 0 and 240 min. A second 240 min sample was analysed following addition of 2 µL of 1 M Na_2SO_4. The samples were deposited as solution drops, and then dried on a polished stainless steel plate. They were analysed using a LabRam 300 spectrometer (Jobin-Yvon) equipped with an Olympus confocal microscope and an Andor Open Electrode iDus CCD detector. The laser sources used were either a Cobolt Samba 500 (532 nm) or a Melles Griot He-Ne laser (632.8 nm). The laser was focused on the target using a x100 objective. The maximum laser beam power was limited to 1.5 mW by using neutral density filters to minimise sample degradation. The integration times ranged from 30 to 50 seconds, depending on the sample. In order to check the homogeneity of the spots, spectra were recorded, with both lasers, on several areas of the sample visualised using a CCD camera. Where necessary, a baseline correction was applied to the recorded spectra using a polynomial regression model and homemade software.

Chapter 8. Summary

The work described in this thesis was primarily focused on the use of NMR to study two general classes of enzymes – the Fe(II)- and 2-oxoglutarate (2OG)-dependent dioxygenases and the β-lactamases. These two enzyme classes are involved in clinically important biological processes, *i.e.* the hypoxic response and antimicrobial resistance, respectively. Both systems are interesting from an NMR perspective because they employ dynamic loops to interact with ligands in catalysis. The work included enzyme mechanistic studies, protein-ligand interaction studies, and method development for inhibitor discovery. **Chapter 1** provided an introduction to the relevant biological systems and to biological applications of NMR spectroscopy. The latter focused on the use of NMR to monitor protein-ligand interactions; such methods can be broadly divided into ligand-observe and protein-observe methods.

In **Chapter 2**, ligand-observe NMR methods were applied to investigate the substrate selectivity of the medicinally important human oxygenase, PHD2. CODD and NODD binding to PHD2 induce different interactions, including changes in the β2β3 and the α3-α4 regions of PHD2 **(Figure 2.3)**. Since the *C*-terminal region differs considerably amongst the human PHD isoforms,[22] the results raise the possibility that isoform-selective PHD inhibition could be achieved. It was found that a single residue substitution, as in the case of P317R PHD2[106] or R396T PHD2,[107] can alter the selectivity of PHD2 towards its ODD substrate **(Figure 2.4)**, which may link to specific disease phenotypes observed (erythrocytosis[106] or breast cancer,[107] respectively). Studies with the *Trichoplax adhaerens* PHD[118] provided insights into the evolutionary substrate preference of the PHD-HIF system **(Figure 2.9)**. Using ^{13}C-labelled peptidyl-substrates, NMR was applied to investigate alternative PHD2 substrates/interaction partners **(Figure 2.11)**. Such binding might alter PHD2 activity by

modulating substrate binding. Interestingly, some PHD2-interacting partners[123, 127] were able to bind to VCB in their hydroxylated form **(Figure 2.14)**, indicating that they might regulate the PHD-HIF system.

Chapter 3 describes studies on the product release mechanism of PHD2. The results suggest a new feedback mechanism in the HIF system and raise the possibility that, in some circumstances, *i.e.* when 2OG is limiting, binding of hydroxylated HIF-α to the PHDs may limit HIF-α degradation. The results reveal that the binding of 2OG strongly discriminates between the binding of HIF and hyHIF to PHD2 **(Figure 3.3)**. Whilst HIF and hyHIF bind equally strongly to *apo*- and metallated-PHD2, a steric clash with the hydroxylated C^4-*endo* proline ring conformation (arising from the *gauche* effect)[30] can disrupt PHD2 binding of hyHIF **(Figure 3.10)**. A fluorescence-based method **(Figure 3.5)** was developed to monitor peptide binding to PHD2 – the fluorescence-based method could be applied to other PHD isoforms and other 2OG dioxygenases. The results suggest a new link between the HIF system and the TCA cycle metabolism.

Chapter 4 describes work in which NMR was applied to monitor PHD2 enzyme kinetics and inhibitor interactions. Competition and displacement assays were designed and applied to investigate inhibitor binding modes; these assays showed whether the inhibition mechanism involved general-metal chelation and/or substrate/cosubstrate competition. The clinically used iron chelators Deferoxamine[154] and Deferasirox[155] were shown to have differential inhibition modes; Deferoxamine sequesters Fe(II) in solution **(Figure 4.4)**, whilst Deferasirox binds to PHD2 itself **(Figure 4.2)**. The results are of interest because they shed light on the possibility of achieving more selective results, at least *in vitro*. Comparative studies on the activities and selectivities of PHD inhibitors in clinical trials[157] were presented. All of the clinically used inhibitors tested compete with 2OG. Notably, however, FG-4592 was the only one of the tested inhibitors capable of displacing CODD, whilst Molidustat did

not interfere with neither CODD nor NODD binding (within limits of detection) **(Figure 4.16)**. The results inform on the mechanism of action of the inhibitors and will aid in long-term work on the therapeutic manipulation of the natural hypoxic response.

The work described in **Chapter 5** describes the development of a PrOF NMR approach for the São Paulo MBL (SPM-1). The results provide structural insights into catalysis, β-amino product binding, and the requirements for inhibitor development **(Table 5.1)**. The tested substrates (piperacillin, meropenem, tazobactam, and clavulanate) gave rise to products that only manifested changes in the L3 region, consistent with the proposal that SPM-1 is mechanistically related to the B1 subclass of MBLs.[164b] Interestingly, the results reveal that the hydrolysed β-amino acid products of MBL catalysis can bind to SPM-1, in a manner involving the L3 loop. The results are of interest from the perspective of identifying novel inhibitor scaffolds for SPM-1, and by implication other MBLs, including for the design of non-β-lactam inhibitors that are not susceptible to β-lactamase hydrolysis and/or β-lactams/β-lactam analogues whose hydrolysed products bind/inhibit MBLs. One result arising from the ^{19}F NMR results was that all the inhibitors tested, including the Zn(II) chelator, 1,10-*o*-phenanthroline, manifest substantial changes in both the α3 and L3 regions, emphasising the importance of both regions, and, in particular, the α3 region, for inhibitor development. The results are of further interest because they reveal for the first time that it is possible to catalytically inhibit MBLs *via* a mechanism related mode, which does not involve zinc ion chelation, *i.e.* as observed with an isoquinoline-based inhibitor. The results illustrate the utility of PrOF for detecting metal chelation which is not always readily tractable in studies on metallo enzyme inhibition, new binding modes, stereoisomer binding/epimerisation in solution, and subtle differences in H-bonding and hydrophobic interactions.

The work described in **Chapter 6**, concerned a cyclobutanone derivative, which is a broad-spectrum MBL inhibitor, [203-204] and which is proposed to mimic the intact β-lactam state. The interaction of the cyclobutanone derivative with SPM-1 was studied. ^{19}F-NMR of a fluorine-labelled SPM-1 variant revealed that the cyclobutanone derivative binds to the SPM-1 with micromolar affinity, in a manner causing perturbation of a loop, L3, adjacent to the active site **(Figure 6.4)**. Cyclobutanone derivative binding also causes a smaller effect on more distant helical elements that define the active site cleft **(Figure 6.3)**. A crystal structure of the SPM-1:cyclobutanone complex shows the binding mode of a hydrated cyclobutanone, including *via* interactions with one of the two active-site zinc ions, stabilisation of the hydrate by hydrogen bonding to zinc-bound water, and hydrophobic contacts with aromatic side chains adjacent to the active site **(Figure 6.6)**. ^{13}C-NMR analysis of a labelled cyclobutanone derivative supported assignment of the bound species as the hydrated, rather than the ketone, form **(Figure 6.7)**. These data reveal a possible mode by which MBLs may bind tetrahedral oxyanionic species and support investigation of similar analogues as effective inhibitors against multiple β-lactamase classes.

The clinical administration of avibactam for use in combination with ceftazidime, a cephalosporin,[209] represents a major advance in antimicrobial therapy, since avibactam is the first non-β-lactam to act similarly to a β-lactam inhibitor.[40] However, the susceptibility of avibactam to Class B MBL-catalysed hydrolysis has not yet been reported. This is an important issue since MBLs are becoming more widespread,[213] and MBL-catalysed avibactam hydrolysis has the potential to impair the potency of β-lactam antibiotic-avibactam combinations against strains producing both SBLs and MBLs.[210] The results described in **Chapter 7** reveal that avibactam is not an MBL inhibitor; instead, it is a poor substrate of most members of all three clinically relevant subclasses of MBLs **(Figure 7.3)**. In some cases, avibactam undergoes slow hydrolysis **(Figure 7.1)** in a process different from that

observed with studied SBLs.[40] The results suggest that whilst the evolution of MBLs that more effectively catalyse avibactam hydrolysis should be anticipated, the development of dual action SBL and MBL inhibitors based on the diazabicyclooctane core of avibactam, or other non-β-lactam cores, is of interest.

Chapter 9. Materials and Methods

Chapter 9. Contents

9.1. Molecular and Biological Techniques

9.1.1. Oligonucleotides Preparation

Oligonucleotide primers were obtained from Sigma-Aldrich as dried pellets and were re-suspended in sterile Milli-Q water giving a primer concentration of 100 µM. A 10-fold dilution was performed and the primers (10 µM) were stored at –20^{o}C.

9.1.2. Site-directed mutagenesis and Polymerase Chain Reaction (PCR)

Site directed mutagenesis[220] of plasmids was performed following the protocol of the QuikChange™ site directed mutagenesis kit from Stratagene. DNA amplification by PCR[221] was carried out in a 50 µL reaction mixture in thin-walled sterile PCR tubes using the following reagents:

Reagents	Volumes
10x PfuTurbo® buffer	5 µL
Plasmid DNA template	3 µL (equivalent to 20 ng)
Deoxynucleotides (dNTPs)	2 µL of 10 mM stock
Reverse primer	1.25 µL of 10 µM stock
Forward primer	1.25 µL of 10 µM stock
Sterile Milli-Q water	36.5 µL
PfuTurbo® DNA polymerase	1 µL

PfuTurbo® DNA polymerase and the corresponding buffer were from Stratagene. dNTP mix was purchased as a 100 mM stock solution from Stratagene and diluted to 10 mM immediately prior to use. A Techne Genius thermal cycler was programmed for an initial hold at 95 °C for 30 seconds as a pre-heating step. This was followed by 18 cycles of:

denaturation at 95°C for 30 seconds,

annealing at 55°C for 1 minute, and

extension at 68°C for 10 minutes (60 s/kbp).

A final extension step at 68°C for 10 minutes was carried out and the samples were held at 4° C before removal from the cycler.

9.1.3. DpnI digestion

The PCR tubes were then centrifuged for 1 minute to bring all the contents into contact with the nuclease and the restriction endonuclease *Dpn*I (1 μL, 10 units.μL^{-1}) was added to each tube. The tubes were then incubated at 37°C for 1-3 hours in a shaking Eppendorf incubator, to digest the parental methylated-DNA template.[222]

9.1.4. Transformation into XL10-Gold® E. coli (Stratagene) cells

Ultracompetent XL10-Gold® *E. coli* (Stratagene) cells were thawed on ice. Plasmid DNA (4 μL) was added to the competent cells (40-50 μL) in pre-chilled 1.5 mL Eppendorf tubes. The tubes were left on ice for 30 minutes. They were then heat-shocked by being placed in a 42°C water bath for 45 seconds. The tubes were returned to ice for 2 min for a recovery step. SOC medium (250 μL) was added to each tube which was then incubated at 37°C for 1 hour. This outgrowth step allows the bacteria time to generate the antibiotic resistance proteins encoded on its plasmid backbone. Each mixture (200 μL) was plated on a 10-cm polystyrene Petri dish agar plate containing ampicillin (50 μg/mL, antibiotic resistance from the plasmid) and chloramphenicol (25 μg/mL, antibiotic resistance from XL10-Gold® *E. coli* (Stratagene) cells) and spread on the plate using a sterile spreader. After the plates

became dry, they were inverted and incubated at 37°C overnight in a Heraeus® TypB 6030 incubator (Thermo Fisher Scientific).

9.1.4.1. XL10-Gold® *E. coli* (Stratagene) cells

According to Stratagene, XL10-Gold® *E. coli* cells are created for transformation of large DNA molecules with high efficiency. XL10-Gold® cells are deficient in all known restriction systems [Δ(mcrA)183 Δ(mcrCB-hsdSMR-mr)173]. The strain is endonuclease deficient (endA), improving the quality of mini-prep DNA, and recombination deficient (recA), helping to ensure insert stability. The lacIqZDM15 gene on the F´episome allows blue-white screening for recombinant plasmids. These cells are chloramphenicol and tetracycline resistant at concentrations of 25 μg/mL and 10 μg/mL, respectively.

9.1.4.2. 2x Tryptone-Yeast Extract (2TY) Medium Preparation

Reagents used per 1 litre are:

16.0 g of bacto-tryptone,

10.0 g of yeast extract, and

5.0 g of NaCl.

All growth media were prepared using sterile Milli-Q water and sterilised by autoclaving at 121^{o}C for 20 min (TouchClaveR II autoclave; LTE Scientific Ltd.). The pH of all growth media was adjusted to 9.0 using conc. HCl or 5.0 M NaOH prior to sterilisation.

9.1.4.3. SOC Medium Preparation

Super Optimal Broth, Catabolite Repressing (SOC) medium (1 mL) was prepared by adding 2TY medium (970 µL) to 20 µL of 2 M glucose and 10 µL of 1 M magnesium chloride.

9.1.4.4. Agar Plates Preparation

Reagents used per 1 litre are:

10.0 g of tryptone,

15.0 g agar,

5.0 g of yeast extract, and

10.0 g of NaCl.

The solution was swirled to be mixed. The top of the flask was covered with an aluminium foil and autoclave tape. The flask was sterilised by autoclaving at 121^{o}C for 20 min (TouchClaveR II autoclave; LTE Scientific Ltd.). After removing the solution from the autoclave, it was allowed to cool at 55^{o}C. The appropriate amounts of the desired antibiotics were added to the solution mixture and the agar solution (20 mL) was poured in a 10-cm polystyrene Petri dish in a laminar flow hood HeraSafe® Model KS12 Class II Biosafety Cabinet (Thermo Fisher Scientific) using sterile media and equipment. Agar was allowed to solidify and the lids were placed on the plates, which were inverted, sealed with parafilm and stored at 4^{o}C for a maximum of one month prior to use.

9.1.5. Small Scale Growth for Starter Cultures

2TY media (5 ml (in 50 ml polypropylene tubes, Greiner Bio-One)) containing the appropriate antibiotics (ampicillin (50 µg/mL) and chloramphenicol(25 µg/mL)) were inoculated from a single colony on an agar plate using a sterile pipette tip and grown at 37°C overnight in a G24 environmental incubator shaker (New Brunswick Scientific). The next

day, the pipette tip was removed from the polypropylene tubes and the tubes were centrifuged at 4 000 rpm for 20 min at 4°C in an Allegra™ 21R centrifuge (Beckman Coulter, Inc.; S4180 rotor). The supernatant was discarded and the cell pellets were subjected to mini-prep as described below.

9.1.6. Purification of Plasmid DNA

Plasmid DNA was typically purified from bacterial cultures (5 mL) grown overnight using a QIAprep Spin Miniprep Kit (QIAGEN) according to the manufacturer's instructions. The alkaline lysis method exploits the different sizes and topologies of genomic and plasmid DNA. Under mild alkaline conditions (lysis buffer), the hydrogen bonds between the two DNA strands are broken, thereby separating the two strands. In the case of genomic DNA, this leads to precipitation of the DNA in complex with cellular proteins. The two strands of comparatively small plasmid DNA, however, stay in solution in an interlinked manner due to the closed, circular nature of the plasmid and re-associate on being transferred to a solution at neutral pH (neutralising buffer). Lysing bacterial cells in an alkaline medium is therefore an easy and efficient method to purify plasmid DNA. In this procedure, samples up to 1.5 mL were centrifuged at room temperature using an AccuSpin™ Micro (Fisher Scientific).

9.1.6.1. Plasmid DNA Concentration Determination

The concentration of plasmid DNA was determined using a NanoDrop® ND-1000 spectrometer. DNA can be quantified by using the absorbance maximum of the nucleobases at $\lambda = 260$ nm. The purity of the DNA preparation were estimated by calculating the ratio of measured absorbances at 260 and 280 nm, where protein and single-stranded DNA/RNA contaminants have a stronger absorbance. A 260 nm/280 nm ratio of 1.8 or higher is usually acceptable for molecular biology applications according to NanoDrop® manufacturer's instructions.

9.1.6.2. Plasmid DNA Sequencing

Plasmid DNA was diluted to 100 ng/μL in a final volume of 10 μL and sent to sequencing to the SourceBioscience sequencing facility (Oxford, UK). All constructs plasmids were sequenced using primers complementary to the T7 promoter and T7 terminator sequences.

The T7 promoter primer sequence (20mer) was as follows:

TAATACGACTCACTATAGGG

The T7 terminator primer sequence (20mer) was as follows:

CTAGTTATTGCTCAGCGGTG

The sequencing results were translated into amino acid sequences using the online ExPASy translate tool. The predicted protein sequences were compared to the original protein template sequence using Protein BLAST online tool.

9.1.7. Transformation into BL21(DE3)pLysS® *E. coli* cells

Ultracompetent BL21(DE3)pLysS® *E. coli* cells were thawed on ice. Sequenced plasmid DNA (1 μL) was added to the competent cells (20-25 μL) in pre-chilled 1.5 mL eppendorf. The tubes were left on ice for 30 minutes; they were then heat-shocked by being placed in a 42°C water bath for 45 seconds. The tubes were returned to ice for 2 min for a recovery step. SOC medium (250 μL) was added to each tube which was then incubated at 37°C for 1 hour. This outgrowth step allows the bacteria time to generate the antibiotic resistance proteins encoded on its plasmid backbone. Each mixture (200 μL) was plated on a 10-cm polystyrene Petri dish agar plate containing ampicillin (50 μg/mL, antibiotic resistance from the plasmid) and chloramphenicol (25 μg/mL, antibiotic resistance from BL21(DE3)pLysS® *E. coli* cells) and spread on the plate using a sterile spreader. After the

plates were dry, they were inverted and incubated at 37°C overnight in a Heraeus® TypB 6030 incubator (Thermo Fisher Scientific).

BL21(DE3)pLysS® *E. coli* cells

According to the Stratagene protocol, BL21(DE3)pLysS® *E. coli* cells are created for high-level protein production and easy induction. This *E. coli* B strain lacks both the *lon* protease and the *ompT* outer membrane protease, which can degrade proteins during purification. BL21(DE3)pLysS® competent cells provide tighter control over protein production for expression of toxic genes and are resistant to chloramphenicol. BL21(DE3) strains are intended for use with T7 RNA polymerase-based expression systems. The gene of interest is cloned into an expression cassette downstream of a T7 promoter, synthesis of T7 polymerase (not usually expressed in bacteria) leads to transcription of the RNA of interest and eventually protein synthesis. The DE3-derivatives of BL21 contains an l prophage that encodes the T7 RNA polymerase gene under the control of the lacUV5 promoter. As such, addition of IPTG (or lactose) to medium induces production of T7 polymerase with consequent expression of the gene of interest. BL21(DE3)pLysS contains a plasmid (pLysS with chloramphenicol resistance) that encodes T7 lysozyme to reduce background levels of T7 polymerase prior to induction.

9.1.8. Small Scale Growth for Glycerol Stock Preparation

2TY medium (5 ml in 50 ml polypropylene tubes, Greiner Bio-One) containing the appropriate antibiotics (50 μg/mL ampicillin and 25 μg/mL chloramphenicol) was inoculated from a single colony on an agar plate using a sterile pipette tip and grown at 37°C overnight in a G24 environmental incubator shaker (New Brunswick Scientific). The next day, the pipette tip was removed from the polypropylene tubes and samples of un-induced cells from growths were preserved by gently mixing the culture (750 μL) with 100% sterile glycerol

(250 µL, sterilised by autoclaving at 121°C), flash freezing in liquid nitrogen and storing at –80°C.

9.1.9. Expression Trials

2TY medium (100 mL in 500 mL Duran® flasks, Schott U.K.) containing the appropriate antibiotic was inoculated from a glycerol freeze, and incubated at 37°C overnight in a G24 environmental incubator shaker (New Brunswick Scientific). Expression trials were typically carried out in 500 mL conical flasks containing sterile 2TY growth medium (100 mL). The appropriate antibiotics corresponding to the resistance gene present in the expression plasmid were added (ampicillin (50 µg/mL) and chloramphenicol (25 µg/mL)). The flasks were inoculated directly from the overnight grown starter culture and incubated at 37°C in a shaker (180 rpm) until the end of the linear growth curve was reached, as judged by optical density (OD_{600} of ~0.6). Optical density readings were taken in 1.6 mL cuvettes with 10× dilution in Milli-Q water against a reference sample of the growth media at zero time. The absorbance was measured at 600 nm using a Novaspec® II spectrophotometer (Pharmacia). Protein production was induced by addition of various isopropyl-β-D-thiogalactopyranoside (IPTG) concentrations (0 mM, 0.2 mM, 0.5 mM, 1.0 mM) from a sterile 1 M stock in water. The culture were then incubated at various temperature (18°C, 30°C and 37°C) for various time periods (4 h, 6h, 8 h, 16 h) and the cells were spun down by centrifugation. Cell pellets were resuspended in lysis buffer (5 mL) in 50 mL polycarbonate centrifuge tubes and lysed on ice by sonication (6 x 30 seconds sonication with 30 seconds rest in between) using an MSE Soniprep 150 sonicator (Sanyo) at 10 µm amplitude. After centrifugation in an Avanti™ J-25 centrifuge (Beckman Coulter, Inc.; JA-25.50 rotor, 22000 rpm, 25 min, 4°C), the resulting supernatant was treated as ‘soluble’ protein extract. The resulting pellet was resuspended in 5 mL lysis buffer and treated as ‘insoluble’ protein

fraction. The level of production was subsequently analysed by SDS-PAGE using the method of Laemmli.[223]

9.1.10. Sodium Dodecyl Sulphate-Polyacrylamide Gel Electrophoresis (SDS-PAGE)

Before being loaded onto the gel, protein samples (10 µL) were boiled at 95^{o}C for 5 min with SDS-PAGE Sample loading buffer (10 µL, described below). The mixture (7-10 µL) was loaded in each lane of the gel. Lane 1 was loaded with protein molecular weight markers (7 µL**,** PageRuler Prestained Protein Ladder 10-170 kDa, Thermo Scientific). Polyacrylamide gels (5 % stacking gel, 12.5 % resolving gel) were run using a Bio-Rad Mini Protean II system (Bio-Rad Laboratories Ltd.) and electrophoresis was typically conducted at 180 V for 45 min. After the end of the run, the gels were stained with a Coomassie solution and destained.

9.1.10.1. Resolving Gel (quantities for 1 gel)

Reagents	**Amount at 12.5 % Acrylamide content**
Tris-HCl (1.5 M, pH 8.8)	1.25 mL
Milli-Q water	1.57 mL
30% (w/v) Acrylamide / 1.034% (w/v) Bis-acrylamide stock	2.08 mL
SDS (10% w/v)	50 µL
10% (w/v) APS	50 µL
TEMED	4 µL

9.1.10.2. Stacking Gel (quantities for 1 gel)

Reagent	Amount at 3.0 % acrylamide content
0.5 M Tris-HCl (pH 6.8)	0.63 mL
Milli-Q water	1.57 mL
30% (w/v) Acrylamide / 1.034% (w/v) Bis-acrylamide stock	0.25 mL
10% SDS solution	25 µL
10% (w/v) APS solution	25 µL
TEMED	2.5 µL

The N,N,N',N'-tetramethylethylenediamine (TEMED) and freshly prepared ammonium persulphate (APS) were added just prior to pouring the gels.

9.1.10.3. 10 × SDS-PAGE Running Buffer

Reagents used per litre:

Reagent	Amount (g)
Tris-HCl	30
Glycine	144
SDS	10

9.1.10.4. SDS-PAGE Gel Stain

Reagent	Amount
Acetic acid	10% (v/v)
Methanol	30% (v/v)
Coomassie® brilliant blue R	0.25% (w/v)

The SDS-PAGE gel destain contains the same quantities of reagents except there is no Coomassie® brilliant blue R present.

9.1.10.5. 10 × SDS-PAGE Sample Loading Buffer

Reagents used per 100 mL:

Reagent	Amount
Tris-HCl, 0.5 M, pH 6.8	10 ml
Bromophenol blue (0.2% w/v)	0.2 g
SDS (10% w/v)	20 ml
Glycerol	12 ml
β-mercaptoethanol	5.0 ml

9.1.11. Large Scale Protein Production

2TY medium (100 mL in 500 mL Duran® flasks, Schott U.K.) containing the appropriate antibiotics was inoculated from a glycerol freeze, and grown at 37°C overnight in a G24 environmental incubator shaker (New Brunswick Scientific). Large scale protein production cultures were carried out in 2 L conical flasks containing 2TY growth medium (600 mL). The antibiotics corresponding to the resistance gene present in the expression plasmid were added (ampicillin (50 μg/mL) and chloramphenicol (25 μg/mL)). The flasks were inoculated with the overnight starter culture (6 mL) and incubated at 37°C in a shaker (180 rpm) until the end of the linear growth curve was reached, as judged by optical density (OD_{600} of ~0.6). The protein production was induced by addition of IPTG (0.5 mM) from a sterile 1M stock in water. After 6 h at 30°C, the cultures were pelleted by centrifugation on an Avanti instrument using a JA-10 rotor at 8000 rpm for 8 min and the pellets stored at -80°C until lysis and protein purification.

9.1.11.1. Bacterial Cell Lysis

The pellets were resuspended in 3x His column binding buffer. EDTA-free protease inhibition cocktail (Roche) or PMSF were added to the mixture as well as a spatula DNase I (Roche), lysosyme (Sigma-Aldridge), and 0.2 % Tween-20. The mixture was left on a magnetic stirrer until it became homogenous with cells completely resuspended in the buffer. Bacterial cell lysis was performed by sonication (9.9 sec pulses every 9.9 sec, for 6 min) at 0°C and the cell membrane debris were removed by centrifugation on an Avanti instrument using a JA-25.50 rotor at 24000 rpm for 30 min at 4°C. The clear lysate was sterile-filtered using a 0.2 μm pore size filter and loaded onto the chromatography column.

9.1.11.2. Fast Protein Liquid Chromatography (FPLC)

FPLC for protein purification was carried out using Äkta™ FPLC systems (GE Healthcare) at 4°C. Buffers were freshly prepared in Milli-Q water and filtered through a 0.22 μm filter before use.

Buffer	Composition
His binding buffer	500 mM NaCl 5 mM imidazole 50 mM Tris, pH 7.5
His elution buffer	500 mM NaCl 500 mM imidazole 50 mM Tris, pH 7.5
Gel filtration buffer	200 mM NaCl 20 mM Tris, pH 7.5
Stripping buffer	0.5 M EDTA
Charging buffer	100 mM $NiSO_4$

Samples up to 10 mL were loaded using a Superloop™ (GE Healthcare) with larger samples being loaded using the FPLC pump. Purification procedures were followed by monitoring absorbance at 280 nm with a UPC-900 monitor on the FPLC and by SDS-PAGE. Sample fractions were collected using a Frac-920 fraction collector. All columns were cleaned after each use according to the manufacturers' instructions.

9.1.11.3. Standard His_6 Tagged Protein Purification

Purification of the His_6 tagged proteins was carried out using a 5 mL (settled bed volume) nickel affinity column of His•Bind® resin (Novagen, part of Merck Chemicals) run at 1 mL per minute on an FPLC system. The resin was prepared by washing with:

- 5-10 column volumes of MilliQ water.
- 1 column volume of charging buffer.
- 5-10 column volumes of binding buffer.

Cells were re-suspended in binding buffer and the cell lysate was applied to the column at 1 $mL.min^{-1}$. During elution, the protein was collected in 5 mL fractions. A_{280} trace and SDS-PAGE analyses were used to determine which of the fractions contained the purified protein. The fractions of proteins were combined and concentrated to 2 mL before injection into the gel filtration column. Protein solutions were concentrated using Amicon® Ultra-4 devices (Millipore U.K. Ltd.) with 10000 Da nominal molecular weight limit-membranes in an Allegra™ 21R centrifuge (Beckman Coulter, Inc.; S4180 rotor, 4000 rpm, 4°C).

9.1.11.4. Preparative Size Exclusion Chromatography

Proteins which were still impure (as judged by SDS-PAGE) after purification by nickel affinity chromatography underwent further purification using a 300 mL Superdex™ 75 size exclusion chromatography column (GE Healthcare). The column was equilibrated at 2 $mL.min^{-1}$ with 1 column volume of gel filtration buffer. The concentrated protein sample (2 mL) was injected through the loop to the gel filtration column. The protein was eluted over 1 column volume of buffer at 2 $mL.min^{-1}$ and 5 mL fractions were collected. An A_{280} trace along with SDS-PAGE was used to determine which of the fractions contained the purified protein. The fractions of proteins were combined and concentrated to around 8 mL before 3-C protease cleavage using Amicon® Ultra-4 devices (Millipore U.K. Ltd.) with 15 mL 10000 Da nominal molecular weight limit-membranes in an Allegra™ 21R centrifuge (Beckman Coulter, Inc.; S4180 rotor, 4000 rpm, 4°C).

PHD2 and most of the recombinant MBLs produced were His-tagged and were purified using the same general protocols described above using reported procedures.[60, 109, 143, 179, 188-189]

9.1.12. HRV 3C-Protease Cleavage

Human rhinovirus (HRV) 3C-protease was used to remove the His_6 tag from fusion proteins. The concentration of protein solutions was determined using a NanoDrop® ND-1000 spectrometer using the following considerations. The molar absorption coefficient of a peptide or protein is related to its tryptophan (W), tyrosine (Y) and cysteine (C) amino acid composition. At 280 nm, this value is approximated by the weighted sum of the 280 nm molar absorption coefficients of these three constituent amino acids, as described in the following equation $\varepsilon = (n(W)x5690) + (n(Y)x1280) + (n(C)x120)$ where n is the number of each residue and the stated values are the amino acid molar absorption at 280 nm.[224] The extinction coefficient of SPM-1 variants, for example, is around 30940 $M^{-1}.cm^{-1}$, at 280 nm measured in water and assuming all cysteines were reduced. The extinction coefficient was given using ExPASy protein parameter online tool. Following Novagen manufacturer's protocol, 1 aliquot of 3C-protease was added to every 50 mg of proteins, which were then left at 4^{o}C for between 15 to 18 hours. Human rhinovirus 3C protease (HRV 3C Protease) is a cysteine protease that recognizes the cleavage site Leu-Glu-Val-Leu-Phe-Gln-Gly-Pro, commonly referred to as the PreScission Site. HRV 3C protease cleaves between Gln and Gly. This cleavage site is already included in the plasmid template (MAHHHHHHSSGLEVLFQ*GPKSSDHV) of SPM-1 variants. The recombinant form of the HRV3C protease is a restriction grade protease that has robust activity at 4°C and high specific activity. This HRV 3C Protease is a 22 kDa protein with His tag so it can be removed by Ni-chelating resin, while SPM-1 is a 28 kDa protein which will be missing the His tag after cleavage (Novagen).

9.1.13. Manual His_6 Tagged Protein Purification

Subsequent to gel filtration and 3C protease cleavage, a second His_6 Tagged protein purification was performed to separate the HRV 3C-protease from the protein of interests (SPM-1 variants). At this stage, HRV 3C-protease which is His-tagged will bind to the nickel column. The His-tagged column is washed with:

5 column volumes of His elution buffer,

10 column volumes of His binding buffer, and

5 column volumes of 20 mM imidazole buffer.

The protein mixture containing both HRV 3C-protease and SPM-1 is loaded into the column at $1mL.min^{-1}$ with imidazole buffer (20 mM). Fractions (5 mL) were collected. Protein purity and separation were checked by SDS-PAGE. SPM-1 variants were collected in the second fraction while HRV 3C-protease was usually collected in the third-fifth fractions. The protein of interest was further concentrated to 2 mL and stored at $-80^{o}C$.

9.1.14. Buffer exchange and BTFA Labelling

Several buffering systems were tried before reaching the optimal labelling conditions.

For labelling purposes, a double buffer exchange using PD-10 desalting column (GE Healthcare) and gravity-mediated protocol elution was performed. The column was equilibrated with phosphate buffer (25 mL of 50 mM phosphate buffer, 200 mM NaCl, pH 7.5). The SPM-1 variants (2 mL) were added to the phosphate buffer (5 mL) supplemented with TCEP (2 mM) and $ZnSO_4$. The mixture was then incubated on ice for 30 min. The sample solution (2.5 mL) was added to the PD-10 column and the flow-through was discarded. The protein was then eluted with phosphate buffer (3.5 mL) and further concentrated to 2 mL using 4 mL Amicon® Ultra-4 devices (Millipore U.K. Ltd.) with 10000 Da nominal molecular weight limit-membranes in an Allegra™ 21R centrifuge (Beckman

Coulter, Inc.; S4180 rotor, 4000 rpm, 4°C). The unlabelled samples (1-10 µL) were stored as a control for MS and tryptic-digest studies. The concentration of the protein sample was checked again as stated earlier. The concentrated protein sample (2 mL) was topped up to 2.5 mL with phosphate buffer to which 35-fold excess of 3-bromo-1,1,1-trifluoroacetone was added. The reaction mixture was left for 10 min at room temperature. A new PD-10 column was equilibrated with Tris-buffer (25 mL of 50 mM Tris, 200 mM NaCl, pH 7.5). The sample solution (2.5 mL) was added to the PD-10 column and the flow-through was discarded. Then, the protein was eluted with Tris-buffer (3.5 mL) and further concentrated to 2 mL using 4 mL Amicon® Ultra-4 devices (Millipore U.K. Ltd.) with 10000 Da nominal molecular weight limit-membranes in an Allegra™ 21R centrifuge (Beckman Coulter, Inc.; S4180 rotor, 4000 rpm, 4°C).[170, 206] The ^{19}F-labelled samples (1-10 µL) were stored for further MS and tryptic-digest studies. The protein concentration was checked as stated earlier and aliquots were stored -80°C after being frozen in liquid nitrogen.

9.2. Biochemical and Biophysical Techniques

9.2.1. Mass Spectrometric Studies

9.2.1.1. Protein LC-MS Studies

Low resolution positive ion electrospray ionisation mass spectra (used to record intact protein masses) were recorded using an LCT Premier XE ionisation (Micromass®) mass spectrometer interfaced with a Acquity™ Ultra Performance liquid chromatography (UPLC) system using a Acquity™ UPLCR BEH300 C18 column at 50°C (Waters Corporation). The protein (1 mg.mL^{-1}, 0.5 µL) was injected and eluted at 0.3 mL.min^{-1} using a gradient system from Solvent A (95 % water, 0.1 % (v/v) formic acid) to Solvent B (95 % acetonitrile, 0.1 % (v/v) formic acid) according to the following conditions:

Time (Minutes)	%A	%B	Curve
0.00	95	5	Initial
8.00	5	95	6
8.01	95	5	6
10.00	95	5	6

The eluent was injected directly into the mass spectrometer. The following MS parameters were used: Capillary voltage – 3,000 V; Sample cone voltage – 35 V; Desolvation temperature – 250^{o}C; Source temperature – 80^{o}C; Cone gas flow – 100 L.h^{-1}; Desolvation gas flow (N_2) – 400 L.h^{-1}; V optics. Sodium formate was used as the calibrant. Spectra were processed using MassLynx™ v4.0 and v4.1 (Waters Corporation) with the Maximum Entropy method (MaxEnt1).

9.2.1.2. In-Solution Trypsin Digestion

All reagents were prepared in Tris buffer (100 mM, pH 7.8). Samples (< 500 µg) were dried in a Vacufuge® vacuum concentrator (*Eppendorf*) connected to an external diaphragm pump and then resuspended in 6 M urea (100 µL). Disulfides were reduced at room temperature (30 min) by addition of dithiothreitol (DTT, 5 µL, 200 mM), and subsequently alkylated at room temperature (30 min) with iodoacetamide (30 µL, 200 mM). Unreacted alkylating reagent was consumed by addition of DTT solution (30 µL, 30 min). The sample was then diluted with Tris buffer (775 µL), mixed with Sequencing Grade Modified Porcine Trypsin (*Promega*) at trypsin:protein sample ratio of ca. 1:50, and digested at 37°C for 12 h. Digestion was stopped by adjusting the sample to pH 3-4 by addition of concentrated acetic acid. Digested samples were subsequently purified and desalted by solid-phase extraction using Sep-Pak C18 Plus Light Cartridges (*Waters*, 130 mg sorbent per cartridge, 55-105 µM particle size) following the manufacturer's protocol. The samples were then dried using a

Vacufuge® machine, then re-dissolved in typically 50% CH_3CN/0.1% CF_3COOH (v/v) (15-30 μL) for analysis by MALDI-ToF-MS.[206]

9.2.1.3. MALDI-ToF-MS and MS/MS Studies

Matrix-assisted laser desorption/ionization time of flight mass spectrometry (MALDI-ToF-MS) and MS/MS analyses were performed using a *Bruker Daltonics* Ultraflex™ MALDI-ToF/ToF machine, using flexControl™ 3.0 software. Spectra were recorded in the positive ion reflectron mode, typically with 32-38 % laser energy. Calibration was performed on each day prior to the measurements using Peptide Calibration Standard II (*Bruker Daltonics*). Data were processed using *Bruker Daltonics* flexAnalysis™ 3.0 software and assigned manually. For MALDI measurements, the sample (1 μL) was mixed with 2,5-dihydroxybenzoic acid (4 μL, DHB, 20 mg/ml in 50% CH_3CN/0.1% CF_3COOH) matrix and this sample-matrix mixture spotted (2 μL) onto a 24 x 16 MTP AnchorChip™ 384 ToF MALDI target and allowed to air-dry before analysis.[206]

9.2.1.4. Non-Denaturing ESI-MS Studies

Recombinant PHD2 was desalted using a Bio-Spin 6 Column (Bio-Rad, Hemel Hempstead, U.K.) in 15 mM ammonium acetate (pH 7.5). The stock solution was diluted with the same buffer to a final concentration of 100 μM. Compounds at a 60 mM stock concentration in DMSO were further diluted in ammonium acetate to a concentration of 100 μM. $MnSO_4$ and 2OG were dissolved in MilliQ water at a concentration of 100 mM. This was then diluted with MilliQ water to give a final working concentration of 100 μM. The protein was mixed with Mn(II), compounds, and 2OG to give final concentrations of 15 μM PHD2, 15 μM Mn(II), and 15 μM compound and 15 μM 2OG. ESI-MS analysis was performed immediately without incubation. Mass spectrometric data were acquired using a Q-TOF mass spectrometer (Q-TOF micro, Micromass, Altrincham, U.K.) interfaced with a NanoMate (Advion Biosciences, Ithaca, NY) with a chip voltage of 1.70 kV and a delivery pressure 0.5

psi. The sample cone voltage was typically 30 V with a source temperature of 60 °C and with an acquisition/scan time of 1 s/1 s. Calibration and sample acquisition were performed in the positive ion mode in the range of 2000-3700 m/z. The pressure at the interface between the atmospheric source and the high vacuum region was fixed at 6.30 mbar. External instrument calibration was achieved using a 2:1 mixture of myglobin/trypsinogen. Data were processed with the MassLynx 4.0 (Waters).[108, 140]

9.2.1.5. Hydroxylation Assays by MALDI-ESI

The PHD2 mass spectrometry-based activity assay was performed by determining the extent of hydroxylation of HIF-1α CODD peptide substrate (HIF-1α residues 556-574) by matrix-assisted laser desorption/ionization time-of-flight mass spectrometry (MALDI-TOF MS) using a Waters® Micromass® MALDI micro MX™ mass spectrometer and MassLynx™ 4.1 as previously described.[109] The optimised hydroxylation assay involved incubation of PHD2 (1 μM) with inhibitor (1 % *v*/*v* in DMSO) in the presence of Fe(II) (10 μM), 2OG (60 μM), ascorbate (100 μM) and HIF-1α $CODD_{556-574}$ (50 μM) in HEPES (50 mM, pH 7.5) at 37 °C for 15 min. Reactions were quenched with formic acid (1 % *v*/*v*). Samples were prepared by mixing reaction mixture (1 μL) with α-cyano-4-hydrocinnamic acid (CHCA) solution (water: acetonitrile 1:1) (1 μL). Dose-response was assessed in 8-point triplicates. Data were analysed using GraphPad Prism® 5.04. For inhibition assays, enzymes were pre-incubated with inhibitor for 5 min before initiation of the reaction with all other reagents. Data were normalised to both a no enzyme negative control and a no inhibitor positive control.

9.2.2. Circular Dichroism Studies

Circular Dichroism (CD) measurements were carried out using a Chirascan CD spectrometer (Applied Photophysics) equipped with a Peltier temperature-controlled cell

holder. Experiments were performed at 23 °C in a 0.1 cm pathlength cuvette using 0.2 mg/mL protein in 10 mM sodium phosphate buffer (pH 8.0) supplemented with 50 mM $ZnSO_4$. Data were recorded from 260 to 185 nm at 0.5 nm intervals; each data point was averaged for 1 s. Spectra were baseline corrected and smoothed using the Savitzky–Golay filter. Data recorded in the 190–240 nm range were analysed using DichroWeb; the CDSSTR deconvolution method was used to estimate secondary structural content using reference set 4. To minimize the effects of differences in protein concentration, the data were normalized at 207 nm.[63-64]

9.2.3. Steady-State Kinetic Studies

The hydrolysis of meropenem was monitored at 25 °C in 50 mM HEPES buffer (pH 7.2) supplemented with 1 mg/mL BSA, 1 mM $ZnSO_4$ and 0.01% Triton X-100. Analyses were carried out in triplicate ($n \geq 3$); the absorbance values were read using a BMG Labtech Pherastar FS plate reader at 300 nm for meropenem hydrolysis or 486 nm for nitrocefin. Extinction coefficients were determined by plotting the absorbance units against decreasing concentrations of the substrate. Kinetic constants (K_M and k_{cat}) were obtained by determining the initial rate of the reaction at different substrate concentrations. The concentration-dependence of the initial rate was fitted and analysed using GraphPad Prism 5.01 software to generate Michaelis–Menten curves.[188]

9.2.4. Differential Scanning Fluorimetric Studies

Differential Scanning Fluorimetric (DSF) was performed using a MiniOpticon Real-Time PCR Detection System (Bio-Rad), monitoring protein unfolding using SYPRO orange (Invitrogen) according to reported method. FAM (492 nm) and ROX (610 nm) filters were used for excitation and emission, respectively. Reaction mixes contained 2 µM protein, 50 µM Mn(II), 200 µM compounds, and 1×SYPRO orange in a final volume of 50 µL. Reagents

were prepared in HEPES buffer except metals, which were dissolved as 100 mM stocks in 20 mM HCl, and then further diluted in Milli-Q water. Compounds tested were prepared in 100% DMSO and added such that the final concentration of DMSO was 5% (v/v). Fluorescence readings were taken every 1°C in the range 25−95°C, with the temperature increased linearly by 1°C.min^{-1}. The software provided was used to perform global minimum subtraction. The inflection point, representing T_m, was calculated by fitting the Boltzmann equation to the sigmoidal curves obtained; data were processed using GraphPad Prism 5.0. The T_m shift caused by the addition of small molecules/fragments was determined by subtraction of the "reference" T_m (protein incubated with metal and 5% DMSO) from the T_m obtained in the presence of the compound.[35]Conditionswere tested in triplicate, with standard deviations typically <1°C.[63]

9.2.5. Fluorescence Polarisation Studies

The affinity of the tracer (*N*-fluorescein tagged HIF-1α $CODD_{556-574}$) for PHD2 in various forms was determined by measuring the polarisation of the tracer across a 2-fold dilution series of PHD2 from 25 µM to 24 nM in 50 mM Tris pH 7.5 buffer. For the *apo*-PHD2, there were no further buffer components; to saturate PHD2 with Zn, 50 µM $Zn(SO_4)_2.7H_2O$ was included in the buffer; to saturate with Zn and 2OG, 50 µM $Zn(SO_4)_2.7H_2O$ and 100 µM 2OG were included in the buffer. Quenching of the tracer was observed upon binding to the protein, so to account for this the signal intensity was plotted against the concentration of PHD2 and the data fitted to establish the intensity of the bound tracer. Free tracer intensity was established from the no protein wells. From these data the affinity of the tracer was determined under each condition. Competition assays were used to determine the affinity of CODD and hyCODD for PHD2 using the same buffer conditions and cofactor concentrations as above with the addition of 5% (*v*/*v*) DMSO. A 2-fold dilution series of competitor peptides from 1000 µM to 15.6 µM were used with the following protein

concentrations: 3 µM for *apo*-PHD2, 1.5 µM for PHD2.Zn, 0.5 µM for PHD2.Zn.2OG. The data were fitted using a competitive model for the peptides with the top and bottom values of the fit constrained for each condition to be the same for experiments with CODD and hyCODD. In the case of *apo*-PHD2.Zn.2OG.CODD near complete competition of the tracer was observed over the concentration range used, indicating tight binding but making EC_{50} determination less reliable.[132, 136]

9.2.6. Nuclear Magnetic Resonance Spectroscopic Studies

Nuclear Magnetic Resonance (NMR) spectra were recorded using either a Bruker AVIII 700 MHz NMR spectrometer equipped with a 5-mm inverse cryoprobe or a Bruker AVIII 600 with BB-$^{19}F/^{1}H$ Prodigy N_2 cryoprobe using 5 mm diameter NMR tubes (Norell) or 3 mm MATCH NMR tubes (Cortectnet). Data were processed with Bruker 3.1 software. *Specific experimental details are given at the end of each chapter.*

Appendices

A. Protein and Peptide Sequences

Full length HIF-1α Amino Acid Sequence

MEGAGGANDK KKISSERRKE KSRDAARSRR SKESEVFYEL AHQLPLPHNV
SSHLDKASVM RLTISYLRVR KLLDAGDLDI EDDMKAQMNC FYLKALDGFV
MVLTDDGDMI YISDNVNKYM GLTQFELTGH SVFDFTHPCD HEEMREMLTH
RNGLVKKGKE QNTQRSFFLR MKCTLTSRGR TMNIKSATWK VLHCTGHIHV
YDTNSNQPQC GYKKPPMTCL VLICEPIPHP SNIEIPLDSK TFLSRHSLDM
KFSYCDERIT ELMGYEPEEL LGRSIYEYYH ALDSDHLTKT HHDMFTKGQV
TTGQYRMLAK RGGYVWVETQ ATVIYNTKNS QPQCIVCVNY VVSGIIQHDL
IFSLQQTECV LKPVESSDMK MTQLFTKVES EDTSSLFDKL KKEPDALTLL
APAAGDTIIS LDFGSNDTET DDQQLEEVPL YNDVMLPSPN EKLQNINLAM
SPLPTAETPK PLRSSADPAL NQEVALKLEP NPESLELSFT MPQIQDQTPS
PSDGSTRQSS PEPNSPSEYC FYVDSDMVNE FKLELVEKLF AEDTEAKNPF
STQDTDLDLE MLAPYIPMDD DFQLRSFDQL SPLESSSASP ESASPQSTVT
VFQQTQIQEP TANATTTTAT TDELKTVTKD RMEDIKILIA SPSPTHIHKE
TTSATSSPYR DTQSRTASPN RAGKGVIEQT EKSHPRSPNV LSVALSQRTT
VPEEELNPKI LALQNAQRKR KMEHDGSLFQ AVGIGTLLQQ PDDHAATTSL
SWKRVKGCKS SEQNGMEQKT IILIPSDLAC RLLGQSMDES GLPQLTSYDC
EVNAPIQGSR NLLQGEELLR ALDQVN

CODD HIF-1α Amino Acid Sequence

DLDLEMLAPYIPMDDDFQL

NODD HIF-1α Amino Acid Sequence

EELAQLAPTPGDAIISLDF

eEF2 Amino Acid Sequence

ENIMLGQLAPAGTGCFDLLLD

Rbp1 Amino Acid Sequence

GRYVEPIEDVPCGNIVGLVGVDQFL

PHD2-$_{181-426}$ Amino Acid Sequence

PNGQTKPLPA LKLALEYIVP CMNKHGICVV DDFLGKETGQ QIGDEVRALH DTGKFTDGQL VSQKSDSSKD IRGDKITWIE GKEPGCETIG LLMSSMDDLI RHCNGKLGSY KINGRTKAMV ACYPGNGTGY VRHVDNPNGD GRCVTCIYYL NKDWDAKVSG GILRIFPEGK AQFADIEPKF DRLLFFWSDR RNPHEVQPAY ATRYAITVWY FDADERARAK VKYLTGEKGV RVELNKPSDS VGKDVF

SPM-1 Amino Acid Sequence (before 3C-cleavage)

MAHHHHHHSS GLEVLFQGPK SSDHVDLPYN LTATKIDSDV FVVTDRDFYS SNVLVAKMLD GTVVIVSSPF ENLGTQTLMD WVAKTMKPKK VVAINTHFHL DGTGGNEIYK KMGAETWSSD LTKQLRLEEN KKDRIKAAEF YKNEDLKRRI LSSHPVPADN VFDLKQGKVF SFSNELVEVS FPGPAHSPDN VVVYFPKKKL LFGGCMIKPK ELGYLGDANV KAWPDSARRL KKFDAKIVIP GHGEWGGPEM VNKTIKVAEK AVGEMRL

SPM-1 Amino Acid Sequence (after 3C-cleavage)

GPKSSDHVDL PYNLTATKID SDVFVVTDRD FYSSNVLVAK MLDGTVVIVS SPFENLGTQT LMDWVAKTMK PKKVVAINTH FHLDGTGGNE IYKKMGAETW SSDLTKQLRL EENKKDRIKA AEFYKNEDLK RRILSSHPVP ADNVFDLKQG KVFSFSNELV EVSFPGPAHS PDNVVVYFPK KKLLFGGCMI KPKELGYLGD ANVKAWPDSA RRLKKFDAKI VIPGHGEWGG PEMVNKTIKV AEKAVGEMRL

B. List of Publications and Presentations

Parts of the work described in this thesis have been presented at conferences and/or published in the scientific literature as follows.

Oral Presentations

^{19}F-NMR analyses of SPM-1 reveal loop dyanmics and hydrolysed substrates binding. Invited Seminar Talk at the Annual Royal Society NMR-Discussion Group Meeting, 2016 Jun, Oxford, U.K.

Towards new β-lactamase inhibitor development and screening methods. Invited Seminar Talk. 2015 Nov 4th, Begbroke Science Park, University of Oxford, U.K.

Poster Presentations

Abboud M.I., Brem J., Makena A., Claridge T.D.W., Schofield C.J. Studying the conformational changes and interactions of SPM-1 with various substrates and inhibitors using ^{19}F-NMR. Antimicrobial Resistance Mechanisms (ARM) Conference, organised by BSAC (British Society of Antimicrobial Chemotherapy), Birmingham, U.K., 26 Nov 2015.

Abboud M.I., Brem J., Leung I.K.H., Claridge T.D.W., Schofield C.J. Using NMR to study proteins and their interactions. Departmental Symposium and Poster Graduate Session,

Department of Chemistry, University of Oxford, U.K., 28 Oct 2015. ***Winner of a Pfizer-sponsored Prize for the Best Poster***.

Abboud M.I., Brem J., Chowdhury R., Leung I.K.H., Schofield C.J., Claridge T.D.W. Applications of ^{19}F-NMR to study protein-ligand interactions and protein conformational changes in solution. EUROMAR, Prague, Czech Republic, 6 Jul 2015. ***Royal Society NMR-DG Award and AMPERE Award, London/Paris***. And the 29th Annual Protein Symposium, organized by the Protein Society, Barcelona, Spain, 22 Jul 2015. ***Special Grant from St John's College, Oxford***.

Abboud M.I., Brem J., Leung I.K.H., Demetriades M., Pfeffer I., Claridge T.D.W., Schofield C.J. Using ^{19}F-NMR to study the inhibition of SPM-1 by clavulanic acid. Bio-NMR workshop, Wolfson College, Oxford, 7 Jul 2014.

Abboud M.I., Brem J., Pfeffer I., Leung I.K.H., Demetriades M., Claridge T.D.W., Schofield C.J. Using ^{19}F-NMR and native MS to study the inhibition of SPM-1, 12th β-lactamase meeting, Gran Canaria, Spain, 30 Jun 2014. ***Special Grant from St John's College, Oxford***.

Publications

Abboud M.I., Hinchliffe P., Brem J., Macsics R., Pfeffer I., Makena A., Umland K.D., Rydzik A.M., Li G.B., Spencer J., Claridge T.D.W., Schofield C.J. ^{19}F-NMR Reveals the Role of Active Loops in Product and Inhibitor Binding by the São Paulo Metallo-β-Lactamase. ***Angewandte Chemie International Edition***. Jan 2017. (accepted)

Li G.B., **Abboud M.I.**, Brem J., Someya H., Lohans C.T., Yang S.Y., Spencer J., Wareham D.W., McDonough M.A., Schofield C.J. NMR-filtered Virtual Screening Leads to Non-Metal Chelating Metallo-β-Lactamase Inhibitors. ***Chemical Science***. Dec 2016. doi:10.1039/C6SC04524C

Chowdhury R., Leung I.K.H., Tian Y-M., **Abboud M.I**., Ge W., Domene C., Rahman M.Z., Cantrelle F-X., Landrieu I., Hardy A.P., Pugh C.W., Ratcliffe P.J., Claridge T.D.W., Schofield C.J. Structural Basis for Oxygen Degradation Domain Selectivity of the HIF Prolyl Hydroxylases. ***Nature Communications***. Aug 2016. doi:10.1038/ncomms12673

Koukourakis M.I., Giatromanolaki A., Zois C.E., Kalamida D., Pouliliou S., Karagounis I., Yeh T-L., **Abboud M.I.**, Claridge T.D.W., Schofield C.J., Sivridis E., Simopoulos C., Tokmakidis S.P., Harris A.L. Normal tissue radioprotection by amifostine *via* Warburg-type effects. ***Scientific Reports***. Aug 2016. doi:10.1038/srep30986

Abboud M.I., Damblon C., Brem J., Smargiasso N., Mercuri P., Gilbert B., Rydzik A.M., Claridge T.D.W., Schofield C.J., Frère J-M. Interactions of Avibactam with class B metallo-β-lactamases. ***Antimicrobial Agents and Chemotherapy***. Jul 2016. doi:10.1128/AAC.00897-16

Wang D.Y.*, **Abboud M.I**.*, Markoulides M.S., Brem J., Schofield C.J. The road to avibactam – the first clinically useful non-β-lactam working somewhat like a β-lactam. Special issue on antibiotic drug discovery. ***Future Medicinal Chemistry***. Jun 2016. doi:10.4155/fmc-2016-0078

Wilkins S.E., **Abboud M.I**., Hancock R.L., Schofield C.J. Targeting Protein-Protein Interactions in the HIF System. Special issue on protein-protein interactions. ***ChemMedChem***. Mar 2016. doi:10.1002/cmdc.201600012

Makena A., Duzgun A.O., Brem J., McDonough M.A., Rydzik A.M., **Abboud M.I.**, Saral A., Cicek A.S., Sandalli C., Schofield C.J. Comparison of Verona Integron-Borne Metallo-β-Lactamase Variants Reveals Differences in Stability and Inhibition Profiles. ***Antimicrobial Agents and Chemotherapy***. Dec 2015. doi:10.1128/AAC.01768-15

Abboud M.I., Brem J., Chowdhury C., Leung I.K.H., Claridge T.D.W., Schofield C.J. Applications of ^{19}F-NMR to study protein-ligand interactions and protein conformational changes in solution. Conference paper in ***Protein Science***. Vol 24, Oct 2015, doi:10.1002/pro.2823

Lippl K., **Abboud M.I.**, Loenarz C., Schofield C.J. Exploring the Substrate Selectivity of Oxygen Sensing Prolyl Hydroxylases. Conference paper in ***Protein Science***. Vol 24, Oct 2015, doi:10.1002/pro.2823

References

1. Michiels, C., Physiological and pathological responses to hypoxia. *The American Journal of Pathology* **2004,** *164* (6), 1875-82.

2. (a) Semenza, G. L.; Wang, G. L., A Nuclear Factor Induced by Hypoxia *Via* Denovo Protein- Synthesis Binds to the Human Erythropoietin Gene Enhancer at a Site Required for Transcriptional Activation. *Molecular and Cellular Biology* **1992,** *12* (12), 5447-5454; (b) Wang, G. L.; Semenza, G. L., General involvement of hypoxia-inducible factor 1 in transcriptional response to hypoxia. *Proceedings of the National Academy of Sciences of the United States of America* **1993,** *90* (9), 4304-8; (c) Forsythe, J. A.; Jiang, B. H.; Iyer, N. V.; Agani, F.; Leung, S. W.; Koos, R. D.; Semenza, G. L., Activation of vascular endothelial growth factor gene transcription by hypoxia-inducible factor 1. *Molecular and Cellular Biology* **1996,** *16* (9), 4604-13.

3. Prigione, A.; Rohwer, N.; Hoffmann, S.; Mlody, B.; Drews, K.; Bukowiecki, R.; Blumlein, K.; Wanker, E. E.; Ralser, M.; Cramer, T.; Adjaye, J., HIF-1α modulates cell fate reprogramming through early glycolytic shift and upregulation of PDK1-3 and PKM2. *Stem Cells* **2014,** *32* (2), 364-76.

4. (a) Schofield, C. J.; Ratcliffe, P. J., Signalling hypoxia by HIF hydroxylases. *Biochemical and Biophysical Research Communications* **2005,** *338* (1), 617-626; (b) Webb, J. D.; Coleman, M. L.; Pugh, C. W., Hypoxia, hypoxia-inducible factors (HIF), HIF hydroxylases and oxygen sensing. *Cellular and Molecular Life Sciences* **2009,** *66* (22), 3539-54; (c) Fandrey, J.; Gassmann, M., Oxygen sensing and the activation of the hypoxia inducible factor 1 (HIF-1)-invited article. *Advances in Experimental Medicine and Biology* **2009,** *648*, 197-206.

5. Schofield, C. J.; Ratcliffe, P. J., Oxygen sensing by HIF hydroxylases. *Nature Reviews. Molecular Cell Biology* **2004,** *5* (5), 343-54.

6. Kallio, P. J.; Okamoto, K.; O'Brien, S.; Carrero, P.; Makino, Y.; Tanaka, H.; Poellinger, L., Signal transduction in hypoxic cells: inducible nuclear translocation and recruitment of the CBP/p300 coactivator by the hypoxia-inducible factor-1α. *EMBO Journal* **1998,** *17* (22), 6573-86.

7. (a) Pugh, C. W.; O'Rourke, J. F.; Nagao, M.; Gleadle, J. M.; Ratcliffe, P. J., Activation of hypoxia-inducible factor-1; definition of regulatory domains within the α-subunit. *The Journal of Biological Chemistry* **1997,** *272* (17), 11205-14; (b) Semenza, G. L.;

Jiang, B. H.; Leung, S. W.; Passantino, R.; Concordet, J. P.; Maire, P.; Giallongo, A., Hypoxia response elements in the aldolase A, enolase 1, and lactate dehydrogenase A gene promoters contain essential binding sites for hypoxia-inducible factor 1. *The Journal of Biological Chemistry* **1996,** *271* (51), 32529-37.

8. (a) Huang, L. E.; Arany, Z.; Livingston, D. M.; Bunn, H. F., Activation of hypoxia-inducible transcription factor depends primarily upon redox-sensitive stabilization of its α-subunit. *The Journal of Biological Chemistry* **1996,** *271* (50), 32253-9; (b) Jiang, B.-H.; Semenza, G. L.; Bauer, C.; Marti, H. H., Hypoxia-inducible factor 1 levels vary exponentially over a physiologically relevant range of O_2 tension. *American Journal of Physiology* **1996,** *271* (4, Pt. 1), C1172-C1180.

9. Greer, S. N.; Metcalf, J. L.; Wang, Y.; Ohh, M., The updated biology of hypoxia-inducible factor. *EMBO Journal* **2012,** *31* (11), 2448-60.

10. Talks, K. L.; Turley, H.; Gatter, K. C.; Maxwell, P. H.; Pugh, C. W.; Ratcliffe, P. J.; Harris, A. L., The expression and distribution of the hypoxia-inducible factors HIF-1α and HIF-2α in normal human tissues, cancers, and tumor-associated macrophages. *The American Journal of Pathology* **2000,** *157* (2), 411-21.

11. (a) Ivan, M.; Kondo, K.; Yang, H.; Kim, W.; Valiando, J.; Ohh, M.; Salic, A.; Asara, J. M.; Lane, W. S.; Kaelin, W. G., Jr., HIFα targeted for VHL-mediated destruction by proline hydroxylation: Implications for O_2 sensing. *Science* **2001,** *292* (5516), 464-468; (b) Jaakkola, P.; Mole, D. R.; Tian, Y. M.; Wilson, M. I.; Gielbert, J.; Gaskell, S. J.; von Kriegsheim, A.; Hebestreit, H. F.; Mukherji, M.; Schofield, C. J.; Maxwell, P. H.; Pugh, C. W.; Ratcliffe, P. J., Targeting of HIF-α to the von Hippel-Lindau ubiquitylation complex by O_2-regulated prolyl hydroxylation. *Science* **2001,** *292* (5516), 468-472.

12. Appelhoff, R. J.; Tian, Y. M.; Raval, R. R.; Turley, H.; Harris, A. L.; Pugh, C. W.; Ratcliffe, P. J.; Gleadle, J. M., Differential function of the prolyl hydroxylases, PHD1, 2 and 3 in the regulation of Hypoxia inducible factor (HIF). *The Journal of Biological Chemistry* **2004**.

13. Wilkins, S. E.; Abboud, M. I.; Hancock, R. L.; Schofield, C. J., Targeting Protein-Protein Interactions in the HIF System. *ChemMedChem* **2016,** *11* (8), 773-86.

14. Cioffi, C. L.; Liu, X. Q.; Kosinsky, P. A.; Garay, M.; Bowen, B. R., Differential regulation of HIF-1α prolyl-4-hydroxylase genes by hypoxia in human cardiovascular cells. *Biochemical and Biophysical Research Communications* **2003,** *303*, 947-953.

15. Kaluz, S.; Kaluzova, M.; Stanbridge, E. J., Regulation of gene expression by hypoxia: integration of the HIF-transduced hypoxic signal at the hypoxia-responsive element. *Clinica Chimica acta; International Journal of Clinical Chemistry* **2008,** *395* (1-2), 6-13.

16. Ratcliffe, P. J., HIF-1 and HIF-2: working alone or together in hypoxia? *The Journal of Clinical Investigation* **2007,** *117* (4), 862-5.

17. Koivunen, P.; Tiainen, P.; Hyvarinen, J.; Williams, K. E.; Sormunen, R.; Klaus, S. J.; Kivirikko, K. I.; Myllyharju, J., An endoplasmic reticulum transmembrane prolyl 4-hydroxylase is induced by hypoxia and acts on hypoxia-inducible factor α. *The Journal of Biological Chemistry* **2007,** *282* (42), 30544-52.

18. Pientka, F. K.; Hu, J.; Schindler, S. G.; Brix, B.; Thiel, A.; Johren, O.; Fandrey, J.; Berchner-Pfannschmidt, U.; Depping, R., Oxygen sensing by the prolyl-4-hydroxylase PHD2 within the nuclear compartment and the influence of compartmentalisation on HIF-1 signalling. *Journal of Cell Science* **2012,** *125* (Pt 21), 5168-76.

19. Metzen, E.; Berchner-Pfannschmidt, U.; Stengel, P.; Marxsen, J. H.; Stolze, I.; Klinger, M.; Huang, W. Q.; Wotzlaw, C.; Hellwig-Burgel, T.; Jelkmann, W.; Acker, H.; Fandrey, J., Intracellular localisation of human HIF-1α hydroxylases: implications for oxygen sensing. *Journal of Cell Science* **2003,** *116* (Pt 7), 1319-26.

20. Minamishima, Y. A.; Moslehi, J.; Padera, R. F.; Bronson, R. T.; Liao, R.; Kaelin, W. G., Jr., A feedback loop involving the Phd3 prolyl hydroxylase tunes the mammalian hypoxic response in vivo. *Molecular and Cellular Biology* **2009,** *29* (21), 5729-41.

21. Marxsen, J. H.; Stengel, P.; Doege, K.; Heikkinen, P.; Jokilehto, T.; Wagner, T.; Jelkmann, W.; Jaakkola, P.; Metzen, E., Hypoxia-inducible factor-1 (HIF-1) promotes its degradation by induction of HIF-α-prolyl-4-hydroxylases. *The Biochemical Journal* **2004,** *381*, 761-7.

22. Huang, J.; Zhao, Q.; Mooney, S. M.; Lee, F. S., Sequence determinants in hypoxia-inducible factor-1α for hydroxylation by the prolyl hydroxylases PHD1, PHD2 and PHD3. *Journal of Biological Chemistry* **2002,** *277*, 39792-39800.

23. Tarhonskaya, H.; Chowdhury, R.; Leung, I. K.; Loik, N. D.; McCullagh, J. S.; Claridge, T. D.; Schofield, C. J.; Flashman, E., Investigating the contribution of the active site environment to the slow reaction of hypoxia-inducible factor prolyl hydroxylase domain 2 with oxygen. *The Biochemical Journal* **2014**.

24. Chowdhury, R.; McDonough, M. A.; Mecinovic, J.; Loenarz, C.; Flashman, E.; Hewitson, K. S.; Domene, C.; Schofield, C. J., Structural basis for binding of hypoxia-inducible factor to the oxygen-sensing prolyl hydroxylases. *Structure* **2009,** *17* (7), 981-9.

25. Aik, W. S.; Chowdhury, R.; Clifton, I. J.; Hopkinson, R. J.; Leissing, T.; McDonough, M. A.; Nowak, R.; Schofield, C. J.; Walport, L. J., CHAPTER 2 Introduction to Structural Studies on 2-Oxoglutarate-Dependent Oxygenases and Related Enzymes. In *2-Oxoglutarate-Dependent Oxygenases*, The Royal Society of Chemistry: 2015; pp 59-94.

26. McDonough, M. A.; Loenarz, C.; Chowdhury, R.; Clifton, I. J.; Schofield, C. J., Structural studies on human 2-oxoglutarate dependent oxygenases. *Current Opinion in Structural Biology* **2010,** *20* (6), 659-72.

27. McNeill, L. A.; Flashman, E.; Buck, M. R.; Hewitson, K. S.; Clifton, I. J.; Jeschke, G.; Claridge, T. D.; Ehrismann, D.; Oldham, N. J.; Schofield, C. J., Hypoxia-inducible factor prolyl hydroxylase 2 has a high affinity for ferrous iron and 2-oxoglutarate. *Molecular BioSystems* **2005,** *1* (4), 321-4.

28. Masson, N.; Willam, C.; Maxwell, P. H.; Pugh, C. W.; Ratcliffe, P. J., Independent function of two destruction domains in hypoxia-inducible factor-α chains activated by prolyl hydroxylation. *EMBO Journal* **2001,** *20* (18), 5197-206.

29. Kageyama, Y.; Koshiji, M.; To, K. K.; Tian, Y. M.; Ratcliffe, P. J.; Huang, L. E., Leu-574 of human HIF-1α is a molecular determinant of prolyl hydroxylation. *FASEB Journal* **2004,** *18* (9), 1028-30.

30. Loenarz, C.; Mecinovic, J.; Chowdhury, R.; McNeill, L. A.; Flashman, E.; Schofield, C. J., Evidence for a stereoelectronic effect in human oxygen sensing. *Angewandte Chemie International Edition* **2009,** *DOI: 10.1002/anie.200805427*.

31. Illingworth, C. J.; Loenarz, C.; Schofield, C. J.; Domene, C., Chemical basis for the selectivity of the von Hippel Lindau tumor suppressor pVHL for prolyl-hydroxylated HIF-1α. *Biochemistry* **2010,** *49* (32), 6936-44.

32. McDonough, M. A.; Li, V.; Flashman, E.; Chowdhury, R.; Mohr, C.; Lienard, B. M.; Zondlo, J.; Oldham, N. J.; Clifton, I. J.; Lewis, J.; McNeill, L. A.; Kurzeja, R. J.; Hewitson, K. S.; Yang, E.; Jordan, S.; Syed, R. S.; Schofield, C. J., Cellular oxygen sensing: Crystal structure of hypoxia-inducible factor prolyl hydroxylase (PHD2). *Proceedings of the National Academy of Sciences of the United States of America* **2006,** *103* (26), 9814-9.

33. (a) Boucher, H. W.; Talbot, G. H.; Bradley, J. S.; Edwards, J. E.; Gilbert, D.; Rice, L. B.; Scheld, M.; Spellberg, B.; Bartlett, J., Bad bugs, no drugs: no ESKAPE! An update from the Infectious Diseases Society of America. *Clinical Infectious Diseases* **2009,** *48* (1), 1-12;

(b) Donadio, S.; Maffioli, S.; Monciardini, P.; Sosio, M.; Jabes, D., Antibiotic discovery in the twenty-first century: current trends and future perspectives. *The Journal of Antibiotics* **2010,** *63* (8), 423-30; (c) Fisher, J. F.; Meroueh, S. O.; Mobashery, S., Bacterial resistance to β-lactam antibiotics: compelling opportunism, compelling opportunity. *Chemical Reviews* **2005,** *105* (2), 395-424.

34. Alanis, A. J., Resistance to antibiotics: are we in the post-antibiotic era? *Archives of Medical Research* **2005,** *36* (6), 697-705.

35. *Reducing Healthcare Associated Infection in Hospitals in England* House of Commons, Public Accounts Committee United Kingdom, 2009.

36. Livermore, D. M.; Woodford, N., The β-lactamase threat in *Enterobacteriaceae*, *Pseudomonas* and *Acinetobacter*. *Trends in Microbiology* **2006,** *14* (9), 413-20.

37. Drawz, S. M.; Bonomo, R. A., Three decades of β-lactamase inhibitors. *Clinical Microbiology Reviews* **2010,** *23* (1), 160-201.

38. (a) Frere, J. M.; Page, M. G., Penicillin-binding proteins: evergreen drug targets. *Current Opinion in Pharmacology* **2014,** *18*, 112-9; (b) Buynak, J. D., Cutting and stitching: the cross-linking of peptidoglycan in the assembly of the bacterial cell wall. *ACS Chemical Biology* **2007,** *2* (9), 602-5.

39. Toussaint, K. A.; Gallagher, J. C., β-Lactam/β-lactamase inhibitor combinations: from then to now. *The Annals of Pharmacotherapy* **2015,** *49* (1), 86-98.

40. Wang, D. Y.; Abboud, M. I.; Markoulides, M. S.; Brem, J.; Schofield, C. J., The road to avibactam: the first clinically useful non-β-lactam working somewhat like a β-lactam. *Future Medicinal Chemistry* **2016,** *8* (10), 1063-84.

41. Chellat, M. F.; Raguz, L., Targeting Antibiotic Resistance. **2016,** *55* (23), 6600-26.

42. Peleg, A. Y.; Hooper, D. C., Hospital-acquired infections due to Gram-negative bacteria. *The New England Journal of Medicine* **2010,** *362* (19), 1804-13.

43. Walsh, T. R.; Toleman, M. A.; Poirel, L.; Nordmann, P., Metallo-β-lactamases: the quiet before the storm? *Clinical Microbiology Reviews* **2005,** *18* (2), 306-25.

44. Ghuysen, J. M., Serine β-lactamases and penicillin-binding proteins. *Annual Review of Microbiology* **1991,** *45*, 37-67.

45. Davies, J.; Davies, D., Origins and evolution of antibiotic resistance. *Microbiology and Molecular Biology Reviews* **2010,** *74* (3), 417-33.

46. (a) Palzkill, T., Metallo-β-Lactamase Structure and Function. *Annals of the New York Academy of Sciences* **2013,** *1277*, 91-104; (b) Karsisiotis, A. I.; Damblon, C. F.; Roberts, G.

C., A variety of roles for versatile zinc in metallo-β-lactamases. *Metallomics: integrated Biometal Science* **2014,** *6* (7), 1181-97.

47. Garau, G.; Garcia-Saez, I.; Bebrone, C.; Anne, C.; Mercuri, P.; Galleni, M.; Frere, J. M.; Dideberg, O., Update of the standard numbering scheme for class B β-lactamases. *Antimicrobial Agents and Chemotherapy* **2004,** *48* (7), 2347-9.

48. Ambler, R. P., The Structure of β-Lactamases. *Philosophical Transactions of the Royal Society of London B: Biological Sciences* **1980,** *289* (1036), 321-331.

49. (a) Carfi, A.; Pares, S.; Duee, E.; Galleni, M.; Duez, C.; Frere, J. M.; Dideberg, O., The 3-D structure of a zinc metallo-β-lactamase from *Bacillus cereus* reveals a new type of protein fold. *EMBO Journal* **1995,** *14* (20), 4914-21; (b) Crowder, M. W.; Spencer, J.; Vila, A. J., Metallo-β-lactamases: novel weaponry for antibiotic resistance in bacteria. *Accounts of Chemical Research* **2006,** *39* (10), 721-8.

50. (a) Wang, Z.; Fast, W.; Valentine, A. M.; Benkovic, S. J., Metallo-β-lactamase: structure and mechanism. *Current Opinion in Chemical Biology* **1999,** *3* (5), 614-22; (b) Wang, Z.; Fast, W.; Benkovic, S. J., On the mechanism of the metallo-β-lactamase from *Bacteroides fragilis*. *Biochemistry* **1999,** *38* (31), 10013-23.

51. (a) Concha, N. O.; Rasmussen, B. A.; Bush, K.; Herzberg, O., Crystal structure of the wide-spectrum binuclear zinc β-lactamase from *Bacteroides fragilis*. *Structure* **1996,** *4* (7), 823-36; (b) Dal Peraro, M.; Vila, A. J.; Carloni, P.; Klein, M. L., Role of zinc content on the catalytic efficiency of B1 metallo β-lactamases. *Journal of the American Chemical Society* **2007,** *129* (10), 2808-16.

52. Yuan, Q.; He, L.; Ke, H., A potential substrate binding conformation of β-lactams and insight into the broad spectrum of NDM-1 activity. *Antimicrobial Agents and Chemotherapy* **2012,** *56* (10), 5157-63.

53. Brem, J.; van Berkel, S. S.; Zollman, D.; Lee, S. Y.; Gileadi, O.; McHugh, P. J.; Walsh, T. R.; McDonough, M. A.; Schofield, C. J., Structural Basis of Metallo-β-Lactamase Inhibition by Captopril Stereoisomers. *Antimicrobial Agents and Chemotherapy* **2015,** *60* (1), 142-50.

54. Strynadka, N. C.; Adachi, H.; Jensen, S. E.; Johns, K.; Sielecki, A.; Betzel, C.; Sutoh, K.; James, M. N., Molecular structure of the acyl-enzyme intermediate in β-lactam hydrolysis at 1.7 A resolution. *Nature* **1992,** *359* (6397), 700-5.

55. King, D. T.; Worrall, L. J.; Gruninger, R.; Strynadka, N. C., New Delhi metallo-β-lactamase: structural insights into β-lactam recognition and inhibition. *Journal of the American Chemical Society* **2012,** *134* (28), 11362-5.

56. Meini, M. R.; Llarrull, L. I.; Vila, A. J., Evolution of Metallo-β-lactamases: Trends Revealed by Natural Diversity and in vitro Evolution. *Antibiotics* **2014,** *3* (3), 285-316.

57. Moran-Barrio, J.; Gonzalez, J. M.; Lisa, M. N.; Costello, A. L.; Peraro, M. D.; Carloni, P.; Bennett, B.; Tierney, D. L.; Limansky, A. S.; Viale, A. M.; Vila, A. J., The metallo-β-lactamase GOB is a mono-Zn(II) enzyme with a novel active site. *The Journal of Biological Chemistry* **2007,** *282* (25), 18286-93.

58. Ullah, J. H.; Walsh, T. R.; Taylor, I. A.; Emery, D. C.; Verma, C. S.; Gamblin, S. J.; Spencer, J., The crystal structure of the L1 metallo-β-lactamase from *Stenotrophomonas maltophilia* at 1.7 A resolution. *Journal of Molecular Biology* **1998,** *284* (1), 125-36.

59. Payne, D. J.; Cramp, R.; Winstanley, D. J.; Knowles, D. J., Comparative activities of clavulanic acid, sulbactam, and tazobactam against clinically important β-lactamases. *Antimicrobial Agents and Chemotherapy* **1994,** *38* (4), 767-72.

60. Ehmann, D. E.; Jahic, H.; Ross, P. L.; Gu, R. F.; Hu, J.; Kern, G.; Walkup, G. K.; Fisher, S. L., Avibactam is a covalent, reversible, non-β-lactam β-lactamase inhibitor. *Proceedings of the National Academy of Sciences of the United States of America* **2012,** *109* (29), 11663-8.

61. Toney, J. H.; Moloughney, J. G., Metallo-β-lactamase inhibitors: promise for the future? *Current Opinion in Investigational Drugs* **2004,** *5* (8), 823-6.

62. Palzkill, T., Metallo-β-lactamase structure and function. *Annals of the New York Academy of Sciences* **2013,** *1277*, 91-104.

63. Makena, A.; Brem, J.; Pfeffer, I.; Geffen, R. E.; Wilkins, S. E.; Tarhonskaya, H.; Flashman, E.; Phee, L. M.; Wareham, D. W.; Schofield, C. J., Biochemical characterization of New Delhi metallo-β-lactamase variants reveals differences in protein stability. *The Journal of Antimicrobial Chemotherapy* **2015,** *70* (2), 463-9.

64. Makena, A.; Duzgun, A. O.; Brem, J.; McDonough, M. A.; Rydzik, A. M.; Abboud, M. I.; Saral, A.; Cicek, A. C.; Sandalli, C.; Schofield, C. J., Comparison of Verona Integron-Borne Metallo-β-Lactamase (VIM) Variants Reveals Differences in Stability and Inhibition Profiles. *Antimicrobial Agents and Chemotherapy* **2016,** *60* (3), 1377-84.

65. Pettinati, I.; Brem, J.; Lee, S. Y.; McHugh, P. J.; Schofield, C. J., The Chemical Biology of Human Metallo-β-Lactamase Fold Proteins. *Trends in Biochemical Sciences* **2016**.

66. Pellecchia, M.; Sem, D. S.; Wuthrich, K., NMR in drug discovery. *Nature Reviews. Drug Discovery* **2002,** *1* (3), 211-9.

67. Skinner, A. L.; Laurence, J. S., High-field Solution NMR Spectroscopy as a Tool for Assessing Protein Interactions with Small Molecule Ligands. *Journal of Pharmaceutical Sciences* **2008,** *97* (11), 4670-95.

68. Pellecchia, M.; Bertini, I.; Cowburn, D.; Dalvit, C.; Giralt, E.; Jahnke, W.; James, T. L.; Homans, S. W.; Kessler, H.; Luchinat, C.; Meyer, B.; Oschkinat, H.; Peng, J.; Schwalbe, H.; Siegal, G., Perspectives on NMR in drug discovery: a technique comes of age. *Nature Reviews. Drug Discovery* **2008,** *7* (9), 738-45.

69. Claridge, T. D. W., *High-Resolution NMR Techniques in Organic Chemistry*. Third ed.; Elsevier: 2016.

70. Peng, J. W.; Lepre, C. A.; Fejzo, J.; Abdul-Manan, N.; Moore, J. M., Nuclear magnetic resonance-based approaches for lead generation in drug discovery. *Methods in Enzymology* **2001,** *338*, 202-30.

71. Meyer, B.; Peters, T., NMR spectroscopy techniques for screening and identifying ligand binding to protein receptors. *Angewandte Chemie International Edition* **2003,** *42* (8), 864-90.

72. Camacho, C. J.; Vajda, S., Protein-protein association kinetics and protein docking. *Current Opinion in Structural Biology* **2002,** *12* (1), 36-40.

73. Shortridge, M. D.; Hage, D. S.; Harbison, G. S.; Powers, R., Estimating Protein-Ligand Binding Affinity using High-Throughput Screening by NMR. *Journal of Combinatorial Chemistry* **2008,** *10* (6), 948-58.

74. Fielding, L., NMR methods for the determination of protein-ligand dissociation constants. *Current Topics in Medicinal Chemistry* **2003,** *3* (1), 39-53.

75. (a) Jahnke, W.; Floersheim, P.; Ostermeier, C.; Zhang, X.; Hemmig, R.; Hurth, K.; Uzunov, D. P., NMR reporter screening for the detection of high-affinity ligands. *Angewandte Chemie International Edition* **2002,** *41* (18), 3420-3; (b) Dalvit, C.; Flocco, M.; Knapp, S.; Mostardini, M.; Perego, R.; Stockman, B. J.; Veronesi, M.; Varasi, M., High-throughput NMR-based screening with competition binding experiments. *Journal of the American Chemical Society* **2002,** *124* (26), 7702-9.

76. Hulme, E. C.; Trevethick, M. A., Ligand binding assays at equilibrium: validation and interpretation. *British Journal of Pharmacology* **2010,** *161* (6), 1219-1237.

77. Cheng, Y.; Prusoff, W. H., Relationship between the inhibition constant and the concentration of inhibitor which causes 50 per cent inhibition of an enzymatic reaction. *Biochemical Pharmacology* **1973,** *22* (23), 3099-108.

78. (a) Arac, D.; Murphy, T.; Rizo, J., Facile detection of protein-protein interactions by one-dimensional NMR spectroscopy. *Biochemistry* **2003,** *42* (10), 2774-80; (b) Dalvit, C.; Ardini, E.; Flocco, M.; Fogliatto, G. P.; Mongelli, N.; Veronesi, M., A general NMR method for rapid, efficient, and reliable biochemical screening. *Journal of the American Chemical Society* **2003,** *125* (47), 14620-5.

79. Lepre, C. A.; Moore, J. M.; Peng, J. W., Theory and applications of NMR-based screening in pharmaceutical research. *Chemical Reviews* **2004,** *104* (8), 3641-76.

80. Kovermann, M.; Rogne, P.; Wolf-Watz, M., Protein dynamics and function from solution state NMR spectroscopy. *Quarterly Reviews of Biophysics* **2016,** *49*.

81. Orts, J.; Walti, M. A.; Marsh, M.; Vera, L.; Gossert, A. D.; Guntert, P.; Riek, R., NMR-Based Determination of the 3D Structure of the Ligand-Protein Interaction Site without Protein Resonance Assignment. *Journal of the American Chemical Society* **2016,** *138* (13), 4393-400.

82. Balaram, P.; Bothner-By, A. A.; Dadok, J., Negative nuclear Overhuaser effects as probes of macromolecular structure. *Journal of the American Chemical Society* **1972,** *94* (11), 4015-4017.

83. Dalvit, C.; Fogliatto, G.; Stewart, A.; Veronesi, M.; Stockman, B., WaterLOGSY as a method for primary NMR screening: practical aspects and range of applicability. *Journal of Biomolecular NMR* **2001,** *21* (4), 349-59.

84. Dalvit, C.; Pevarello, P.; Tato, M.; Veronesi, M.; Vulpetti, A.; Sundstrom, M., Identification of compounds with binding affinity to proteins *via* magnetization transfer from bulk water. *Journal of Biomolecular NMR* **2000,** *18* (1), 65-8.

85. Fielding, L.; Rutherford, S.; Fletcher, D., Determination of protein-ligand binding affinity by NMR: observations from serum albumin model systems. *Magnetic Resonance in Chemistry* **2005,** *43* (6), 463-70.

86. (a) Radeglia, R., Neuhaus, D.; Williamson, M.: The nuclear overhauser effect in structural and conformational analysis. XXII, 522 S., 200 Abb., 80 Tab., 16 × 24 cm. New York: VCH Publishers, Inc. 1989. Pappeinband, 194,- DM. *Journal für Praktische Chemie* **1990,** *332* (5), 658-658; (b) Chen, A.; Shapiro, M. J., NOE Pumping: A Novel NMR Technique for Identification of Compounds with Binding Affinity to Macromolecules. *Journal of the American Chemical Society* **1998,** *120* (39), 10258-10259; (c) Chen, A.;

Shapiro, M. J., NOE Pumping. 2. A High-Throughput Method To Determine Compounds with Binding Affinity to Macromolecules by NMR. *Journal of the American Chemical Society* **2000,** *122* (2), 414-415.

87. Parella, T., Pulsed field gradients: a new tool for routine NMR. *Magnetic Resonance in Chemistry* **1998,** *36* (7), 467-495.

88. Parella, T.; Belloc, J., Spin-state-selective excitation in selective 1D inverse NMR experiments. *Journal of Magnetic Resonance* **2001,** *148* (1), 78-87.

89. Castañar, L.; Parella, T., Chapter Four - Recent Advances in Small Molecule NMR: Improved HSQC and HSQMBC Experiments. In *Annual Reports on NMR Spectroscopy*, Graham, A. W., Ed. Academic Press: 2015; Vol. Volume 84, pp 163-232.

90. (a) Manzenrieder, F.; Frank, A. O.; Kessler, H., Phosphorus NMR spectroscopy as a versatile tool for compound library screening. *Angewandte Chemie International Edition* **2008,** *47* (14), 2608-11; (b) Dalvit, C., Fluorine NMR Spectroscopy for Biochemical Screening in Drug Discovery. In *NMR of Biomolecules*, Wiley-VCH Verlag GmbH & Co. KGaA: 2012; pp 314-327.

91. (a) Ziarek, J. J.; Peterson, F. C.; Lytle, B. L.; Volkman, B. F., Binding site identification and structure determination of protein-ligand complexes by NMR a semiautomated approach. *Methods in Enzymology* **2011,** *493*, 241-75; (b) Williamson, M. P., Using chemical shift perturbation to characterise ligand binding. *Progress in Nuclear Magnetic Resonance Spectroscopy* **2013,** *73*, 1-16.

92. Rajagopal, P.; Waygood, E. B.; Reizer, J.; Saier, M. H.; Klevit, R. E., Demonstration of protein—protein interaction specificity by NMR chemical shift mapping. *Protein Science* **1997,** *6* (12), 2624-2627.

93. (a) Arntson, K. E.; Pomerantz, W. C., Protein-Observed Fluorine NMR: A Bioorthogonal Approach for Small Molecule Discovery. *Journal of Medicinal Chemistry* **2016,** *59* (11), 5158-71; (b) Gee, C. T.; Arntson, K. E.; Urick, A. K.; Mishra, N. K.; Hawk, L. M. L.; Wisniewski, A. J.; Pomerantz, W. C. K., Protein-observed ^{19}F-NMR for fragment screening, affinity quantification and druggability assessment. *Nature Protocols* **2016,** *11* (8), 1414-1427; (c) Danielson, M. A.; Falke, J. J., Use of ^{19}F NMR to probe protein structure and conformational changes. *Annual Review of Biophysics and Biomolecular structure* **1996,** *25*, 163-95.

94. (a) He, T.; Gershenson, A.; Eyles, S. J.; Lee, Y. J.; Liu, W. R.; Wang, J.; Gao, J.; Roberts, M. F., Fluorinated Aromatic Amino Acids Distinguish Cation-pi Interactions from Membrane Insertion. *The Journal of Biological Chemistry* **2015,** *290* (31), 19334-42; (b)

Mishra, N. K.; Urick, A. K.; Ember, S. W. J.; Schönbrunn, E.; Pomerantz, W. C., Fluorinated Aromatic Amino Acids Are Sensitive ^{19}F NMR Probes for Bromodomain-Ligand Interactions. *ACS Chemical Biology* **2014,** *9* (12), 2755-2760.

95. Tkachenko, A. N.; Mykhailiuk, P. K.; Afonin, S.; Radchenko, D. S.; Kubyshkin, V. S.; Ulrich, A. S.; Komarov, I. V., A ^{19}F NMR label to substitute polar amino acids in peptides: a CF3-substituted analogue of serine and threonine. *Angewandte Chemie International Edition* **2013,** *52* (5), 1486-9.

96. Kitevski-LeBlanc, J. L.; Evanics, F.; Scott Prosser, R., Optimizing ^{19}F NMR protein spectroscopy by fractional biosynthetic labeling. *Journal of Biomolecular NMR* **2010,** *48* (2), 113-21.

97. Whittaker, J. W., Selective isotopic labeling of recombinant proteins using amino acid auxotroph strains. *Methods in Molecular Biology (Clifton, N.J.)* **2007,** *389*, 175-88.

98. Kim, H. W.; Perez, J. A.; Ferguson, S. J.; Campbell, I. D., The specific incorporation of labelled aromatic amino acids into proteins through growth of bacteria in the presence of glyphosate. Application to fluorotryptophan labelling to the H(+)-ATPase of *Escherichia coli* and NMR studies. *FEBS Letters* **1990,** *272* (1-2), 34-6.

99. Jones, D. H.; Cellitti, S. E.; Hao, X.; Zhang, Q.; Jahnz, M.; Summerer, D.; Schultz, P. G.; Uno, T.; Geierstanger, B. H., Site-specific labeling of proteins with NMR-active unnatural amino acids. *Journal of Biomolecular NMR* **2010,** *46* (1), 89-100.

100. Hammill, J. T.; Miyake-Stoner, S.; Hazen, J. L.; Jackson, J. C.; Mehl, R. A., Preparation of site-specifically labeled fluorinated proteins for ^{19}F-NMR structural characterization. *Nature Protocols* **2007,** *2* (10), 2601-7.

101. Chen, H.; Viel, S.; Ziarelli, F.; Peng, L., ^{19}F NMR: a valuable tool for studying biological events. *Chemical Society Reviews* **2013,** *42* (20), 7971-7982.

102. (a) Bruick, R. K.; McKnight, S. L., A conserved family of prolyl-4-hydroxylases that modify HIF. *Science* **2001,** *294* (5545), 1337-1340; (b) Epstein, A. C.; Gleadle, J. M.; McNeill, L. A.; Hewitson, K. S.; O'Rourke, J.; Mole, D. R.; Mukherji, M.; Metzen, E.; Wilson, M. I.; Dhanda, A.; Tian, Y. M.; Masson, N.; Hamilton, D. L.; Jaakkola, P.; Barstead, R.; Hodgkin, J.; Maxwell, P. H.; Pugh, C. W.; Schofield, C. J.; Ratcliffe, P. J., *C. elegans* EGL-9 and mammalian homologs define a family of dioxygenases that regulate HIF by prolyl hydroxylation. *Cell* **2001,** *107* (1), 43-54; (c) Masson, N.; Willam, C.; Maxwell, P. H.; Pugh, C. W.; Ratcliffe, P. J., Independent function of two destruction domains in hypoxia-inducible factor-α chains activated by prolyl hydroxylation. *EMBO Journal* **2001,** *20* (18), 5197-206.

103. (a) Chan, D. A.; Sutphin, P. D.; Yen, S. E.; Giaccia, A. J., Coordinate regulation of the oxygen-dependent degradation domains of hypoxia-inducible factor 1α. *Molecular and Cellular Biology* **2005,** *25* (15), 6415-26; (b) Tian, Y. M.; Yeoh, K. K.; Lee, M. K.; Eriksson, T.; Kessler, B. M.; Kramer, H. B.; Edelmann, M. J.; Willam, C.; Pugh, C. W.; Schofield, C. J.; Ratcliffe, P. J., Differential sensitivity of hypoxia inducible factor hydroxylation sites to hypoxia and hydroxylase inhibitors. *Journal of Biological Chemistry* **2011,** *286* (15), 13041-51.

104. (a) Hirsila, M.; Koivunen, P.; Gunzler, V.; Kivirikko, K. I.; Myllyharju, J., Characterization of the human prolyl 4-hydroxylases that modify the hypoxia-inducible factor. *Journal of Biological Chemistry* **2003,** *278* (33), 30772-80; (b) Huang, J.; Zhao, Q.; Mooney, S. M.; Lee, F. S., Sequence determinants in hypoxia-inducible factor-1α for hydroxylation by the prolyl hydroxylases PHD1, PHD2, and PHD3. *Journal of Biological Chemistry* **2002,** *277* (42), 39792-800.

105. Berra, E.; Benizri, E.; Ginouves, A.; Volmat, V.; Roux, D.; Pouyssegur, J., HIF prolyl-hydroxylase 2 is the key oxygen sensor setting low steady-state levels of HIF-1α in normoxia. *EMBO Journal* **2003,** *22* (16), 4082-90.

106. Lee, F. S.; Percy, M. J., The HIF pathway and erythrocytosis. *Annual Review of Pathology* **2011,** *6*, 165-92.

107. Kato, H.; Inoue, T.; Asanoma, K.; Nishimura, C.; Matsuda, T.; Wake, N., Induction of human endometrial cancer cell senescence through modulation of HIF-1α activity by EGLN1. *International Journal of Cancer* **2006,** *118* (5), 1144-53.

108. Mecinovic, J.; Chowdhury, R.; Flashman, E.; Schofield, C. J., Use of mass spectrometry to probe the nucleophilicity of cysteinyl residues of prolyl hydroxylase domain 2. *Analytical Biochemistry* **2009,** *393* (2), 215-21.

109. Flashman, E.; Bagg, E. A.; Chowdhury, R.; Mecinovic, J.; Loenarz, C.; McDonough, M. A.; Hewitson, K. S.; Schofield, C. J., Kinetic rationale for selectivity toward *N*- and *C*-terminal oxygen-dependent degradation domain substrates mediated by a loop region of hypoxia-inducible factor prolyl hydroxylases. *The Journal of Biological Chemistry* **2008,** *283* (7), 3808-15.

110. Flashman, E.; Hoffart, L. M.; Hamed, R. B.; Bollinger, J. M., Jr.; Krebs, C.; Schofield, C. J., Evidence for the slow reaction of hypoxia-inducible factor prolyl hydroxylase 2 with oxygen. *FEBS Journal* **2010,** *277* (19), 4089-99.

111. Chan, M. C.; Atasoylu, O.; Hodson, E.; Tumber, A.; Leung, I. K.; Chowdhury, R.; Gomez-Perez, V.; Demetriades, M.; Rydzik, A. M.; Holt-Martyn, J.; Tian, Y. M.; Bishop, T.; Claridge, T. D.; Kawamura, A.; Pugh, C. W.; Ratcliffe, P. J.; Schofield, C. J., Potent and Selective Triazole-Based Inhibitors of the Hypoxia-Inducible Factor Prolyl-Hydroxylases with Activity in the Murine Brain. *PloS One* **2015,** *10* (7), e0132004.

112. Leung, I. K.; Demetriades, M.; Hardy, A. P.; Lejeune, C.; Smart, T. J.; Szollossi, A.; Kawamura, A.; Schofield, C. J.; Claridge, T. D., Reporter ligand NMR screening method for 2-oxoglutarate oxygenase inhibitors. *Journal of Medicinal Chemistry* **2013,** *56* (2), 547-55.

113. Chowdhury, R.; Leung, I. K.; Tian, Y. M.; Abboud, M. I.; Ge, W.; Domene, C.; Cantrelle, F. X.; Landrieu, I.; Hardy, A. P.; Pugh, C. W.; Ratcliffe, P. J.; Claridge, T. D.; Schofield, C. J., Structural basis for oxygen degradation domain selectivity of the HIF prolyl hydroxylases. *Nature Communications* **2016,** *7*, 12673.

114. Bamford, S.; Dawson, E.; Forbes, S.; Clements, J.; Pettett, R.; Dogan, A.; Flanagan, A.; Teague, J.; Futreal, P. A.; Stratton, M. R.; Wooster, R., The COSMIC (Catalogue of Somatic Mutations in Cancer) database and website. *British Journal of Cancer* **2004,** *91* (2), 355-8.

115. (a) Arsenault, P. R.; Pei, F.; Lee, R.; Kerestes, H.; Percy, M. J.; Keith, B.; Simon, M. C.; Lappin, T. R.; Khurana, T. S.; Lee, F. S., A knock-in mouse model of human PHD2 gene-associated erythrocytosis establishes a haploinsufficiency mechanism. *Journal of Biological Chemistry* **2013,** *288* (47), 33571-84; (b) Percy, M. J.; Zhao, Q.; Flores, A.; Harrison, C.; Lappin, T. R.; Maxwell, P. H.; McMullin, M. F.; Lee, F. S., A family with erythrocytosis establishes a role for prolyl hydroxylase domain protein 2 in oxygen homeostasis. *Proceedings of the National Academy of Sciences of the United States of America* **2006,** *103* (3), 654-9.

116. Maxwell, P. H.; Eckardt, K. U., HIF prolyl hydroxylase inhibitors for the treatment of renal anaemia and beyond. *Nature Reviews. Nephrology* **2015**.

117. Rytkonen, K. T.; Williams, T. A.; Renshaw, G. M.; Primmer, C. R.; Nikinmaa, M., Molecular evolution of the metazoan PHD-HIF oxygen-sensing system. *Molecular Biology and Evolution* **2011,** *28* (6), 1913-26.

118. Loenarz, C.; Coleman, M. L.; Boleininger, A.; Schierwater, B.; Holland, P. W.; Ratcliffe, P. J.; Schofield, C. J., The hypoxia-inducible transcription factor pathway regulates oxygen sensing in the simplest animal, Trichoplax adhaerens. *EMBO Reports* **2011,** *12* (1), 63-70.

119. (a) Giaccia, A. J.; Simon, M. C.; Johnson, R., The biology of hypoxia: the role of oxygen sensing in development, normal function, and disease. *Genes & Development* **2004,** *18* (18), 2183-94; (b) Majmundar, A. J.; Wong, W. J.; Simon, M. C., Hypoxia-inducible factors and the response to hypoxic stress. *Molecular Cell* **2010,** *40* (2), 294-309; (c) Aragones, J.; Fraisl, P.; Baes, M.; Carmeliet, P., Oxygen sensors at the crossroad of metabolism. *Cell Metabolism* **2009,** *9* (1), 11-22.

120. Loenarz, C.; Coleman, M. L.; Boleininger, A.; Schierwater, B.; Holland, P. W.; Ratcliffe, P. J.; Schofield, C. J., The hypoxia-inducible transcription factor pathway regulates oxygen sensing in the simplest animal, *Trichoplax adhaerens*. *EMBO Reports* **2011,** *12* (1), 63-70.

121. Gorres, K. L.; Raines, R. T., Prolyl 4-hydroxylase. *Critical Reviews in Biochemistry and Molecular Biology* **2010,** *45* (2), 106-24.

122. Cummins, E. P.; Berra, E.; Comerford, K. M.; Ginouves, A.; Fitzgerald, K. T.; Seeballuck, F.; Godson, C.; Nielsen, J. E.; Moynagh, P.; Pouyssegur, J.; Taylor, C. T., Prolyl hydroxylase-1 negatively regulates IkB kinase-β, giving insight into hypoxia-induced NFkB activity. *Proceedings of the National Academy of Sciences of the United States of America* **2006,** *103* (48), 18154-9.

123. Kuznetsova, A. V.; Meller, J.; Schnell, P. O.; Nash, J. A.; Ignacak, M. L.; Sanchez, Y.; Conaway, J. W.; Conaway, R. C.; Czyzyk-Krzeska, M. F., von Hippel-Lindau protein binds hyperphosphorylated large subunit of RNA polymerase II through a proline hydroxylation motif and targets it for ubiquitination. *Proceedings of the National Academy of Sciences of the United States of America* **2003,** *100* (5), 2706-11.

124. Xie, L.; Xiao, K.; Whalen, E. J.; Forrester, M. T.; Freeman, R. S.; Fong, G.; Gygi, S. P.; Lefkowitz, R. J.; Stamler, J. S., Oxygen-regulated β2-adrenergic receptor hydroxylation by EGLN3 and ubiquitylation by pVHL. *Science Signaling* **2009,** *2* (78), ra33.

125. Koditz, J.; Nesper, J.; Wottawa, M.; Stiehl, D. P.; Camenisch, G.; Franke, C.; Myllyharju, J.; Wenger, R. H.; Katschinski, D. M., Oxygen-dependent ATF-4 stability is mediated by the PHD3 oxygen sensor. *Blood* **2007,** *110* (10), 3610-7.

126. Chan, M. C.; Holt-Martyn, J. P.; Schofield, C. J.; Ratcliffe, P. J., Pharmacological targeting of the HIF hydroxylases - A new field in medicine development. *Molecular Aspects of Medicine* **2016,** *47-48*, 54-75.

127. Romero-Ruiz, A.; Bautista, L.; Navarro, V.; Heras-Garvín, A.; March-Díaz, R.; Castellano, A.; Gómez-Díaz, R.; Castro, M. J.; Berra, E.; López-Barneo, J.; Pascual, A., Prolyl Hydroxylase-dependent Modulation of Eukaryotic Elongation Factor 2 Activity and

Protein Translation under Acute Hypoxia. *The Journal of Biological Chemistry* **2012,** *287* (12), 9651-8.

128. Groulx, I.; Lee, S., Oxygen-dependent ubiquitination and degradation of hypoxia-inducible factor requires nuclear-cytoplasmic trafficking of the von Hippel-Lindau tumor suppressor protein. *Molecular Cell Biology* **2002,** *22* (15), 5319-36.

129. Haase, V. H., The VHL/HIF oxygen-sensing pathway and its relevance to kidney disease. *Kidney International* **2006,** *69* (8), 1302-7.

130. Mack, F. A.; Rathmell, W. K.; Arsham, A. M.; Gnarra, J.; Keith, B.; Simon, M. C., Loss of pVHL is sufficient to cause HIF dysregulation in primary cells but does not promote tumor growth. *Cancer Cell* **2003,** *3* (1), 75-88.

131. Maxwell, P. H.; Wiesener, M. S.; Chang, G. W.; Clifford, S. C.; Vaux, E. C.; Cockman, M. E.; Wykoff, C. C.; Pugh, C. W.; Maher, E. R.; Ratcliffe, P. J., The tumour suppressor protein VHL targets hypoxia-inducible factors for oxygen-dependent proteolysis. *Nature* **1999,** *399* (6733), 271-5.

132. Buckley, D. L.; Van Molle, I.; Gareiss, P. C.; Tae, H. S.; Michel, J.; Noblin, D. J.; Jorgensen, W. L.; Ciulli, A.; Crews, C. M., Targeting the von Hippel-Lindau E3 ubiquitin ligase using small molecules to disrupt the VHL/HIF-1α interaction. *Journal of the American Chemical Society* **2012,** *134* (10), 4465-8.

133. Owicki, J. C., Fluorescence polarization and anisotropy in high throughput screening: perspectives and primer. *Journal of Biomolecular Screening* **2000,** *5* (5), 297-306.

134. Stebbins, C. E.; Kaelin, W. G.; Pavletich, N. P., Structure of the VHL-ElonginC-ElonginB complex: Implications for VHL tumor suppressor function. *Science* **1999,** *284* (5413), 455-461.

135. Hon, W. C.; Wilson, M. I.; Harlos, K.; Claridge, T. D. W.; Schofield, C. J.; Pugh, C. W.; Maxwell, P. H.; Ratcliffe, P. J.; Stuart, D. I.; Jones, E. Y., Structural basis for the recognition of hydroxyproline in α IF-1 α by pVHL. *Nature* **2002,** *417* (6892), 975-978.

136. Buckley, D. L.; Gustafson, J. L.; Van Molle, I.; Roth, A. G.; Tae, H. S.; Gareiss, P. C.; Jorgensen, W. L.; Ciulli, A.; Crews, C. M., Small-molecule inhibitors of the interaction between the E3 ligase VHL and HIF1α. *Angewandte Chemie International Edition* **2012,** *51* (46), 11463-7.

137. Aguilar, J. A.; Nilsson, M.; Bodenhausen, G.; Morris, G. A., Spin echo NMR spectra without J modulation. *Chemical Communications* **2012,** *48* (6), 811-3.

138. Selak, M. A.; Armour, S. M.; MacKenzie, E. D.; Boulahbel, H.; Watson, D. G.; Mansfield, K. D.; Pan, Y.; Simon, M. C.; Thompson, C. B.; Gottlieb, E., Succinate links TCA

cycle dysfunction to oncogenesis by inhibiting HIF-α prolyl hydroxylase. *Cancer Cell* **2005,** *7* (1), 77-85.

139. (a) Pektas, S.; Knapp, M. J., Substrate preference of the HIF-prolyl hydroxylase-2 (PHD2) and substrate-induced conformational change. *Journal of Inorganic Biochemistry* **2013,** *126*, 55-60; (b) Flashman, E.; Bagg, E. A. L.; Chowdhury, R.; Mecinovic, J.; Loenarz, C.; McDonough, M. A.; Hewitson, K. S.; Schofield, C. J., Kinetic Rationale for Selectivity toward *N*- and *C*-terminal Oxygen-dependent Degradation Domain Substrates Mediated by a Loop Region of Hypoxia-Inducible Factor Prolyl Hydroxylases. *The Journal of Biological Chemistry* **2008,** *283* (7), 3808-3815.

140. Mecinovic, J.; Chowdhury, R.; Lienard, B. M.; Flashman, E.; Buck, M. R.; Oldham, N. J.; Schofield, C. J., ESI-MS studies on prolyl hydroxylase domain 2 reveal a new metal binding site. *ChemMedChem* **2008,** *3* (4), 569-72.

141. Bacia, K.; Haustein, E.; Schwille, P., Fluorescence correlation spectroscopy: principles and applications. *Cold Spring Harbor Protocols* **2014,** *2014* (7), 709-25.

142. Xu, W.; Podoll, J. D.; Dong, X.; Tumber, A.; Oppermann, U.; Wang, X., Quantitative Analysis of Histone Demethylase Probes Using Fluorescence Polarization. *Journal of Medicinal Chemistry* **2013,** *56* (12), 5198-5202.

143. Leung, I. K.; Flashman, E.; Yeoh, K. K.; Schofield, C. J.; Claridge, T. D., Using NMR solvent water relaxation to investigate metalloenzyme-ligand binding interactions. *Journal of Medicinal Chemistry* **2010,** *53* (2), 867-75.

144. (a) Cario, H.; Schwarz, K.; Jorch, N.; Kyank, U.; Petrides, P. E.; Schneider, D. T.; Uhle, R.; Debatin, K. M.; Kohne, E., Mutations in the von Hippel-Lindau (VHL) tumor suppressor gene and VHL-haplotype analysis in patients with presumable congenital erythrocytosis. *Haematologica* **2005,** *90* (1), 19-24; (b) Gordeuk, V. R.; Sergueeva, A. I.; Miasnikova, G. Y.; Okhotin, D.; Voloshin, Y.; Choyke, P. L.; Butman, J. A.; Jedlickova, K.; Prchal, J. T.; Polyakova, L. A., Congenital disorder of oxygen sensing: association of the homozygous Chuvash polycythemia VHL mutation with thrombosis and vascular abnormalities but not tumors. *Blood* **2004,** *103* (10), 3924-3932; (c) Walmsley, S. R.; McGovern, N. N.; Whyte, M. K.; Chilvers, E. R., The HIF/VHL pathway: from oxygen sensing to innate immunity. *American Journal of Respiratory Cell and Molecular Biology* **2008,** *38* (3), 251-5.

145. (a) Andronesi, O. C.; Kim, G. S.; Gerstner, E.; Batchelor, T.; Tzika, A. A.; Fantin, V. R.; Vander Heiden, M. G.; Sorensen, A. G., Detection of 2-hydroxyglutarate in IDH-mutated glioma patients by in vivo spectral-editing and 2D correlation magnetic resonance

spectroscopy. *Science Translational Medicine* **2012,** *4* (116), 116ra4; (b) Chen, C.; Liu, Y.; Lu, C.; Cross, J. R.; Morris, J. P. t.; Shroff, A. S.; Ward, P. S.; Bradner, J. E.; Thompson, C.; Lowe, S. W., Cancer-associated IDH2 mutants drive an acute myeloid leukemia that is susceptible to Brd4 inhibition. *Genes & Development* **2013,** *27* (18), 1974-85; (c) Dang, L.; White, D. W.; Gross, S.; Bennett, B. D.; Bittinger, M. A.; Driggers, E. M.; Fantin, V. R.; Jang, H. G.; Jin, S.; Keenan, M. C.; Marks, K. M.; Prins, R. M.; Ward, P. S.; Yen, K. E.; Liau, L. M.; Rabinowitz, J. D.; Cantley, L. C.; Thompson, C. B.; Vander Heiden, M. G.; Su, S. M., Cancer-associated IDH1 mutations produce 2-hydroxyglutarate. *Nature* **2010,** *465* (7300), 966; (d) Figueroa, M. E.; Abdel-Wahab, O.; Lu, C.; Ward, P. S.; Patel, J.; Shih, A.; Li, Y.; Bhagwat, N.; Vasanthakumar, A.; Fernandez, H. F.; Tallman, M. S.; Sun, Z.; Wolniak, K.; Peeters, J. K.; Liu, W.; Choe, S. E.; Fantin, V. R.; Paietta, E.; Lowenberg, B.; Licht, J. D.; Godley, L. A.; Delwel, R.; Valk, P. J.; Thompson, C. B.; Levine, R. L.; Melnick, A., Leukemic IDH1 and IDH2 mutations result in a hypermethylation phenotype, disrupt TET2 function, and impair hematopoietic differentiation. *Cancer Cell* **2010,** *18* (6), 553-67.

146. (a) Walport, L. J.; Hopkinson, R. J.; Chowdhury, R., Arginine demethylation is catalysed by a subset of JmjC histone lysine demethylases. *Nature Communications* **2016,** *7*, 11974; (b) Hopkinson, R. J.; Hamed, R. B.; Rose, N. R.; Claridge, T. D. W.; Schofield, C. J., Monitoring the Activity of 2-Oxoglutarate Dependent Histone Demethylases by NMR Spectroscopy: Direct Observation of Formaldehyde. *ChemBioChem* **2010,** *11* (4), 506-510.

147. Chowdhury, R.; Flashman, E.; Mecinovic, J.; Kramer, H. B.; Kessler, B. M.; Frapart, Y. M.; Boucher, J. L.; Clifton, I. J.; McDonough, M. A.; Schofield, C. J., Studies on the reaction of nitric oxide with the hypoxia-inducible factor prolyl hydroxylase domain 2 (EGLN1). *Journal of Molecular Biology* **2011,** *410* (2), 268-79.

148. Bernheim-Groswasser, A.; Shusterman, R.; Krichevsky, O., Fluorescence correlation spectroscopy analysis of segmental dynamics in actin filaments. *The Journal of Chemical Physics* **2006,** *125* (8), 084903.

149. (a) Martin-Puig, S.; Tello, D.; Aragones, J., Novel perspectives on the PHD-HIF oxygen sensing pathway in cardioprotection mediated by IPC and RIPC. *Frontiers in Physiology* **2015,** *6*, 137; (b) Chen, R. L.; Ogunshola, O. O.; Yeoh, K. K.; Jani, A.; Papadakis, M.; Nagel, S.; Schofield, C. J.; Buchan, A. M., HIF prolyl hydroxylase inhibition prior to transient focal cerebral ischaemia is neuroprotective in mice. *Journal of Neurochemistry* **2014,** *131* (2), 177-89; (c) Hu, Y.; Liu, J.; Huang, H., Recent Agents targeting HIF-1α for cancer therapy. *Journal of Cellular Biochemistry* **2013,** *114* (3), 498-

509; (d) Goswami, S. K.; Das, D. K., Oxygen Sensing, Cardiac Ischemia, HIF-1α and Some Emerging Concepts. *Current Cardiology Reviews* **2010,** *6* (4), 265-73.

150. (a) Oh, S. W.; Ahn, J. M.; Lee, Y. M.; Kim, S.; Chin, H. J.; Chae, D. W.; Na, K. Y., Activation of hypoxia-inducible factor by cobalt is associated with the attenuation of tissue injury and apoptosis in cyclosporine-induced nephropathy. *The Tohoku Journal of Experimental Medicine* **2012,** *226* (3), 197-206; (b) Schleisner, P., Cobalt in anaemia. *Acta Medica Scandinavica* **1956,** *154* (3), 177-85.

151. (a) Baader, E.; Tschank, G.; Baringhaus, K.-H.; Burghard, H.; Gunzler, V., Inhibition of prolyl 4-hydroxylase by oxalyl amino acid derivatives in vitro, in isolated microsomes and in embryonic chicken tissues. *Biochemical Journal* **1994,** *300*, 525-530; (b) Nagel, S.; Papadakis, M.; Chen, R.; Hoyte, L. C.; Brooks, K. J.; Gallichan, D.; Sibson, N. R.; Pugh, C.; Buchan, A. M., Neuroprotection by dimethyloxalylglycine following permanent and transient focal cerebral ischemia in rats. *Journal of Cerebral Blood Flow and Metabolism* **2011,** *31* (1), 132-43.

152. (a) Peurala, E.; Koivunen, P.; Bloigu, R.; Haapasaari, K. M.; Jukkola-Vuorinen, A., Expressions of individual PHDs associate with good prognostic factors and increased proliferation in breast cancer patients. *Breast Cancer Research and Treatment* **2012,** *133* (1), 179-88; (b) Moser, S. C.; Bensaddek, D.; Ortmann, B.; Maure, J. F.; Mudie, S.; Blow, J. J.; Lamond, A. I.; Swedlow, J. R.; Rocha, S., PHD1 links cell-cycle progression to oxygen sensing through hydroxylation of the centrosomal protein Cep192. *Developmental Cell* **2013,** *26* (4), 381-92; (c) Luo, W.; Lin, B.; Wang, Y.; Zhong, J.; O'Meally, R.; Cole, R. N.; Pandey, A.; Levchenko, A.; Semenza, G. L., PHD3-mediated prolyl hydroxylation of non-muscle actin impairs polymerization and cell motility. *Molecular Biology of the Cell* **2014**; (d) Xu, W.; Yang, H.; Liu, Y.; Yang, Y.; Wang, P.; Kim, S. H.; Ito, S.; Yang, C.; Wang, P.; Xiao, M. T.; Liu, L. X.; Jiang, W. Q.; Liu, J.; Zhang, J. Y.; Wang, B.; Frye, S.; Zhang, Y.; Xu, Y. H.; Lei, Q. Y.; Guan, K. L.; Zhao, S. M.; Xiong, Y., Oncometabolite 2-hydroxyglutarate is a competitive inhibitor of α-ketoglutarate-dependent dioxygenases. *Cancer Cell* **2011,** *19* (1), 17-30; (e) Ratcliffe, P. J., HIF-1 and HIF-2: working alone or together in hypoxia? *J. Clin. Invest.* **2007,** *117* (4), 862-865; (f) Ratcliffe, P. J.; Pugh, C. W.; Maxwell, P. H., Targeting tumors through the HIF system. *Nature Medicine* **2000,** *6* (12), 1315-1316.

153. Cho, E. A.; Song, H. K.; Lee, S. H.; Chung, B. H.; Lim, H. M.; Lee, M. K., Differential in vitro and cellular effects of iron chelators for hypoxia inducible factor hydroxylases. *Journal of Cellular Biochemistry* **2013,** *114* (4), 864-73.

154. (a) Woo, K. J.; Lee, T. J.; Park, J. W.; Kwon, T. K., Desferrioxamine, an iron chelator, enhances HIF-1α accumulation via cyclooxygenase-2 signaling pathway. *Biochemical and Biophysical Research Communications* **2006,** *343* (1), 8-14; (b) Hirsila, M.; Koivunen, P.; Xu, L.; Seeley, T.; Kivirikko, K. I.; Myllyharju, J., Effect of desferrioxamine and metals on the hydroxylases in the oxygen sensing pathway. *FASEB Journal* **2005,** *19* (10), 1308-10; (c) Wang, G. L.; Semenza, G. L., Desferrioxamine induces erythropoietin gene expression and hypoxia-inducible factor 1 DNA-binding activity:implications for models of hypoxia signal transduction. *Blood* **1993,** *82*, 3610-3615.

155. (a) Choi, J. G.; Kim, J. L.; Park, J.; Lee, S.; Park, S. J.; Kim, J. S.; Choi, C. W., Effects of oral iron chelator deferasirox on human malignant lymphoma cells. *The Korean Journal of Hematology* **2012,** *47* (3), 194-201; (b) Zhao, Y.; Rempe, D. A., Prophylactic neuroprotection against stroke: low-dose, prolonged treatment with deferoxamine or deferasirox establishes prolonged neuroprotection independent of HIF-1 function. *Journal of Cerebral Blood Flow and Metabolism* **2011,** *31* (6), 1412-23.

156. (a) Epstein, A. C. R.; Gleadle, J. M.; McNeill, L. A.; Hewitson, K. S.; O'Rourke, J.; Mole, D. R.; Mukherji, M.; Metzen, E.; Wilson, M. I.; Dhanda, A.; Tian, Y.-M.; Masson, N.; Hamilton, D. L.; Jaakkola, P.; Barstead, R.; Hodgkin, J.; Maxwell, P. H.; Pugh, C. W.; Schofield, C. J.; Ratcliffe, P. J., C. elegans EGL-9 and mammalian homologs define a family of dioxygenases that regulate HIF by prolyl hydroxylation. *Cell* **2001,** *107* (1), 43-54; (b) Mole, D. R.; Schlemminger, I.; McNeill, L. A.; Hewitson, K. S.; Pugh, C. W.; Ratcliffe, P. J.; Schofield, C. J., 2-oxoglutarate analogue inhibitors of HIF prolyl hydroxylase. *Bioorganic & Medicinal Chemistry Letters* **2003,** *13* (16), 2677-80; (c) Schlemminger, I.; Mole, D. R.; McNeill, L. A.; Dhanda, A.; Hewitson, K. S.; Tian, Y. M.; Ratcliffe, P. J.; Pugh, C. W.; Schofield, C. J., Analogues of Dealanylalahopcin are Inhibitors of Human HIF Prolyl Hydroxylases. *Bioorganic & Medicinal Chemistry Letters* **2003,** *13*, 1451.

157. (a) Beuck, S.; Schanzer, W.; Thevis, M., Hypoxia-inducible factor stabilizers and other small-molecule erythropoiesis-stimulating agents in current and preventive doping analysis. *Drug Testing and Analysis* **2012,** *4* (11), 830-45; (b) Eltzschig, H. K.; Bratton, D. L.; Colgan, S. P., Targeting hypoxia signalling for the treatment of ischaemic and inflammatory diseases. *Nature Reviews. Drug discovery* **2014,** *13* (11), 852-69; (c) Higashijima, Y.; Tanaka, T.; Nangaku, M., Structure-based drug design for hypoxia-inducible factor prolyl-hydroxylase inhibitors and its therapeutic potential for the treatment of erythropoiesis-stimulating agent-resistant anemia: raising expectations for exploratory clinical trials. *Expert Opinion on Drug Discovery* **2013,** *8* (8), 965-76; (d) Koury, M. J.;

Haase, V. H., Anaemia in kidney disease: harnessing hypoxia responses for therapy. *Nature Reviews. Nephrology* **2015,** *11* (7), 394-410; (e) Rabinowitz, M. H., Inhibition of hypoxia-inducible factor prolyl hydroxylase domain oxygen sensors: tricking the body into mounting orchestrated survival and repair responses. *Journal of Medicinal Chemistry* **2013,** *56* (23), 9369-402; (f) Rose, N. R.; McDonough, M. A.; King, O. N.; Kawamura, A.; Schofield, C. J., Inhibition of 2-oxoglutarate dependent oxygenases. *Chemical Society Reviews* **2011,** *40* (8), 4364-97; (g) Yan, L.; Colandrea, V. J.; Hale, J. J., Prolyl hydroxylase domain-containing protein inhibitors as stabilizers of hypoxia-inducible factor: small molecule-based therapeutics for anemia. *Expert Opinion on Therapeutic Patents* **2010,** *20* (9), 1219-45.

158. Chowdhury, R.; Candela-Lena, J. I.; Chan, M. C.; Greenald, D. J.; Yeoh, K. K.; Tian, Y. M.; McDonough, M. A.; Tumber, A.; Rose, N. R.; Conejo-Garcia, A.; Demetriades, M.; Mathavan, S.; Kawamura, A.; Lee, M. K.; van Eeden, F.; Pugh, C. W.; Ratcliffe, P. J.; Schofield, C. J., Selective small molecule probes for the hypoxia inducible factor (HIF) prolyl hydroxylases. *ACS Chemical Biology* **2013,** *8* (7), 1488-96.

159. Raval, R. R.; Lau, K. W.; Tran, M. G. B.; Sowter, H. M.; Mandriota, S. J.; Li, J.-L.; Pugh, C. W.; Maxwell, P. H.; Harris, A. L.; Ratcliffe, P. J., Contrasting properties of hypoxia-inducible factor 1 (HIF-1) and HIF-2 in von Hippel-Lindau-associated renal cell carcinoma. *Molecular and Cellular Biology* **2005,** *25* (13), 5675-5686.

160. (a) Grundmann, H.; Kropec, A.; Hartung, D.; Berner, R.; Daschner, F., Pseudomonas aeruginosa in a neonatal intensive care unit: reservoirs and ecology of the nosocomial pathogen. *The Journal of Infectious Diseases* **1993,** *168* (4), 943-7; (b) Carvalho, A. P.; Albano, R. M.; de Oliveira, D. N.; Cidade, D. A.; Teixeira, L. M.; Marques Ede, A., Characterization of an epidemic carbapenem-resistant *Pseudomonas aeruginosa* producing SPM-1 metallo-β-lactamase in a hospital located in Rio de Janeiro, Brazil. *Microbial Drug Resistance* **2006,** *12* (2), 103-8; (c) Salabi, A. E.; Toleman, M. A.; Weeks, J.; Bruderer, T.; Frei, R.; Walsh, T. R., First report of the metallo-β-lactamase SPM-1 in Europe. *Antimicrobial Agents and Chemotherapy* **2010,** *54* (1), 582.

161. Toleman, M. A.; Simm, A. M.; Murphy, T. A.; Gales, A. C.; Biedenbach, D. J.; Jones, R. N.; Walsh, T. R., Molecular characterization of SPM-1, a novel metallo-β-lactamase isolated in Latin America: report from the SENTRY antimicrobial surveillance programme. *The Journal of Antimicrobial Chemotherapy* **2002,** *50* (5), 673-9.

162. (a) Poirel, L.; Magalhaes, M.; Lopes, M.; Nordmann, P., Molecular analysis of metallo-β-lactamase gene *bla(SPM-1)*-surrounding sequences from disseminated *Pseudomonas aeruginosa* isolates in Recife, Brazil. *Antimicrobial Agents and Chemotherapy*

2004, *48* (4), 1406-9; (b) Zavascki, A. P.; Gaspareto, P. B.; Martins, A. F.; Goncalves, A. L.; Barth, A. L., Outbreak of carbapenem-resistant *Pseudomonas aeruginosa* producing SPM-1 metallo-β-lactamase in a teaching hospital in southern Brazil. *The Journal of Antimicrobial Chemotherapy* **2005,** *56* (6), 1148-51; (c) Doi, Y.; de Oliveira Garcia, D.; Adams, J.; Paterson, D. L., Coproduction of novel 16S rRNA methylase RmtD and metallo-β-lactamase SPM-1 in a panresistant *Pseudomonas aeruginosa* isolate from Brazil. *Antimicrobial Agents and Chemotherapy* **2007,** *51* (3), 852-6; (d) Martins, A. F.; Zavascki, A. P.; Gaspareto, P. B.; Barth, A. L., Dissemination of *Pseudomonas aeruginosa* producing SPM-1-like and IMP-1-like metallo-β-lactamases in hospitals from southern Brazil. *Infection* **2007,** *35* (6), 457-60; (e) Castanheira, M.; Fritsche, T. R.; Sader, H. S.; Jones, R. N., RmtD 16S RNA methylase in epidemiologically unrelated SPM-1-producing *Pseudomonas aeruginosa* isolates from Brazil. *Antimicrobial Agents and Chemotherapy* **2008,** *52* (4), 1587-8; author reply 1588; (f) Fuentefria, D. B.; Ferreira, A. E.; Graf, T.; Corcao, G., Spread of Metallo-β-lactamases: screening reveals the presence of a *BLA SPM-1* gene in hospital sewage in southern Brazil. *Brazilian Journal of Microbiology* **2009,** *40* (1), 82-5; (g) Polotto, M.; Casella, T.; de Lucca Oliveira, M. G.; Rubio, F. G.; Nogueira, M. L.; de Almeida, M. T.; Nogueira, M. C., Detection of P. aeruginosa harboring *bla CTX-M-2, bla GES-1 and bla GES-5, bla IMP-1* and *bla SPM-1* causing infections in Brazilian tertiary-care hospital. *BMC Infectious Diseases* **2012,** *12*, 176.

163. (a) Galetti, R.; Andrade, L. N.; Climaco, E. C.; Pitondo-Silva, A.; Ferreira, J. C.; Darini, A. L., Genomic diversification and virulence features in SPM-1-producing *Pseudomonas aeruginosa* 13 years later. *Diagnostic Microbiology and Infectious Disease* **2015,** *82* (2), 179-80; (b) Ghamgosha, M.; Shahrekizahedani, S.; Kafilzadeh, F.; Bameri, Z.; Taheri, R. A.; Farnoosh, G., Metallo-β-Lactamase VIM-1, SPM-1, and IMP-1 Genes Among Clinical *Pseudomonas aeruginosa* Species Isolated in Zahedan, Iran. *Jundishapur Journal of Microbiology* **2015,** *8* (4), e17489; (c) Moosavian, M.; Rahimzadeh, M., Molecular detection of metallo-β-lactamase genes, *bla IMP-1, bla VIM-2* and *bla SPM-1* in imipenem resistant *Pseudomonas aeruginosa* isolated from clinical specimens in teaching hospitals of Ahvaz, Iran. *Iranian Journal of Microbiology* **2015,** *7* (1), 2-6; (d) Hopkins, K. L.; Meunier, D.; Findlay, J.; Mustafa, N.; Parsons, H.; Pike, R.; Wright, L.; Woodford, N., SPM-1 metallo-β-lactamase-producing *Pseudomonas aeruginosa* ST277 in the UK. *Journal of Medical Microbiology* **2016**.

164. (a) Murphy, T. A.; Catto, L. E.; Halford, S. E.; Hadfield, A. T.; Minor, W.; Walsh, T. R.; Spencer, J., Crystal structure of *Pseudomonas aeruginosa* SPM-1 provides insights into

variable zinc affinity of metallo-β-lactamases. *Journal of Molecular Biology* **2006,** *357* (3), 890-903; (b) Brem, J.; Struwe, W. B.; Rydzik, A. M.; Tarhonskaya, H.; Pfeffer, I.; Flashman, E.; van Berkel, S. S.; Spencer, J.; Claridge, T. D.; McDonough, M. A.; Benesch, J. L.; Schofield, C. J., Studying the active-site loop movement of the Sao Paolo metallo-β-lactamase-1. *Chemical Science* **2015,** *6* (2), 956-963.

165. Murphy, T. A.; Simm, A. M.; Toleman, M. A.; Jones, R. N.; Walsh, T. R., Biochemical characterization of the acquired metallo-β-lactamase SPM-1 from *Pseudomonas aeruginosa*. *Antimicrobial Agents and Chemotherapy* **2003,** *47* (2), 582-7.

166. Gonzalez, L. J.; Moreno, D. M.; Bonomo, R. A.; Vila, A. J., Host-specific enzyme-substrate interactions in SPM-1 metallo-β-lactamase are modulated by second sphere residues. *PLoS Pathogens* **2014,** *10* (1), e1003817.

167. Toney, J. H.; Hammond, G. G.; Fitzgerald, P. M.; Sharma, N.; Balkovec, J. M.; Rouen, G. P.; Olson, S. H.; Hammond, M. L.; Greenlee, M. L.; Gao, Y. D., Succinic acids as potent inhibitors of plasmid-borne IMP-1 metallo-β-lactamase. *The Journal of Biological Chemistry* **2001,** *276* (34), 31913-8.

168. Garau, G.; Bebrone, C.; Anne, C.; Galleni, M.; Frere, J. M.; Dideberg, O., A metallo-β-lactamase enzyme in action: crystal structures of the monozinc carbapenemase CphA and its complex with biapenem. *Journal of Molecular Biology* **2005,** *345* (4), 785-95.

169. Chen, H.; Viel, S.; Ziarelli, F.; Peng, L., 19F NMR: a valuable tool for studying biological events. *Chemical Society Reviews* **2013,** *42* (20), 7971-82.

170. Rydzik, A. M.; Brem, J.; van Berkel, S. S.; Pfeffer, I.; Makena, A.; Claridge, T. D.; Schofield, C. J., Monitoring conformational changes in the NDM-1 metallo-β-lactamase by ^{19}F NMR spectroscopy. *Angewandte Chemie International Edition* **2014,** *53* (12), 3129-33.

171. (a) Huestis, W. H.; Raftery, M. A., Bromotrifluoroacetone alkylates hemoglobin at cysteine β93. *Biochemical and Biophysical Research Communications* **1978,** *81* (3), 892-899; (b) Brown, W. E.; Seamon, K. B., Quantitation and characterization of the trifluoroacetonyl derivative of cysteine: A useful NMR probe. *Analytical Biochemistry* **1978,** *87* (1), 211-222.

172. Dalvit, C.; Vulpetti, A., Weak Intermolecular Hydrogen Bonds with Fluorine: Detection and Implications for Enzymatic/Chemical Reactions, Chemical Properties, and Ligand/Protein Fluorine NMR Screening. *Chemistry* **2016,** *22* (22), 7592-601.

173. Stoesz, J. D.; Malinowski, D. P.; Redfield, A. G., Nuclear magnetic resonance study of solvent exchange and nuclear Overhauser effect of the histidine protons of bovine superoxide dismutase. *Biochemistry* **1979,** *18* (21), 4669-75.

174. (a) Dalvit, C.; Fagerness, P. E.; Hadden, D. T.; Sarver, R. W.; Stockman, B. J., Fluorine-NMR experiments for high-throughput screening: theoretical aspects, practical considerations, and range of applicability. *Journal of the American Chemical Society* **2003,** *125* (25), 7696-703; (b) Vulpetti, A.; Dalvit, C., Fluorine local environment: from screening to drug design. *Drug discovery today* **2012,** *17* (15-16), 890-7; (c) Veronesi, M.; Romeo, E.; Lambruschini, C.; Piomelli, D.; Bandiera, T.; Scarpelli, R.; Garau, G.; Dalvit, C., Fluorine NMR-based screening on cell membrane extracts. *ChemMedChem* **2014,** *9* (2), 286-9.

175. Bush, K., Classification of β-lactamases: groups 1, 2a, 2b, and 2b'. *Antimicrobial Agents and Chemotherapy* **1989,** *33* (3), 264-70.

176. Motara, H.; Mistry, D.; Brown, D. R.; Cryan, R. A.; Nigen, M.; Page, M. I., pH and basicity of ligands control the binding of metal-ions to *B. cereus* B1 β-lactamase. *Chemical Science* **2014,** *5* (8), 3120-3129.

177. (a) Liepinsh, E.; Otting, G., Organic solvents identify specific ligand binding sites on protein surfaces. *Nature Biotechnology* **1997,** *15* (3), 264-268; (b) Dalvit, C.; Floersheim, P.; Zurini, M.; Widmer, A., Use of organic solvents and small molecules for locating binding sites on proteins in solutions. *Journal of Biomolecular NMR* **1999,** *14* (1), 23-32.

178. Spicer, T.; Minond, D.; Enogieru, I.; Saldanha, S. A.; Allais, C.; Liu, Q.; Mercer, B. A.; Roush, W. R.; Hodder, P., ML302, a Novel B-lactamase (BLA) Inhibitor. In *Probe Reports from the NIH Molecular Libraries Program*, Bethesda (MD), 2010.

179. Brem, J.; van Berkel, S. S.; Aik, W.; Rydzik, A. M.; Avison, M. B.; Pettinati, I.; Umland, K. D.; Kawamura, A.; Spencer, J.; Claridge, T. D.; McDonough, M. A.; Schofield, C. J., Rhodanine hydrolysis leads to potent thioenolate mediated metallo-β-lactamase inhibition. *Nature Chemistry* **2014,** *6* (12), 1084-90.

180. Heinz, U.; Bauer, R.; Wommer, S.; Meyer-Klaucke, W.; Papamichaels, C.; Bateson, J.; Adolph, H. W., Coordination geometries of metal ions in D- or L-captopril-inhibited metallo-β-lactamases. *The Journal of Biological Chemistry* **2003,** *278* (23), 20659-66.

181. Brem, J.; van Berkel, S. S.; Zollman, D.; Lee, S. Y.; Gileadi, O.; McHugh, P. J.; Walsh, T. R.; McDonough, M. A.; Schofield, C. J., Structural Basis of Metallo-β-Lactamase Inhibition by Captopril Stereoisomers. *Antimicrobial Agents and Chemotherapy* **2016,** *60* (1), 142-50.

182. Lienard, B. M.; Garau, G.; Horsfall, L.; Karsisiotis, A. I.; Damblon, C.; Lassaux, P.; Papamicael, C.; Roberts, G. C.; Galleni, M.; Dideberg, O.; Frere, J. M.; Schofield, C. J., Structural basis for the broad-spectrum inhibition of metallo-β-lactamases by thiols. *Organic & Biomolecular Chemistry* **2008,** *6* (13), 2282-94.

183. Makena, A.; Duzgun, A. O.; Brem, J.; McDonough, M. A.; Rydzik, A. M.; Abboud, M. I.; Saral, A.; Cicek, A. C.; Sandalli, C.; Schofield, C. J., Comparison of Verona Integron-Borne Metallo-β-lactamase Variants Reveals Differences in Stability and Inhibition Profiles. *Antimicrobial Agents and Chemotherapy* **2015**.

184. Ehmann, D. E.; Jahic, H.; Ross, P. L.; Gu, R. F.; Hu, J.; Durand-Reville, T. F.; Lahiri, S.; Thresher, J.; Livchak, S.; Gao, N.; Palmer, T.; Walkup, G. K.; Fisher, S. L., Kinetics of avibactam inhibition against Class A, C, and D β-lactamases. *The Journal of Biological Chemistry* **2013,** *288* (39), 27960-71.

185. Abboud, M. I.; Damblon, C.; Brem, J.; Smargiasso, N.; Mercuri, P.; Gilbert, B.; Rydzik, A. M.; Claridge, T. D.; Schofield, C. J.; Frere, J. M., Interaction of Avibactam with Class B Metallo-β-lactamases. *Antimicrobial Agents and Chemotherapy* **2016**.

186. Didenko, T.; Liu, J. J.; Horst, R.; Stevens, R. C.; Wuthrich, K., Fluorine-19 NMR of integral membrane proteins illustrated with studies of GPCRs. *Current Opinion in Structural Biology* **2013,** *23* (5), 740-7.

187. Cahill, S. T.; Tarhonskaya, H.; Rydzik, A. M.; Flashman, E.; McDonough, M. A.; Schofield, C. J.; Brem, J., Use of Ferrous Iron by Metallo-β-Lactamases. *Journal of Inorganic Biochemistry*.

188. van Berkel, S. S.; Brem, J.; Rydzik, A. M.; Salimraj, R.; Cain, R.; Verma, A.; Owens, R. J.; Fishwick, C. W.; Spencer, J.; Schofield, C. J., Assay platform for clinically relevant metallo-β-lactamases. *Journal of Medicinal Chemistry* **2013,** *56* (17), 6945-53.

189. van Berkel, S. S.; Nettleship, J. E.; Leung, I. K.; Brem, J.; Choi, H.; Stuart, D. I.; Claridge, T. D.; McDonough, M. A.; Owens, R. J.; Ren, J.; Schofield, C. J., Binding of (5*S*)-penicilloic acid to penicillin binding protein 3. *ACS Chemical Biology* **2013,** *8* (10), 2112-6.

190. Ghebre-Sellassie, I.; Hem, S. L.; Knevel, A. M., Epimerization of benzylpenicilloic acid in alkaline media. *Journal of Pharmaceutical Sciences* **1984,** *73* (1), 125-8.

191. Badarau, A.; Llinas, A.; Laws, A. P.; Damblon, C.; Page, M. I., Inhibitors of metallo-β-lactamase generated from β-lactam antibiotics. *Biochemistry* **2005,** *44* (24), 8578-89.

192. (a) Brown, R. P.; Aplin, R. T.; Schofield, C. J.; Frydrych, C. H., Mass spectrometric studies on the inhibition of TEM-2 β-lactamase by clavulanic acid derivatives. *The Journal of Antibiotics* **1997,** *50* (2), 184-5; (b) Imtiaz, U.; Billings, E.; Knox, J. R.; Manavathu, E. K.; Lerner, S. A.; Mobashery, S., Inactivation of class A β-lactamases by clavulanic acid: the role of arginine-244 in a proposed nonconcerted sequence of events. *Journal of the American Chemical Society* **1993,** *115* (11), 4435-4442.

193. Vulpetti, A.; Hommel, U.; Landrum, G.; Lewis, R.; Dalvit, C., Design and NMR-based screening of LEF, a library of chemical fragments with different local environment of fluorine. *Journal of the American Chemical Society* **2009,** *131* (36), 12949-59.

194. Jhoti, H.; Cleasby, A.; Verdonk, M.; Williams, G., Fragment-based screening using X-ray crystallography and NMR spectroscopy. *Current Opinion in Chemical Biology* **2007,** *11* (5), 485-93.

195. Liang, Z.; Li, L.; Wang, Y.; Chen, L.; Kong, X.; Hong, Y.; Lan, L.; Zheng, M.; Guang-Yang, C.; Liu, H.; Shen, X.; Luo, C.; Li, K. K.; Chen, K.; Jiang, H., Molecular basis of NDM-1, a new antibiotic resistance determinant. *PloS One* **2011,** *6* (8), e23606.

196. Makena, A.; van Berkel, S. S.; Lejeune, C.; Owens, R. J.; Verma, A.; Salimraj, R.; Spencer, J.; Brem, J.; Schofield, C. J., Chromophore-linked substrate (CLS405): probing metallo-β-lactamase activity and inhibition. *ChemMedChem* **2013,** *8* (12), 1923-9.

197. Kabsch, W., XDS. *Acta Crystallographica Section D* **2010,** *66* (2), 125-132.

198. Winn, M. D.; Ballard, C. C.; Cowtan, K. D.; Dodson, E. J.; Emsley, P.; Evans, P. R.; Keegan, R. M.; Krissinel, E. B.; Leslie, A. G. W.; McCoy, A.; McNicholas, S. J.; Murshudov, G. N.; Pannu, N. S.; Potterton, E. A.; Powell, H. R.; Read, R. J.; Vagin, A.; Wilson, K. S., Overview of the CCP4 suite and current developments. *Acta Crystallographica Section D: Biological Crystallography* **2011,** *67* (Pt 4), 235-42.

199. McCoy, A. J.; Grosse-Kunstleve, R. W.; Adams, P. D.; Winn, M. D.; Storoni, L. C.; Read, R. J., Phaser crystallographic software. *Journal of Applied Crystallography* **2007,** *40* (4), 658-674.

200. Adams, P. D.; Afonine, P. V.; Bunkoczi, G.; Chen, V. B.; Davis, I. W.; Echols, N.; Headd, J. J.; Hung, L.-W.; Kapral, G. J.; Grosse-Kunstleve, R. W.; McCoy, A. J.; Moriarty, N. W.; Oeffner, R.; Read, R. J.; Richardson, D. C.; Richardson, J. S.; Terwilliger, T. C.; Zwart, P. H., PHENIX: a comprehensive Python-based system for macromolecular structure solution. *Acta Crystallographica Section D* **2010,** *66* (2), 213-221.

201. Emsley, P.; Cowtan, K., Coot: model-building tools for molecular graphics. *Acta Crystallographica Section D* **2004,** *60* (12 Part 1), 2126-2132.

202. Chen, V. B.; Arendall, W. B.; Headd, J. J.; Keedy, D. A.; Immormino, R. M.; Kapral, G. J.; Murray, L. W.; Richardson, J. S.; Richardson, D. C., MolProbity: all-atom structure validation for macromolecular crystallography. *Acta Crystallographica Section D* **2010,** *66* (1), 12-21.

203. Johnson, J. W.; Evanoff, D. P.; Savard, M. E.; Lange, G.; Ramadhar, T. R.; Assoud, A.; Taylor, N. J.; Dmitrienko, G. I., Cyclobutanone Mimics of Penicillins: Effects of

Substitution on Conformation and Hemiketal Stability. *The Journal of Organic Chemistry* **2008,** *73* (18), 6970-6982.

204. Johnson, J. W.; Gretes, M.; Goodfellow, V. J.; Marrone, L.; Heynen, M. L.; Strynadka, N. C.; Dmitrienko, G. I., Cyclobutanone analogues of β-lactams revisited: insights into conformational requirements for inhibition of serine- and metallo-β-lactamases. *Journal of the American Chemical Society* **2010,** *132* (8), 2558-60.

205. (a) Turano, H.; Gomes, F.; Medeiros, M.; Oliveira, S.; Fontes, L. C.; Sato, M. I.; Lincopan, N., Presence of high-risk clones of OXA-23-producing *Acinetobacter baumannii* (ST79) and SPM-1-producing *Pseudomonas aeruginosa* (ST277) in environmental water samples in Brazil. *Diagnostic Microbiology and Infectious Disease* **2016**; (b) Fonseca, E. L.; Marin, M. A.; Encinas, F.; Vicente, A. C., Full characterization of the integrative and conjugative element carrying the metallo-β-lactamase *bla SPM-1* and bicyclomycin *bcr1* resistance genes found in the pandemic *Pseudomonas aeruginosa* clone SP/ST277. *The Journal of Antimicrobial Chemotherapy* **2015,** *70* (9), 2547-50.

206. Brem, J.; Struwe, W. B.; Rydzik, A. M.; Tarhonskaya, H.; Pfeffer, I.; Flashman, E.; van Berkel, S. S.; Spencer, J.; Claridge, T. D.; McDonough, M. A.; Benesch, J. L.; Schofield, C. J., Studying the active-site loop movement of the Sao Paolo metallo-β-lactamase-1. *Chemical Science* **2015,** *6* (2), 956-963.

207. Bebrone, C.; Lassaux, P.; Vercheval, L.; Sohier, J. S.; Jehaes, A.; Sauvage, E.; Galleni, M., Current challenges in antimicrobial chemotherapy: focus on β-lactamase inhibition. *Drugs* **2010,** *70* (6), 651-79.

208. Ding, Y.-S.; Prestwich, G. D., Chemical studies of proteins that degrade pheromones. *Journal of Chemical Ecology* **1988,** *14* (11), 2033-2046.

209. Ceftazidime/Avibactam (Avycaz) - a new intraveneous antibiotic. *The Medical Letter on Drugs and therapeutics* **2015,** *57* (1469), 79-80.

210. Fernea, A.; Galleni, M.; Frere, J. M., Kinetics of the interaction between avibactam and the CHE-1 class C β-lactamase. *The Journal of Antimicrobial Chemotherapy* **2015,** *70* (3), 951-3.

211. (a) Stachyra, T.; Pechereau, M. C.; Bruneau, J. M.; Claudon, M.; Frere, J. M.; Miossec, C.; Coleman, K.; Black, M. T., Mechanistic studies of the inactivation of TEM-1 and P99 by NXL104, a novel non-β-lactam β-lactamase inhibitor. *Antimicrobial Agents and Chemotherapy* **2010,** *54* (12), 5132-8; (b) Bonnefoy, A.; Dupuis-Hamelin, C.; Steier, V.; Delachaume, C.; Seys, C.; Stachyra, T.; Fairley, M.; Guitton, M.; Lampilas, M., In vitro

activity of AVE1330A, an innovative broad-spectrum non-β-lactam β-lactamase inhibitor. *The Journal of Antimicrobial Chemotherapy* **2004,** *54* (2), 410-7.

212. (a) Flamm, R. K.; Farrell, D. J.; Sader, H. S.; Jones, R. N., Ceftazidime/avibactam activity tested against Gram-negative bacteria isolated from bloodstream, pneumonia, intra-abdominal and urinary tract infections in US medical centres (2012). *The Journal of Antimicrobial Chemotherapy* **2014,** *69* (6), 1589-98; (b) Flamm, R. K.; Farrell, D. J.; Sader, H. S.; Jones, R. N., Antimicrobial activity of ceftaroline combined with avibactam tested against bacterial organisms isolated from acute bacterial skin and skin structure infections in United States medical centers (2010-2012). *Diagnostic Microbiology and Infectious Disease* **2014,** *78* (4), 449-56.

213. (a) Bebrone, C., Metallo-β-Lactamases (Classification, Activity, Genetic Organization, Structure, Zinc Coordination) and Their Superfamily. *Biochemical pharmacology* **2007,** *74* (12), 1686-1701; (b) Bush, K., Extended-spectrum β-lactamases in North America, 1987-2006. *Clinical Microbiology and Infection* **2008,** *14 Suppl 1*, 134-43; (c) Bush, K., Alarming β-lactamase-mediated resistance in multidrug-resistant Enterobacteriaceae. *Current Opinion in Microbiology* **2010,** *13* (5), 558-64.

214. (a) Bebrone, C.; Anne, C.; De Vriendt, K.; Devreese, B.; Rossolini, G. M.; Van Beeumen, J.; Frere, J. M.; Galleni, M., Dramatic broadening of the substrate profile of the *Aeromonas hydrophila* CphA metallo-β-lactamase by site-directed mutagenesis. *The Journal of Biological Chemistry* **2005,** *280* (31), 28195-202; (b) Lassaux, P.; Traore, D. A.; Loisel, E.; Favier, A.; Docquier, J. D.; Sohier, J. S.; Laurent, C.; Bebrone, C.; Frere, J. M.; Ferrer, J. L.; Galleni, M., Biochemical and structural characterization of the subclass B1 metallo-β-lactamase VIM-4. *Antimicrobial Agents and Chemotherapy* **2011,** *55* (3), 1248-55; (c) Laraki, N.; Franceschini, N.; Rossolini, G. M.; Santucci, P.; Meunier, C.; de Pauw, E.; Amicosante, G.; Frere, J. M.; Galleni, M., Biochemical characterization of the *Pseudomonas aeruginosa* 101/1477 metallo-β-lactamase IMP-1 produced by *Escherichia coli*. *Antimicrobial Agents and Chemotherapy* **1999,** *43* (4), 902-6; (d) Mercuri, P. S.; Garcia-Saez, I.; De Vriendt, K.; Thamm, I.; Devreese, B.; Van Beeumen, J.; Dideberg, O.; Rossolini, G. M.; Frere, J. M.; Galleni, M., Probing the specificity of the subclass B3 FEZ-1 metallo-β-lactamase by site-directed mutagenesis. *The Journal of Biological Chemistry* **2004,** *279* (32), 33630-8.

215. Galleni, M.; Lamotte-Brasseur, J.; Rossolini, G. M.; Spencer, J.; Dideberg, O.; Frere, J. M.; Metallo-β-lactamases Working, G., Standard numbering scheme for class B β-lactamases. *Antimicrobial Agents and Chemotherapy* **2001,** *45* (3), 660-3.

216. Xu, G.; Evans, J. S., The application of "excitation sculpting" in the construction of selective one-dimensional homonuclear coherence-transfer experiments. *Journal of Magnetic Resonance. Series B* **1996,** *111* (2), 183-5.

217. (a) Testa, R.; Canton, R.; Giani, T.; Morosini, M. I.; Nichols, W. W.; Seifert, H.; Stefanik, D.; Rossolini, G. M.; Nordmann, P., In vitro activity of ceftazidime, ceftaroline and aztreonam alone and in combination with avibactam against European Gram-negative and Gram-positive clinical isolates. *International Journal of Antimicrobial Agents* **2015,** *45* (6), 641-6; (b) Vasoo, S.; Cunningham, S. A.; Cole, N. C.; Kohner, P. C.; Menon, S. R.; Krause, K. M.; Harris, K. A.; De, P. P.; Koh, T. H.; Patel, R., In Vitro Activities of Ceftazidime-Avibactam, Aztreonam-Avibactam, and a Panel of Older and Contemporary Antimicrobial Agents against Carbapenemase-Producing Gram-Negative Bacilli. *Antimicrobial Agents and Chemotherapy* **2015,** *59* (12), 7842-6; (c) Wang, X.; Zhang, F.; Zhao, C.; Wang, Z.; Nichols, W. W.; Testa, R.; Li, H.; Chen, H.; He, W.; Wang, Q.; Wang, H., In vitro activities of ceftazidime-avibactam and aztreonam-avibactam against 372 Gram-negative bacilli collected in 2011 and 2012 from 11 teaching hospitals in China. *Antimicrobial Agents and Chemotherapy* **2014,** *58* (3), 1774-8.

218. Biedenbach, D. J.; Kazmierczak, K.; Bouchillon, S. K.; Sahm, D. F.; Bradford, P. A., In vitro activity of aztreonam-avibactam against a global collection of Gram-negative pathogens from 2012 and 2013. *Antimicrobial Agents and Chemotherapy* **2015,** *59* (7), 4239-48.

219. (a) Livermore, D. M.; Mushtaq, S.; Warner, M.; Zhang, J.; Maharjan, S.; Doumith, M.; Woodford, N., Activities of NXL104 combinations with ceftazidime and aztreonam against carbapenemase-Producing Enterobacteriaceae. *Antimicrobial Agents and Chemotherapy* **2011,** *55* (1), 390-4; (b) Pillar, C. M.; Stoneburner, A.; Shinabarger, D. L.; Krause, K. M.; Nichols, W. W., The postantibiotic effect and post-β-lactamase-inhibitor effect of ceftazidime, ceftaroline and aztreonam in combination with avibactam against target Gram-negative bacteria. *Letters in Applied Microbiology* **2016,** *63* (2), 96-102.

220. McKnight, S. L.; Kingsbury, R., Transcriptional control signals of a eukaryotic protein-coding gene. *Science* **1982,** *217* (4557), 316-24.

221. Oste, C., Polymerase chain reaction. *BioTechniques* **1988,** *6* (2), 162-7.

222. Lu, L.; Patel, H.; Bissler, J. J., Optimizing DpnI digestion conditions to detect replicated DNA. *BioTechniques* **2002,** *33* (2), 316-8.

223. Laemmli, U. K., Cleavage of structural proteins during the assembly of the head of bacteriophage T4. *Nature* **1970,** *227* (5259), 680-5.

224. Gill, S. C.; von Hippel, P. H., Calculation of protein extinction coefficients from amino acid sequence data. *Analytical Biochemistry* **1989,** *182* (2), 319-26.